Regulation of phagosome maturation and bacterial killing by the TPL-2 complex

Felix Breyer

University College London

and

The Francis Crick Institute

PhD Supervisor: Professor Steven C. Ley

A thesis submitted for the degree of

Doctor of Philosophy

University College London

November 2020

Declaration

I, Felix Breyer confirm that the work presented in this thesis is my own. Where information has been derived from other sources, I confirm that this has been indicated in the thesis.

List of Publications

Breyer, F., Härtlova, A., Thurston, T., Flynn, H.R., Chakravarty, P., Janzen, J., Peltier, J., Heunis, T., Snijders, A.P., Trost, M., Ley, S.C. TPL-2 kinase induces phagosome acidification to promote macrophage killing of bacteria. Manuscript under review at *The EMBO Journal*.

Ventura, S*., Cano, F*., Kannan, Y*., **Breyer, F**., Pattison, M.J., Wilson, M.S., and Ley, S.C. (2018). A20-binding inhibitor of NF-κB (ABIN) 2 negatively regulates allergic airway inflammation. *J. Exp. Med*. 215, 2737–2747.

* Joint first authors

Abstract

A fundamental role of the innate immune response involves the killing of phagocytosed pathogens, such as bacteria, by macrophages. During phagocytosis, bacteria are internalised into membrane-bound vacuoles called phagosomes. The nascent phagosome undergoes a complex maturation process, which involves sequential membrane fusion and fission events with the endosomal compartment and ultimately with lysosomes to form a phagolysosome. The mature phagolysosome is an acidic, hydrolytic and highly oxidative organelle, which efficiently degrades internalised bacteria.

Toll-like receptor (TLR) activation of mitogen-activated protein (MAP) kinases in macrophages is mediated by tumour progression locus 2 (TPL-2), a MAP 3 kinase that is critical for inflammatory immune responses to bacteria, viruses, and fungi. In unstimulated macrophages, TPL-2 forms a ternary complex with NF-κB1 p105 and A20-binding inhibitor of NF-κB-2 (ABIN-2). TLR-induced activation of the IκB kinase (IKK) complex leads to p105 phosphorylation and its proteasomal degradation. This liberates TPL-2 to activate MAP kinase signalling, which results in gene expression of numerous inflammatory mediators. ABIN-2 is also released, however, its physiological function in innate immune responses has remained unclear.

I discovered that the TPL-2 complex promotes bead phagosome maturation in macrophages. Genetic inactivation of TPL-2 catalytic activity or ABIN-2 ubiquitin binding substantially altered the composition of the phagosome proteome in primary mouse macrophages. Further, I found that TPL-2 catalytic activity induced phagosome proteolytic activity and phagosome acidification, while ABIN-2 ubiquitin binding promoted phagosome proteolysis without affecting phagosome acidification. My genetic and pharmacological experiments indicated that TPL-2 regulates phagosome function independently of its known ability to activate MAP kinases. I demonstrated that induction of phagosome maturation was mediated by TPL-2-dependent regulation of V-ATPase function via serine 1903 phosphorylation of DMXL1, a V-ATPase-interacting regulatory protein. Importantly, I showed that TPL-2 catalytic activity also induced phagosome maturation independently of MAP kinase

signalling in primary human macrophages, establishing the clinical relevance of my findings. Furthermore, my results revealed that ubiquitin binding to ABIN-2 promotes phagosome proteolytic activity independently of TPL-2 regulation of MAP kinase signalling.

Consistent with these findings analysing bead phagosomes, I discovered that TPL-2 catalytic activity and ABIN-2 ubiquitin binding are required for efficient killing of internalised *Staphylococcus aureus* by macrophages. Genetic inactivation of TPL-2 catalytic activity or ABIN-2 ubiquitin binding impaired maturation of *S. aureus* phagosomes. I also found that TPL-2 catalytic activity was required for optimal killing of phagocytosed *Citrobacter rodentium* by inducing phagosomal acidification. Moreover, I demonstrated that ABIN-2 ubiquitin binding was essential for efficient killing of *Salmonella typhimurium*. Together, these discoveries demonstrated that both TPL-2 catalytic activity and ABIN-2 ubiquitin binding are important for the killing of several bacterial species, Gram-negative and Gram-positive as well as extracellular and intracellular microbes.

In conclusion, my research identified novel signalling pathways that promote phagosome maturation and pathogenic bacterial killing by macrophages. This work increases our understanding of a critical process in innate immune responses and may lead to development of novel therapeutic approaches for acute bacterial infections.

Impact Statement

Diseases caused by bacteria are a global threat to human health and treatment of bacterial diseases represents a major unmet medical need. Effective vaccines for many bacterial diseases do not exist. Antimicrobials, including antibiotics, are widely used medicines to treat bacterial infections in the clinic and have, historically, proven very successful in fighting bacteria-causing diseases. However, antimicrobial resistance, a phenomenon that occurs when bacteria are no longer susceptible to antibiotics, has become widespread and has given rise to so-called 'superbugs', which are bacterial infections that are resistant to traditional antibiotic therapies. The World Health Organization has declared antibiotic-resistant bacteria as one of the major threats to global public health. To develop novel therapeutic approaches for the treatment of bacterial infections, it is critical to better understand the molecular pathways underlying host immunity. A key early step in the innate immune response is the killing of phagocytosed bacteria by macrophages. This killing mechanism involves a process called phagosome maturation, in which phagocytosed bacteria are trafficked into a series of increasingly microbicidal membrane-bound vacuoles and then degraded. The molecular understanding of host immune signalling pathways that regulate phagosome maturation has remained limited. My research identified novel signalling pathways that induce phagosome maturation and pathogenic bacterial killing by macrophages. I discovered that two key components of the TPL-2 complex, namely TPL-2 and ABIN-2, stimulate macrophage phagosome maturation independently of their established functions in the innate immune system. Besides, I consolidated that one of these signalling pathways is conserved in human immune cells, which raises the possibility that further elucidation of this signalling network may identify potential drug targets that could possibly be exploited to develop a novel class of antimicrobial agents for the treatment of bacterial infections. Of particular relevance is my discovery that the pathways identified are important in promoting the killing of *Staphylococcus aureus*, a bacterial species that frequently develops antimicrobial resistance. Methicillin-resistant *Staphylococcus aureus* (MRSA) causes severe infections, with poor clinical prognosis and MRSA 'superbug' infections put significant burden on patients and healthcare systems across the world.

Acknowledgement

First and foremost, I would like to sincerely thank my supervisor Professor Steve Ley for providing me with the great opportunity to work on an exciting project in his laboratory. I am extremely grateful for his scientific guidance, continuous support and constructive criticism over the past four years.

I am also very thankful to my dear colleagues Dr Louise Blair, Julia Janzen, Dr Joan Manils, Dr Louise Webb, Dr Michael Pattison, Dr Sonia Ventura, Dr Florencia Cano and Dr Ashleigh Howes for their insightful discussions, helpful scientific advice and technical support. It has been a joy sharing a fridge and freezer with Louise for several years, and I have been very lucky that she has shared, or at times rather withstood, my particular sense of humour.

I have been fortunate to have enjoyed the great support of many colleagues across The Francis Crick Institute, including Dr Bram Snijders, Dr Helen Flynn, Probir Chakravarty, Dr Simone Kunzelmann, Dr Jeremy Carlton, Dr Antonio Tedeschi and Robert Moore. Moreover, I also gratefully acknowledge the fantastic scientific support I have received from my colleagues working in the Biological Research, Advanced Light Microscopy, Advanced Sequencing and Media Preparation Science Technology Platforms.

I would also like to extend many thanks to my thesis committee members Professor Henning Walczak, Professor Julian Downward and Dr Owen Williams for their excellent discussions and scientific advice.

I have thoroughly enjoyed working with remarkable collaborators throughout my PhD. I am very thankful to Professor Matthias Trost, Assistant Professor Anetta Härtlova, Professor David Holden and Dr Teresa Thurston for their invaluable support.

I am also very thankful to Professor Sir Philip Cohen for his mentorship and early scientific training, which prepared me well for the PhD.

I have been particularly fortunate to be part of the Boehringer Ingelheim Fonds community. I would like to thank all members of the BIF team for their support and all BIF Fellows for enjoyable conferences, seminars and, most importantly, socials.

I would also like to send many thanks to Daniel, Tim and David for their special friendship over the years.

Ein ganz besonderes Dankeschön geht auch an meine Eltern (euch Vieren) und Bruder für die wunderbare Unterstützung.

Table of Contents

List of Publications **3**
Abstract **4**
Impact Statement **6**
Acknowledgement **7**
Table of Contents **9**
Table of figures **12**
List of tables **17**
Abbreviations **18**
Chapter 1.Introduction **26**
1.1 The immune system **26**
1.1.1 The innate immune response 27
1.1.2 Immune cells of the innate and adaptive response 27
1.1.3 Hallmarks of macrophages 29
1.1.4 Macrophage polarisation 30
1.2 Regulation of innate immune signalling by post-translational modifications **32**
1.2.1 Protein phosphorylation 33
1.2.2 Protein ubiquitylation 34
1.2.3 Linkage-specific functions of ubiquitin chains 35
1.2.4 Ubiquitin-binding proteins 37
1.3 Pathogen recognition by innate immune receptors **38**
1.3.1 TLR4 signalling 41
1.3.2 The MyD88-dependent signalling pathway 42
1.3.3 The TRIF-dependent signalling pathway 46
1.3.4 MAP kinase signalling in innate immunity 49
1.3.5 Functions of MAPKs in innate immune cells 50
1.4 Ternary TPL-2 complex **52**
1.4.1 TPL-2 protein kinase 52
1.4.2 Discovery of TPL-2 and its role in cancer 52
1.4.3 Regulation of TPL-2 activity and stability by NF-κB1 p105 54
1.4.4 Regulation of TPL-2 activity by phosphorylation 57
1.4.5 Regulation of TPL-2 stability by ABIN-2 57
1.4.6 Regulation of innate signalling pathways by TPL-2 58
1.4.7 Regulation of inflammatory and innate immune responses by TPL-261
1.4.8 TPL-2 kinase as a drug target to treat inflammatory diseases 63
1.5 The ABIN-2 adaptor protein **65**
1.5.1 ABIN-2 regulation of inflammation 66
1.5.2 ABIN-2 interaction with ESCRT-I 68
1.6 Phagocytosis **69**
1.6.1 Phagosome formation 70
1.6.2 Phagosome maturation 72
1.6.3 Phagosome acidification 78
1.6.4 Reactive oxygen and nitrogen species 79
1.6.5 Antimicrobial peptides and enzymes 81
1.7 Thesis Aims **83**

Chapter 2.Materials & Methods 84
2.1 Materials 84
2.1.1 Chemicals 84
2.1.2 Antibodies 86
2.1.3 Proteins 89
2.1.4 Mice 90
2.1.5 Buffers 91
2.2 Methods 93
2.2.1 Mammalian cell culture 93
2.2.2 Primary Cells 94
2.2.3 Immortalised cell lines 96
2.2.4 Biochemistry techniques 98
2.2.5 Microbiology techniques 104
2.2.6 Surface staining for flow cytometry 106
2.2.7 Techniques to study phagocytosis and phagosome biology 107
2.2.8 Mass spectrometry techniques 111
2.2.9 Immunofluorescence 118
2.2.10 Statistical Analysis 121
2.2.11 Molecular biology techniques 121
2.2.12 RNA sequencing 124
Chapter 3.Biochemical characterisation of ABIN-2 126
3.1 Introduction 126
3.2 Results 127
3.2.1 Characterisation of *Abin2* point mutations 127
3.2.2 The role of ABIN-2 in TLR4 and TNF receptor signalling 132
3.2.3 Regulation of TLR4-mediated gene expression by ABIN-2/A20 complexes 136
3.3 Conclusion 139
3.3.1 Specificity of *Abin2* mutation effects on ABIN-2 interactions 139
3.3.2 ABIN-2 is not a regulator of TLR4 or TNF receptor-mediated signalling in macrophages 141
Chapter 4.A novel role for the TPL-2 complex in promoting phagosome maturation 142
4.1 Introduction 142
4.2 Results 143
4.2.1 ABIN-2 ubiquitin binding and TPL-2 kinase activity induce phagosome proteolysis 143
4.2.2 TPL-2 kinase activity promotes phagosome acidification 146
4.2.3 ABIN-2 ubiquitin binding and TPL-2 kinase activity drive ROS production upon phagocytosis 149
4.2.4 TPL-2 induces phagosome maturation independently of MAP kinase activation 150
4.2.5 TPL-2 catalytic activity promotes phagosome maturation in primary human macrophages independently of MAP kinase activation 154
4.2.6 TPL-2 and ABIN-2 regulate the protein composition of phagosomes 157
4.2.7 *Tpl2*^{D270A} and *Abin2*^{D310N} mutation do not affect ubiquitin abundance on phagosomes 164

4.2.8 Analysis of the TPL-2-dependent phosphoproteome during phagocytosis 165
4.2.9 TPL-2 promotes phosphorylation of DMXL1 following phagocytosis 175
4.2.10 TPL-2 promotes AKT signalling following phagocytosis 180
4.2.11 AKT signalling induces phagosome maturation 183
4.2.12 TPL-2-dependent transcriptome following phagocytic uptake of LPS-coated latex beads 187
4.2.13 TPL-2 interacts with the endosomal protein EEA1 following LPS stimulation 192
4.2.14 ESCRT-I binding to ABIN-2 promotes phagosomal proteolysis 195
4.3 Conclusion 198
4.3.1 Bead particles trigger scavenger receptor-mediated phagocytosis 199
4.3.2 ABIN-2 induces phagosome maturation 199
4.3.3 A role for ABIN-2 in the interplay between ubiquitin and ESCRT during phagosome maturation 201
4.3.4 How does ABIN-2 regulate phagosome maturation? 202
4.3.5 TPL-2 stimulates phagosome maturation 203
4.3.6 TPL-2 induces DMXL1 phosphorylation to induce phagosome acidification 204
4.3.7 Endosomal activation of AKT signalling by TPL-2 promotes phagosome maturation 206
4.3.8 Endosomal activation of type I interferon expression 208
Chapter 5.TPL-2 and ABIN-2 promote killing of Gram-positive and Gram-negative bacteria 210
5.1 Introduction 210
5.2 Results 211
5.2.1 TPL-2 and ABIN-2 promote macrophage killing of *Escherichia coli* 211
5.2.2 TPL-2 promotes macrophage killing of *Citrobacter rodentium* 212
5.2.3 TPL-2 and ABIN-2 promote macrophage killing of *Staphylococcus aureus* 214
5.2.4 TPL-2 and ABIN-2 regulate macrophage killing of *Salmonella typhimurium* 230
5.3 Conclusion 235
5.3.1 ABIN-2 is a regulator of bacterial killing in macrophages 236
5.3.2 ABIN-2 ubiquitin binding promotes phagosome maturation following *S. aureus* infection 238
5.3.3 A novel role for TPL-2 in promoting bacterial killing by macrophages 240
5.3.4 TPL-2 catalytic activity promotes phagosome maturation during *S. aureus* infection 241
5.3.5 TPL-2 catalytic activity suppresses type I interferon expression during *S. aureus* infection 243
5.3.6 Loss of TPL-2 catalytic activity protects against *S. typhimurium* infection 245
Reference List 247

Table of figures

Figure 1 Macrophage polarisation 32
Figure 2 Different types of ubiquitylation and chain-specific biological functions ... 36
Figure 3 Pattern recognition receptors in innate immunity 39
Figure 4 MyD88-dependent signalling 45
Figure 5 TRIF-dependent signalling pathway 48
Figure 6 Structure of the ternary TPL-2 complex 54
Figure 7 TPL-2 signalling pathway 55
Figure 8 ABIN-2 domain structure 65
Figure 9 Phagosome maturation 73
Figure 10 ABIN-2^{D309N} selectively abrogates ubiquitin binding to ABIN-2 128
Figure 11 ABIN-2^{E255K} selectively reduces A20 binding to ABIN-2 129
Figure 12 ABIN-2^{Y230A} selectively abrogates ESCRT-I binding to ABIN-2 130
Figure 13 ABIN-2 point mutations do not impair binding to TPL-2/p105 complexes 131
Figure 14 ABIN-2 and TPL-2 levels are normal in knock-in mouse strains 132
Figure 15 ABIN-2 is recruited to TNFR1 upon stimulation 133
Figure 16 A20 and ubiquitin binding to ABIN-2 do not regulate TLR4 and TNFR1 signalling 135
Figure 17 Regulation of gene expression by ABIN-2/A20 complexes in response to TLR4 activation 137
Figure 18 *Abin2*^{E256K} mutation does not regulate expression of select innate immune genes upon LPS stimulation 138
Figure 19 Genetically-modified mouse strains to decipher ABIN-2 and TPL-2 signalling 140
Figure 20 *Tpl2*^{D270A} and *Abin2*^{D310N} mutation impair phagosomal proteolysis 145
Figure 21 *Tpl2*^{D270A} and *Abin2*^{D310N} mutation reduce cathepsin activity 146
Figure 22 *Tpl2*^{D270A} mutation blocks phagosomal acidification following uptake of BCECF-coupled silica beads 147
Figure 23 *Tpl2*^{D270A} mutation blocks phagosomal acidification following uptake of LPS-coated BCECF-coupled silica beads 148

Figure 24 *Tpl2*^{D270A} mutation reduces abundance of acidic compartments following bead uptake 149
Figure 25 *Tpl2*^{D270A} and *Abin2*^{D310N} mutation reduce ROS levels following uptake of latex beads 150
Figure 26 *Nfkb1*^{SSAA} mutation does not impair phagosomal proteolysis or acidification 152
Figure 27 Pharmacological inhibition of ERK1/2 and p38α activation does not impair phagosomal proteolysis 153
Figure 28 Pharmacological inhibition of TPL-2, but not MAP kinases, impairs phagosome maturation in BMDMs 154
Figure 29 FACS analysis of positive selection for CD14^{+} monocytes 155
Figure 30 Pharmacological inhibition of TPL-2, but not MAP kinases, impairs phagosome maturation in primary human macrophages 156
Figure 31 Biological processes downregulated by *Tpl2*^{D270A} and *Abin2*^{D310N} mutation 158
Figure 32 *Tpl2*^{D270A} and *Abin2*^{D310N} mutation reduce abundance of critical regulators of phagosome maturation 159
Figure 33 Selected phagosomal proteins downregulated by *Tpl2*^{D270A} and *Abin2*^{D310N} mutation 160
Figure 34 *Tpl2*^{D270A} and *Abin2*^{D310N} mutation decrease Rab GTPases on phagosomes 161
Figure 35 *Tpl2*^{D270A} mutation reduces V-ATPase abundance on phagosomes 162
Figure 36 *Tpl2*^{D270A} and *Abin2*^{D310N} mutation reduce abundance of AP2 proteins on phagosomes 163
Figure 37 *Tpl2*^{D270A} and *Abin2*^{D310N} decrease LAMP1 and RAB5 protein levels on phagosomes 164
Figure 38 Ubiquitin chain abundance on isolated phagosomes from *Tpl2*$^{D270A/D270A}$ and *Abin2*$^{D310N/D310N}$ BMDMs 165
Figure 39 TPL-2-dependent phosphoproteome following uptake of latex beads 166
Figure 40 TPL-2-dependent phosphoproteome following uptake of LPS-coated latex beads 170
Figure 41 Biological pathways regulated by *Tpl2*^{D270A} mutation following uptake of LPS-coated beads 171

Figure 42 TPL-2-dependent phosphoproteome following uptake of LPS-coated latex beads 172
Figure 43 TPL-2 catalytic activity promotes DMXL1 phosphorylation on S1903 upon phagocytosis 176
Figure 44 TPL-2 catalytic activity induces phagosome maturation in iBMDMs 177
Figure 45 Knockdown of *Dmxl1*, but not *Dmxl2*, impairs phagosome maturation in iBMDMs 178
Figure 46 Phosphorylation of DMXL1 on S1903/S1904 regulates phagosome maturation 179
Figure 47 *Tpl2*^{D270A} mutation impairs AKT signalling following uptake of LPS-coated latex beads 181
Figure 48 *Abin2*^{D310N} mutation does not regulate AKT signalling following uptake of LPS-coated latex beads 182
Figure 49 *Tpl2*^{D270A} mutation reduces AKT activation following phagocytic uptake of latex beads 183
Figure 50 AKT inhibition by Akti-1/2 impairs phagosomal proteolysis and acidification 184
Figure 51 mTOR inhibition by AZD8055 impairs phagosomal proteolysis and acidification 185
Figure 52 AKT knockdown impairs phagosome maturation in iBMDMs 186
Figure 53 TPL-2-dependent transcriptome following phagocytic uptake of LPS-coated latex beads 188
Figure 54 Selected up- and downregulated processes in the TPL-2-dependent transcriptome following uptake of LPS-coated beads 189
Figure 55 Relative expression of type I interferon genes in WT and *Tpl2*$^{D270A/D270A}$ BMDMs following LPS stimulation and uptake of LPS-coated beads 190
Figure 56 Expression levels of cytokines and type I interferon genes in *Tpl2*$^{D270A/D270A}$ BMDMs following uptake of LPS-coated beads 191
Figure 57 TPL-2 interactome following LPS and TNFα stimulation 194
Figure 58 TPL-2 interacts with EEA1 upon LPS stimulation 195
Figure 59 *Abin2*^{Y231A} mutation impairs phagosomal proteolysis while acidification remains unaffected 196
Figure 60 TSG101 knockdown reduces phagosomal proteolysis 197
Figure 61 TPL-2 and ABIN-2 promote phagosome maturation in macrophages .. 198

Figure 62 *Tpl2*^{D270A} and *Abin2*^{D310N} mutation impair macrophage killing of *E. coli* 211
Figure 63 *Tpl2*^{D270A} mutation impairs macrophage killing of *C. rodentium* 213
Figure 64 *Tpl2*^{D270A} mutation impairs acidification of *C. rodentium* phagosomes . 214
Figure 65 Infection of primary macrophages with YFP-labelled *S. aureus* 215
Figure 66 *Tpl2*^{D270A} and *Abin2*^{D310N} mutation impair macrophage killing of *S. aureus* 216
Figure 67 *Tpl2*^{D270A} and *Abin2*^{D310N} mutation do not impair pyroptosis upon *S. aureus* infection 217
Figure 68 *Tpl2*^{D270A} and *Abin2*^{D310N} mutation reduce cathepsin activity in *S. aureus* phagosomes 218
Figure 69 *Tpl2*^{D270A} mutation impairs acidification of *S. aureus* phagosomes 219
Figure 70 *Tpl2*^{D270A} mutation reduces co-localisation of YFP-*S. aureus* with EEA1 220
Figure 71 *Tpl2*^{D270A} and *Abin2*^{D310N} mutation reduce co-localisation of YFP-*S. aureus* with LAMP1 220
Figure 72 *Abin2*^{D310N} mutation reduces co-localisation of YFP-*S. aureus* with ubiquitin 221
Figure 73 TPL-2 activates ERK1/2 from the cell surface following *S. aureus* infection 223
Figure 74 TPL-2 catalytic activity has pronounced effects on the global transcriptome of *S. aureus*-infected BMDMs 224
Figure 75 Selected pathways that are up- and downregulated by *Tpl2*^{D270A} mutation following *S. aureus* infection 225
Figure 76 *Tpl2*^{D270A} mutation dysregulates expression of innate immune genes . 226
Figure 77 *Tpl2*^{D270A} mutation upregulates type I interferon and interferon-stimulated genes during *S. aureus* infection 227
Figure 78 Endosomal activation of AKT following *S. aureus* infection 228
Figure 79 TPL-2 activates AKT signalling from endosomes following *S. aureus* infection 229
Figure 80 Infection of BMDMs with *S. typhimurium* 231
Figure 81 *Abin2*^{D310N} mutation impairs macrophage killing of *S. typhimurium* 232
Figure 82 Impaired acidification mediated by *Tpl2*^{D270A} mutation restricts *S. typhimurium* growth 233

Figure 83 *Tpl2*^{D270A} and *Abin2*^{D310N} mutation do not impair pyroptosis upon *S. typhimurium* infection 234
Figure 84 TPL-2 and ABIN-2 induce killing of *S. aureus* by promoting phagosome maturation 235

List of tables

Table 1 Commercial primary antibodies for immunoblotting 86
Table 2 Custom-made primary antibodies for immunoblotting 88
Table 3 Secondary antibodies for immunoblotting 88
Table 4 Primary antibodies for immunofluorescence 88
Table 5 Secondary antibodies for immunofluorescence 89
Table 6 Primary FACS antibodies 89
Table 7 Proteins 89
Table 8 Buffers 91
Table 9 Cell culture growth media 93
Table 10 Inhibitors 98
Table 11 Agonists 99
Table 12 siRNA pools 103
Table 13 Bacterial strains 105
Table 14 Synthetic ubiquitin peptides 113
Table 15 Plasmids 122
Table 16 FAM-MGB-coupled qRT-PCR probes 124
Table 17 Selected phospho-sites in MAP kinases and TPL-2 following bead uptake 167
Table 18 Selected phospho-sites in proteins implicated in vesicle trafficking following bead uptake 168
Table 19 Significantly downregulated phospho-sites in DMXL1 following bead uptake 168
Table 20 Selected phospho-sites in MAP kinases and TPL-2 following uptake of LPS-coated beads 170
Table 21 Selected phospho-sites in proteins implicated in vesicle trafficking following uptake of LPS-coated beads 173
Table 22 Significantly downregulated phospho-sites in DMXL1 following uptake of LPS-coated beads 174
Table 23 Significantly regulated phospho-sites in proteins of the mTOR signalling pathway following uptake of LPS-coated beads 175
Table 24 TPL-2-interacting proteins upon LPS stimulation 193

Abbreviations

A20	TNFα-induced protein 3
ABIN	A20-binding inhibitor of NF-κB
ADP	adenosine diphosphate
AHD	ABIN homology domain
Ala (A)	alanine
AP2	adaptor protein-2
APS	ammonium persulfate
Arp2/3	actin-related protein 2/3
ATP	adenosine triphosphate
β-ME	β-mercaptoethanol
BCR	B cell receptor
BMDM	bone marrow-derived macrophage
BSA	bovine serum albumin
CAP	cationic antimicrobial peptide
CCL	C-C motif ligand
Cdc42	cell division control protein 42
CFU	colony forming unit
CHMP2B	charged multivesicular body protein 2B
CLR	C-type lectin receptor
cm	centrimetre
CR	complement receptor
CXCL	C-X-C motif ligand
Da	dalton
DAMP	damage-associated molecular pattern
DAPI	4′,6-diamidino-2-phenylindole
DD	death domain
DMEM	Dulbecco's Modified Eagle Medium
DMSO	dimethyl sulfoxide
DNA	deoxyribonucleic acid
DPBS	Dulbecco's phosphate-buffered saline
DSS	dextran sulphate sodium

DSTT	Division of Signal Transduction Therapy
DTT	dithiothreitol
DUB	deubiquitylating enzyme
DUSP1	dual-specificity protein phosphatase 1
EAE	experimental autoimmune encephalomyelitis
EBR	ESCRT-I binding region
ECM	extracellular matrix
EDA-ID	anhidrotic ectodermal dysplasia with immunodeficiency
EDTA	ethylenediaminetetraacetic acid
EEA1	early endosome antigen 1
EGTA	ethylene glycol tetraacetic acid
EIF	eukaryotic initiation factor
em	emission
EPS15L1	epidermal growth factor receptor substrate 15-like 1
ERK	extracellular signal-regulated kinase
ESCRT	endosomal sorting complex required for transport
EV	empty vector
ex	excitation
FACS	fluorescence-activated cell sorting
FBS	foetal bovine serum
FcγR	Fcγ receptors
fMLP	N-formylmethionyl-leucyl-phenylalanine
fmol	femtomole
FSC	forward scatter
FYVE	Fab1, YOTB, Vac 1, and EEA1
Gab2	Grb2-associated binder
GAP	GTPase-activating protein
GAPVD1	GAP and VPS9 domain-containing protein 1
GDI	GDP dissociation inhibitor
GEF	guanine nucleotide exchange factor
GFP	green fluorescent protein
GM-CSF	granulocyte-macrophage colony stimulation factor
GPI	glycosylphosphatidylinositol

Grb2	growth factor receptor-bound protein 2
GSEA	gene set enrichment analysis
GST	glutathione S-transferase
h	hour
HDM	house dust mite
HEK293	human embryonic kidney 293 cells
HEPES	4-(2-hydroxyethyl)-1-piperazineethanesulfonic acid
HOPS	homotypic fusion and protein sorting
HRP	horseradish-peroxidase
HSP	heat-shock protein
iBMDM	immortalised bone marrow-derived macrophage
IF	immunofluorescence
IFN	interferon
Ig	immunoglobulin
IκB	inhibitory proteins of κB
IKK	IκB kinase
IL	interleukin
ILV	intraluminal vesicle
IMF	intestinal sub-epithelial myofibroblast
iNOS	nitric oxide synthase
IntDen	integrated density
IP	immunoprecipitation
IRAK	IL-1 receptor-associated kinase
IRF	IFN regulatory factor
ISG	interferon-stimulated gene
ISRE	interferon-stimulated response element
ITAM	tyrosine-based activation motif
JAK	Janus-activated kinase
JNK	c-Jun N-terminal kinase
kDa	kilodalton
KI	knock-in
KO	knockout
L	litre

LAMP	lysosome-associated membrane protein
LAT	linker of activated T cells
LB	Luria Bertani
LBP	LPS binding protein
LBPA	lysobisphosphatidic acid
LC	Liquid chromatography
LDH	lactate dehydrogenase
LPS	lipopolysaccharides
LRR	leucine-rich repeat
LUBAC	linear ubiquitin assembly complex
Lys (K)	lysine
LysC	lysyl endopeptidase
m	milli
M	molar
MAP	mitogen activated protein
MAPK	mitogen activated protein kinase
MCP-1	monocyte chemoattractant protein-1
MD-2	myeloid differentiation factor 2
MDSC	myeloid-derived suppressor cell
MEF	mouse embryonic fibroblasts
MEK	MAPK/ERK kinase
MEKK	MAPK/ERK kinase kinase
Met (M)	methionine
mg	milligram
MHC	major histocompatibility
min	minute
MKK	MAP kinase kinase
ml	millilitre
mm	millimetre
mM	millimolar
MMP	matrix metalloproteinase
MOI	multiplicity of infection
mol	mole

MOPS	3-(N-morpholino)propanesulfonic acid
MS	mass spectrometry
MS/MS	tandem mass spectrometry
MSK	mitogen- and stress-activated kinase
MSR1	macrophage SR 1
mTOR	mammalian target of rapamycin
MVB	multivesicular body
MyD88	myeloid differentiation primary response gene 88
n	nano
NADPH	nicotinamide adenine dinucleotide phosphate
NEM	N-Ethylmaleimide
NEMO	NF-κB essential modulator
NF-κB	nuclear factor κB
ng	nanogram
NK	natural killer
NKLAM	natural killer lytic-associated molecule
NLR	NOD-like receptor
nM	nanomolar
nm	nanometre
NO	nitric oxides
NOX2	NADPH oxidase
NRAMP1	natural resistance-associated macrophage protein 1
ns	not significant
OPTN	optineurin
ORPL1	oxysterol-binding protein-related protein 1
P	phospho
p70S6K	ribosomal S6 kinase p70
PA	phosphatidic acid
PAMP	pathogen-associated molecular pattern
PBMC	peripheral blood mononuclear cells
PBS	phosphate-buffered saline
PCA	principal component analysis
PCR	polymerase chain reaction

PD	pulldown
PDCD6	programmed cell death protein 6
PDK1	phosphatidyl-inositide-dependent kinase 1
PEI	polyethylenimine
PEST	proline, glutamic acid, aspartic acid, serine and threonine-rich
PGE_2	prostaglandin E_2
$PI(3,4,5)P_3$	phosphatidylinositol-3,4,5-trisphosphate
$PI(3,5)P_2$	phosphatidylinositol-(3,5)-bisphosphate
PI(3)P	phosphatidylinositol-3-phosphate
$PI(4,5)P_2$	phosphatidylinositol-4,5-bisphosphate
PI3K	phosphoinositide 3-kinase
PID	processing inhibitory domain
PIP5K3	PIKfyve kinase
PKB	protein kinase B
PLD	phospholipase D
PMSF	phenylmethylsulfonyl fluoride
PRM	parallel reaction monitoring
PRR	pattern recognition receptor
PSG	L-glutamine-penicillin-streptomycin
PTM	post-translational modification
PVDF	polyvinylidene difluoride
qRT-PCR	real-time quantitative reserve transcription PCR
Rabex-5	rabaptin-5-associated exchange factor for RAB5
Rac	Ras-related C3 botulinum toxin substrate
RFU	relative fluorescence units
RIG	retinoic acid-inducible gene
RILP	RAB7-interacting lysosomal protein
RIP1	receptor-interacting serine/threonine-protein kinase 1
RLR	RIG-I-like receptors
RNA	ribonucleic acid
RNA-seq	RNA sequencing
RNI	nitrogen intermediate
ROS	reactive oxygen species

rpm	revolutions per minute
RT	room temperature
RU	relative units
S1K	Schedule 1 kill
SARM	sterile α and HEAT-Armadillo motifs-containing protein
$SCF^{\beta TrCP}$	SKP1-cullin-1-F-box complex containing βTrCP
SDS	sodium dodecyl sulfate
SDS-PAGE	SDS polyacrylamide gel electrophoresis
sec	second
SEM	standard error of the mean
Ser (S)	serine
SH2	Src homology 2
SNARE	soluble N-ethylmaleimide-sensitive-factor attachment protein receptor
SOC	super optimal broth with catabolite repression
SPI	Salmonella pathogenicity island
SQSTM1	sequestosome 1
SR	scavenger receptor
STAT	signal transducer and activator of transcription
STX	syntaxin
SYK	spleen tyrosine kinase
T3SS	type III secretion system
TAB	TAK1-binding protein
TACE	TNFα-converting enzyme
TAK1	transforming growth factor β-activated kinase-1
TAM	tumour associated macrophage
TBK1	TANK binding kinase 1
TCR	T cell receptor
TEAB	triethylammonium bicarbonate
TECEP	tris(2-carboxyethyl)phosphine
TEMED	tetramethylethylenediamine
TFA	trifluoroacetic acid
TGFβ	transforming growth factor β
T_H	T helper

Thr (T)	threonine
TIR	Toll/IL-1 receptor
TIRAP	TIR domain-containing adaptor protein
TLR	Toll-like receptor
TMT	tandem mass tag
TNF	tumour necrosis factor
TPL-2	tumour progression locus 2
TRAF	TNF receptor-associated factor
TRAM	TRIF-related adaptor molecule
TRIF	TIR domain-containing adaptor inducing IFN-β
TSC	tuberous sclerosis protein
TSG101	tumour susceptibility gene 101
Tyr (Y)	tyrosine
Ub-AQUA	absolute quantification of ubiquitin
UBAN	ubiquitin binding in ABIN and NEMO
UBD	ubiquitin-binding domain
UEV	E2 variant domain
US	unstimulated
v	volume
V-ATPase	vacuolar ATPase
VAMP	vesicle-associated membrane protein
VPS	vacuolar protein sorting
w	weight
WCL	whole cell lysate
WT	wild type
YFP	yellow fluorescent protein
µ	micro
µg	microgram
µl	microlitre
µm	micrometre
µM	micromolar

Chapter 1. Introduction

1.1 The immune system

Throughout lifetime, humans and other mammals are continuously exposed to a plethora of invading pathogens, which pose a threat to health. The host organism has to closely monitor for the presence of pathogenic microbes, including bacteria, viruses and fungi, to maintain tissue integrity and organ function (Akira *et al*, 2006). Upon microbial infection, the immune system has to rapidly respond to minimise replication and spread of pathogens within the host. The innate immune system is the first line of defence against pathogenic invasion. Germline encoded receptors recognise invariant pathogen molecules, which then trigger the expression of genes encoding cytokines and chemokines. Together, cytokines and chemokines promote immune cell recruitment to the site of infection to rapidly clear invading pathogenic microbes.

In vertebrate organisms, innate immune responses are a prerequisite for activation of the adaptive immune system (Mogensen, 2009). Adaptive immune responses take several days to mount and involve highly specific receptors for pathogens on T and B lymphocytes, encoded by genes that undergo complex somatic rearrangements of germline gene elements. In addition, the adaptive immune system provides immunological memory, which allows for more rapid clearance of pathogens on reinfection. The body's ability to rapidly induce production of high-affinity antibodies by B lymphocytes upon secondary infection with the same pathogen is integral to acquired immunity (Chaplin, 2010).

A coherent synergy between both arms of the immune system, innate and adaptive, is critical for healthy development of all vertebrates. Defective responses may lead to immunodeficiencies, which result in susceptibility to infection and possibly life-threatening conditions (Etzioni, 2003). However, sustained activation of the immune response may cause autoimmune disorders, chronic immune diseases and sepsis (Chang, 2014; Straub & Schradin, 2016). Therefore, tight regulation of immune responses is vital to ensure a balance in the immune response and to maintain tissue homeostasis.

1.1.1 The innate immune response

The innate immune system is activated either by recognition of non-self molecules or by mechanical stress experienced by host cells of the epithelium. Epithelial cells form a physical barrier (e.g. keratinocytes of the skin) protecting the body from continuous exposure to microbes present in the host's environment. In the event of tissue damage during microbial invasion, epithelial cells release chemokines to rapidly recruit innate immune cells (Chaplin, 2010). In addition, innate immune cells, in particular tissue-resident macrophages and dendritic cells, express a plethora of pathogen receptors, which recognise microbes during initial stages of infection and activate other immune cells upon sensing of non-self material in the extracellular environment (Takeuchi & Akira, 2010; Davies *et al*, 2013). A complex network of signalling pathways is triggered to clear pathogenic infection, resulting in inflammation. Inflammation is a condition, which is characterised by common symptoms, including fever, swelling, pain and redness of skin (Chen *et al*, 2018). These clinical symptoms result from pro-inflammatory mediators, which are released by innate immune cells. Inflammatory mediators promote vasodilation, immune cell infiltration at sites of infection, and fever (Iwasaki & Medzhitov, 2015). The lipid-based second messenger prostaglandin E_2 (PGE_2), which is released by activated immune cells, acts upon the endothelium of the hypothalamus to cause fever (Dinarello *et al*, 1999). Elevated temperature is a protective response of the host as a temperature rise causes microbes to be more susceptible to immune cell cytotoxicity (Netea *et al*, 2000). Inflammation is essential to prevent pathogen spread and to trigger the adaptive immune response, however, an excessive inflammatory response may lead to chronic inflammatory diseases.

1.1.2 Immune cells of the innate and adaptive response

Cells of the immune system are highly specialised white blood cells, referred to as leukocytes. Immune cell lineages involved in both the innate and adaptive response originate from pluripotent hematopoietic stem cells in the bone marrow, except for tissue-resident macrophages, which are derived from the yolk sac during early embryonic development (Varol *et al*, 2015). Hematopoietic stem cells either

differentiate into common myeloid progenitors (myeloid stem cells) or common lymphoid progenitors (Kondo, 2010).

Cell populations derived from myeloid stem cells orchestrate the innate immune response. Progenitors of the myeloid lineage differentiate into mast cells, granulocytes, comprising basophils, eosinophils and neutrophils, as well as monocytes (Chaplin, 2010). The monocyte lineage includes macrophages and dendritic cells (DCs). Neutrophils and monocytes are among the first immune cells to accumulate at sites of microbial invasion and play an important role in bacterial killing, either by phagocytosis or by releasing anti-microbial products into the extracellular milieu (Kolaczkowska & Kubes, 2013).

Phagocytosis involves the engulfment of an invading microbe and subsequent destruction of the microorganism within an intracellular vacuole called the phagosome. A combination of proteases, reactive oxygen species and microbicidal peptides in the phagosome lead to effective killing of engulfed pathogens (Flannagan *et al*, 2012). In addition, neutrophils and monocytes switch on gene expression to encode and release pro-inflammatory mediators, which include cytokines and chemokines. Both cytokines and chemokines initiate activation and infiltration of additional granulocytes at sites of infection (Vieira *et al*, 2009; Kolaczkowska & Kubes, 2013). Following binding to microbes, granulocytes promote pathogenic clearance by releasing proteolytic granules into the extracellular environment. In addition, basophils release histamines to induce vasodilation, thus aiding in the process of immune cell recruitment to sites of infection (White, 1990).

DCs are important to initiate the adaptive stage of the immune response. DCs present small fragments of digested pathogens as antigenic peptides in a complex with major histocompatibility (MHC) molecules on their cell surface. Proteolytic digestion of microbial proteins following phagocytosis is critical for antigen presentation on MHC molecules (Joffre *et al*, 2012; Roche & Furuta, 2015). Microbial antigens presented on MHC molecules are recognised by T lymphocytes, which belong to the lymphoid lineage (Jakubzick *et al*, 2017). Common lymphoid progenitors in the bone marrow differentiate into mature lymphocytes, including B and T lymphocytes as well as natural killer (NK) cells, all of which drive the adaptive immune response (Lai & Kondo, 2008). Interaction between the antigen-MHC

complex on DCs and a unique antigen-specific T cell receptor (TCR) on T lymphocytes results in T lymphocyte activation (Smith-Garvin *et al*, 2009). Besides the TCR, T lymphocytes express CD4 or CD8 co-receptors, which define the T lymphocyte lineage (Taniuchi, 2018). Activated $CD8^+$ T lymphocytes, also referred to as cytotoxic T cells, have the cytotoxic ability to clear infected and cancerous cells (Hukelmann *et al*, 2016; Chaplin, 2010). Activated $CD4^+$ T lymphocytes, also known as T helper (T_H) cells, undergo rapid proliferation and induce isotype switching in naïve B cells, which involves the rearrangement of antibody-encoding gene elements in B lymphocytes (Chaplin, 2010; Cantrell, 1996; Lebman *et al*, 1988; Parker, 1993). As a result, B lymphocytes are able to synthesise antibodies of different isotypes, however with identical antigenic specificity against the invading pathogen (Lebman *et al*, 1988; Parker, 1993). The immunoglobulin G (IgG) isotype, which is the most abundant isotype in blood and extracellular fluids, has the highest antigen affinity among isotype classes (Janeway *et al*, 2001). B lymphocytes produce highly pathogen-specific antibodies, which bind to target sites on the microbe. As a result, immune cells, including phagocytes, are recruited to antibody-coated pathogens to initiate their engulfment and clearance. The interplay between innate and adaptive immune systems orchestrates an effective immune response to clear infection.

1.1.3 Hallmarks of macrophages

Macrophages belong to the mononuclear phagocytic system, which originates from hematopoietic stem cells in the bone marrow. Besides macrophages, the mononuclear phagocytic system comprises monocytes and DCs (Geissmann *et al*, 2010). Macrophages, monocytes, DCs and neutrophils are highly phagocytic cells and are thus termed ‘professional’ phagocytes (Mantovani *et al*, 1972). In addition, cells belonging to the mononuclear phagocytic pool are critical for cytokine secretion and antigen presentation during infection. Monocytes are macrophage precursors, which enter the circulatory system following release from the bone marrow. Differentiation of monocytes into monocyte-derived macrophages in the circulatory system is initiated upon infection (Murray & Wynn, 2011). During steady-state, monocytes migrate through the circulatory system, extravasate through the endothelial layer into local tissues, and differentiate into tissue-resident

macrophages. Monocytes are vital for constantly replenishing the macrophage pool to maintain tissue homeostasis (Bain *et al*, 2014).

Tissue-resident macrophages with specialised functions include microglia (brain), Kupffer cells (liver), osteoclasts (bone) and alveolar macrophages (lung). In addition, secondary lymphoid organs, including the spleen and lymph nodes, are populated by tissue-resident macrophages (Wynn *et al*, 2013). More specifically, splenic marginal zone macrophages and subcapsular sinus macrophages in lymph nodes promote immune suppression and antiviral humoral immunity, respectively (McGaha *et al*, 2011; Iannacone *et al*, 2010; Junt *et al*, 2007). Regardless of tissue specificity, tissue-resident macrophages promote pathogenic clearance and antigen presentation. During inflammation, tissue-resident macrophages attract high levels of monocyte-derived macrophages from the circulatory system to clear infection (Murray & Wynn, 2011).

1.1.4 Macrophage polarisation

Following differentiation, macrophages can either polarise into classically activated (M1) macrophages or alternatively activated (M2) macrophages (Figure 1). Plasticity enables macrophages to dynamically switch between polarisation phenotypes (Shapouri-Moghaddam *et al*, 2018). M1 macrophages are pro-inflammatory, responsible for pathogen clearance and strengthen anti-tumour immunity (Lee, 2019). Stimuli including interferon γ (IFNγ), lipopolysaccharide (LPS) and granulocyte-macrophage colony stimulation factor (GM-CSF) mediate macrophage polarisation into the M1 subset (Martinez & Gordon, 2014). Priming of macrophages by IFNγ results in increased responsiveness to inflammatory signals, in particular LPS and type I interferons, while inducing resistance to anti-inflammatory signals such as glucocorticoids, interleukin (IL)-4 and IL-10 (Martinez & Gordon, 2014). IFNγ, the only type II class interferon, is a cytokine predominantly released by NK cells, innate lymphoid cells and T helper 1 (T_H1) cells of the adaptive immune lineage (Schroder *et al*, 2004).

M1 polarised macrophages produce a variety of pro-inflammatory mediators, including IL-1, IL-6, IL-12, IL-23 and tumour necrosis factor α (TNFα) (Duque & Descoteaux, 2014). Moreover, M1 macrophages actively produce anti-microbial and anti-tumourigenic products, in particular nitric oxides (NO) and reactive oxygen species (ROS) (Mantovani *et al*, 2004). Despite the importance of M1 macrophages in clearing pathogens, sustained activation of pro-inflammatory M1 macrophages may lead to tissue damage. In contrast, M2 macrophages are anti-inflammatory, mediate wound healing and possess tumourigenic characteristics (Ley, 2017). There are multiple subsets of M2 macrophages, including IL-10-secreting regulatory macrophages, tumour associated macrophages (TAMs) and myeloid-derived suppressor cells (MDSCs) (Roszer, 2015; Mantovani *et al*, 2002). Both IL-4 and IL-13, released by T helper 2 (T_H2) cells, basophils and eosinophils, mediate macrophage polarisation into the M2 subset (Van Dyken & Locksley, 2013). In response to polarisation, M2 macrophages share high expression profiles of anti-inflammatory IL-10 and transforming growth factor β (TGFβ), while only expressing low levels of pro-inflammatory IL-12 (Gong *et al*, 2012; Mantovani *et al*, 2004). In addition, M2 macrophages express high levels of arginase-1, a metabolic enzyme converting L-arginine into L-ornithine to promote collagen synthesis for tissue repair (Campbell *et al*, 2013). L-arginine is required by nitric oxide synthase (iNOS) to generate NO and thus, increased arginase-1 expression reduces NO production, thereby limiting cytotoxicity of M2 macrophages (Rath *et al*, 2014).

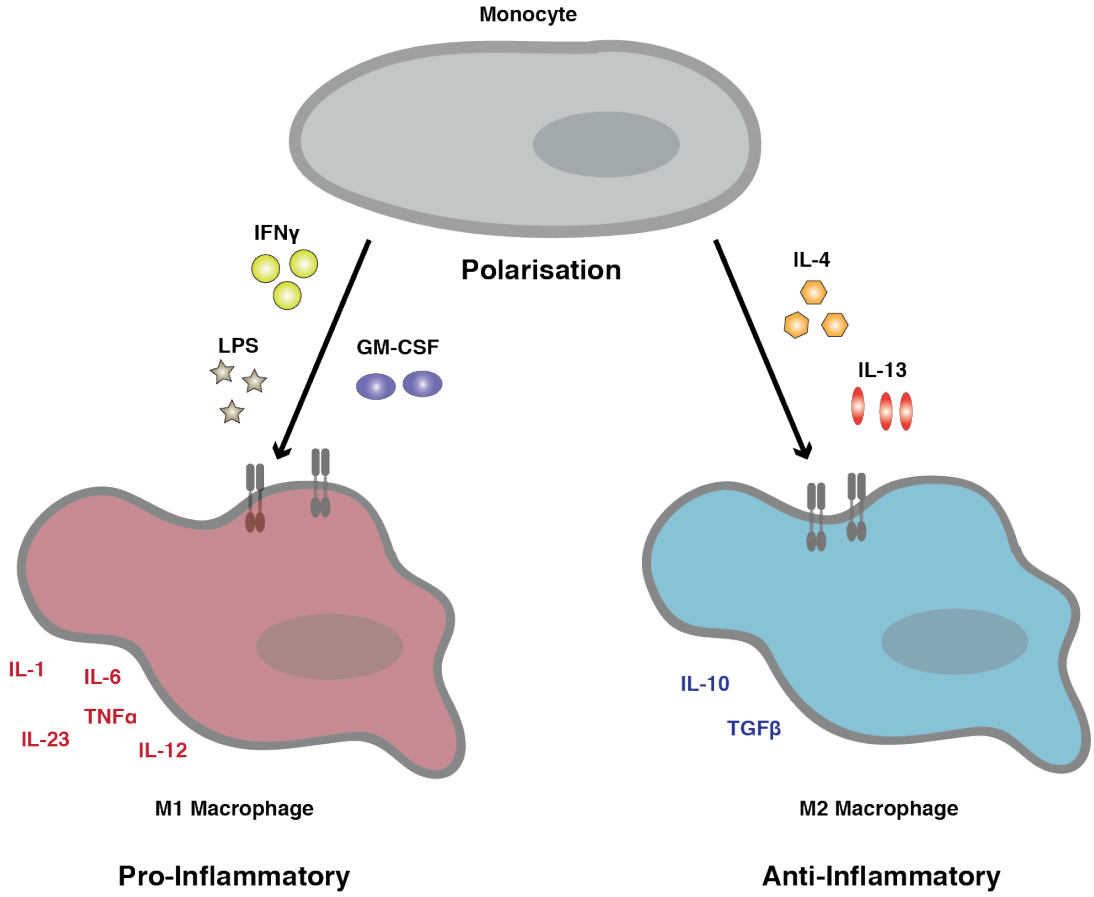

Figure 1 Macrophage polarisation

Stimulation of monocytes triggers polarisation of macrophages into either a pro-inflammatory M1 phenotype, or an anti-inflammatory M2 phenotype. Signals that lead to M1 polarisation include IFNγ, LPS or GM-CSF. Once in an M1 state, macrophages induce expression of pro-inflammatory cytokines, including IL-1, IL-6, IL-12, IL-23 and TNFα. Alternatively, priming of macrophages with IL-4 or IL-13 leads to polarisation into an M2 state. Resolving macrophages induce expression of anti-inflammatory mediators, including IL-10 and TGFβ. Macrophage polarisation is highly dynamic and macrophages are able to reversibly switch between M1 and M2 phenotypes.

1.2 Regulation of innate immune signalling by post-translational modifications

A prerequisite for a potent innate immune response is the ability of immune cells to rapidly respond to signals in the extracellular environment and to convert these stimuli into a cellular response. Signal transduction describes the process by which extracellular signals induce a complex network of intracellular signalling pathways to

elicit a response at the cellular level. Following engagement of a receptor in the plasma membrane, adaptor proteins and signalling molecules with enzymatic activity are recruited and activated to amplify the extracellular signal (Ferrell, 1996). Signal transduction orchestrates intracellular signalling to convert receptor activation into a physiological response. The underlying mechanism by which all signalling pathways remain balanced is the regulation of post-translational modifications (PTMs). PTMs regulate activity, stability and folding of proteins, thereby controlling all aspects of protein function. PTM involves the covalent attachment of a new functional group to a protein. Examples of PTMs include phosphorylation, ubiquitylation, methylation, glycosylation, and acetylation. The covalent addition or removal of a PTM can significantly alter physical interactions and cellular localisation of the target protein. The tight regulation of PTMs is critical to prevent the development of inflammatory diseases.

1.2.1 Protein phosphorylation

Protein phosphorylation involves the transfer of a γ-phosphate group from adenosine triphosphate (ATP) to the hydroxyl group of serine, threonine or tyrosine amino acid residues in the target protein. More specifically, ATP and substrate bind to the active site of a protein kinase, which catalyses γ-phosphate transfer to the target residue, after which adenosine diphosphate (ADP) and substrate are released from the protein kinase (Fischer & Krebs, 1955; Cohen, 2002; Hanks *et al*, 1988). The reverse reaction, substrate dephosphorylation, is catalysed by protein phosphatases (Ingebritsen & Cohen, 1983). Attachment or removal of a phosphate group alters the surface charge, which may induce a conformational change, thus regulating protein-protein interactions, substrate stability, localisation or enzymatic activity. In eukaryotes, protein kinases are one of the largest gene families encoding for more than 530 protein kinases (Wilson *et al*, 2018). In addition, more than 160 protein phosphatases have been identified (Wilson *et al*, 2018).

Substrate specificity is critical to ensure that protein kinases phosphorylate their physiological target sites. Molecular mechanisms to ensure substrate specificity are multifaceted (Ubersax & Ferrell, 2007). Firstly, structural confirmation,

hydrophobicity and surface charge of the active site are features that determine substrate complementarity. Secondly, distal docking sites on the substrate interact with domains spatially separated from the active site on the kinase to increase the binding affinity of kinases for particular substrates (Holland & Cooper, 1999; Biondi & Nebreda, 2003). Thirdly, some protein kinases, such as cyclin-dependent kinases, utilise modular binding partners containing docking domains, which allows for a single kinase to target multiple substrates in a context-dependent manner (Jeffrey *et al*, 1995; Schulman *et al*, 1998). Fourthly, conditional docking sites allow for high-affinity recruitment of kinases to substrates. More specifically, this involves substrate priming by phosphorylation adjacent or distant from the secondary phosphorylation site (Pinna & Ruzzene, 1996). In addition, localisation of kinases to subcellular compartments can locally increase kinase concentration in distinct parts of the cell to facilitate the rate of phosphorylation. Lastly, scaffolding proteins provide signalling platforms for protein kinases and substrates to be recruited to close proximity. Scaffolds share some similarity with modular binding partners, however, while modular binding partners interact stably with the protein kinase, scaffolds provide a more dynamic signalling platform for kinases (Pawson & Scott, 1997; Bhattacharyya *et al*, 2006). Due to high substrate specificities, clinical application of kinase inhibitors for the treatment of inflammatory diseases and cancer has been extensively investigated by the pharmaceutical industry over the past two decades (Cohen & Alessi, 2013; Bain *et al*, 2007, 2003).

1.2.2 Protein ubiquitylation

Protein ubiquitylation involves the transfer of a ubiquitin moiety onto a target protein. Ubiquitin is a highly conserved protein comprising 76 amino acids (Goldstein *et al*, 1975). It is covalently attached via its C-terminus, to either another ubiquitin molecule or to a lysine (Lys, K) residue of a substrate protein (Goldknopf & Busch, 1977). Ubiquitylation involves the enzymatic activity of three distinct protein families: E1 ubiquitin-activating enzymes, E2 ubiquitin-conjugating enzymes, and E3 ubiquitin-ligating enzymes (Swatek & Komander, 2016). The E1 ubiquitin-activating enzyme catalyses the formation of a thioester bond between a cysteine residue present in its active site and the C-terminal glycine residue of a ubiquitin molecule. Thioester bond

formation is an ATP-dependent process. Subsequently, ubiquitin is transferred to the cysteine residue in the active site of an E2 ubiquitin-conjugating enzyme. E3 ubiquitin ligases associate with both the protein substrate and the ubiquitin-bound E2 ubiquitin-conjugating enzyme. More specifically, E3 ubiquitin ligases transfer the ubiquitin on E2 enzymes to the ε-amino group of a lysine residue on the protein substrate (Li *et al*, 2016).

In humans, two E1s, more than 35 E2s, and approximately 600 E3s have been identified (Jin *et al*, 2007; Wijk & Timmers, 2010; Moulder *et al*, 2016; Li *et al*, 2008). The large number of E3 ubiquitin ligases provides specificity and ensures that substrates are appropriately ubiquitylated. Ubiquitylation was originally discovered as a degradation signal to target proteins for proteolysis by the 26S proteasome (Ciechanover *et al*, 1978; Hershko *et al*, 1979). However, over the past decade the importance of ubiquitylation as a PTM, to regulate a plethora of cellular processes, has been established. In particular, ubiquitylation plays an essential role in regulating signalling pathways underlying innate immune responses (Schwartz & Hochstrasser, 2003; Hu & Sun, 2016). The reverse reaction, substrate deubiquitylation, is catalysed by deubiquitylating enzymes (DUBs). To date, approximately 100 distinct DUBs have been identified (Clague *et al*, 2019; Hutchins *et al*, 2013). Enzymatic activity of E3 ligases relative to DUBs determines the ubiquitylation state of substrates (Heride *et al*, 2014). Importantly, DUBs constitutively replenish the cellular pool of free ubiquitin by processing ubiquitin chains from proteins destined for proteasomal degradation.

1.2.3 Linkage-specific functions of ubiquitin chains

In mammalian cells, more than half of ubiquitylation events comprise the covalent attachment of a single ubiquitin molecule to a lysine residue in the substrate. This is referred to as monoubiquitylation (Figure 2). Approximately 20% of total ubiquitin is present in polyubiquitin structures, where multiple ubiquitin molecules are attached to form polyubiquitin chains (Swatek & Komander, 2016). Ubiquitin contains seven lysine residues (Lys6, Lys11, Lys27, Lys29, Lys33, Lys48, Lys63), which are all able to serve as a substrate for another ubiquitin molecule, thus leading to the formation of polyubiquitin chains (Akutsu *et al*, 2016). In addition, ubiquitin contains an N-

terminal methionine (Met, M) residue, which is able to form a stable isopeptide bond with the glycine residue at the C-terminus of another ubiquitin molecule. This results in the formation of linear, or Met1 (M1)-linked polyubiquitin chains (Kirisako *et al*, 2006; Ikeda & Dikic, 2008). Ubiquitin chains of different linkage specificities display significant structural diversity and regulate distinct cellular processes.

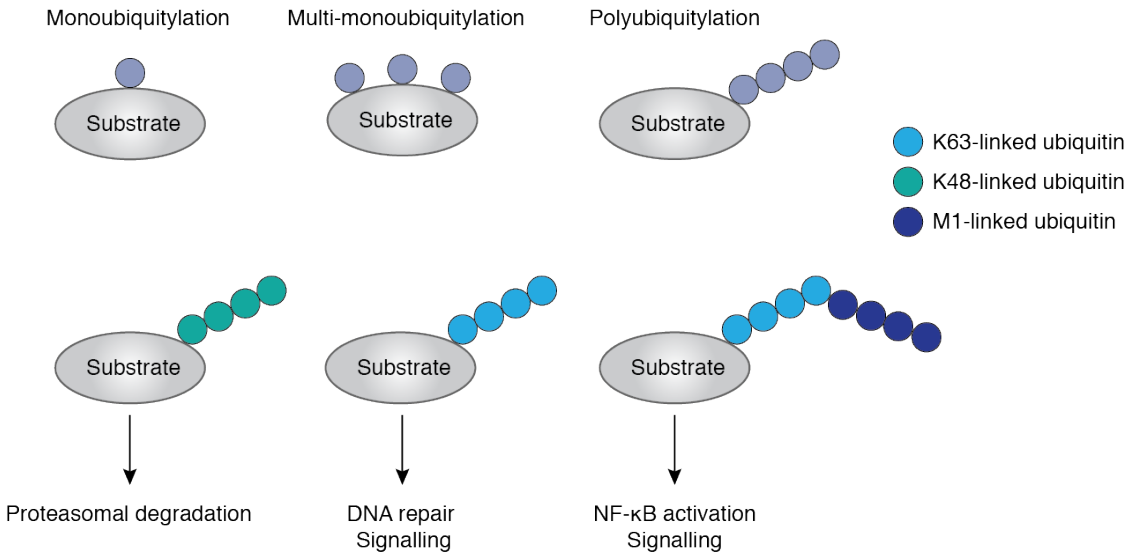

Figure 2 Different types of ubiquitylation and chain-specific biological functions

Protein substrates can be ubiquitylated with a single ubiquitin moiety to a single lysine residue, which is known as monoubiquitylation. Alternatively, a substrate can be ubiquitylated with a single ubiquitin at several different lysine residues, which is referred to as multi-monoubiquitylation. Polyubiquitylation refers to the attachment of multiple ubiquitin moieties to a single lysine residue. Polyubiquitin chains may be homogeneous (identical chain linkages) or hybrid (different chain linkages). K48-linked polyubiquitin marks substrates for proteasomal degradation. In contrast, K63-linked polyubiquitin chains regulate DNA repair and immune signalling. Similarly, hybrid K63/M1-linked polyubiquitin chains regulate NF-κB activation and innate immune signalling.

K48-linked ubiquitin chains are the most abundant linkage type in cells as K48-linked chains target proteins for proteasomal degradation (Chau *et al*, 1989). K63-linked ubiquitin chains are the second most abundant chain linkage type and are involved in non-degradative processes, including DNA repair and cell signalling (Hu & Sun, 2016; Spence *et al*, 1995). In contrast to the compact structural conformation of K48-linked ubiquitin chains, K63- and M1-linked polyubiquitin chains adopt a more elongated and accessible conformation for signalling molecules to bind (Tenno *et al*, 2004; Varadan *et al*, 2004; Komander *et al*, 2009). In recent years, both K63-linked

and M1-linked polyubiquitin chains have been extensively studied in the context of nuclear factor κB (NF-κB) signalling (Haas *et al*, 2009; Gerlach *et al*, 2011). Formation of both linkage types is required for NF-κB activation and elicitation of an inflammatory response during infection (Li *et al*, 2016). In recent years, the formation of 'hybrid' ubiquitin chains has also been described, where polyubiquitin chains are composed of multiple linkage types (Figure 2). More specifically, K63/M1-linked as well as K48/K63-linked hybrid ubiquitin chains have been shown to regulate innate immune signalling, particularly NF-κB activation (Emmerich *et al*, 2013, 2016; Ohtake *et al*, 2016). Every linkage type has a highly specific set of 'writers' (E3 ubiquitin ligases), 'readers' (ubiquitin-binding proteins), and 'erasers' (DUBs), which all contribute to the ubiquitin code that translates ubiquitylation into a biological response (Komander & Rape, 2012).

1.2.4 Ubiquitin-binding proteins

Ubiquitylation is recognised by 'reader' proteins containing ubiquitin-binding domains (UBDs). Ubiquitin-binding proteins, or ubiquitin receptors, contain at least one UBD and based on their modes of interaction with ubiquitin, UBDs have been classified into more than 20 distinct families comprising more than 200 proteins (Dikic *et al*, 2009). While UBDs are structurally different, the majority of UBDs bind non-covalently to the hydrophobic patch adjacent to the Ile44 of ubiquitin (Husnjak & Dikic, 2012). Ubiquitin-binding proteins commonly contain multiple signalling domains, which are involved in regulating localisation, enzymatic activity or adaptor recruitment.

Decoding of M1-linked ubiquitin signals is mediated by the ubiquitin binding in ABIN and NEMO (UBAN) domain. The UBAN domain was originally discovered in A20-binding inhibitor of NF-κB-1 (ABIN-1), ABIN-2, ABIN-3, NF-κB essential modulator (NEMO) and optineurin (Wagner *et al*, 2008; Agou *et al*, 2004; Ea *et al*, 2006; Zhu *et al*, 2007; Heyninck *et al*, 2003). Structural studies into the UBAN domain of NEMO revealed that the UBAN domain interacts with the Ile44-adjacent hydrophobic patch in the proximal ubiquitin. In addition, strong interactions are formed between the UBAN domain and the linker residues between two M1-linked ubiquitin molecules

(Husnjak & Dikic, 2012). UBAN domains are able to interact with K63-linked ubiquitin chains, however, studies have shown that the UBAN domain binds M1-linked ubiquitin chains with a 100-fold stronger affinity (Lo *et al*, 2009; Rahighi *et al*, 2009). The ability of NEMO to interact with M1-linked ubiquitin via its UBAN domain is required for the regulation NF-κB activation in response to TNFα, IL-1 and Toll-like receptor (TLR) agonists (Emmerich *et al*, 2013; Chen & Chen, 2013; Clark *et al*, 2013). Human point mutations in NEMO, which disrupt polyubiquitin binding to its UBAN domain, have been shown to lead to the development of anhidrotic ectodermal dysplasia with immunodeficiency (EDA-ID) (Hubeau *et al*, 2011). EDA-ID is a syndrome that causes developmental abnormalities and severe susceptibility to bacterial as well as viral pathogens. Moreover, mice harbouring a point mutation in the *Abin1* gene, which abrogates ubiquitin binding, develop hallmarks of autoimmunity since ABIN-1 is critical for negatively regulating NF-κB activation downstream of TLRs (Nanda *et al*, 2011).

1.3 Pathogen recognition by innate immune receptors

During infection of the host, germline-encoded innate immune receptors, also known as pattern recognition receptors (PRRs), sense the presence of pathogens (Akira *et al*, 2006). PRRs are highly expressed on macrophages, neutrophils and DCs, but also found on non-professional immune cells. PRRs bind to pathogen-associated molecular patterns (PAMPs), which are strongly conserved structures expressed by microbial species (Takeuchi & Akira, 2010). Importantly, PAMPs are exclusively expressed by invading pathogens, thus allowing the host to distinguish between 'self' and 'non-self' (Mogensen, 2009). In addition to PAMPs, PRRs also recognise damage-associated molecular patterns (DAMPs). DAMPs are stress signals, which are released by damaged or apoptotic host cells during cellular stress or tissue injury. DAMPs are endogenous danger signals, including extracellular matrix (ECM) components, histones, heat-shock proteins (HSPs), all of which are very potent to induce inflammation when recognised by PRRs (Roh & Sohn, 2018).

Four distinct PRR families have been identified: TLRs, NOD-like receptors (NLRs), C-type lectin receptors (CLRs) and retinoic acid-inducible gene (RIG)-I-like receptors (RLRs) (Takeuchi & Akira, 2010). Stimulation of PRRs by PAMPs and DAMPs leads to induction of genes regulating the inflammatory response (Figure 3). These include chemokines, cytokines, type I interferons, microbicidal proteins and regulators of PRR signalling (Kawai & Akira, 2010).

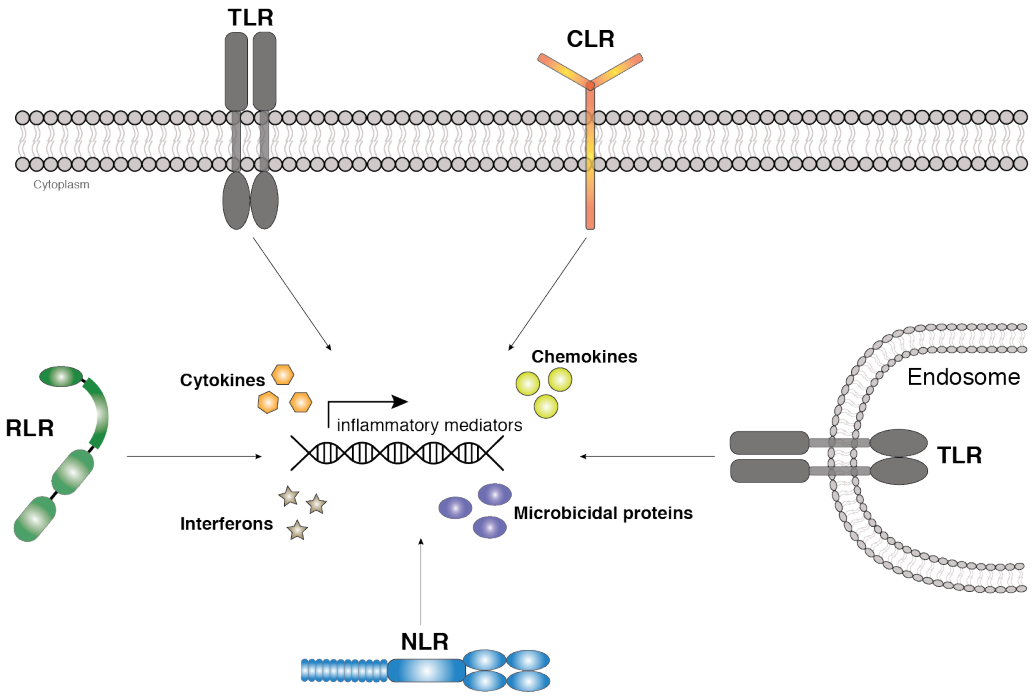

Figure 3 Pattern recognition receptors in innate immunity

A diverse repertoire of PRRs responds to the presence of PAMPs and DAMPs. Four PRR families have been identified, including Toll-like receptors (TLRs), NOD-like receptors (NLRs), C-type lectin receptors (CLRs) and retinoic acid-inducible gene (RIG)-I-like receptors (RLRs). PRRs are found in the plasma membrane, on endosomal membranes and in the cytosol. Upon activation, PRRs mediate a complex network of signalling pathways, which lead to the production of inflammatory mediators. These include chemokines, cytokines, interferons as well as microbicidal proteins. PRR, pattern recognition receptor; PAMP, pathogen-associated molecular pattern; DAMP, damage-associated molecular pattern.

TLRs were originally discovered in *Drosophila melanogaster* and have also been described in plant species including *Arabidopsis thaliana*, which demonstrates the evolutionary importance of TLRs in innate immunity across biological kingdoms (Lemaitre *et al*, 1996; Chan *et al*, 2010). TLRs are located on the outer plasma

membrane as well as on membranes of cytosolic vesicles to sense extracellular and intracellular pathogens, respectively (Kawasaki & Kawai, 2014). TLRs are type I transmembrane glycoproteins comprising an N-terminal extracellular, central transmembrane, and C-terminal intracellular domain (Botos *et al*, 2011). Receptors of the TLR family share N-terminal recognition leucine-rich repeat (LRR) motifs, a central transmembrane helix and a C-terminal signalling Toll/IL-1 receptor (TIR) domain (O'Neill & Bowie, 2007). Tandem repeats of LRRs are involved in antigen binding and while repeating leucine residues in LRRs are conserved, other residues are variable to ensure a broad ligand specificity among the TLR family. Therefore, LRR motifs among the TLR family are highly diverse and vary significantly between different TLRs (Botos *et al*, 2011). In contrast, transmembrane and TIR domains are highly conserved among the TLR family. The intracellular TIR domain is also conserved in some interleukin receptors, including the IL-1 receptor (O'Neill & Bowie, 2007). Unlike some other receptors, such as receptor tyrosine kinases, which possess catalytic C-termini, the TIR domain of TLRs has no catalytic activity. Instead, TLR-mediated signal transduction is induced when TIR domain-containing adaptor proteins are recruited to TLRs upon activation (Kawasaki & Kawai, 2014).

In humans, ten distinct TLRs have been characterised, while in mice 12 TLRs have been identified. Different TLRs recognise distinct molecular structures and differ in cellular localisation. TLRs located on the plasma membrane include TLR1, 2, 4, 5, 6 and 11, while intracellular TLRs include TLR3, 7, 8, 9 and 10 (Beutler, 2004). Importantly, TLRs respond to a broad spectrum of microbial ligands, including lipoproteins (TLR1, 2 and 6), double-stranded RNA (TLR3), LPS (TLR4), flagellin (TLR5), single-stranded RNA (TLR7 and 8) and viral DNA (TLR9) (Zhang *et al*, 2007; Andersen-Nissen *et al*, 2005; Barton *et al*, 2006; Alexopoulou *et al*, 2001; Hoebe *et al*, 2003; Campos *et al*, 2001). Ligand binding to N-terminal LRR motifs promotes dimerisation of two TLRs to form either homo- or heterodimers (Botos *et al*, 2011). Dimerisation of antigen-bound ectodomains brings C-terminal TIR domains of two adjacent TLRs in close proximity. Dimerisation induces adaptor recruitment to initiate downstream signalling cascades. While the TLR family is subdivided into plasma membrane and endosomal TLRs, a number of studies have shown that plasma membrane TLRs have the ability to also signal from endosomal compartments (Zanoni *et al*, 2011; Kagan *et al*, 2008a; Stuart *et al*, 2005; Stack *et al*, 2014).

Historically, it was believed that localisation of TLRs from the plasma membrane to endosomal compartments downregulates TLR-mediated signalling to dampen the innate immune response (Latz *et al*, 2003; Husebye *et al*, 2006; Tan *et al*, 2015). However, for some TLRs endocytic uptake has been shown to be essential for downstream signalling. LPS-induced endocytosis of TLR4 is a prerequisite for activation of the type I interferon pathway (Kagan *et al*, 2008a; Zanoni *et al*, 2011). Similarly, localisation of cell surface TLR2 to endosomes is required for type I interferon induction following infection of macrophages with herpes viruses or the bacterium *Staphylococcus aureus* (Stack *et al*, 2014).

1.3.1 TLR4 signalling

TLR4 binds to LPS and endogenous DAMPs, including HSPs, β-defensin 2 and hyaluronic acid. LPS is a major structural component of the outer membrane of Gram-negative bacteria, consisting of an O side chain, an oligosaccharide core and lipid A. Lipid A is the conserved PAMP, which is recognised by TLR4 (Poltorak *et al*, 1998a, 1998b). LPS binding protein (LBP), a soluble shuttle glycoprotein, mediates the interaction between LPS and CD14, a glycosylphosphatidylinositol (GPI)-anchored protein in the plasma membrane (Tobias *et al*, 1986; Wright *et al*, 1989; Pugin *et al*, 1993). Cell surface TLR4 is in a complex with myeloid differentiation factor 2 (MD-2), which has an LPS-binding motif and facilitates PAMP recognition when LPS is transferred from CD14 to the TLR4/MD-2 complex (Pugin *et al*, 1994; Da Silva Correia *et al*, 2001; Da Silva Correia & Ulevitch, 2002). Upon LPS binding, two TLR4/MD-2 complexes oligomerise to form a homodimer. This brings C-terminal TIR domains of two adjacent TLR4 molecules in close proximity, thus enabling recruitment of TIR domain-containing adaptor proteins to induce signal transduction (Park & Lee, 2013).

The five distinct TIR domain-containing signalling adaptors in mammalian cells include myeloid differentiation primary response gene 88 (MyD88), TIR domain-containing adaptor protein (TIRAP, also known as Mal), TIR domain-containing adaptor inducing IFNβ (TRIF), TRIF-related adaptor molecule (TRAM) and sterile α and HEAT-Armadillo motifs-containing protein (SARM) (O'Neill & Bowie, 2007).

While different TLRs recruit specific TIR domain-containing adaptor proteins, TLR4 has been shown to recruit all five adaptor proteins in a context-dependent manner (Lu *et al*, 2008). MyD88 was originally identified as a signalling adaptor for the TIR domain-containing IL-1 receptor (Burns *et al*, 1998). The importance of MyD88 was demonstrated using MyD88 knockout mice, which are resistant to LPS-induced sepsis (Roger *et al*, 2009; Muzio *et al*, 1997). In addition, knockout of MyD88 in macrophages prevents the expression of pro-inflammatory cytokines in response to LPS stimulation, while NF-κB activation is delayed and type I interferon expression remains unaffected (Kawai *et al*, 2001; Adachi *et al*, 1998; Kawai & Adachi, 1999). These findings suggested distinct TLR4-mediated signalling cascades induced by different TIR domain-containing adaptor proteins. TIRAP contains a phosphatidylinositol 4,5-bisphosphate (PIP_2) binding domain, which facilitates its recruitment to TLR4 in the plasma membrane (Kagan & Medzhitov, 2006). In addition, TIRAP mediates the recruitment of MyD88 to trigger the MyD88-dependent pathway, which leads to pro-inflammatory cytokine expression (Horng *et al*, 2001). The MyD88-independent pathway is initiated when TRAM binds to TLR4, which promotes the recruitment of TRIF to the receptor. The MyD88-independent, or TRIF-dependent, pathway leads to expression of type I interferons and interferon-stimulated genes (ISGs) (Rowe *et al*, 2006; Yamamoto *et al*, 2003b, 2003a).

1.3.2 The MyD88-dependent signalling pathway

The MyD88-dependent signalling pathway is not exclusively utilised by TLR4, but also by other TLRs, including TLR2 (Kawasaki & Kawai, 2014; Kawai & Akira, 2011). In addition to a TIR domain, MyD88 also contains a death domain (DD), which mediates recruitment of DD-containing signalling proteins via homotypic interactions to TLR4 upon LPS stimulation (Ohnishi *et al*, 2009). Following recruitment to TIRAP, MyD88 binds and activates DD-containing IL-1 receptor-associated kinase 4 (IRAK4). Subsequently, IRAK4 promotes association of IRAK1, IRAK2 and/or IRAK3 with the receptor to form a signalling complex known as the Myddosome (Figure 4). Kinase activity of IRAK4 is critical for TLR4 signalling and similarly to MyD88 deficiency, IRAK4 deficiency or inactivation of IRAK4 kinase activity by knock-in mutations protects from septic shock and abrogates expression of pro-inflammatory cytokines

(Cheng *et al*, 2007; Motshwene *et al*, 2009; Lin *et al*, 2010; Tae *et al*, 2007). IRAK1 catalytic activity is not essential for TLR-induced signal transduction, however, it promotes caspase-1 activation (Pauls *et al*, 2013; Lin *et al*, 2014). IRAK2 and 3 in turn lack conserved amino acid residues required for catalytic activity, and thus IRAK2 and 3 are known as pseudokinases (Wesche *et al*, 1999). Although kinase activity of IRAK1, 2 and 3 are redundant for TLR signalling, they are structurally important for the formation of the Myddosome.

IRAK1, 2 and 3 contain a C-terminal motif, which recruits TNF receptor-associated factor 6 (TRAF6), an E3 ubiquitin ligase, to the Myddosome (Ye *et al*, 2002; Lin *et al*, 2010). In the presence of the UBE2V1-Ubc13 heterodimer, an E2 ubiquitin-conjugating enzyme, TRAF6 catalyses the formation of K63-linked polyubiquitin chains (Deng *et al*, 2000). K63-linked chains are attached to the Myddosome, in particular to IRAK1, as well as to TRAF6 itself (Lamothe *et al*, 2007; Walsh *et al*, 2008; Cohen, 2014). Besides TRAF6, E3 ubiquitin ligases belonging to the Pellino family have also been shown to generate K63-linked ubiquitin chains following Myddosome assembly (Ordureau *et al*, 2008; Butler *et al*, 2007). The formation of K63-linked polyubiquitin is essential for the activation of transforming growth factor β-activated kinase-1 (TAK1, also known as MAP3K7) and for the formation of M1-linked polyubiquitin chains (Kanayama *et al*, 2004; Wang *et al*, 2001; Xia *et al*, 2009).

In mammalian cells, the TAK1 complex consists of TAK1, the catalytic component, and TAK1-binding protein 1 (TAB1) and either TAB2 or TAB3. Both TAB2 and TAB3 contain a ubiquitin-binding zinc finger domain, which specifically interacts with K63-linked ubiquitin chains (Kulathu *et al*, 2009). Following K63-linked ubiquitin chain formation by TRAF6, the TAK1 complex binds to K63-linked chains either via TAB2 or TAB3 (Figure 4). Ubiquitin binding to the TAK1 complex induces a conformational change in TAK1, which activates its kinase activity (Wang *et al*, 2001). TAK1 is a mitogen-activated protein (MAP) kinase kinase kinase (MAP3K), which initiates signalling cascades leading to the activation of MAP kinases, including p38 and c-Jun N-terminal kinases (JNKs) (Cohen, 2014).

TRAF6-generated K63-linked ubiquitin chains are a prerequisite for the formation of M1-linked polyubiquitin chains (Emmerich *et al*, 2013). The linear ubiquitin assembly

complex (LUBAC), an E3 ubiquitin ligase exclusively catalysing M1-linked ubiquitin, uses K63-linked ubiquitin chains as a substrate to generate K63/M1-linked hybrid ubiquitin chains (Kirisako *et al*, 2006; Gerlach *et al*, 2011; Emmerich *et al*, 2013). More specifically, HOIP is the catalytic subunit of LUBAC, which interacts with K63-linked ubiquitin via its zinc finger domain to covalently attach M1-linked ubiquitin moieties to existing K63-linked ubiquitin molecules (Gerlach *et al*, 2011; Emmerich *et al*, 2013). M1-linked ubiquitin chains activate the inhibitory proteins of κB (IκB) kinase (IKK) complex, which comprises the catalytic subunits IKKα and IKKβ as well as the adaptor protein NEMO, also known as IKKγ (Zandi *et al*, 1997; Yamaoka *et al*, 1998). NEMO interacts with M1-linked ubiquitin chains via its UBAN domain, thus localising the canonical IKK complex to ubiquitin (Marienfeld *et al*, 2006; Rahighi *et al*, 2009). The hybrid nature of K63/M1-linked ubiquitin chains brings the TAK1 and IKK complex in close proximity, allowing for TAK1 to phosphorylate and activate IKKβ (Emmerich *et al*, 2013; Cohen, 2014) (Figure 4).

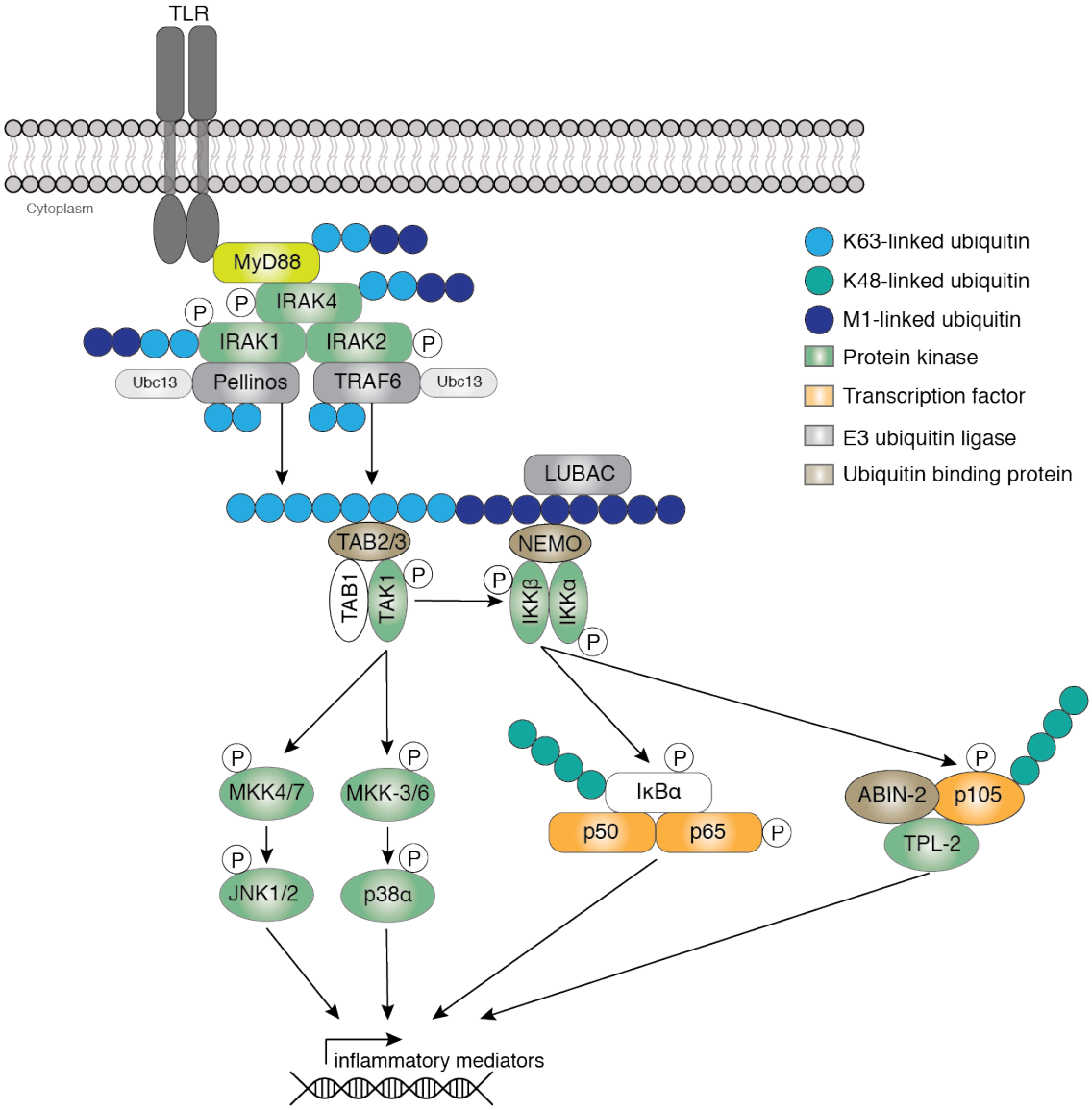

Figure 4 MyD88-dependent signalling

Activation of TLRs mediates the localisation of MyD88 to the receptor, which results in formation of the Myddosome. The E3 ubiquitin ligases TRAF6 and members of the Pellino family generate, together with the E2 conjugating enzyme Ubc13, K63-linked polyubiquitin chains. These act as a substrate for the E3 ubiquitin ligase LUBAC, which generates M1-linked polyubiquitin chains. Recruitment of the TAK1 complex to K63-linked ubiquitin chains induces TAK1 kinase activity, which in turn activates IKKβ of the IKK complex. The IKK complex binds to M1-linked ubiquitin chains via NEMO. Both TAK1 and IKKβ activate a plethora of protein kinases and transcription factors, which control the expression of inflammatory mediators.

IKKβ phosphorylates the cytoplasmic NF-κB inhibitory protein IκBα leading to its K48-linked polyubiquitylation by the SKP1-cullin-1-F-box complex-containing βTrCP ($SCF^{\beta TrCP}$), an E3 ubiquitin ligase complex (Winston *et al*, 1999; Spencer *et al*, 1999;

Yaron *et al*, 1998). K48-linked polyubiquitylation of IκBα promotes its degradation by the proteasome. This liberates IκBα-associated NF-κB p65-p50 heterodimers to translocate into the nucleus and activate expression of NF-κB-dependent genes, including pro-inflammatory mediators (Oeckinghaus & Ghosh, 2009). Besides IκBα, IKKβ also phosphorylates NF-κB1 p105 (p105), a precursor of the p50 subunit of NF-κB. Similar to IκBα phosphorylation, IKKβ-induced phosphorylation of p105 leads to K48-linked polyubiquitylation by $SCF^{\beta TrCP}$ and subsequent proteasomal degradation. In addition to proteasomal degradation, $SCF^{\beta TrCP}$-independent proteolytic digestion cleaves p105 into its mature p50 form, which assembles with p65 to form an active NF-κB transcription factor heterodimer (Moorthy *et al*, 2006). Proteolysis of p105 releases and activates tumour progression locus 2 (TPL-2), a MAP3K that initiates MAP kinase cascades to activate extracellular signal-regulated kinase (ERK) 1 and ERK2 (Lang *et al*, 2003; Waterfield *et al*, 2004; Dumitru *et al*, 2000).

Protein kinases activated in the MyD88-dependent pathway phosphorylate hundreds of signalling proteins that regulate gene expression, stability, processing and release of inflammatory mediators (Cohen, 2014).

1.3.3 The TRIF-dependent signalling pathway

The localisation and repertoire of signalling adaptors determine which pathways are activated downstream of TLRs. TLR2, 4 and 5 recognise PAMPs of bacterial cell walls and these receptors are thus present on the cell surface to induce cytokine production during microbial infection. In contrast, TLR3, 7 and 9 recognise viral nucleic acids and are predominantly found on endosomal vesicles (Kawai & Akira, 2006). TLR7 and TLR9 signal via MyD88 to promote type I interferon expression while TLR3 utilises TRIF to induce the type I interferon response (Kawai & Akira, 2010, 2011). Type I interferon production is critical for anti-viral responses and elevated type I interferon levels are protective during acute viral infection (Teijaro, 2016). The ability to drive both MyD88-dependent and -independent pathways is unique to TLR4 (Kawasaki & Kawai, 2014; Shen *et al*, 2008). Studies in MyD88-deficient macrophages revealed that MyD88 is critical for the expression of pro-inflammatory cytokines downstream of TLR4 (Kawai *et al*, 2001). However, strikingly

TLR4 activation of NF-κB and MAP kinases (MAPKs), as well as expression of type I interferons, remains largely unaffected when MyD88 is absent due to activation of the TRIF-dependent signal transduction pathway (Kawai *et al*, 2001).

TLR4 sequentially activates the MyD88-dependent and TRIF-dependent pathway from the plasma membrane and endosomal compartments, respectively (Kagan *et al*, 2008a). At the plasma membrane, a PIP_2-rich environment promotes TIRAP-MyD88 binding to TLR4 (Kagan & Medzhitov, 2006). Following initial MyD88-dependent signalling, TLR4 is internalised by a dynamin-dependent process (Husebye *et al*, 2006). As PIP_2 levels decrease during endocytosis, TIRAP-MyD88 complexes dissociate from TLR4. This allows the TIR domain-containing adaptor protein TRAM to bind to TLR4 and recruit TRIF via homotypic TIR domain interactions (Horng *et al*, 2001). A seven amino acid myristoylation motif in TRAM ensures localisation to early endosomes (Rowe *et al*, 2006). Pharmacological inhibition of dynamin-mediated endocytosis blocks LPS-induced internalisation of TLR from the cell surface and IFN induction (Kagan *et al*, 2008a).

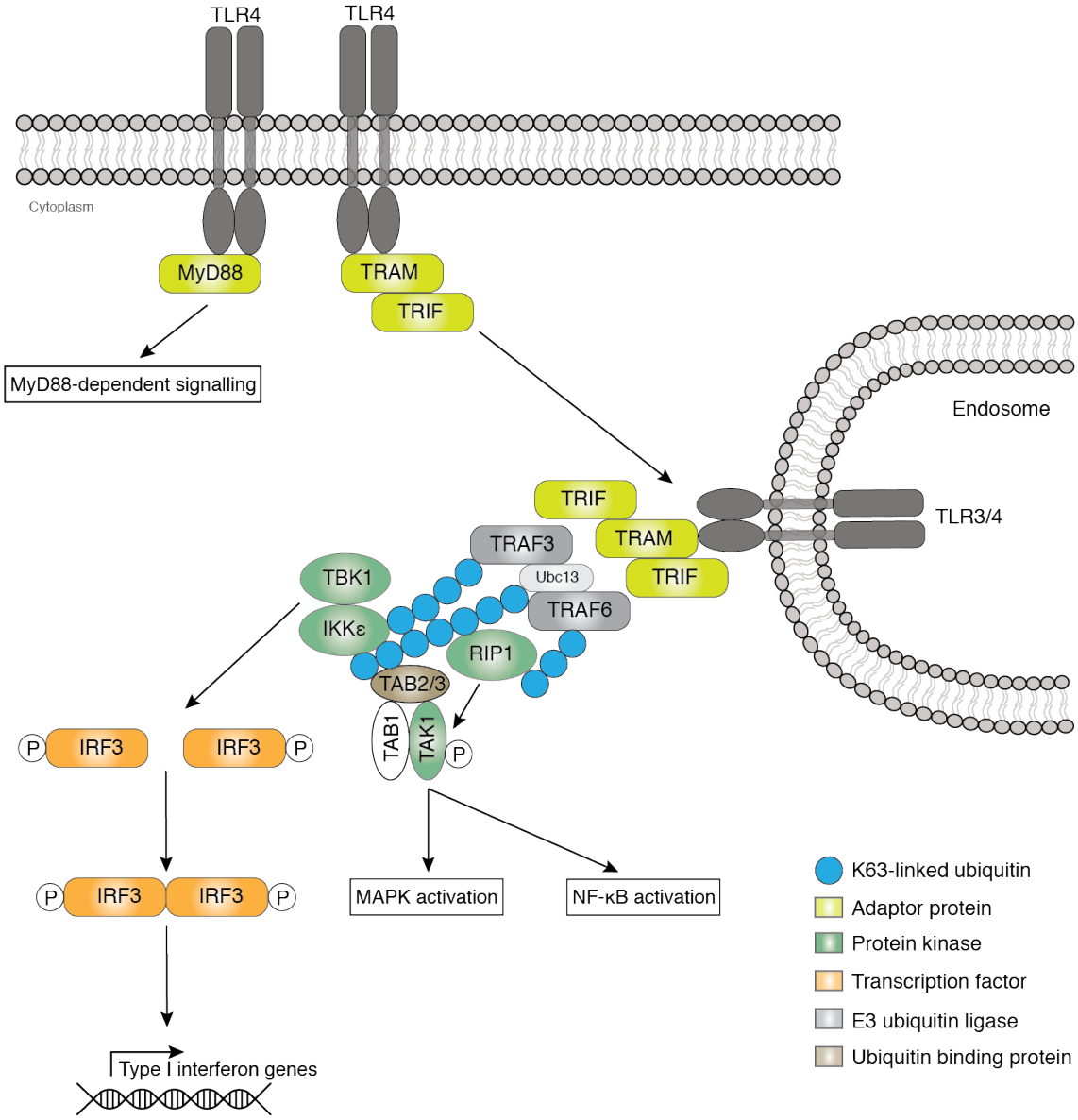

Figure 5 TRIF-dependent signalling pathway

Following internalisation, TLR4 signalling becomes TRIF-dependent, while TLR3 exclusively signals via the adaptor protein TRIF. The E3 ubiquitin ligases TRAF3 and TRAF6 are recruited to the TLR/TRAM/TRIF signalling complex. Both TRAF3 and TRAF6 generate K63-linked polyubiquitin chains. TRAF6 ubiquitylates RIP1, which in turn phosphorylates TAK1. TAK1 drives activation of MAP kinases and NF-κB. TRAF3 ubiquitylates IKKε and TBK1, which phosphorylate IRF3. Phosphorylation induces IRF3 dimerisation and subsequent nuclear translocation to promote expression of type I interferon genes.

TRIF promotes recruitment of the E3 ubiquitin ligases TRAF3 and TRAF6 to TLR4. TRAF6 recruits and ubiquitylates the receptor-interacting serine/threonine-protein kinase 1 (RIP1), which in turn phosphorylates and activates TAK1 to induce MyD88-independent activation of NF-κB transcription factors and MAP kinases (Kawai &

Akira, 2011) (Figure 5). In addition, TRAF3 binds to and ubiquitylates the IKK-related kinases IKKε (also known as IKKi) and TANK binding kinase 1 (TBK1, also known as NAK) (Hildebrand *et al*, 2011). Besides TRAF proteins, members of the Pellino family of E3 ubiquitin ligases have also been studied in the context of TLR signalling. TBK1 and IKKε phosphorylate Pellino-1, thus promoting Pellino-1-mediated ubiquitylation of RIP1 to further drive TAK1 activation (Smith *et al*, 2011). Both TBK1 and IKKε phosphorylate IFN regulatory factor 3 (IRF3) on C-terminal residues (McWhirter *et al*, 2004; Häcker & Karin, 2006). In unstimulated cells, IRF3 resides latently in the cytoplasm, however, upon phosphorylation IRF3 homodimerises. The dimeric IRF3/IRF3 transcription factor translocates into the nucleus and binds to interferon-stimulated response elements (ISREs), which are upstream consensus sequences of IFNα/β genes (Figure 5). IRF3/IRF3 binding to ISREs drives expression of type I interferon genes (DeFilippis *et al*, 2006; Yoneyama *et al*, 1998).

1.3.4 MAP kinase signalling in innate immunity

MAP kinase signalling is activated in macrophages and DCs downstream of all four PRR classes during the innate immune response. MAP kinase signalling pathways describe a cascade of at least three distinct kinases, where a MAP3K phosphorylates and activates a MAP2K, which in turn activates a MAPK by dual phosphorylation of a conserved Thr-X-Tyr motif (X represents any amino acid residue) in the kinase activation loop (Arthur & Ley, 2013). In mammals, a total of 14 MAPKs have been identified. In the context of innate immune responses, three MAPK families, including the classical ERK MAPKs (ERK1 and ERK2,) p38 MAPKs (p38α, p38β, p38γ and p38δ) and JNK MAPKs (JNK1, JNK2 and JNK3), have been most extensively studied (Arthur & Ley, 2013; Morrison, 2012).

In fibroblasts ERK1/2 activation is driven by RAF, an oncogenic serine/threonine MAP3K (Schaeffer & Weber, 1999; Moodie *et al*, 1993). However, in innate immune cells, TPL-2 MAP3K drives ERK1/2 activation (Gantke *et al*, 2012). More specifically, TPL-2 phosphorylates MEK kinase 1 (MKK1) and MKK2, which are MAP2Ks that in turn activate ERK1/2 (Beinke *et al*, 2004; Roget *et al*, 2012). The p38 MAPKs are activated by MKK3 and MKK6 downstream of a different set of MAP3Ks, including

TAK1, MAP3K1 (also known as MAPK/ERK kinase kinase [MEKK1]) as well as MAP3K4 (MEKK4) (Sato *et al*, 2005; Jiang *et al*, 1997; Zarubin & Han, 2005). Interestingly, p38 and JNK MAPK families share identical upstream MAP3Ks, however, JNKs are activated by two different MAP2Ks, namely MKK4 and MKK7 (Yang *et al*, 1997; Tournier *et al*, 2001). Extracellular stimuli determine the relative contribution of different protein kinases in MAPK signal transduction. While both MKK4 and MKK7 are required for optimal JNK activation in response to ultraviolet light, pro-inflammatory stimuli predominately activate JNKs via MKK7 (Tournier *et al*, 2001; Zou *et al*, 2007). Substrate specificity between MAP2Ks and downstream MAPKs is ensured by MAPK-specific docking sites in MAP2Ks (Bardwell, 2006). Similarly, MAP3Ks phosphorylate respective MAP2Ks in a context-dependent manner, which is regulated by signalling adaptors (Symons *et al*, 2006; Arthur & Ley, 2013). TAK1 is the MAP3K that initiates protein cascades to activate p38 and JNK MAPK pathways (Sato *et al*, 2005). However, via an indirect activating pathway TAK1 phosphorylates the IKK complex, which also leads to activation of TPL-2 (Beinke *et al*, 2004; Robinson *et al*, 2007; Zhang *et al*, 2014). It is the assembly of multiprotein signalling complexes by adaptor proteins, which links distinct tiers of the MAPK pathways to achieve substrate specificity and signal propagation (Arthur & Ley, 2013).

1.3.5 Functions of MAPKs in innate immune cells

The JNK family comprises three homologues, however, while JNK3 is predominantly expressed in neuronal tissues, JNK1 and JNK2 regulate the JNK signalling axis in myeloid cells (Rincón & Davis, 2009). Myeloid-specific deletion of JNKs protects against the development of insulin resistance in response to high-fat diet and inhibits macrophage polarisation into the M1 subset (Han *et al*, 2013). JNK1 and JNK2 have pro-inflammatory immune functions by mediating the expression of inflammatory mediators, including IL-1, IL-12, IL-6 and TNFα (Han *et al*, 2013; Martinez *et al*, 2009).

The classical MAPKs, which include ERK1 and ERK2, are involved in both the transcriptional and post-transcriptional regulation of cytokine production in innate immune cells upon infection. In macrophages, ERK1 and ERK2 promote expression

of TNFα, IL-1β and IL-10, while reducing expression of IL-12, IFNβ and iNOS (Dumitru *et al*, 2000; Kaiser *et al*, 2009; Mielke *et al*, 2009). In TPL-2-deficient mice, ERK1/2-driven gene expression of pro- and anti-inflammatory mediators is abrogated, which results in increased susceptibility of TPL-2-deficient mice to bacterial infection (Mielke *et al*, 2009; McNab *et al*, 2013). Besides, TPL-2-induced inhibition of IFNβ is critical for protecting against bacterial infections (McNab *et al*, 2013).

The p38 family of MAPKs has been shown to exhibit both pro- and anti-inflammatory functions depending on physiological context (O'Keefe *et al*, 2007). Macrophage-specific deletion of p38α significantly reduces TLR-dependent expression of TNFα, resulting in increased resistance of mice to endotoxic shock (Kang *et al*, 2008). In macrophages, p38 activation has been shown to promote production of pro-inflammatory mediators. However, essential cell type-specific functions such as the activation of negative feedback loops to suppress inflammation have been attributed to p38 signalling (Guma *et al*, 2012). More specifically, p38α signalling reduces skin inflammation induced by ultraviolet light in myeloid cells, whereas ultraviolet light-induced skin inflammation is exacerbated by p38α in epithelial cells (Kim *et al*, 2008). In myeloid cells, p38 pathways suppress inflammation by promoting transcription of anti-inflammatory mediators and by negatively regulating upstream signalling. Firstly, p38α phosphorylates TAB1 and/or TAB3 on Ser423/Thr431 and Ser60/Thr404, respectively (Cheung *et al*, 2003). Phosphorylation of the TAB complex by p38α inhibits TAK1, thus inhibiting inflammatory signalling (Mendoza *et al*, 2008). In addition, p38α-mediated phosphorylation of mitogen- and stress-activated kinases (MSKs) promotes expression of anti-inflammatory IL-10 and induces expression of dual-specificity protein phosphatase 1 (DUSP1), which dephosphorylates and deactivates p38α itself as well as JNKs to dampen the inflammatory response (Ananieva *et al*, 2008; Kim *et al*, 2008).

1.4 Ternary TPL-2 complex

1.4.1 TPL-2 protein kinase

TPL-2 (also known as COT or MAP3K8) is a serine/threonine MAP3K that is activated downstream of TNF receptor 1 (TNFR1), IL-1 receptor and TLRs (Gantke *et al*, 2012). TPL-2 is widely expressed, with particularly high expression levels in spleen, thymus, lungs and the gut (Patriotis *et al*, 1993; Makris *et al*, 1993; Koliaraki *et al*, 2012). In mammalian cells, two isoforms of TPL-2 are expressed, a 58 kDa and a 52 kDa protein, respectively. The translational initiation from methionine at either position one or position 30 determines whether the high or low molecular weight isoform of TPL-2 is expressed (Aoki *et al*, 1993). Both isoforms are localised in the cytosol and the functional difference between both TPL-2 isoforms remains unknown (Miyoshi *et al*, 1991).

1.4.2 Discovery of TPL-2 and its role in cancer

TPL-2 was discovered by three laboratories in the 1990s. Initially, TPL-2 was discovered as an oncogene in a human thyroid carcinoma cell line (cancer Osaka thyroid, *Cot* gene), which has the ability to transform the SHOK hamster embryonic cell line (Miyoshi *et al*, 1991). The murine homolog of the *Cot* gene, referred to as TPL-2, was identified as a target of provirus insertion in Moloney murine leukaemia virus-induced T cell lymphomas, a phenomenon later confirmed in two genome-wide studies (Patriotis *et al*, 1993; Mikkers *et al*, 2002; Lund *et al*, 2002). In addition, the *Tpl2* gene was identified as a site of mouse mammary tumour virus proviral integration in mammary carcinomas in mice (Erny *et al*, 1996). For consistency, all mammalian homologs in this thesis are referred to as *Tpl2*. Proviral activation of the *Tpl2* gene most commonly results in expression of TPL-2 with a C-terminal truncation, which provided initial evidence that the C-terminal region is critical for regulation of TPL-2 kinase activity (Ceci *et al*, 1997). Upon expression of C-terminally truncated TPL-2 in T lymphocytes, mice develop T cell lymphomas (Ceci *et al*, 1997). C-terminal truncation causes TPL-2-induced oncogenic transformation since an intact C-terminus exhibits autoinhibition of TPL-2 catalytic activity. Moreover, C-terminal truncation eliminates a degron sequence, comprising amino acid residues 435 to 457,

thus preventing proteasomal degradation (Gandara *et al*, 2003). This results in aberrantly high expression of catalytically active TPL-2. Furthermore, C-terminal truncation of TPL-2 abrogates binding to p105, an inhibitor of TPL-2 signalling (Beinke *et al*, 2003).

A recent study provided the first clinical evidence that C-terminal truncation of TPL-2 is a driver of human malignancies. More specifically, the study revealed that C-terminal truncation of TPL-2 promotes oncogenesis in one-third of spitzoid melanoma cases (Newman *et al*, 2019). However, despite the striking oncogenic potential of truncated TPL-2 in mouse models, a more general role for TPL-2 kinase activity in driving other human cancers has not been demonstrated. Amongst 477 primary tumour biopsies from human patients, which were analysed by DNA sequencing at the Wellcome Trust Sanger Institute, only one tumour biopsy from a patient diagnosed with glioblastoma multiforme harboured a point mutation in the *Tpl2* gene (Parsons *et al*, 2008). However, whether this mutation contributed to tumourigenesis was not determined. One study of a primary human lung adenocarcinoma identified a mutation in *Tpl2*, which leads to C-terminal truncation (Clark *et al*, 2004). In other studies of malignancies, including renal carcinomas, anaplastic large-cell lymphoma and multiple myeloma, overexpression of TPL-2 has been linked to oncogenesis (Lee *et al*, 2013; Jeong *et al*, 2011; Fernández *et al*, 2011; Hebron *et al*, 2013).

Multiple studies have provided evidence that TPL-2 may function as a tumour suppressor. More specifically, reduced TPL-2 expression in squamous cell carcinomas and lung adenocarcinomas corresponds to reduced survival of lung cancer patients (Gkirtzimanaki *et al*, 2013). In accordance with these findings, TPL-2-deficient mice develop increased numbers of urethane-induced lung tumours at an earlier onset relative to wild type (WT) control mice (Tuveson & Jacks, 1999). Furthermore, azoxymethane- and dextran sulphate-induced tumourigenesis in colons of mice is suppressed in TPL-2-deficient mice (Koliaraki *et al*, 2012).

1.4.3 Regulation of TPL-2 activity and stability by NF-κB1 p105

Originally NF-κB1 p105 was identified as a TPL-2-binding protein in a yeast two-hybrid screen (Belich *et al*, 1999). Almost all TPL-2 in unstimulated macrophages is complexed with p105, while only approximately 5% of total cellular p105 is bound to TPL-2 (Belich *et al*, 1999; Beinke *et al*, 2004). TPL-2 interacts stoichiometrically with the C-terminal region of NF-κB1 p105 via two direct interactions (Figure 6). Firstly, the C-terminal 70 amino acids of TPL-2 interact with a domain in p105 adjacent to the ankyrin repeat region. This binding region is a highly conserved helical domain located within the processing inhibitory domain (PID) (Gantke *et al*, 2011a). The PID mediates p105 dimerisation, thereby preventing proteolytic cleavage of p105 into p50, as the p105 dimer is inaccessible to the proteasome (Cohen *et al*, 2006; Savinova *et al*, 2009). Secondly, the kinase domain of TPL-2 directly interacts with the C-terminal DD of p105, thus limiting substrate accessibility to the kinase domain of TPL-2 (Beinke *et al*, 2003) (Figure 6).

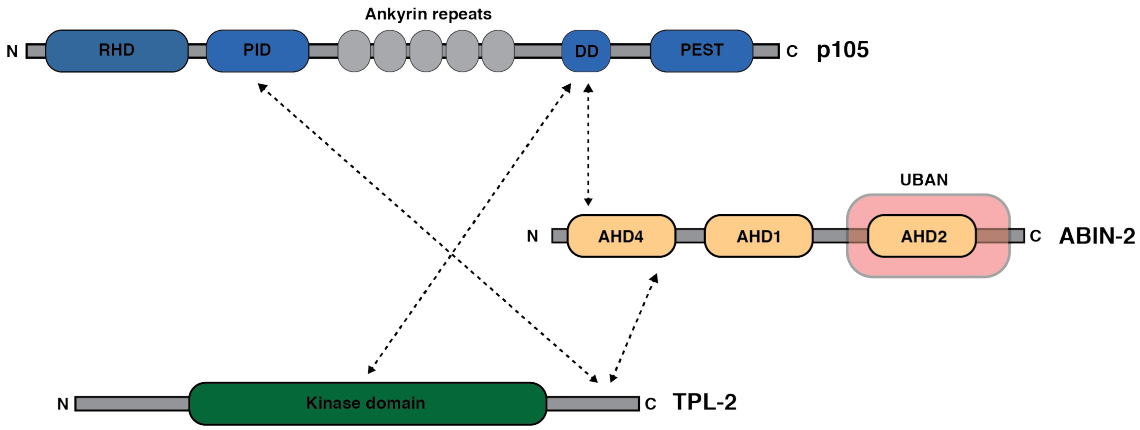

Figure 6 Structure of the ternary TPL-2 complex

In unstimulated cells, TPL-2 forms a complex with ABIN-2 and NF-κB1 p105. The kinase domain of TPL-2 directly interacts with the death domain (DD) of NF-κB1 p105, which regulates TPL-2 MEK kinase activity. The C-terminal region of TPL-2 interacts with the processing inhibitory domain (PID) of p105, which facilitates p105 dimerisation. Both interactions ensure a strong association between p105 and TPL-2. The TPL-2 C-terminus also interacts with ABIN-2, more specifically with the N-terminal AHD4 of ABIN-2. ABIN-2 association with TPL-2 is required to maintain TPL-2 protein stability. RHD, Rel homology domain; PEST, domain rich in proline, glutamate, serine and threonine; DD, death domain; PID, processing inhibitory domain; AHD, ABIN homology domain; UBAN, ubiquitin binding in ABIN and NEMO.

The stoichiometric interaction between p105 and TPL-2 regulates both stability and catalytic activity of TPL-2 (Waterfield *et al*, 2003; Beinke *et al*, 2003). TPL-2 contains a degron sequence, which is blocked by p105 binding thus stabilising TPL-2 expression. In p105-deficient macrophages from *Nfκb1*$^{-/-}$ mice, TPL-2 levels are substantially reduced resulting in impaired MEK1/2 and ERK1/2 activation when BMDMs from these mice are stimulated with LPS (Waterfield *et al*, 2003). p105 binding also inhibits MEK1/2 binding to TPL-2, thus preventing MEK1/2-induced activation of ERK1/2 MAP kinase signalling (Beinke *et al*, 2003; Waterfield *et al*, 2003; Beinke *et al*, 2004). Therefore, in unstimulated macrophages, in which the total cellular TPL-2 pool is associated with p105, TPL-2 cannot activate MEK1/2 and ERK1/2 signalling.

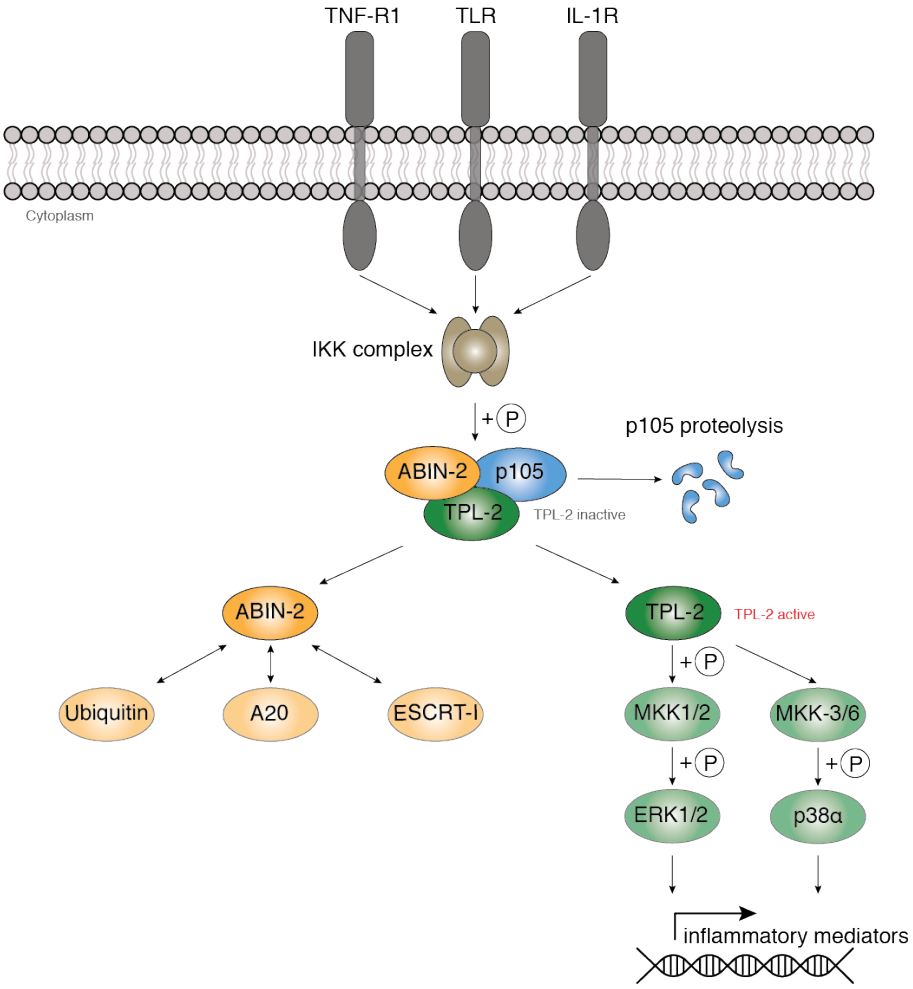

Figure 7 TPL-2 signalling pathway

In unstimulated cells, TPL-2 forms a ternary complex with ABIN-2 and NF-κB1 p105. Stimulation of the TNF receptor 1 (TNFR1), IL-1 receptor (IL-1R) and Toll-like

receptors (TLRs) activates the IκB kinase (IKK) complex, which phosphorylates p105. Phosphorylation of NF-κB1 p105 leads to its proteasomal degradation, which liberates TPL-2 and ABIN-2 from the ternary complex. TPL-2 release triggers phosphorylation and activation of MEK kinase 1 (MKK1) and MKK2, which in turn activate extracellular signal-regulated kinase (ERK) 1 and ERK2. Moreover, TPL-2 phosphorylates MKK3 and MKK6, which phosphorylate p38α. Together, ERK1/2 and p38α regulate gene expression of inflammatory mediators. The physiological signalling functions of ABIN-2 remain unknown, however, ABIN-2 has been shown to interact with ubiquitin, A20 and the ESCRT-I complex.

As previously mentioned, IKKβ-mediated phosphorylation of p105 leads to its proteasomal degradation (Figure 7). IKKβ phosphorylates Ser930 and Ser935 in the proline, glutamic acid, aspartic acid, serine and threonine-rich (PEST) region of murine p105 (Ser927 and Ser932 in humans). Dual phosphorylation mediates $SCF^{\beta TrCP}$ E3 ubiquitin ligase recruitment to p105, which adds K48-linked polyubiquitin chains to trigger proteasomal degradation of p105 (Lang *et al*, 2003; Heissmeyer *et al*, 2001; Orian, 2000). In some cell types, including $CD4^+$ T lymphocytes, $SCF^{\beta TrCP}$-induced proteolysis of p105 leads to complete degradation (Lang *et al*, 2003; Heissmeyer *et al*, 2001). However, in macrophages, $SCF^{\beta TrCP}$-induced proteolysis of p105 in response to IKK phosphorylation leads to proteolytic processing of p105 into p50 (Yang *et al*, 2012). In contrast, signal-induced cleavage of p105 by an $SCF^{\beta TrCP}$-independent mechanism predominantly mediates proteolytic cleavage of p105 to form p50, which interacts with p65 to activate gene expression of NF-κB-dependent genes (Gantke *et al*, 2011a, 2012).

Pharmacological inhibition of the proteasome prevents TPL-2 release from p105 and abrogates LPS-induced ERK1/2 activation in macrophages (Waterfield *et al*, 2004; Beinke *et al*, 2004). Moreover, in macrophages from *Nfκb1*$^{SSAA/SSAA}$ mice in which serine 930 and 935 of p105 are mutated to alanine, p105 is resistant to IKK-mediated degradation. In macrophages, *Nfκb1*^{SSAA} mutation fully blocks p105 phosphorylation, its subsequent degradation, and TPL-2-dependent activation of MEK1/2 as well as ERK1/2 (Yang *et al*, 2012; Sriskantharajah *et al*, 2009). Therefore, the IKK complex regulates both NF-κB and ERK1/2 MAP kinase signalling. Importantly, while TPL-2 is unable to promote ERK1/2 activation when bound to p105, TPL-2 kinase is catalytically active and may therefore phosphorylate downstream substrates other than MEK when complexed with p105 (Robinson *et al*, 2007; Babu *et al*, 2006).

Characterisation of *Nfκb1*$^{SSAA/SSAA}$ mice also led to the discovery that IKKβ-mediated phosphorylation of p105 is essential for TCR-dependent NF-κB activation in CD4$^+$ T lymphocytes and B cell receptor (BCR)-dependent NF-κB activation in B lymphocytes (Sriskantharajah *et al*, 2009; Jacque *et al*, 2014).

1.4.4 Regulation of TPL-2 activity by phosphorylation

Deficiency of p105 is insufficient to activate TPL-2. Retroviral expression of TPL-2 has shown that LPS stimulation is still required to mediate TPL-2-induced activation of ERK1/2 in macrophages from *Nfκb1*$^{-/-}$ mice. These findings imply that a p105-independent activating pathway for TPL-2 exists. Similar to other protein kinases, TPL-2 catalytic activity is regulated by phosphorylation on multiple residues. Two sites in TPL-2, Thr290 in the activation loop of the kinase domain and Ser400 in the C-terminal domain, are particularly important in regulating catalytic activity of TPL-2. Phosphorylation of both T290 and S400 is critical to induce TPL-2 kinase activity (Robinson *et al*, 2007; Luciano *et al*, 2004; Stafford *et al*, 2006). TPL-2 phosphorylation at T290 promotes TPL-2 release from p105 and point mutation of threonine 290 to alanine abrogates MEK activation (Cho *et al*, 2005; Cho & Tsichlis, 2005). Similarly, point mutation of serine 400 to alanine prevents retrovirally expressed mutant TPL-2 to phosphorylate and activate ERK1/2 in macrophages from *Nfκb1*$^{-/-}$ mice upon LPS stimulation (Robinson *et al*, 2007). Both phosphorylation sites in TPL-2, T290 and S400, are predicted to be autophosphorylated (Robinson *et al*, 2007; Xu *et al*, 2018). In addition, TPL-2 is directly phosphorylated by IKKβ at S400, which induces 14-3-3 binding to the C-terminal tail of TPL-2 (Ben-Addi *et al*, 2014). Association of 14-3-3 with the TPL-2 C-terminus increases the efficiency of MEK1 phosphorylation by TPL-2 and is thus required for ERK1/2 activation (Ben-Addi *et al*, 2014).

1.4.5 Regulation of TPL-2 stability by ABIN-2

In the early 2000s, proteomic mapping of the NF-κB pathway and tandem-affinity purification identified ABIN-2 as a binding partner of p105 (Bouwmeester *et al*, 2004; Lang *et al*, 2004). A20-binding inhibitor of NF-κB-2 (ABIN-2) can also associate with

free TPL-2 but binds to p105-bound TPL-2 with much higher affinity to form a ternary ABIN-2/TPL-2/p105 complex. ABIN-2 was initially discovered in a yeast two-hybrid screen as an A20-interacting protein that inhibits NF-κB when overexpressed (Van Huffel *et al*, 2001). siRNA-mediated gene knockdown of *Abin2* (also termed *Tnip2*) in HEK293 cells causes a severe loss of TPL-2 protein abundance (Lang *et al*, 2004; Symons *et al*, 2006). Furthermore, endogenous TPL-2 levels are dramatically reduced in primary cells, including macrophages and DCs, from *Abin2*$^{-/-}$ mice (Papoutsopoulou *et al*, 2006). Therefore, ABIN-2 is essential to maintain protein stability of TPL-2. Importantly, TPL-2 is also vital to stabilise ABIN-2 and thus *Tpl2*$^{-/-}$ mice are also deficient in both TPL-2 and ABIN-2 (Sriskantharajah *et al*, 2014).

In macrophages from *Abin2*$^{-/-}$ mice, LPS-induced ERK1/2 activation is significantly reduced, but not abrogated, due to minimal TPL-2 expression (Papoutsopoulou *et al*, 2006). Since phosphorylation of ERK1/2 is solely dependent on TPL-2 activity in primary macrophages, this implies that minimally expressed TPL-2 in *Abin2*$^{-/-}$ macrophages is thus catalytically active (Dumitru *et al*, 2000). Consistent with this, retrovirally expressed TPL-2 in macrophages from *Abin2*$^{-/-}$ mice rescues ERK1/2 phosphorylation upon LPS stimulation (Papoutsopoulou *et al*, 2006). While ABIN-2 is important to stabilise TPL-2, ABIN-2 is not required to activate TPL-2 kinase. Moreover, ABIN-2 does not interact with free TPL-2, which phosphorylates and activates MEK1/2 (Lang *et al*, 2004). Upon IKKβ-mediated phosphorylation of p105 on Ser930 and Ser935 in response to LPS stimulation, proteasomal degradation of p105 induces the release of TPL-2 and ABIN-2 from the ternary complex (Gantke *et al*, 2011a; Xu *et al*, 2018). While free TPL-2 activates the ERK MAP kinase pathway, the physiological role of ABIN-2 in innate immunity remains unknown.

1.4.6 Regulation of innate signalling pathways by TPL-2

Initial experiments on TPL-2 involved overexpression in cell lines and suggested that TPL-2 activated multiple MAP kinase pathways, NF-κB and nuclear factor of activated T cells (NFAT). The physiological relevance of some of these studies is questionable. Analyses of *Tpl2*$^{-/-}$ mice have been essential to establish the physiological functions of endogenous TPL-2. TPL-2-deficient mice are healthy

under pathogen-free conditions and develop normally compared to WT control mice (Dumitru *et al*, 2000). Furthermore, immune cell development of both innate immune cells and B as well as T lymphocytes is normal in *Tpl2*$^{-/-}$ mice (Dumitru *et al*, 2000; Sriskantharajah *et al*, 2009). Analyses of *Tpl2*$^{-/-}$ mice have indicated important signalling functions for TPL-2 in several cell types involved in innate immune responses.

1.4.6.1 Macrophages

TPL-2 function has been most extensively studied in macrophages, in which ERK1/2 phosphorylation is completely dependent on TPL-2 following TLR stimulation (Gantke *et al*, 2012). In contrast, TLR activation of p38α and JNK are largely independent of TPL-2 expression. TPL-2 is also essential for ERK1/2 activation in macrophages downstream of TNF receptor 1, TLR2 and TLR9 (Dumitru *et al*, 2000; Pattison *et al*, 2016; Bandow *et al*, 2012; Eliopoulos *et al*, 2003).

TPL-2 deficiency in macrophages reduces TLR-induced expression of essential inflammatory mediators, including IL-1β, TNFα, IL-6, IL-10, chemokine C-C motif ligand 7 (CCL7), CCL3, chemokine C-X-C motif ligand 2 (CXCL2) and monocyte chemoattractant protein-1 (MCP-1) (Xu *et al*, 2018; Kaiser *et al*, 2009; Mielke *et al*, 2009; Dasi *et al*, 2005). Strikingly, macrophages are the major cell type secreting TNF during bacterial infection, which consolidates the fundamental role of TPL-2 in innate immune response to bacteria (Dumitru *et al*, 2000; Mielke *et al*, 2009). However, PRR induction of TNF secretion in macrophages is not always TPL-2-dependent. For example, dectin-1 activation by curdlan leads to TNF secretion via a TPL-2-independent pathway (Mielke *et al*, 2009; Gringhuis *et al*, 2009).

TPL-2 promotes mRNA abundance of many inflammatory mediators in macrophages, primarily via direct ERK1/2 modulation of transcription factors (Yang *et al*, 2019). However, TPL-2 also regulates TNF expression via a post-translational mechanism. TPL-2 has been proposed to induce the processing of pre-TNF into soluble TNF by promoting ERK1/2-mediated phosphorylation and activation of TNFα-converting enzyme (TACE) on T735 (Soond *et al*, 2005). In contrast, TPL-2 also inhibits mRNA

expression of inflammatory mediators in macrophages, including IL-12 and IFNβ (Kaiser *et al*, 2009; Tomczak *et al*, 2006). TPL-2 signalling, therefore, exhibits complex pro- and anti-inflammatory roles.

1.4.6.2 Neutrophils

TPL-2 also regulates MAP kinase activation in neutrophils and DCs. Neutrophils are the most abundant circulating leukocyte and have key roles in innate immune responses, including phagocytosing and killing microbes as well as removing apoptotic cells. Neutrophils from *Tpl2*$^{-/-}$ mice secrete reduced levels of TNF in response to LPS stimulation, similar to macrophages (Acuff *et al*, 2017b). Pharmacological inhibition of TPL-2 in neutrophils blocks expression of other pro-inflammatory mediators, including IL-8, CCL3 and CCL4, in response to TLR4 activation (Senger *et al*, 2017). In addition, superoxide generation in *Tpl2*$^{-/-}$ neutrophils is impaired upon stimulation with N-formylmethionyl-leucyl-phenylalanine (fMLP), a chemotactic peptide, while WT neutrophils produce high levels of superoxide upon activation of the formyl peptide receptor 1 in response to fMLP stimulation (Acuff *et al*, 2017b). Superoxide is an important class of ROS, which promotes neutrophil cytotoxicity to clear bacterial infection. Consistent with this, neutrophils from *Tpl2*$^{-/-}$ mice are unable to effectively kill internalised *C. rodentium* compared to WT neutrophils (Acuff *et al*, 2017b).

1.4.6.3 Fibroblasts

In embryonic fibroblasts, TPL-2 promotes ERK1/2 and JNK phosphorylation in response to TNFα and IL-1β stimulation. TPL-2 activation also contributes to NF-κB activation (Dasi *et al*, 2005; Xu *et al*, 2018). The ability of TPL-2 to directly phosphorylate the upstream activators of all three distinct MAP kinase pathways, namely MKK1, MKK4 and MKK6, makes TPL-2 a critical regulatory node of innate immune responses. It is not clear why TPL-2 makes differential contributions to activation of specific MAP kinases in different cell types. A possible explanation is that cell type-specific expression of other MAP3Ks that function redundantly with TPL-2 differentially contribute to MAP kinase activation.

1.4.7 Regulation of inflammatory and innate immune responses by TPL-2

Analyses of *Tpl2*$^{-/-}$ mice have demonstrated important roles for TPL-2 in the regulation of inflammation and immune responses to multiple pathogens.

1.4.7.1 Inflammation

TPL-2 deficiency has been shown to reduce inflammation in a variety of mouse models mimicking human diseases (Watford *et al*, 2010; Gantke *et al*, 2011b; Kuriakose *et al*, 2015; Xu *et al*, 2018). *Tpl2*$^{-/-}$ mice produce very low levels of TNF and IL-1β after intraperitoneal LPS injection and are resistant to endotoxic shock (Mielke *et al*, 2009). Furthermore, TPL-2 is required for the development of TNF-induced Crohn's-like inflammatory bowel disease (Kontoyiannis *et al*, 2002, 1999). In addition, *Tpl2*$^{-/-}$ mice are protected in drug-induced models of liver fibrosis, thrombocytopenia, pancreatitis, and experimental autoimmune encephalomyelitis (EAE), a mouse model for multiple sclerosis (Sriskantharajah *et al*, 2014; Van Acker *et al*, 2007; Perugorria *et al*, 2013; Kyrmizi *et al*, 2013). Such studies have suggested that TPL-2 would be a good anti-inflammatory drug target (George & Salmeron, 2009).

1.4.7.2 Citrobacter rodentium

TPL-2 is required for optimal clearance of the Gram-negative extracellular bacterium *C. rodentium* (Acuff *et al*, 2017b, 2017a). *Tpl2*$^{-/-}$ mice infected with *C. rodentium* experience increased bacterial burden and elevated systemic dissemination of *C. rodentium* to both spleen and liver (Acuff *et al*, 2017a). In addition, *C. rodentium*-infected *Tpl2*$^{-/-}$ mice recruit decreased numbers of neutrophils and monocytes to the colon, which contributes to increased bacterial infection in *Tpl2*$^{-/-}$ mice compared to WT controls (Acuff *et al*, 2017a).

1.4.7.3 Listeria monocytogenes

Tpl2$^{-/-}$ mice are more susceptible to infection with the intracellular Gram-positive bacterium *Listeria monocytogenes* (Mielke *et al*, 2009; McNab *et al*, 2013). *Tpl2*$^{-/-}$ mice produce significantly reduced levels of IL-1β and increased type I IFNs. McNab *et al*. showed using double knockout mice, which are deficient in both TPL-2 and the IFN receptor, that increased bacterial burden resulting from the loss of TPL-2 is indeed due to elevated type I IFN induction in TPL-2-deficient mice (McNab *et al*, 2013).

1.4.7.4 Mycobacterium tuberculosis

Tpl2$^{-/-}$ mice are more susceptible to the intracellular bacterium *Mycobacterium tuberculosis* (McNab *et al*, 2013). Further investigations into the transcriptomic landscape of *M. tuberculosis*-infected macrophages have demonstrated that negative regulation of type I IFN production by TPL-2 via ERK1/2 signalling, which is impaired in *Tpl2*$^{-/-}$ mice, contributes to clearance of *M. tuberculosis* infection (McNab *et al*, 2013). Importantly, *Tpl2*$^{-/-}$ *Rag1*$^{-/-}$ mice, which lack adaptive immune cells, have a greater bacterial burden following *M. tuberculosis* and *L. monocytogenes* infection compared to WT controls. Thus, a defective innate immune response in *Tpl2*$^{-/-}$ mice results in susceptibility to bacterial infection.

1.4.7.5 Influenza

TPL-2 is critical for reducing morbidity as well as mortality in response to influenza virus infection. Notably, *Tpl2*$^{-/-}$ mice are more susceptible to infection with influenza virus and TPL-2 expression is essential for optimal production of IFNγ upon viral infection *in vitro* and *in vivo* (Kuriakose *et al*, 2015). Loss of TPL-2 reduces antigen-specific CD8^{+} T lymphocyte responses, thereby enhancing influenza infection. Interestingly, TPL-2 has been shown to differentially regulate interferon induction in response to viral ligands in a cell type-specific manner (Kuriakose *et al*, 2015). More specifically, TPL-2 promotes IFNα/β and IFNγ induction in DCs following stimulation

with viral ligands, whereas TPL-2 inhibits IFNβ production in macrophages (Kuriakose *et al*, 2015).

1.4.7.6 Toxoplasma gondii

TPL-2 signalling has also been implicated in the host defence against parasitic pathogens. *Tpl2*$^{-/-}$ mice mount an impaired immune response upon infection with *Toxoplasma gondii*, a single-celled protozoan parasite (Watford *et al*, 2008). TPL-2-deficient mice are unable to efficiently clear *T. gondii* infection and produce reduced levels of IFNγ (Watford *et al*, 2008). Importantly, Watford *et al.* showed that the weakened host immune response in *Tpl2*$^{-/-}$ mice in response to *T. gondii* results from a T lymphocyte-intrinsic defect (Watford *et al*, 2008). Therefore, TPL-2 is an important regulator of T-lymphocyte-mediated immune responses to parasites *in vivo*.

1.4.8 TPL-2 kinase as a drug target to treat inflammatory diseases

Disease aetiology of many inflammatory and autoimmune disorders, including Crohn's disease and rheumatoid arthritis, is frequently driven by pro-inflammatory cytokines such as TNF, IL-1β and IL-6 (Zhang & An, 2007; Sanchez-Muñoz *et al*, 2008). In the clinic, however, not all patients respond well to anti-TNF antibodies and other anti-cytokine therapies (Gantke *et al*, 2011a). In addition, antibody therapies are very expensive and require injection. Consequently, there is an unmet clinical need for low-cost and orally administered medicines. In order to limit production of TNF and other pro-inflammatory cytokines, pharmacological inhibition of signalling pathways that promote expression of pro-inflammatory mediators is a potential avenue to treat inflammatory and autoimmune diseases (Cohen, 2009; Cohen & Alessi, 2013).

As previously described, TPL-2 is required for TLR-mediated production of TNF and other pro-inflammatory cytokines in innate immune cells (Dumitru *et al*, 2000; Mielke *et al*, 2009). In addition, analyses of *Tpl2*$^{-/-}$ mice have shown that TPL-2 promotes inflammation in a number of disease models and TPL-2 has become an attractive drug target (Dumitru *et al*, 2000). Since TPL-2 activates the MEK-ERK signalling axis

exclusively in innate immune responses, targeting TPL-2 with specific inhibitors may have reduced adverse effects than blocking ERK1/2 directly, which would also block RAF activation of ERK1/2 (Gantke *et al*, 2011a; Wellbrock *et al*, 2004). Moreover, the kinase domain of TPL-2 has low sequence homology to other members of the mammalian kinome. More specifically, a unique proline residue at position 145 in the human sequence instead of a conserved glycine residue is exclusive to the kinase domain of TPL-2 among the human kinase family (Luciano *et al*, 2004). The unique structural feature of the TPL-2 kinase domain may provide an opportunity to develop very selective TPL-2 inhibitors with high clinical potency and low off-target effects.

Initially, the pharmaceutical company Wyeth Research (Pfizer) developed a number of selective TPL-2 inhibitors, which potently block LPS- and IL-1β-induced production of TNFα in primary human monocytes and in mice following intraperitoneal injection. In addition, these TPL-2 inhibitors block ERK-mediated expression of IL-6, IL-8, PGE_2 and matrix metalloproteinases 1 (MMP-1) and MMP-3 (Hall *et al*, 2007; Hu *et al*, 2006). In 2009, Abbott Laboratories identified thieno[2,3-c]pyridines as a novel class of TPL-2 kinase inhibitors, which inhibit TPL-2-induced ERK1/2 activation *in vitro* (George *et al*, 2008). At a similar time, Wyeth Research (Pfizer) identified 8-halo-4-(3-chloro-4-flu- oro-phenylamino)-6-[(1H-[1,2,3]triazol-4-ylmethyl)-amino]-quinoline-3-carbonitriles (C4) as potent inhibitors of TPL-2 kinase activity. Further structural substitutions and modifications of the triazole moiety within candidate compounds identified the addition of a cyclic amine group to the triazole moiety as beneficial. Structural optimisation of cyclic amine groups led to the development of 8-chloro-4-(3-chloro-4-fluorophenylamino)-6-((1-(1-ethylpiperidin-4-yl)-1H-1,2,3-triazol-4-yl)methylamino) quinoline-3-carbonitrile (C34). C34 is a highly selective and potent TPL-2 inhibitor, which blocks LPS-induced TNFα production in a rat inflammation model *in vivo* (Wu *et al*, 2009).

Despite the discovery of TPL-2 inhibitors for *in vitro* and *in vivo* studies, limited structural insight into TPL-2 has hindered the development of chemical candidates for clinical applications (George & Salmeron, 2009). A study by Novartis identified the X-ray crystal structure of human TPL-2, which revealed that the kinase domain of TPL-2 exists in two distinct conformations, which are unique to TPL-2 compared to other protein kinases (Gutmann *et al*, 2015). More specifically, a 15 amino acid

sequence precedes the active site P-loop. This short amino acid insert in the catalytic domain regulates folding of the active site, thus enabling the kinase domain of TPL-2 to be more structurally dynamic. This in-depth structural insight may provide a critical understanding of TPL-2 structure to design highly selective TPL-2 kinase inhibitors for future clinical studies.

1.5 The ABIN-2 adaptor protein

Originally, ABIN-2 was identified as an A20-binding protein in a yeast two-hybrid screen (Van Huffel *et al*, 2001; Heyninck *et al*, 1999) (Figure 8). A20 (TNFα-induced protein 3; TNFAIP3) is a ubiquitin-binding protein, which is a key regulator of inflammation, apoptosis and autophagy (Catrysse *et al*, 2014). Besides ABIN-2, the yeast-two hybrid screen identified ABIN-1, a structurally related protein (Heyninck *et al*, 1999). Bioinformatic analysis led to the discovery of ABIN-3, which shares sequence homology with both ABIN-1 and ABIN-2 (Wullaert *et al*, 2007). ABIN family members share the ability to interact with A20, negatively regulate NF-κB activation when overexpressed, and contain homologous short amino acid motifs called ABIN homology domains (AHDs) (Kumar *et al*, 2004; Hoffmann *et al*, 2006; Gilmore, 2006).

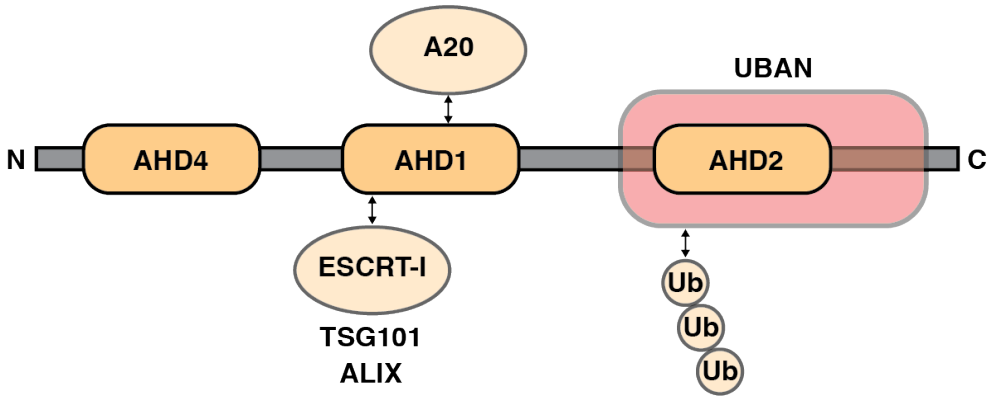

Figure 8 ABIN-2 domain structure

ABIN-2 comprises three ABIN homology domains (AHDs), namely AHD1, AHD2 and AHD4. While AHD4 is located at the amino-, or N-terminus, AHD1 is centrally located within the ABIN-2 peptide sequence. Tyrosine at position 231 interacts with TSG101 and ALIX of the ESCRT-I complex, whereas glutamic acid at position 256 interacts with A20. The ubiquitin binding in ABIN and NEMO (UBAN) domain at the carboxyl, or C-terminus of ABIN-2 comprises AHD2. Aspartic acid at position 310 within the UBAN domain interacts with ubiquitin.

All members of the ABIN family share AHD1, 2 and 4, however, ABIN-2 lacks AHD3 (Wullaert *et al*, 2007; Heyninck *et al*, 2003). Moreover, among the murine ABIN family, ABIN-3 lacks AHD2. As previously outlined, ABIN family members contain a UBAN domain, which specifically interacts with M1-linked ubiquitin and to a lesser extent with K63-linked ubiquitin (Wagner *et al*, 2008). The UBAN domain plays an important role in signal transduction pathways and is also present in NEMO, which mediates NF-κB activation in response to PRR activation. The C-terminal UBAN domain comprises AHD2, while the central AHD1 interacts with the zinc finger domain in the C-terminus of A20 (Wagner *et al*, 2008; Verstrepen *et al*, 2009). Importantly, ABIN-2 does not exert enzymatic activity and thus its biological function is dependent on molecular interactions and localisation (Verstrepen *et al*, 2009). ABIN-2 is a cytosolic 49 kDa protein, which shares 78% sequence homology between human and mouse (Van Huffel *et al*, 2001; Liu *et al*, 2003; Hughes *et al*, 2003). Deletion of the N-terminal 195 amino acid residues mediates nuclear translocation, which indicates that the N-terminus of ABIN-2 is critical to maintain its cytosolic localisation (Liu *et al*, 2003).

1.5.1 ABIN-2 regulation of inflammation

Originally, biochemical studies in HEK293 cells indicated that transiently overexpressed ABIN-2 negatively regulates TNFα- and IL-1-induced NF-κB activation downstream of RIP1, TRAF2 and TRAF6 as well as IRAK1 (Huang *et al*, 2008; Van Huffel *et al*, 2001). In contrast, overexpression of ABIN-2 does not inhibit NF-κB activation resulting from overexpression of IKKβ, which suggests that ABIN-2 regulates NF-κB upstream of the IKK complex (Van Huffel *et al*, 2001). Moreover, ABIN-2 contains a NEMO-binding motif, which shares high homology with the NEMO-binding domain in RIP1 (Ye *et al*, 2000). Overexpression studies suggest that ABIN-2 negatively regulates NF-κB activation by directly competing with RIP1 for NEMO binding, thus interfering with NEMO-RIP1 complex formation, which is a prerequisite for TNFα-induced NF-κB signalling (Liu *et al*, 2004). Furthermore, it was proposed that ubiquitin binding to the UBAN domain of ABIN-2 is required for NF-κB inhibition (Wagner *et al*, 2008). However, subsequent studies have shown that endogenous ABIN-2 does not regulate NF-κB activation in primary cells. Macrophages from *Abin2*$^{-/-}$ mice activate NF-κB similarly to macrophages from WT

control mice in response to LPS and TNFα stimulation (Papoutsopoulou *et al*, 2006). Similarly, ABIN-2 does not regulate NF-κB activation downstream of TLR4 and antigen receptors in B lymphocytes or upon antigen receptor- and CD28-mediated NF-κB activation in T lymphocytes.

Analyses of ABIN-2-deficient cells have demonstrated that ABIN-2 maintains TPL-2 stability and consequently, ABIN-2 positively regulates ERK1/2 MAP kinase signalling mediated by TPL-2 kinase (Papoutsopoulou *et al*, 2006). For example, LPS activation of ERK1/2 is impaired in *Abin2*$^{-/-}$ macrophages due to TPL-2 deficiency. The specific functions of ABIN-2 in inflammation have been elucidated using knock-in mice with specific mutations in ABIN-2, which block ABIN-2 signalling function without affecting TPL-2 protein expression or signalling.

1.5.1.1 ABIN-2 binding to A20 inhibits allergic airway inflammation

Studies using *Tpl2*$^{-/-}$ mice have shown that TPL-2 deficiency exacerbates allergic airway inflammation induced by house dust mite (HDM). TPL-2 expression in lung DCs is critical to negatively regulate expression of pro-inflammatory C-C motif chemokine ligand 24 (CCL24), which promotes the recruitment of eosinophils and T lymphocytes to inflamed lungs following HDM challenge. However, HDM-induced allergic responses are normal in *Tpl2*$^{D270A/D270A}$ mice expressing catalytically inactive TPL-2, indicating that blocked TPL-2 signalling does not explain the phenotype of *Tpl2*$^{-/-}$ mice. Rather, the absence of TPL-2 reduces expression of ABIN-2 and consequently the formation of a complex between ABIN-2 and the key negative regulator of inflammation, A20, which is genetically linked to the development of asthma (Schuijs *et al*, 2015). The molecular mechanism by which the formation of ABIN-2/A20 complexes reduces HDM-induced airway inflammation remains to be fully understood.

1.5.1.2 ABIN-2 binding to ubiquitin inhibits DSS-induced colitis

Tpl2$^{-/-}$ mice are hypersensitive to dextran sulphate sodium (DSS)-induced colitis, due to TPL-2 deficiency in intestinal sub-epithelial myofibroblasts (IMFs) (Roulis *et*

al, 2014). A recent study has demonstrated that *Abin2*^{D310N} mutation, which blocks ABIN-2 binding to M1/K63-linked polyubiquitin chains, phenocopies the effect of *Tpl2* null mutation in DSS-induced colitis (Nanda *et al*, 2018), but does not affect TPL-2 activation of ERK1/2. Biochemical analyses of IMFs suggest that the hypersensitivity of *Tpl2*$^{-/-}$ mice to DSS-induced colitis is caused by the absence of ABIN-2 ubiquitin binding, which reduces IL-1β upregulation of PGE_2 production in IMFs by a TPL-2-independent pathway.

1.5.2 ABIN-2 interaction with ESCRT-I

In 2016, Banks *et al.* discovered that a central motif in ABIN-2 mediates its interaction with endosomal sorting complex required for transport (ESCRT)-I (Banks *et al*, 2016). This ESCRT and ALIX binding region (EABR), which was originally identified in CEP-55 that regulates cytokinesis, is not present in ABIN-1 or NEMO, suggesting that ESCRT-associated functions may be exclusive to ABIN-2 within the UBAN protein family. The EABR in ABIN-2 mediates a direct interaction with tumour susceptibility gene 101 (TSG101, also called VPS23), a core complex component of ESCRT-I. Previous studies have shown that tyrosine 187 in CEP55 is critical for ESCRT-I binding (Hyung *et al*, 2008). Mutation of the equivalent residue in the EABR of human ABIN-2 (tyrosine 230 to alanine) abrogates ESCRT-I binding (Banks *et al*, 2016).

Functioning sequentially, ESCRT-I, ESCRT-II and ESCRT-III complexes remodel membranes, regulating a number of membrane fission processes. These include the formation of multivesicular bodies (MVBs) in late endosomes (Lefebvre *et al*, 2018a) and the fusion of late endosomes and autophagosomes with lysosomes (Metcalf & Isaacs, 2010). The interaction of ABIN-2 with ESCRT-I raised the possibility that ABIN-2 may regulate ESCRT-I functions during innate immune responses.

In mammalian cells, four distinct ESCRT complexes, ESCRT-0, I, II and III, orchestrate MVB biogenesis. MVBs are late endosomal vesicles, which are involved in the degradation of endocytosed particles, including cell surface receptors. As endosomes mature into MVBs, intraluminal vesicles (ILVs) form within the MVB by inward budding and scission of the endosomal membrane (Lefebvre *et al*, 2018a). A

critical role of ESCRT complexes is the delivery of endocytosed particles to ILVs within MVBs. Moreover, ESCRT complexes also mediate topologically comparable membrane-budding events, including viral budding and abscission of cells to complete cytokinesis (Stuchell *et al*, 2004). Ubiquitylated cargo on endosomal membranes is sequestered by ESCRT-0, which contains membrane- and ubiquitin-binding domains. More specifically, ESCRT-0 consists of two subunits, namely Hrs and STAM1/2. The Hrs subunit contains a Fab1, YOTB, Vac 1, and EEA1 (FYVE) zinc finger domain, which anchors ESCRT-0 to PI(3)P on endosomal membranes (Mao *et al*, 2000; Raiborg *et al*, 2006). Moreover, Hrs and STAM1/2 associate with ubiquitin, which enables ESCRT-0 to bind to cargo-enriched endosomes (Henne *et al*, 2011). Since ESCRT-I only interacts with membranes through weak electrostatic interactions, ESCRT-I recruitment to membranes is ESCRT-0-dependent (Kostelansky *et al*, 2007). Here, the E2 variant domain (UEV) on TSG101 of the ESCRT-I complex interacts with the PTAP-like motif on Hrs of ESCRT-0 (Katzmann *et al*, 2003). Subsequently, ubiquitylated cargo is transferred from ESCRT-0 to ESCRT-I and ESCRT-II, both of which also contain UBDs and mediate inward budding of the MVB membrane to engulf cargo proteins (Lefebvre *et al*, 2018a). Deficiency or mutation of several ESCRT complex components, including TSG101, has been shown to lead to the accumulation of autophagosomes since downstream membrane fission events are impaired (Doyette *et al*, 2005).

1.6 Phagocytosis

TPL-2 expression is required for efficient killing of phagocytosed *C. rodentium* and quantitative proteomics showed that TPL-2 catalytic activity may regulate vesicle trafficking (Acuff *et al*, 2017b; Pattison *et al*, 2016). Furthermore, the ability of ABIN-2 to interact with ubiquitin and ESCRT-I raised the possibility that ABIN-2 may function as an adaptor protein during internalisation of bacteria. Therefore, a major aim of this thesis was to investigate the role of TPL-2 and ABIN-2 in phagocytosis.

Phagocytosis, defined as the engulfment of particles ≥ 0.5 μm, is a critical process of innate immune responses (Gordon, 2016). Phagocytes, including macrophages, DCs and neutrophils, are specialised innate immune cells, which internalise and kill

bacteria, fungi as well as viruses during infection (Chaplin, 2010). Phagocytosis is therefore an essential first line of defence against pathogenic invasion as well as a prerequisite for antigen presentation and mounting the adaptive immune response (Freeman & Grinstein, 2014). Phagocytosis, which is evolutionarily highly conserved, is not exclusively limited to innate immune cells as fibroblasts, epithelial and endothelial cells also perform phagocytosis to clear apoptotic cells, thereby maintaining tissue integrity and homeostasis (Flannagan *et al*, 2012; Boulais *et al*, 2010).

Following phagocytic engulfment, microorganisms are trapped with extracellular fluid in an intracellular vesicle, called the phagosome. Therefore, the lumen of a nascent phagosome is innocuous and undergoes dynamic changes, including numerous fusion and fission events with distinct compartments of the endocytic pathway, to become a highly degradative and microbicidal vacuole (Kinchen & Ravichandran, 2008). The dynamic conversion of the nascent phagosome into a hydrolytic, acidic and oxidative vacuole is referred to as phagosome maturation (Kinchen & Ravichandran, 2008; Pauwels *et al*, 2017). The process of phagocytosis can be subdivided into two distinct stages: phagosome formation, or phagocytic uptake, and phagosome maturation.

1.6.1 Phagosome formation

Initiation of phagocytic uptake requires recognition of the microorganism by receptors expressed on the surface of phagocytes. PRRs, in particular TLRs, on innate immune cells recognise conserved PAMPs such as carbohydrates, peptidoglycans or lipoproteins exposed on the surface of microbes (Flannagan *et al*, 2012). An additional class of PRRs recognising non-opsonised PAMPs are scavenger receptors (SRs). The class A scavenger receptor (SR-A) is a highly expressed phagocytic receptor on macrophages, which mediates internalisation of numerous bacterial pathogens, including *Staphylococcus aureus* and *Listeria monocytogenes* (Flannagan *et al*, 2009). SR-A, also called macrophage SR 1 (MSR1), recognises LPS from Gram-negative bacteria, lipoteichoic acid from the cell wall of Gram-

positive bacteria and CpG islands in bacterial DNA (Plüddemann *et al*, 2011; Peiser *et al*, 2000).

Phagocytic receptors on macrophages and other phagocytes also recognise opsonins, which are host factors that coat invading pathogens and mediate immune cell activation. Opsonins include IgG and numerous components of the complement system. IgG-coated microbes are recognised by Fcγ receptors (FcγRs), whereby the constant (Fc) region of antibodies binds to the extracellular domain of the FcγR (Rosales & Uribe-Querol, 2017; Anderson *et al*, 1990). Murine FcγR classes include FcγRI, FcγRII, FcγRIII, FcγRIV and FcγRIIB, which differ in receptor affinity towards IgG (Anderson *et al*, 1990). Alternatively, PRRs recognise PAMPs and initiate the complement system via the classical, lectin or alternative pathway (Flannagan *et al*, 2012; Vachon *et al*, 2007). Despite molecular differences between these complement pathways, all three cascades result in the formation of the complement protein fragment C3b, which binds and activates complement receptor 1 (CR1) on phagocytes. Moreover, C3b can be further cleaved into the opsonin C3bi, which activates CR3 (also called Mac-1) and CR4 (Ross *et al*, 1992).

Signalling pathways activated downstream of phagocytic receptors are stimulus- and receptor-dependent. The molecular cascades triggered in response to FcγR activation have been most extensively studied. IgG-coated pathogens mediate receptor clustering at the plasma membrane, which leads to phosphorylation of immunoreceptor tyrosine-based activation motifs (ITAMs) within the cytoplasmic tail of FcγR receptors (Griffin *et al*, 1975; Jones *et al*, 1985; Odin *et al*, 1991; Holowka *et al*, 2007). ITAM dual phosphorylation is catalysed by tyrosine kinases of the Src family (Hck, Lyn and Fgr), which triggers recruitment and activation of spleen tyrosine kinase (SYK) (Hamada *et al*, 1993; Gulle *et al*, 1998; Ghazizadeh *et al*, 1994). Two Src homology 2 (SH2) domains in SYK bind to the dually phosphorylated ITAMs in FcγRs, which facilitates SYK activation (Ghazizadeh *et al*, 1995; Johnson *et al*, 1995).

Linker of activated T cells (LAT), a transmembrane adaptor protein, is phosphorylated by SYK, which triggers recruitment of growth factor receptor-bound protein 2 (Grb2), an additional adaptor protein (Tridandapani *et al*, 2000; Zhang *et*

al, 1998). Grb2 in turn mediates the recruitment of the Grb2-associated binder (Gab2) (Yu *et al*, 2006). Gab2 is phosphorylated by Lyn and associates with p85, the regulatory subunit of class IA phosphoinositide 3-kinase (PI3K) (Gu *et al*, 2003). Gab2 mediates localisation of PI3K to its substrate phosphatidylinositol-4,5-bisphosphate [$PI(4,5)P_2$] at the membrane of the phagocytic cup. Subsequently, class IA PI3Ks generate phosphatidylinositol-3,4,5-trisphosphate [$PI(3,4,5)P_3$] from $PI(4,5)P_2$ (Gu *et al*, 2003). In addition, PI3K activation induces protein kinase B (PKB, also called AKT) signalling.

Increased levels of $PI(3,4,5)P_3$ lead to activation of Ras-related C3 botulinum toxin substrate (Rac) GTPases. SYK-mediated $PI(3,4,5)P_3$ signalling leads to pseudopod extension accompanied by actin polymerisation, a process driven by Rho family GTPases Rac1, Rac2 and the cell division control protein 42 (Cdc42) (Hoppe & Swanson, 2004; Caron & Hall, 1998). This involves Rho GTPase signalling activation of the multiprotein actin-related protein 2/3 (Arp2/3) complex, a major component of the actin cytoskeleton and mediator of actin polymerisation (Higgs & Pollard, 2000; May *et al*, 2000). $PI(3,4,5)P_3$ also contributes to phagosome formation by activating the actin-associated contractile protein myosin X. Myosin X facilitates pseudopod extension and closure of the phagosomal membrane to form the nascent phagosome (Cox *et al*, 2002; Mansfield *et al*, 2000). Upon FcγR clustering, phospholipase D (PLD) is recruited to the phagocytic cup and catalyses the formation of phosphatidic acid (PA), a lipid that mediates negative curvature of the phagosomal membrane to promote membrane fission during internalisation (Iyer *et al*, 2004; Corrotte *et al*, 2006).

1.6.2 Phagosome maturation

Following scission and sealing of the phagosome from the surface membrane, the nascent phagosome undergoes a highly orchestrated series of sequential fusions with early and late endosomes and ultimately with lysosomes to acquire microbicidal properties (Pauwels *et al*, 2017). Maturation of the phagosome causes the phagosomal lumen to become highly oxidative, hydrolytic and acidic, a milieu that drives effective bacterial degradation following internalisation (Kinchen &

Ravichandran, 2008) (Figure 9). The sequential maturation process from nascent phagosome to the terminal phagolysosome comprises three distinct stages, including the early phagosome, the late phagosome and the phagolysosome (Flannagan *et al*, 2009).

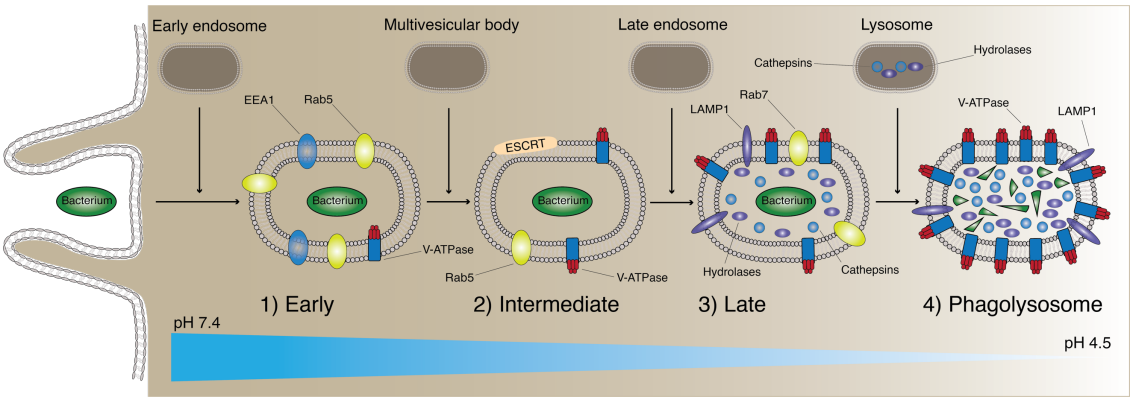

Figure 9 Phagosome maturation

Following internalisation of a bacterium, phagosomes undergo a sequential maturation process, which includes an early, intermediate and late maturation stage as well as the mature phagolysosome. As maturation proceeds, phagosomes interact with sub-components of the endocytic pathway, including multivesicular bodies, late endosomes and lysosomes. Early phagosomes acquire the early endosome antigen 1 (EEA1) and RAB5 GTPases. Multiprotein proton pumps, so called V-ATPases, are gradually acquired by phagosomes to decrease phagosomal pH, thereby restricting bacterial replication and activating pH-sensitive cathepsin proteases. ESCRT complexes are present during the intermediate maturation stage to facilitate multivesicular body formation and phagolysosomal fusion. Membranes of the late phagosome are characterised by the presence of lysosomal-associated membrane protein 1 (LAMP1) and RAB7 GTPases, both of which promote the formation of the highly acidic and hydrolytic phagolysosome.

1.6.2.1 Early phagosome

The early phagosome fuses with sorting and recycling endosomes, maintains a mildly acidic pH of 6.1 to 6.5 and its hydrolytic potential within the lumen remains low (Mukherjee *et al*, 1997). Composition of phagosomal membranes and its lumen is orchestrated by Rab GTPases (Stenmark, 2009), which switch between two states, an active GTP-bound state and an inactive GDP-bound state. Guanine nucleotide exchange factor (GEF) proteins promote GTP loading of Rab GTPases, thus facilitating formation of the active GTP-bound state. In contrast, GTPase-activating

proteins (GAPs) induce Rab GTPase activity, which leads to GTP hydrolysis and switching to the inactive GDP-bound state (Stenmark, 2009).

The Rab GTPase family comprises almost 70 related proteins. More than 20 Rab GTPases have been shown to localise to phagosomes, however, their respective molecular functions remain, in most cases, to be fully understood (Hu *et al*, 2019; Freeman & Grinstein, 2014). Fusion of phagosomes with early (sorting) endosomes involves acquisition of RAB5, a critical mediator of early phagosome trafficking and biogenesis (Zeigerer *et al*, 2012; Nielsen *et al*, 1999; Vieira *et al*, 2003a). Following phagocytic uptake of apoptotic cells, RAB5 is activated by the GEF proteins GAP and VPS9 domain-containing protein 1 (GAPVD1) as well as by rabaptin-5-associated exchange factor for RAB5 (Rabex-5) (Kitano *et al*, 2008). RAB22A GTPase facilitates recruitment of Rabex-5 to early phagosomes, thereby promoting RAB5 activation (Zhu *et al*, 2009). RAB10 localisation to phagosomes has been shown to precede RAB5 recruitment (Gutierrez, 2013; Cardoso *et al*, 2010). Moreover, RAB10-mediated re-shuttling of GPI-anchored proteins to the cell surface is required for effective phagosome remodelling (Cardoso *et al*, 2010).

Once recruited, RAB5 activity is essential for phagosome maturation as deficiency leads to maturation arrest and a constitutively active GTP-bound RAB5 mutant mediates formation of enlarged phagosomes (Duclos *et al*, 2000; Flannagan *et al*, 2012; Vieira *et al*, 2003a). RAB5 promotes maturation by interacting with the p150-vacuolar protein sorting 34 (VPS34) PI3K complex (Flannagan *et al*, 2009). p150 is a serine/threonine kinase, which associates with VPS34, a class III PI3K driving the production of phosphatidylinositol-3-phosphate [PI(3)P] from phosphatidylinositol on the phagosomal membrane (Vieira *et al*, 2001; Araki *et al*, 1996). PI(3)P anchors proteins containing a FYVE zinc finger domain to the cytosolic face of the phagosomal membrane (Fratti *et al*, 2001; Williams & Urbé, 2007). One such effector protein includes the early endosome antigen 1 (EEA1) (Christoforidis *et al*, 1999; Simonsen *et al*, 1998). Besides PI(3)P-mediated binding of EEA1 to the phagosome, EEA1 is also recruited to early phagosome via direct interactions with RAB5 (Mishra *et al*, 2010).

EEA1 mediates docking and fusion events with early endosomes and recruits syntaxin 13 (STX13), which is a soluble N-ethylmaleimide-sensitive fusion protein attachment protein receptor (SNARE) protein (McBride *et al*, 1999; Collins *et al*, 2002). STX13 is required for membrane fusion events with endosomes (Collins *et al*, 2002). SNARE proteins are important drivers of membrane fusion events, where a v-SNARE on the donating early endosomal membrane interacts with a t-SNARE on the recipient membrane of the nascent phagosome. Hairpin-like complexes between SNARE proteins bring fusing membranes into close proximity to facilitate vesicle maturation (Flannagan *et al*, 2012).

The dynamic maturation process of the early phagosome also involves the retrieval of phagosomal proteins to the plasma membrane (Driskell *et al*, 2007; Traer *et al*, 2007). Both RAB4 and RAB11 are involved in promoting the recycling pathway to the plasma membrane (Damiani *et al*, 2004; Lindsay *et al*, 2002; Cox *et al*, 2000). To shuttle membrane-associated cargo from the phagosome to other sites, inwards budding and pinching of the limiting phagosomal membrane results in the formation of an MVB-like compartment, which mediates cargo retrieval.

1.6.2.2 Late phagosome

As the early phagosome matures into the late phagosome, the luminal pH decreases to 5.5 to 6.0 (Flannagan *et al*, 2012). Phagosomal acidification is mediated by vacuolar ATPases (V-ATPases), which accumulate on the phagosomal membrane to pump protons from the cytosol into the lumen of the phagosome. V-ATPases are multimeric protein complexes, which hydrolyse ATP to transport H^+ ions across the phagosomal membrane (Kinchen & Ravichandran, 2008; Flannagan *et al*, 2009). V-ATPases are trafficked from the *trans*-Golgi to phagosomes and delivered by fusion with V-ATPase-containing endosomes (Vergne *et al*, 2004; Sturgill-Koszycki *et al*, 1994).

The vacuolar fusion protein Mon1 is recruited to early phagosomes and is responsible for recruitment of the key regulator RAB7 (Poteryaev *et al*, 2010; Kinchen & Ravichandran, 2010). Firstly, Mon1 localises the vacuolar fusion protein

CCZ1 to the phagosomal membrane, forming a Mon1/CCZ1 complex (Kinchen & Ravichandran, 2010). Mon1 disrupts binding of the RAB5 GEF protein Rabex-5 to the phagosomal membrane. This results in RAB5 inactivation and suppression of RAB5-mediated early maturation signalling events (Poteryaev *et al*, 2010). Moreover, CCZ1 interacts with RAB7 and disrupts binding of the GDP dissociation inhibitor (GDI) to RAB7, thereby facilitating RAB7 activation (Kinchen & Ravichandran, 2010).

Besides the Mon1/CCZ1 complex, the homotypic fusion and protein sorting (HOPS) complex contributes to RAB7 activation (Rink *et al*, 2005). The HOPS complex, comprising VPS21, VPS16, VPS18 and VPS33 subunits, associates with VPS41 and VPS39 at the phagosomal membrane. VPS39 is a GEF protein involved in RAB7 activation (Wurmser *et al*, 2000). Significantly, Mon1 directly interacts with HOPS subunits, thus mediating an interplay between Mon1/CCZ1 and HOPS complexes to drive RAB7 activation (Poteryaev *et al*, 2010).

Defects in RAB7 activation inhibit fusion of phagosomes with lysosomes and prevent phagosomal acidification (Harrison *et al*, 2003). RAB7 concentrates effector proteins, including RAB7-interacting lysosomal protein (RILP) and oxysterol-binding protein-related protein 1 (ORPL1), at the membrane of late phagosomes (Johansson *et al*, 2007; Cantalupo *et al*, 2001). Both RILP and ORPL1 promote dynein-driven microtubule-mediated transport (Johansson *et al*, 2007). Transport of phagosomes to the perinuclear region is essential for fusion of late phagosomes with lysosomes (Vieira *et al*, 2003a). Besides Mon1/CCZ1 complex-dependent RAB7 recruitment, lysosome-associated membrane protein 1 (LAMP1) and LAMP2 are membrane proteins of lysosomes, late phagosomes as well as endosomes, which promote RAB7 recruitment (Huynh *et al*, 2007; Binker *et al*, 2007).

ILV formation during the intermediate to late phagosome maturation stage is critical to retrieve and dispose of redundant membrane components. By inward budding, ILVs form within the lumen of the late phagosome (Fader & Colombo, 2009; Manil-Segalén *et al*, 2015; Flannagan *et al*, 2012). Lysobisphosphatidic acid (LBPA) is a lipid, which is present on late endosomes and phagosomes. The ESCRT-I accessory protein ALIX binds to LBPA, thereby linking ESCRT-I, ESCRT-II, and ESCRT-III complexes to promote inward budding from the phagosomal membrane (Odorizzi,

2006). Moreover, PI(3)P facilitates anchoring of multiple ESCRT proteins to the phagosomal membrane, thereby contributing to ILV formation (Schmidt & Teis, 2012). Both ESCRT-I and ESCRT-II drive invagination of the phagosomal membrane to form ILVs, while ESCRT-III induces membrane scission, which releases ILVs from the membrane (Hanson *et al*, 2008; Muzioł *et al*, 2006). The FYVE finger-containing phosphoinositide kinase PIP5K3 (PIKfyve kinase) binds and phosphorylates PI(3)P on the phagosomal membrane, thus converting PI(3)P to phosphatidylinositol-(3,5)-bisphosphate [PI(3,5)P_2] (Zolov *et al*, 2012). The VPS24 subunit of ESCRT-III interacts with PI(3,5)P_2, thereby mediating ESCRT-III recruitment to the phagosome to drive ILV scission (Whitley *et al*, 2003).

While RAB7 has important roles in phagosome maturation during the late stages, other Rab GTPases have also been implicated in late phagosome maturation. Loss of RAB20, RAB22B, RAB32, RAB34, RAB38 or RAB43 activity prevents cathepsin D localisation to phagosomes (Seto *et al*, 2011). Since RAB22B, RAB32, RAB34 and RAB38 are Golgi-associated Rab GTPases, it has been hypothesised that these Rab GTPases do not only directly promote maturation of late phagosomes, but also indirectly by facilitating pro-cathepsin D delivery to lysosomes, which ultimately fuse with late phagosomes (Seto *et al*, 2011; Ng *et al*, 2007; Wasmeier *et al*, 2006; Wang & Hong, 2002).

1.6.2.3 Phagolysosome

The phagolysosome refers to the mature phagosome, which results from fusion of late phagosomes with lysosomes. The phagolysosome is the highly microbicidal and degradative vacuole, which efficiently digests and kills internalised pathogens (Kinchen & Ravichandran, 2008; Flannagan *et al*, 2009). Phagolysosomal fusion is mediated by the assembly of the SNARE complex, which comprises syntaxin 7 (STX7) and vesicle-associated membrane protein 7 (VAMP7) (Griffin *et al*, 1975; Tsai & Discher, 2008). STX7, a t-SNARE, on the phagosomal membrane interacts with VAMP7, a v-SNARE, on the lysosomal membrane to induce vesicle fusion. As phagosomes mature into phagolysosomes, PI(3)P and LBPA levels decrease (Gillooly *et al*, 2000; Kobayashi *et al*, 1998). By fusion with lysosomes, the luminal

pH of the phagolysosome decreases to 4.5 to 5.0 and becomes highly enriched in active cathepsins (Flannagan *et al*, 2012). Acidification is critical for the optimal catalytic activity of lysosomal hydrolases, such as cathepsins. Besides phagosome acidification and acquisition of hydrolytic enzymes, the phagolysosome is enriched in reactive oxygen and nitrogen species as well as in a diverse repertoire of antimicrobial proteins (Flannagan *et al*, 2009, 2012; Kinchen & Ravichandran, 2008).

1.6.3 Phagosome acidification

Acidification of the phagosome continuously occurs throughout the maturation process by acquisition of V-ATPases and is further driven by membrane fusion with highly acidic lysosomes (Lukacs *et al*, 1990, 1991). Phagosomal acidification is mediated V-ATPases, which accumulate on the phagosomal membrane as the phagosome matures (Kinchen & Ravichandran, 2008). Since phagosomes have minimal passive proton permeability, which prevents H^+ ion efflux from the phagosomal lumen, V-ATPases can rapidly increase the H^+ ion concentration within the maturing phagosome.

The V-ATPase is a high molecular weight protein complex, comprising two multiprotein V_0 and V_1 subcomplexes. The V_1 complex is located in the cytosol and consists of eight distinct proteins, which drive ATP hydrolysis (Marshansky & Futai, 2008; Flannagan *et al*, 2012). The V_0 complex is located in the phagosomal membrane and assembles the pore, which enables proton transport into the phagosomal lumen (Marshansky & Futai, 2008). To maintain a physiological ion potential across the phagosomal membrane despite rapid H^+ ion influx, additional ion transporters shuttle chloride anions into the phagolysosome and potassium as well as sodium cations into the cytosol (Steinberg *et al*, 2010; Graves *et al*, 2008).

Acidification facilitates the microbicidal properties of the phagolysosome in multiple ways. Firstly, acidification activates pH-dependent proteolytic enzymes, including cathepsin D and cathepsin L (Turk *et al*, 2000, 1993). Secondly, low pH directly blocks pathogen replication by interfering with enzymes and structural components of microbes (Flannagan *et al*, 2009; Kinchen & Ravichandran, 2008). Moreover,

phagosome acidification activates natural resistance-associated macrophage protein 1 (NRAMP1), which is a divalent metal ion transporter. The electrochemical gradient resulting from V-ATPase-mediated proton influx into the phagosome provides a source of energy for NRAMP1 to transport metal ions from the lumen into the cytosol (Jabado *et al*, 2000). These metal ions are critical co-factors for the life cycle of bacteria, and thus metal deprivation restricts bacterial growth (Flannagan *et al*, 2012). Lastly, acidification also leads to increased production of anti-microbial ROS (Winterbourn, 2008; DeCoursey, 2010). Importantly, the degree of phagosomal acidification is cell type-specific. While phagosomes in macrophages become strongly acidic to maximise pathogen killing, the pH of phagosomes in DCs only decreases to approximately 6.0 (Flannagan *et al*, 2012; Kinchen & Ravichandran, 2008). This limits phagosomal proteolysis and increases the ability of DCs to present antigen fragments on MHC molecules. In addition, phagosomal pH in neutrophils is more alkaline than in macrophages as preformed cytoplasmic granules are rapidly delivered to form non-acidic phagosomes (Foote *et al*, 2019; Nordenfelt & Tapper, 2011).

1.6.4 Reactive oxygen and nitrogen species

ROS production by the NADPH oxidase (NOX2) in phagolysosomes is critical for killing invading microbes. NOX2 is a multiprotein complex, which drives the production of superoxide anions (O_2^-) by transferring electrons from nicotinamide adenine dinucleotide phosphate (NADPH) onto molecular oxygen (Babior, 2004). NOX2 is located in the phagosomal membrane and comprises transmembrane proteins $gp91^{phox}$ and $gp22^{phox}$, which form the flavocytochrome b_{558}. In addition, NOX2 consists of cytosolic proteins $p40^{phox}$, $p47^{phox}$ and $p67^{phox}$ (Rybicka *et al*, 2010; Savina *et al*, 2006; Mantegazza *et al*, 2008). Upon NOX2 activation by pro-inflammatory stimuli, the cytosolic proteins interact with the small GTPases Rac1 and Rac2, thus mediating the assembly with flavocytochrome b_{558} (Hordijk, 2006). The intact NOX2 complex transports electrons across the phagosomal membrane into the lumen of the phagolysosome to generate O_2^-. While the resulting O_2^- is cytotoxic, it is rapidly converted into hydrogen peroxide (H_2O_2), which is highly microbicidal and can lead to further downstream generation of highly toxic hydroxyl radicals

(Flannagan *et al*, 2012; Babior, 2004). In addition, H_2O_2 can be used by the phagolysosomal myeloperoxidase to drive enzymatic conversion of chloride ions into hypochlorous acid, which is highly toxic to engulfed microbes (Winterbourn, 2008). PI(3)P production by VPS34 class III PI3K is required for $p40^{phox}$ activity at the phagosomal membrane (Anderson *et al*, 2010).

In addition to ROS, reactive nitrogen intermediates (RNI) contribute to the microbicidal milieu in phagolysosomes (Serbina *et al*, 2003). Nitrous oxide synthase 2, also referred to as iNOS, drives the formation of nitrous oxides (NO), an important class of RNI (Förstermann & Sessa, 2012). While ROS production requires the assembly of existing protein subunits, RNI production requires expression of iNOS (*Nos2* gene), which is induced by pro-inflammatory signals downstream of MAP kinase, NF-κB and Janus-activated kinase-signal transducer and activator of transcription (JAK-STAT) signalling cascades (Pautz *et al*, 2010; Chen *et al*, 1999; Martin *et al*, 1994). Functional iNOS exists in a homodimer, which contains an N-terminal oxygenase domain for substrate interaction with L-arginine and a C-terminal domain with reductase activity, which binds to the electron donor NADPH (Tzeng *et al*, 1995; Aktan, 2004). iNOS transfers electrons from NADPH to subsequently oxidise L-arginine, thus resulting in NO generation. NO generation occurs at the cytosolic side of the phagosomal membrane-bound iNOS (Aktan, 2004). Following oxidation, NO diffuses into the phagolysosomal lumen, where it reacts with ROS to yield a number of microbicidal RNIs, including peroxynitrite.

The interplay between ROS and RNI is critical to create a highly toxic phagosomal lumen for invading pathogens (Flannagan *et al*, 2012). More specifically, NO and ROS frequently interact with metabolic processes, including the respiratory chain of many microbes to inhibit ATP synthesis, and induce DNA damage by oxidation to cause instability within the microbial genome (Mastroeni *et al*, 2000; Chakravortty & Hensel, 2003).

1.6.5 Antimicrobial peptides and enzymes

A plethora of antimicrobial factors in mature phagosomes either directly digest invading microbes or indirectly interfere with the life cycle and metabolic machinery of pathogens (Flannagan *et al*, 2009). Iron is a metal cofactor critical for bacterial DNA replication. Lactoferrin, an iron-binding protein, is present in phagosomes to capture iron, thus blocking its acquisition by engulfed bacteria (Molloy & Winterbourn, 1990; Jenssen & Hancock, 2009). In addition, as previously mentioned, NRAMP1 is an ion transporter, which transports zinc and manganese ions into the cytosol (Jabado *et al*, 2000). NRAMP1 is acquired by phagosomes upon fusion with endosomes and lysosomes. Zinc and manganese ions are important nutrients for bacterial growth and thus metal ion deprivation restricts bacterial replication (Searle *et al*, 1998; Gruenheid *et al*, 1997). An important digestive enzyme, which directly targets microbes for destruction, includes lysozyme. Lysozyme is a glycoside hydrolase, which breaks down the peptidoglycan layer in Gram-positive bacteria (Ganz, 2004; Miyauchi *et al*, 1985). While Gram-negative bacteria are protected against lysozyme-mediated hydrolysis of the outer peptidoglycan layer, cationic antimicrobial peptides (CAPs) in the phagosome provide microbicidal activity against these bacterial strains (Risso, 2000). CAPs include defensins, which are cysteine-rich cationic antimicrobial peptides penetrating the outer membrane of Gram-negative bacteria (Diamond *et al*, 2009; Arnett *et al*, 2011). The cationic properties of CAPs induce ion diffusion from the microbe into the phagosomal lumen upon pore formation (Zhang *et al*, 2010).

In a mature phagolysosome, more than 50 lysosomal hydrolases maintain a highly microbicidal environment. Antimicrobial lysosomal enzymes broadly include phosphatases, glycosidases, lipases, proteases as well as nucleases. Cathepsins are lysosomal proteases, which include cysteine proteases (cathepsins B, C, F, H, K, L, O, S, V, X and W), aspartate proteases (cathepsins D and E), as well as serine proteases (cathepsins A and G) (Flannagan *et al*, 2009, 2012). Proteolytic activity of cathepsins is induced by decreasing pH and as the maturing phagosome fuses with endosomes and lysosomes, it continuously acquires increasing levels of cathepsins. The NADPH oxidase NOX2 negatively regulates phagosomal proteolysis by cathepsins in a pH-independent manner and independently of cathepsin delivery to

the phagosome (Rybicka *et al*, 2012). More specifically, NOX2 oxidises cysteine cathepsins, which results in their inactivation. This regulatory mechanism illustrates the interplay between local redox states within the phagosomal lumen and hydrolase activity (Rybicka *et al*, 2010).

1.7 Thesis Aims

Prior to this thesis, a study by the Ley laboratory demonstrated that TPL-2 catalytic activity promotes phosphorylation of several proteins implicated in endocytosis, vesicle trafficking and GTPase signalling (Pattison *et al*, 2016). Although the regulation of gene expression during innate immune responses by TPL-2 had been extensively studied, the role of TPL-2 in regulating intracellular trafficking had not been investigated (Gantke *et al*, 2011a; Xu *et al*, 2018). Despite the discovery that ABIN-2 forms a ternary complex with TPL-2 and NF-κB1 p105 almost two decades ago, the physiological role of ABIN-2 in innate immune signalling had remained uncharacterised (Lang *et al*, 2004).

In the third chapter, I set out to biochemically characterise point mutations in ABIN-2, which disrupt the association with its binding partners A20, ubiquitin and TSG101. To elucidate the biological roles of ABIN-2, it was a prerequisite to study whether individual ABIN-2 point mutations disrupt interactions with its other known binding partners. Moreover, I intended to investigate whether ubiquitin or A20 binding to ABIN-2 regulate innate immune signalling, in particular TLR4 and TNF receptor-mediated pathways.

In the fourth chapter, I aimed to explore whether TPL-2 or ABIN-2 regulate phagosome maturation in primary macrophages. I used a combination of fluorescence-based bead assays, phagosome proteomics, phosphoproteomics and confocal microscopy to characterise the regulatory roles of TPL-2 catalytic activity and ABIN-2 ubiquitin binding in phagosome maturation.

In the fifth chapter, I focused on the regulation of bacterial killing in macrophages by TPL-2 catalytic activity and ABIN-2 ubiquitin binding. I investigated a diverse set of bacterial species, including *Staphylococcus aureus*, *Citrobacter rodentium* and *Salmonella typhimurium*. I decided to focus on *S. aureus* to study in detail how TPL-2 catalytic activity and ABIN-2 ubiquitin binding regulate the maturation of bacteria-containing phagosomes.

Chapter 2. Materials & Methods

2.1 Materials

2.1.1 Chemicals

Albumin, ammonium bicarbonate, ammonium persulfate (APS), ampicillin, aprotinin, β-glycerophosphate, bafilomycin A1, bovine serum albumin (BSA), cyanamide, dithiothreitol (DTT), ethanol, Fluoromount™ Aqueous Mounting Medium, foetal bovine serum (FBS), formic acid, gelatin from cold water fish skin, gentamicin, glycerol, glycine, HPLC Grade water, hydrogen peroxide, hydroxylamine, imidazole, iodoacetamide, L-glutamine-penicillin-streptomycin (PSG), leupeptin, M2 Anti-FLAG Affinity Gel, N-Ethylmaleimide (NEM), NP-40, okadaic acid, phenylmethylsulfonyl fluoride (PMSF), phosphoric acid, potassium chloride, RPMI-1640 medium, sodium azide, sodium borate, sodium borohydride, sodium deoxycholate, sodium dodecyl sulfate (SDS), sodium fluoride, sodium orthovanadate, sodium pyrophosphate, sodium pyruvate, sterile-filtered Ethylenediaminetetraacetic acid (EDTA), sucrose, sulphuric acid, super optimal broth with catabolite repression (SOC) medium, triethylammonium bicarbonate (TEAB), Triton X-100, trypan blue, trypsin-EDTA solution, Tween-20 and urea were obtained from Sigma-Aldrich. 4′,6-diamidino-2-phenylindole (DAPI) stain, β-mercaptoethanol (β-ME), Bioscience™ IC fixation buffer, cytochalasin D, DQ Green BSA, Dulbecco's Modified Eagle Medium (DMEM), High-Select Fe-NTA phosphopeptide enrichment kit, High-Select TiO2 phosphopeptide enrichment kit, HPLC Grade triethylamine, LC/MS Grade acetic acid, LC/MS Grade acetonitrile, LC/MS Grade Optima water, LC/MS Grade trifluoroacetic acid (TFA), LysoTracker Red DND-99, Pierce High pH Reversed-Phase Peptide Fractionation Kit, Pierce Protease and Phosphatase Inhibitor Mini Tablets, Pierce™ Coomassie Protein Assay Kit, Qiagen EndoFree Plasmid Maxi Kit, Qiagen RNase-free DNase set and Qiagen RNeasy Mini Kits were purchased from Thermo Fisher Scientific. Magic Red cathepsin L substrate, Precision Plus Protein™ Dual Colour marker, polyvinylidene difluoride (PVDF) membranes, tetramethylethylenediamine (TEMED) and Tris/Glycine/SDS running buffer were from Bio-Rad Laboratories. EDTA solution, ethylene glycol tetraacetic acid (EGTA) solution, Luria Bertani (LB) medium, sodium chloride solution, Tris/HCl pH 7.5 solution and L929 cell supernatant were provided

by the Media Preparation and Cell Services STP at The Francis Crick Institute. 10% Bis-Tris NuPAGE gels, 4-12% Bis-Tris NuPAGE gradient gels, 3-(N-morpholino)propanesulfonic acid (MOPS) SDS running buffer and SuperScript VILO cDNA Synthesis Kits were purchased from Invitrogen. ECL Western Blotting Detection Reagent, Ficoll Paque Plus and glutathione Sepharose 4B resin were from GE Healthcare. BCA Protein Assay Kit, MS-grade porcine trypsin and tris(2-carboxyethyl)phosphine (TCEP) were obtained from Pierce. Lipopolysaccharides (LPS) and purified M1-linked (2, 4, 8) polyubiquitin chains were from Enzo Life Sciences. Akti-1/2 inhibitor and reactive oxygen species (ROS) Deep Red dye were purchased from Abcam. Mouse GM-CSF and tumour necrosis factor α (TNFα) were from Peprotech. Dulbecco's phosphate-buffered saline (DPBS) and *E. coli* DH5α cells were obtained from Life Technologies. AZD8055 inhibitor and VX-745 inhibitor were from Selleckchem. 4-(2-hydroxyethyl)-1-piperazineethanesulfonic acid (HEPES) was from BioWhittaker. Acrylamide ProtoGel 30% solution was from National Diagnostics. Avidin was purchased from Callbiochem. C34 inhibitor was synthesised by Medchem Express. Carboxylated silica beads were obtained from Kisker Biotech. CD14 MicroBeads were from MACS Miltenyi Biotec. cOmplete Mini EDTA-free Protease Inhibitor Cocktail tablets were obtained from Roche. Dimethyl sulfoxide (DMSO) was from Fisher Chemical. Dried milk powder was from Marvel. Human GM-CSF was purchased from STEMCELL Technologies. Immobilon Western Chemiluminescent HRP Substrate was from Millipore. Latex beads were obtained from Estapor Merck Chimie SAS. Lysyl endopeptidase (LysC) was from FUJIFILM Wako Pure Chemical Corporation. Nuclease-free water was from Ambion. Pam_3CSK_4 was obtained from InvivoGen. PD0325901 inhibitor was synthesised by the DSTT. siRNA buffer was from Horizon Discovery. TaqMan Universal PCR Master Mix was purchased from Applied Biosystems. Viromer Green was obtained from Lipocalyx.

2.1.2 Antibodies

Commercial and custom-made antibodies for immunoblotting that were raised against unmodified peptides were diluted in blocking buffer supplemented with 0.01% (w/v) sodium azide. Antibodies raised against phospho-peptides were diluted in 5% (w/v) BSA in PBST (Table 8) containing 0.01% (w/v) sodium azide. Membranes were incubated with antibody solutions overnight at 4°C. Secondary antibodies for immunoblotting were diluted in blocking buffer (Table 8) and incubated with membranes for 1h at room temperature (RT).

Table 1 Commercial primary antibodies for immunoblotting

Antibody	Working dilution	Catalogue number	Source
3xFLAG (M2)	1:1000	F1804	Sigma-Aldrich
A20 (D13H3)	1:1000	5630	Cell Signaling Technology
Actin (C-11)	1:1000	sc-1615	Santa Cruz Biotechnology
AKT	1:1000	9272	Cell Signaling Technology
EEA1 (Clone 14)	1:1000	610457	BD Biosciences
ERK1/2	1:1000	9102	Cell Signaling Technology
GSDMD	1:1000	G7422	Sigma-Aldrich
GST	1:1000	A7340	Sigma-Aldrich
HA (3F10)	1:1000	11867423001	Roche
His_6 (HIS-1)	1:2000	A7058	Sigma-Aldrich
HSP90 (H-114)	1:1000	sc-7947	Santa Cruz Biotechnology
IkB-α (C-21)	1:1000	sc-371	Santa Cruz Biotechnology
K63 Ubiquitin (HWA4C4)	1:1000	05-1313	Merck
K63 Ubiquitin (D7A11)	1:1000	5621	Cell Signaling Technology
LAMP1 (1D4B)	1:1000	AB_528127	DSHB
M1 Ubiquitin (LUB9)	1:1000	MABS451	Merck

p-4EBP1 (T37/46)	1:1000	9459	Cell Signaling Technology
p-Akt (S473 site)	1:1000	9271L	Cell Signaling Technology
p-Akt (T308) (L32A4)	1:1000	5106	Cell Signaling Technology
p-eIF2A (S52)	1:1000	44-728G	Invitrogen
p-eIF4B (S422)	1:1000	3591	Cell Signaling Technology
p-ERK1/2 (T202/Y204)	1:1000	9101	Cell Signaling Technology
p-FOXO1 (T24)/p-FOXO3a (T32)	1:1000	9464	Cell Signaling Technology
p-JNK1/2 (T183/Y185)	1:1000	44-682G	Invitrogen
p-p105 (S933) (18E6)	1:1000	4806	Cell Signaling Technology
p-p38 (T180/Y182) (D3F9)	1:1000	4511	Cell Signaling Technology
p-p70 S6 kinase (T389) (108D2)	1:1000	9234	Cell Signaling Technology
p-p70S6K (T421/S424)	1:1000	9204	Cell Signaling Technology
p-S6 (S240/244)	1:1000	2215	Cell Signaling Technology
p-STAT1 (Y701) (58D6)	1:1000	9167	Cell Signaling Technology
p-STAT3 (Y705)	1:1000	9131	Cell Signaling Technology
p105	1:1000	4717	Cell Signaling Technology
RAB5 (C8B1)	1:1000	3547	Cell Signaling Technology
SHIP1 (D1163)	1:1000	2728	Cell Signaling Technology
STAT1	1:1000	9172	Cell Signaling Technology

TPL-2 (M-20)	1:1000	sc-720	Santa Cruz Biotechnology
TSG101 (C-2)	1:1000	sc-7964	Santa Cruz Biotechnology
Ubiquitin	1:1000	3933	Cell Signaling Technology
Vimentin (H5)	1 µg/ml	AB_528506	DSHB

Table 2 Custom-made primary antibodies for immunoblotting

Antibody	Working dilution	Catalogue number	Source
ABIN-1	1 µg/ml	S010C (Bleed 3)	DSTT
ABIN-2	1 µg/ml	4934	Harlan Sprague Dawley Inc.
p-DMXL1 (S1903)	1 µg/ml	DA048 (Bleed 2)	DSTT

Table 3 Secondary antibodies for immunoblotting

Antibody	Working dilution	Catalogue number	Source
Goat anti-rabbit IgG(H+L)	1:5000	4050-05	SouthernBiotech
Rabbit anti-sheep IgG(H+L)	1:5000	6156-05	SouthernBiotech
Goat anti-mouse IgG(H+L)	1:5000	1010-05	SouthernBiotech
Rabbit anti-goat IgG(H+L)	1:5000	6164-05	SouthernBiotech
Goat anti-rat IgG(H+L)	1:5000	3051-05	SouthernBiotech
Goat anti-chicken IgY(H+L)	1:5000	6100-05	SouthernBiotech

Table 4 Primary antibodies for immunofluorescence

Antibody	Working dilution	Catalogue number	Source
EEA1 (C-14)	1:200	610457	BD Biosciences
LAMP1 (1D4B)	1:200	AB_528127	DSHB
Ubiquitin	1:200	3933	Cell Signaling Technology

Table 5 Secondary antibodies for immunofluorescence

Antibody	Working dilution	Catalogue number	Source
Alexa Fluor 594 anti-rat	1:1000	A-11007	Thermo Fisher Scientific
Alexa Fluor 647 anti-rabbit	1:1000	A-21245	Thermo Fisher Scientific
Alexa Fluor 647 anti-mouse	1:1000	A-21235	Thermo Fisher Scientific

Table 6 Primary FACS antibodies

Molecular target & conjugate	Working dilution	Catalogue number	Source
CD14 APC	1:200	17-0141-81	eBioscience
α-human CD14 APC	1:200	561383	BD Biosciences
F4/80 Pacific Blue	1:200	123124	BioLegend

2.1.3 Proteins

GST-fusion proteins (Table 7) were expressed and purified by the Division of Signal Transduction Therapy (DSTT) Protein Production Team at the University of Dundee, led by Dr James C. Hastie. Protein sequences and purity were confirmed by mass spectrometry and SDS-PAGE.

Table 7 Proteins

Protein	Species	ID	Source
GST-ABIN-2	Human	DU3714	DSTT
GST-ABIN-2 Y230A	Human	DU63999	DSTT
GST-ABIN-2 E255K	Human	DU56529	DSTT
GST-ABIN-2 D309N	Human	DU8638	DSTT
3xFLAG-TNF	Human	N/A	Professor Henning Walczak (University College London)

2.1.4 Mice

All mice in this study were bred and maintained under specific pathogen-free conditions at The Francis Crick Institute. All experiments were performed in full compliance with UK Home Office regulations and under a project license to Professor Steven C. Ley (Ley 70/8819). Mouse strains used in this thesis were maintained as homozygous lines and were all fully backcrossed on to a C57BL/6Jax background (The Jackson Laboratory). C57BL/6Jax mice were used as WT controls throughout this study.

For the purpose of clarity protein rather than gene names of TPL-2 (*Map3k8*) and ABIN-2 (*Tnip2*) were used for mouse nomenclature throughout this thesis. In addition, homozygous *Nfkb1*^{S930A,S935A} knock-in mice were referred to as *Nfkb1*$^{SSAA/SSAA}$ mice. *Tpl2*$^{D270A/D270A}$ (Sriskantharajah *et al*, 2014), *Nfkb1*$^{SSAA/SSAA}$ (Sriskantharajah *et al*, 2009), *Abin2*$^{-/-}$ (Papoutsopoulou *et al*, 2006) and *Abin2*$^{E256K/E256K}$ (Ventura *et al*, 2018) mice were generated by the Ley laboratory and have previously been described. *Tpl2*$^{D270A/D270A}$ and *Nfkb1*$^{SSAA/SSAA}$ mice were crossed and bred to homozygosity to generate compound knock-in *Nfkb1*$^{SSAA/SSAA}$ *Tpl2*$^{D270A/D270A}$ mice. *Abin2*$^{D310N/D310N}$ mice (Nanda *et al*, 2018) were generated and kindly provided by Professor Sir Philip Cohen (MRC Protein Phosphorylation and Ubiquitylation Unit, University of Dundee). *Abin2*$^{D310N/D310N}$ mice were fully backcrossed on to C57BL/6Jax mice at The Francis Crick Institute. *Abin2*$^{Y231A/Y231A}$ mice were generated by the Genetic Modification Service (GeMS) at The Francis Crick Institute. Using CRISPR/Cas9 gene editing technology the point mutation was introduced into the C57BL/6Jax background via zygote injection. *Tpl2*$^{3xFLAG/3xFLAG}$ mice were generated by the Ley laboratory. A gene targeting construct was created by Gene Bridges GmbH (Heidelberg, Germany). This construct was used to target the endogenous TPL-2, *Map3k8*, locus to insert a 3xFLAG sequence with an adjacent GGGS linker after the ATG start codon in exon 2 and upstream the TPL-2 coding sequence. Therefore, *Tpl2*$^{3xFLAG/3xFLAG}$ mice express N-terminally 3xFLAG-tagged TPL-2.

2.1.5 Buffers

Table 8 Buffers

Buffer	Composition
Lysis Buffer	Unless otherwise stated this lysis buffer was used for lysis of mammalian cells. 50 mM Tris/HCl pH 7.5, 150 mM sodium chloride, 1% (v/v) Triton X-100, 10 mM sodium fluoride, 1 mM sodium pyrophosphate, 10 mM β-glycerophosphate, 2 mM EDTA, 100 µM sodium orthovanadate, 10% (v/v) glycerol, supplemented with one EDTA-free protease inhibitor cocktail tablet per 10 ml lysis buffer. If ubiquitin chains were examined 100 mM iodoacetamide was added
Phosphoproteome lysis buffer	8 M urea, 50 mM HEPES pH 8.2, 10 mM β-glycerophosphate, 50 mM sodium fluoride, 5 mM sodium pyrophosphate, 1 mM EDTA, 1 mM sodium orthovanadate, 1 mM DTT, 1 mM phenylmethylsulfonyl fluoride, 1 µg/ml aprotinin, 1 µg/ml leupeptin, 100 nM okadaic acid
RIPA lysis buffer	20 mM Tris/HCl pH 7.5, 150 mm sodium chloride, 1 mM EDTA, 1 mM EGTA, 1% (v/v) NP-40, 0.5% (w/v) sodium deoxycholate, 0.1% (w/v) SDS, supplemented with one EDTA-free protease inhibitor cocktail tablet per 10 ml lysis buffer
MEF lysis buffer	30 mM Tris/HCl pH 7.4, 120 mM sodium chloride, 2 mM EDTA, 2 mM potassium chloride, 1% (v/v) Triton X-100, supplemented with one EDTA-free protease inhibitor cocktail tablet per 10 ml lysis buffer
Separating gel buffer	10% (w/v) acrylamide ProtoGel, 0.1% (w/v) ammonium persulfate, 0.1% (v/v) TEMED, 375 mM Tris/HCl pH 8.8, 0.4% (w/v) SDS. Ammonium persulfate and TEMED, which initiate gel solidification, were added last

Stacking gel buffer	4% (w/v) acrylamide ProtoGel, 0.1% (w/v) ammonium persulfate, 0.1% (v/v) TEMED, 125 mM Tris/HCl pH 6.8, 0.1% (w/v) SDS
MOPS SDS running buffer	50 mM MOPS, 50 mM Tris base pH 7.7, 0.1% (w/v) SDS, 1 mM EDTA
Tris/Glycine/SDS running buffer	25 mM Tris base pH 8.3, 192 mM glycine, 0.1% (w/v) SDS
Phosphate-buffered saline	137 mM NaCl, 8.1 mM Na_2HPO_4, 2.7 mM KCl, 1.5 mM KH_2PO_4, pH 7.4
Ubiquitin binding buffer	50 mM Tris/HCl pH 7.5, 150 mM NaCl, 5 mM DTT, 0.1% (v/v) NP-40
Bead assay buffer	DPBS, 5% (v/v) FBS
PBST buffer	PBS, 0.05% (v/v) Tween-20
Blocking buffer	PBS, 0.05% (v/v) Tween-20, 5% (w/v) dried milk powder
Glycine elution buffer	200 mM glycine, 0.05% (v/v) NP-40, pH 2.5
Sample buffer (5X)	250 mM Tris/HCl pH 6.8, 32.5% (v/v) glycerol, 5% (w/v) SDS, 5% (v/v) β-ME
FACS buffer	PBS, 0.1% BSA (w/v)
Hypotonic buffer	250 mM sucrose, 3 mM imidazole pH 7.4, Pierce Protease and Phosphatase Inhibitor Mini Tablets (Thermo Fisher Scientific)
S-Trap binding buffer	90% (v/v) methanol, 100 mM TEAB pH 7.1
LC-MS/MS infection buffer	3% (v/v) DMSO, 0.1% (v/v) formic acid, in HPLC-grade water
LC-MS/MS elution buffer	80% (v/v) HPLC-grade acetonitrile, 3% (v/v) DMSO, 0.1% (v/v) formic acid, in HPLC-grade water
IP-MS buffer A	5% (v/v) DMSO, 0.1% (v/v) formic acid, in HPLC-grade water
IP-MS buffer B	80% (v/v) HPLC-grade acetonitrile, 5% (v/v) DMSO, 0.1% (v/v) formic acid, in HPLC-grade water
CD14 selection buffer	PBS, 0.5% BSA (w/v), 2 mM EDTA

Lysis buffer components

Sodium fluoride, sodium pyrophosphate, okadaic acid and β-glycerophosphate inhibit serine threonine phosphatases. Sodium orthovanadate was used to inactivate

tyrosine phosphatases. EDTA mediates chelation of magnesium and manganese ions resulting in inactivation of protein kinases, while EGTA chelates calcium ions to inactivate calmodulin-dependent protein kinases. A protease inhibitor cocktail (Roche) and phenylmethylsulfonyl fluoride were used to block activity of serine and cysteine proteases. Aprotinin inhibits trypsin and closely related proteases, including chymotrypsin and plasmin. Leupeptin specifically inactivates lysosomal proteases. If ubiquitin chains were studied, iodoacetamide was used to inhibit cysteine peptidases. DTT is a reducing agent that prevents formation of disulphide bonds between cysteine residues.

2.2 Methods

2.2.1 Mammalian cell culture

Mammalian cell culture procedures were performed under aseptic conditions strictly following biological safety regulations. Primary cells and immortalised cell lines were cultured in the appropriate growth medium (Table 9) at 37°C with 5% CO_2 to maintain neutral pH. High humidity of 85-95% to prevent evaporation of growth medium was maintained by a humidity reservoir.

Table 9 Cell culture growth media

Culture medium	Composition
BMDM differentiation medium	RPMI-1640 medium commercially supplemented with L-glutamine and sodium bicarbonate, 10% (v/v) FBS, 10 mM HEPES, 1 mM sodium pyruvate, 100 U/ml penicillin, 100 µg/ml streptomycin, 2 mM L-glutamine, 50 µM β-ME and 20% (v/v) L929 cell supernatant containing M-CSF (provided by The Francis Crick Institute Cell Services)
BMDM seeding medium	RPMI-1640 medium commercially supplemented with L-glutamine and sodium bicarbonate, 10% (v/v) FBS, 10 mM HEPES, 1 mM sodium pyruvate, 100 U/ml penicillin, 100 µg/ml streptomycin, 2 mM L-glutamine, 50 µM β-ME. Only 1% (v/v) FBS was added if experiments did not focus on phagocytosis. If cells were infected with live bacteria, L-

	glutamine-penicillin-streptomycin solution was excluded to maintain an antibiotic-free culture
BMDM lift medium	Magnesium and calcium-free Dulbecco's phosphate-buffered saline (DPBS) supplemented with 5% (v/v) FBS and 2.5 mM EDTA
iBMDM culture medium	RPMI-1640 medium commercially supplemented with L-glutamine and sodium bicarbonate, 10% (v/v) FBS, 10 mM HEPES, 1 mM sodium pyruvate, 100 U/ml penicillin, 100 µg/ml streptomycin, 2 mM L-glutamine, 50 µM β- ME and 10% (v/v) L929 cell supernatant
HEK293 culture medium MEF culture medium	DMEM commercially supplemented with L-glutamine and glucose, 10% (v/v) FBS, 1 mM sodium pyruvate, 100 U/ml penicillin, 100 µg/ml streptomycin, 2 mM L-glutamine
Human macrophage medium	RPMI-1640 medium commercially supplemented with L-glutamine and sodium bicarbonate, 10% (v/v) FBS, 10 mM HEPES, 1 mM sodium pyruvate, 100 U/ml penicillin, 100 µg/ml streptomycin, 2 mM L-glutamine, 50 ng/ml human GM-CSF

2.2.2 Primary Cells

2.2.2.1 Generation of bone marrow-derived macrophages (BMDMs)

Primary macrophages were cultured from 6 to 12-week-old mice. Mice were culled according to Schedule 1 kill (S1K) regulations by the United Kingdom Home Office and subsequently sprayed with 70% ethanol. Using a sterile dissection kit both femurs were extracted and kept in basal RPMI-1640 for short-term storage. Bones were rinsed for 2 min in 70% ethanol before removing residual mouse tissue. Both ends of the femur were removed using scissors and the bone cavity was flushed with 2.5 ml pre-chilled basal RPMI from both ends. Bone marrow cells from one mouse were collected in a 15 ml Falcon tube, centrifuged at 1,000 rpm for 5 min at RT and subsequently resuspended in 6 ml BMDM differentiation medium. Bone marrow cells from one mouse were seeded in six non-treated 140 mm Sterilin petri dishes (Thermo Fisher Scientific). On day 4 of the BMDM culture, cells were fed with 10 ml BMDM differentiation medium. Differentiated BMDMs were harvested from day 6 to 8. Non-adherent cells were aspirated and adherent BMDMs were harvested by

incubation with 5 ml pre-chilled BMDM lift medium (Table 9) for 10 min at RT. Cells were pooled in a 50 ml Falcon tube, centrifuged at 1,000 rpm for 5 min at RT, resuspended in BMDM seeding medium (Table 9) and counted. If the role of TPL-2 and ABIN-2 in phagocytosis was studied, macrophages were seeded in medium supplemented with 10% (v/v) FBS. For all other experiments, macrophages were seeded in starvation medium supplemented with 1% (v/v) FBS. BMDMs were rested overnight at 37°C with 5% CO_2 prior to starting the experiment.

2.2.2.2 Human macrophages

2.2.2.2.1 Isolation of mononuclear cells from human peripheral blood by density gradient centrifugation

Surplus NHS blood donated by healthy volunteers was used for this research, which has been approved by NHS Health Research Authority and complied with the Human Tissue Act 2004. Human peripheral blood mononuclear cells (PBMCs) were isolated from anonymised buffy coat samples (NC07, 50 ml) collected by NHS Blood and Transplant Colindale. Human blood from a 50 ml buffy coat was added to ice-cold 2 mM EDTA in PBS at a final dilution of 1:5 (v/v). In 50 ml Falcon tubes, 35 ml blood suspension was gently pipetted onto 15 ml Ficoll Paque Plus (GE Healthcare) and centrifuged at 1,000×g for 15 min at RT, with deceleration set to 0. The white-coloured interphase cell layer between blood plasma and erythrocytes, consisting of PBMCs, was carefully transferred to a fresh 50 ml Falcon tube. PBMCs were washed with 2 mM EDTA in PBS and centrifuged at 300×g for 10 min at RT. To remove platelets, PBMCs were washed twice with 2 mM EDTA in PBS and centrifuged at 200×g for 15 min at RT. Prior to CD14 selection, cells were resuspended in 2 mM EDTA in PBS and counted.

2.2.2.2.2 Selection of $CD14^+$ mononuclear cells

A total of 1×10^8 PBMCs were resuspended in 800 µl CD14 selection buffer. To label $CD14^+$ mononuclear cells, 200 µl CD14 MicroBeads (130-050-201, MACS Miltenyi Biotec) were added and the mixture was incubated for 15 min at 4°C. Cells were

washed with 20 ml CD14 selection buffer and centrifuged at 300×g for 10 min at RT. The cell pellet was resuspended in 500 µl CD14 selection buffer. The LS column (130-042-401, MACS Miltenyi Biotec) was placed in a MiniMACS separator (MACS Miltenyi Biotec) attached to a MACS MultiStand (MACS Miltenyi Biotec), thus applying a magnetic field to the column. The LS column was calibrated with 3 ml CD14 selection buffer. The CD14-labelled cell suspension was subjected to the column. Cells passing through the column were collected as unlabelled effluent. The column was washed three times with 3 ml CD14 selection buffer. The column was removed from the magnetic field and 5 ml CD14 selection buffer was applied. To elute $CD14^+$ PBMCs, the plunger was firmly pushed into the column and CD14-labelled cells were collected as eluate. Efficiency of $CD14^+$ selection was quantified by flow cytometry (2.2.6).

2.2.2.2.3 Differentiation of $CD14^+$ mononuclear cells into human macrophages

$CD14^+$ PBMCs were seeded at 2×10^7 cells per 140 mm Nunc dish (Sigma-Aldrich) in 25 ml human macrophage medium (Table 9). The culture medium was supplemented with human recombinant GM-CSF (STEMCELL Technologies) at a final concentration of 50 ng/ml to ensure differentiation of monocytes into macrophages. On day 4, cells were fed with 10 ml human macrophage medium. Differentiated human macrophages were harvested on day 7. Cells were harvested similar to BMDMs (2.2.2.1), counted and resuspended in human macrophage medium for seeding.

2.2.3 Immortalised cell lines

2.2.3.1 Generation and passaging of immortalised bone marrow-derived macrophages (iBMDM)

Dr Teresa Thurston (MRC Centre for Molecular Bacteriology and Infection, Imperial College London, United Kingdom) kindly generated immortalised macrophage cell lines from primary BMDMs that were differentiated from WT, *Tpl2*$^{D270A/D270A}$ and *Abin2*$^{D310N/D310N}$ mice provided by the Ley laboratory. Briefly, the Thurston laboratory infected primary BMDMs with a J2 virus containing both v-raf and v-myc oncogenes,

which induced macrophage proliferation to generate immortalised cell lines (Blasi E , Radzioch D , Merletti L, 1989; Bone *et al*, 2018; Gandino & Varesio, 1990). iBMDM cell lines were grown to 75-90% confluency in T175 tissue culture flasks (Corning). Following removal of media, cells were washed with DPBS and incubated with 3 ml trypsin / 0.05% (v/v) EDTA for 5-7 min. Detached cells were centrifuged at 1,000 rpm for 5 min at RT and diluted 1/5 in fresh iBMDM culture medium (Table 9).

2.2.3.2 Human embryonic kidney (HEK) 293 cells

Adherent HEK293 cells were provided by The Francis Crick Institute Cell Services. Cells were maintained in HEK293 culture medium and grown to 85-90% confluency in T175 tissue culture flasks. Experimental procedures for HEK293 cell passaging were identical to iBMDM protocols (2.2.3.1).

2.2.3.3 Mouse embryonic fibroblasts (MEF)

MEFs were previously generated by Dr Michael Pattison (Ley Laboratory) from C57BL/6Jax WT mice. Cells were maintained in MEF culture medium (Table 9) and grown to 85-90% confluency in T175 tissue culture flasks. Experimental procedures for MEF cell passaging were identical to iBMDM protocols (2.2.3.1).

2.2.3.4 Freezing and thawing of immortalised cell lines

iBMDMs in a confluent T175 tissue culture flask were trypsinised and detached cells were centrifuged at 1,000 rpm for 5 min at RT. The cell pellet was resuspended in 2 ml FBS containing 10% (v/v) DMSO, split into two 1.8 ml cryogenic vials (Star Lab) and stored in a polyethylene freezing container (Corning) for 24 h at -80°C. For short-term storage, cells were kept at -80°C, while transfer to liquid nitrogen at -196°C was ensured for long-term storage. iBMDM or MEF cryogenic vials were warmed in a 37°C water bath for 1 min and subsequently resuspended in 10 ml iBMDM or MEF culture medium (Table 9). Following centrifugation at 1,000 rpm for 5 min at RT, the cell pellet was resuspended in 25 ml iBMDM or MEF culture medium and transferred to a T175 tissue culture flask.

2.2.4 Biochemistry techniques

2.2.4.1 Inhibitor and agonist treatment

Inhibitors and agonists used in this thesis are outlined in Table 10 and Table 11, respectively. Inhibitors and agonists were resuspended according to manufacturer instructions, aliquoted and stored at -20°C. If necessary, stock solutions were diluted in the appropriate cell culture medium prior to use. Inhibitors and agonists were directly pipetted into the respective wells or dishes, cells were gently swirled and incubated at 37°C for the times indicated. Since DMSO was used for resuspension of all inhibitors, an equivalent volume of DMSO was used as a vehicle control alongside inhibitor treatments.

Table 10 Inhibitors

Inhibitor	Molecular target	Working concentration	Pre-treatment (min)	Source
PD0325901	MEK1 (Ciuffreda *et al*, 2009)	0.1 µM	10	DSTT
VX-745	p38 (Duffy *et al*, 2011)	1 µM	60	Selleckchem
C34	TPL-2 (Wu *et al*, 2009)	10 µM	60	Medchem Express
Akti-1/2	AKT1, AKT2, AKT3 (Lindsley *et al*, 2005; Barnett *et al*, 2005)	10 µM	60	Abcam
AZD8055	mTOR (Chresta *et al*, 2010)	1 µM	60	Selleckchem
Leupeptin	Serine-cysteine proteases (Libby & Goldberg, 1978)	100 µg/ml	60	Sigma-Aldrich
Bafilomycin A1	V-ATPase	1 µM	15	Sigma-Aldrich

	(Yamamoto *et al*, 1998)			
Cytochalasin D	Actin (Schliwa, 1982)	10 µg/ml	30	Thermo Fisher Scientific

Table 11 Agonists

Agonist	Molecular target	Working concentration	Source
LPS (from *Salmonella minnesota* R595)	TLR4 (Poltorak *et al*, 1998a)	100 ng/ml	Enzo Life Sciences
TNFα	TNFR1, TNFR2 (Thoma *et al*, 1990)	20 ng/ml	Peprotech
Pam_3CSK_4	TLR2 (Tsolmongyn *et al*, 2013)	100 ng/ml	InvivoGen
Carboxylated latex beads	Scavenger receptors (Palecanda *et al*, 1999)	1:50	Estapor, Merck
LPS-coated carboxylated latex beads	TLR4 (Zanoni *et al*, 2011)	1:300	Felix Breyer (2.2.7.7)

2.2.4.2 Cell lysis

Following the described treatment, cells were placed on ice and washed once with ice-cold PBS. If cells were treated with beads or infected with live bacteria, then cells were washed three times. Cells were scraped in lysis buffer, incubated on ice for 15 min and lysates were cleared by centrifugation at 15,000 rpm for 15 min at 4°C. Lysate supernatants were transferred to a new Eppendorf tube.

2.2.4.3 Protein quantification

Protein concentration was determined using the Pierce™ Coomassie Protein Assay Kit following principles of the Bradford protocol (Bradford, 1976). Upon binding of the Coomassie reagent to proteins the optimal absorbance shifts to 595 nm, which is associated with a colour change to blue. In a 96-well plate, 2 µl of cleared lysate was

combined with 200 µl Coomassie reagent, gently shaken and incubated for 2 min at RT. Absorbance was measured at 595 nm. A standard curve was generated based on absorbance measurements from BSA protein standards (0.125 mg/ml to 2 mg/ml). Protein concentrations of samples were calculated using the standard curve.

2.2.4.4 SDS polyacrylamide gel electrophoresis (SDS-PAGE)

Cell lysates were mixed with 5X sample buffer (Table 8) and heated for 10 min at 90°C. SDS induces a negative charge in proteins relative to their molecular weight. While heating of gel samples breaks tertiary and secondary structures, β-ME breaks disulphide bridges to linearise peptides. Samples (15-25 µg) were subjected to SDS-PAGE on a 10% acrylamide gel. Gels were run in Tris/Glycine/SDS running buffer (Table 8) at a constant voltage of 150 V until the sample buffer front migrated through approximately 90% of the gel. Negatively charged peptides migrate towards the positively charged anode proportional to their molecular mass. The Precision Plus Protein™ Dual Colour marker (Bio-Rad Laboratories) was used as molecular weight ladder. If high-molecular-weight proteins (>150 kDa) or ubiquitin chains were studied, samples were subjected to 4-12% Bis-Tris NuPAGE gradient gels (Invitrogen) in MOPS running buffer at a constant voltage of 200 V for 45 min.

2.2.4.5 Western blotting

Proteins were transferred onto PVDF membranes (Bio-Rad Laboratories) using the Trans-Blot Turbo Transfer System (Bio-Rad Laboratories), a system based on experimental principles developed by Towbin (Towbin *et al*, 1979). A constant electric current of 1 A and voltage of up to 25 V was applied for 0.5 h to transfer proteins onto PVDF membranes. Subsequently, membranes were incubated with blocking buffer (Table 8) for 1 h at RT to prevent non-specific binding of antibodies to PVDF membranes. Membranes were incubated with primary antibodies overnight at 4°C (Table 1). On the next day, membranes were washed four times for 15 min in PBST buffer (Table 8). Membranes were incubated with horseradish-peroxidase (HRP)-conjugated secondary antibodies (Table 3) in blocking buffer at 1:5000 for 1 h at RT. Afterwards, membranes were washed four times for 15 min in PBST buffer.

Membranes were incubated with Amersham ECL Western Blotting Detection Reagent (GE Healthcare Life Sciences) for 2 min at RT and visualised with X-ray film and an automatic X-ray film processor. Membranes were exposed to X-ray films (Scientific Laboratory Supplies) for varying times to obtain optimal exposure. If weak signals were observed, membranes were briefly washed in PBST buffer and the Immobilon Western Chemiluminescent HRP Substrate (Millipore) was used as chemiluminescent detection reagent instead.

2.2.4.6 PEI transfection in HEK293 cells

Polyethylenimine (PEI, Polysciences, Inc.) was dissolved in 20 mM HEPES pH 7.5 (Thermo Fisher Scientific) to a final concentration of 1 mg/ml. PEI was subjected to a 0.2 µm filter for sterilisation. HEK293 cells were seeded at 2×10^6 cells per 10 cm dish. To ensure a cDNA to PEI ratio of 1:3, 5 µg cDNA and 15 µg PEI were vortexed for 15 sec in 1 ml basal DMEM (Thermo Fisher Scientific) and incubated for 15 min at RT. The transfection mixture was gently added to a 10 cm dish. After 6 h, basal DMEM was replaced with HEK293 culture medium (Table 9). Cells were harvested and lysed 24 h post-transfection.

2.2.4.7 Immunoprecipitation

M2 Anti-FLAG Affinity Gel (Sigma-Aldrich, 15 µg packed beads) was incubated with 1.5 mg cell lysate for 16 h at 4°C. Beads were washed four times with lysis buffer (Table 8) and once with sterile water to remove any buffering capacity. Beads were dried with a flat gel-loading tip. Immunoprecipitated proteins were released by glycine elution. Briefly, beads were incubated with glycine elution buffer (Table 8) at 1,400 rpm for 3 min, centrifuged at 13,000 rpm for 1 min at RT and the eluate was transferred to a new Eppendorf tube. Elution was repeated three times. To neutralise the acidic pH, 1 M Tris base pH 8 was added at a final concentration of 20% (v/v). Eluates were mixed with 5X sample buffer and heated for 10 min at 90°C. Samples were subjected to SDS-PAGE.

2.2.4.8 Immunoprecipitation of the TNF receptor signalling complex

MEFs were seeded at 3×10^6 cells per 10 cm dish. After overnight resting, MEFs were stimulated with recombinant 3xFLAG-tagged TNF ligand (provided by Professor Henning Walczak, University College London) at 0.5 µg/ml for 15 min (Haas *et al*, 2009). Cells were lysed in MEF lysis buffer (Table 8) for 0.5 h at 4°C. Lysates were centrifuged at 15,000×g for 0.5 h at 4°C. The unstimulated control lysate was mixed with 0.5 µg 3xFLAG-tagged TNF ligand. M2 Anti-FLAG Affinity Gel (20 µg packed beads) was incubated with 2 mg cell lysate for 16 h at 4°C. Beads were washed five times with MEF lysis buffer (Table 8). Proteins were eluted by heating beads in 2X sample buffer for 10 min at 90°C. Samples were subjected to SDS-PAGE.

2.2.4.9 GST pulldown of ABIN-2

Binding proteins of ABIN-2 were transiently overexpressed in HEK293 cells (2.2.4.6). HEK293 cell lysates were pre-cleared by incubating 750 µg cell extract with 2 µg GST protein and glutathione Sepharose 4B resin (10 µg packed beads, GE Healthcare) for 1 h at 4°C. Pre-cleared cell lysates were mixed with 1 µg GST protein (negative binding control) or 2.9 µg GST-ABIN-2 fusion protein and glutathione Sepharose 4B resin (10 µg packed beads). Pulldowns were performed for 16 h at 4°C. Beads were washed six times with lysis buffer (Table 8), which was adjusted to pH 8. Proteins were eluted by heating beads in 2X sample buffer for 10 min at 90°C. Eluates were subjected to SDS-PAGE.

2.2.4.10 GST pulldown of ABIN-2 – Ubiquitin binding

The respective GST-ABIN-2 fusion protein (2.9 µg) was mixed with glutathione Sepharose 4B resin (10 µg packed beads) and M1-linked polyubiquitin at 500 ng/ml in 1 ml ubiquitin binding buffer (Table 8). Purified M1-linked (2, 4, 8) polyubiquitin (Enzo Life Sciences) was used. Ubiquitin pulldowns were incubated for 3 h at 4°C. Beads were washed five times in ubiquitin binding buffer and proteins were eluted by heating beads in 2X sample buffer for 10 min at 90°C. Samples were subjected to SDS-PAGE.

2.2.4.11 siRNA-mediated gene knockdown in iBMDMs

iBMDMs were seeded in iBMDM culture medium at a density of 5×10^4 cells per well in a 24-well plate or 1×10^4 cells per well in a 96-well plate (M0562, Greiner CELLSTAR®) one day prior to transfection. siRNA was resuspended in siRNA buffer (B-002000-UB+100, Horizon Discovery [formerly Dharmacon]) to 20 µM. SMARTpool ON-TARGETplus siRNA was used to target genes of interest (Table 12) while an ON-TARGETplus non-targeting pool was used as siRNA control (D-001810-10-20, Horizon Discovery). iBMDMs were transfected using Viromer Green (Lipocalyx). Manufacturer instructions according to the basic transfection protocol of adherent cells were followed. iBMDMs were transfected with siRNA at a final concentration of 50 nM for 48 h at 37°C. After 48 h, 96-well plates were used for fluorescence-based bead assays, while 24-well plates were used for Western blotting or qRT-PCR analysis to confirm siRNA-mediated knockdown of genes of interest.

Table 12 siRNA pools

Gene target	Catalogue number	Source
Akt1	L-040709-00-0005	Horizon Discovery
Dmxl1	L-055471-01-0005	Horizon Discovery
Dmxl2	L-061928-01-0005	Horizon Discovery
Tsg101	L-049922-01-0005	Horizon Discovery

2.2.4.12 Co-transfection of siRNA and 3xFLAG-DMXL1

Experimental steps for siRNA-mediated gene knockdown of *Dmxl1* were performed as previously described (2.2.4.11). Additional conditions were prepared where *Dmxl1*-specific siRNA was co-transfected with plasmid vectors expressing either 3xFLAG-DMXL1^{WT}[1773-2047] or 3xFLAG-DMXL1^{SSAA}[1773-2047], in which serine residues 1903 and 1904 were replaced with alanines. The empty pcDNA3-3xFLAG plasmid was separately co-transfected with *Dmxl1*-specific siRNA as control. Each individual well in a 24-well and 96-well plate was co-transfected with 125 ng and 50 ng plasmid cDNA, respectively.

2.2.4.13 Cytotoxicity assay

BMDMs of indicated genotypes were seeded in 24-well plates and infected with *S. aureus* (MOI of 10) and *S. typhimurium* (MOI of 5) for the indicated times as previously described. Quadruplicates were prepared per condition. Supernatants were collected, centrifuged at 6,000 rpm for 2 min at RT to remove cell debris, and transferred to new Eppendorf tubes. As MAX control, an uninfected 24-well plate was transferred to -80°C for complete cell lysis and supernatants were collected as outlined above. The Cytotoxicity Detection Kit (11 644 793 001, Roche) was used according to manufacturer instructions to quantify lactate dehydrogenase (LDH) activity released from the cytosol of pyroptotic BMDMs. Briefly, 100 µl supernatant was combined with 100 µl substrate for 5-30 min at RT, protected from light. To terminate the assay, 100 µl 0.16 M sulphuric acid was added. LDH activity was measured in an Infinite microplate reader (TECAN) at 490 nm (absorbance), with the reference wavelength set to 650 nm. MAX control samples corresponded to maximum cytotoxicity of 100%.

2.2.5 Microbiology techniques

2.2.5.1 Bacterial infection

BMDMs were seeded in antibiotic-free BMDM seeding medium (Table 9) at a density of 2×10^6 cells per well in a 6-well plate or 0.5×10^6 cells per well in a 24-well plate one day prior to infection. Bacteria were cultured in 5 ml Luria Bertani (LB) medium for 16 h at 37 °C with constant shaking at 200 rpm. LB medium was supplemented with the respective antibiotic(s) (Table 13). Following overnight culture, bacteria were diluted in antibiotic-free BMDM seeding medium (Table 9) and added to the adherent macrophage monolayer. *E. coli* and *C. rodentium* were added to BMDMs at an MOI of 10:1 and 2:1, respectively. *S. aureus* and *S. typhimurium* were added to cells at an MOI of 10:1 and 5:1, respectively. Immediately after infection, cells were centrifuged at 100×g for 5 min at RT and incubated for the indicated times at 37 °C until cell lysis.

Table 13 Bacterial strains

Bacterial species	Strain	Antibiotic resistance	Description	Source
GFP-*Escherichia coli* K12	BW25113	50 µg/ml ampicillin	BW25113 was transformed with pFPV25.1 (GFP) plasmid	Dr Teresa Thurston
YFP-*Staphylococcus aureus*	RN6390	10 µg/ml chloramphenicol	Transformed RN6390 produces plasmid-encoded EsaB-YFP	Professor Tracy Palmer
GFP-*Citrobacter rodentium*	ICC683	50 µg/ml nalidixic acid; 100 µg/ml chloramphenicol	Untagged *C. rodentium* was transformed with pACYC-GFP plasmid	Professor Gad Frankel
GFP-*Salmonella typhimurium*	12023	50 µg/ml ampicillin	12023 was transformed with pFPV25.1 (GFP) plasmid	Dr Teresa Thurston
Salmonella typhimurium ΔssaV	12023	50 µg/ml kanamycin	12023 lacks ssaV gene, a component of the SPI-2-encoded T3SS	Dr Teresa Thurston

2.2.5.2 Bacterial colony forming unit assay

Bacterial colony forming unit (CFU) assays were performed in 24-well tissue culture plates with two biological replicates and three technical replicates per condition. Following bacterial infection and centrifugation, BMDMs were incubated for 25 min at 37°C to allow phagocytic uptake of extracellular bacteria. Cells were gently washed three times with warm PBS and incubated with BMDM seeding medium (Table 9) supplemented with 50 µg/ml gentamicin for 1 h at 37 °C to remove any extracellular bacteria. After 1 h, the culture medium was changed to BMDM seeding

medium supplemented with 10 µg/ml gentamicin. Infected BMDMs were harvested at the indicated time points. Cells were washed once with ice-cold PBS, lysed in 1 ml 0.1% (v/v) Triton X-100 in PBS for 5 min and transferred to fresh Eppendorf tubes. Cell lysates were diluted in PBS as appropriate and plated on antibiotic-free agar plates (provided by the Media Preparation Team, The Francis Crick Institute). Following overnight incubation at 37°C, bacterial colonies were counted using the Synbiosis aCOLyte (7510/SYN) counting device.

2.2.5.3 Phagocytic uptake of GFP-Salmonella typhimurium

These experiments were performed with Dr Teresa Thurston (MRC Centre for Molecular Bacteriology and Infection, Imperial College London, United Kingdom). BMDMs were infected with GFP-*Salmonella typhimurium* and treated as outlined in 2.2.5.1 and 2.2.5.2. At the indicated times, BMDM seeding media was removed and cells were washed once in pre-warmed PBS. Cells were scraped in 1 ml ice-cold PBS and centrifuged at 300×g for 5 min at 4°C. Cell pellets were gently resuspended in 300 µl PBS and GFP fluorescence intensity was measured using a FACSCalibur flow cytometer (BD Biosciences). At least 10,000 events were acquired. Data was analysed using FlowJo (Version 10.3.0) software.

2.2.6 Surface staining for flow cytometry

Cells were scraped in 1 ml ice-cold PBS and centrifuged at 1,500 rpm for 5 min at 4°C. BMDMs were stained with CD16/CD32 (BioLegend) at 1/50 in FACS buffer (Table 8) for 20 min on ice. CD16/CD32 blocking prevents non-specific binding of immunoglobulin to Fc receptors. Cells were washed in FACS buffer and surface straining of antigens was performed in FACS buffer for 1 h on ice (Table 6). The F4/80 stain recognises a macrophage-specific glycoprotein, thus functioning as a BMDM marker. A live/dead cell stain for UV excitation (Invitrogen) was included for positive selection of viable macrophages. Cells were washed in FACS buffer and analysed using a LSRFortessa A flow cytometer (BD Biosciences). Data was analysed using FlowJo (Version 10.3.0) software. If samples were not immediately

analysed, cells were fixed by incubation in IC fixation buffer (eBioscience) for 15 min at RT. Data acquisition and analysis was carried out with Dr Louise Webb.

2.2.7 Techniques to study phagocytosis and phagosome biology

2.2.7.1 Coupling of Alexa Fluor 488 BSA-coated silica beads

100 µl carboxylated silica beads with a 3 µm diameter (PSI-3.0COOH, Kisker Biotech) were washed three times in PBS by centrifugation at 2,000×g for 1 min. Beads were resuspended in 25 mg/ml cyanamide and incubated at 900 rpm for 15 min at RT on a Thermoshaker (Thermo Fisher Scientific). Cyanamide functions as a cross-linker. Beads were washed twice in 100 mM sodium borate buffer pH 8.0 to remove excess cyanamide. For fluorophore coupling, beads were incubated with 0.1 mg BSA and 2 µl of the 5 mg/ml stock of Alexa Fluor 488 succinimidyl ester (Thermo Fisher Scientific) at 900 rpm for 16 h at RT on a Thermoshaker. Albumin functions as an opsonic ligand for the mannose receptor, thus ensuring localisation of coupled beads to endosomes (Astarie-Dequeker *et al*, 1999). Overnight incubation allows silica bead-coupled albumin to be sufficiently labelled with the amine-reactive fluor. Coupled beads were washed twice in 250 mM glycine in PBS pH 7.2 to remove soluble amine groups. Beads were washed twice in PBS and resuspended in 100 µl PBS supplemented with 0.01% (w/v) sodium azide for long-term storage.

2.2.7.2 Phagocytic uptake assay

Fluorescence-based assays and bead coupling protocols were adapted from methods developed by the Valenzeno and Russell laboratories (Russell *et al*, 1995; Yates & Russell, 2005, 2008). BMDMs were seeded on 96-well plates (M0562, Greiner CELLSTAR®) at 1×10^5 BMDMs/well in BMDM seeding medium (Table 9) and rested overnight. Cells were incubated with Alexa Fluor 488 BSA-coated silica beads at 1:300 dilution in bead assay buffer (Table 8) for 0.5 h at 37°C. Silica beads were removed and 100 µl trypan blue was added to quench extracellular fluorescence of non-phagocytosed beads. Trypan blue was aspirated and cells were washed once with pre-warmed bead assay buffer. Fluorescence intensity was

measured in a Clariostar (BMG Labtech) microplate reader at excitation/emission wavelengths 490/520 nm.

2.2.7.3 Coupling of DQ Green BSA/Alexa Fluor 594-coupled silica beads

Experimental procedures were adapted from 2.2.7.1. Here, 500 µl silica beads were used for coupling. For fluorophore coupling, beads were incubated with 0.5 mg DQ Green BSA (Thermo Fisher Scientific) and 125 µg avidin at 900 rpm for 16 h at RT on a Thermoshaker. Overnight incubation allows DQ Green BSA, the proteolytic sensor, to covalently attach to silica beads via the cyanamide cross-linking agent. Avidin functions as an opsonic ligand for the mannose receptor, thus ensuring localisation of coupled beads to endosomes. DQ Green BSA-coupled beads were washed twice in 250 mM glycine in PBS pH 7.2 to quench the unreacted cyanamide and twice in 100 mM sodium borate buffer pH 8.0 to remove soluble amine groups. Beads were resuspended in 500 µl sodium borate buffer pH 8.0 and supplemented with 5 µl of the 5 mg/ml stock of Alexa Fluor 594 succinimidyl ester (Thermo Fisher Scientific) at 900 rpm for 1 h at RT on a Thermoshaker. Incubation for 1 h is sufficient to label silica beads with the amine-reactive fluor. Coupled beads were washed three times in 250 mM glycine in PBS pH 7.2 to remove soluble amine groups and resuspended in 500 µl PBS supplemented with 0.01% (w/v) sodium azide for long-term storage.

2.2.7.4 Phagosome proteolysis assay

Experimental procedures were adapted from 2.2.7.2. Cells were incubated with DQ Green BSA/Alexa Fluor 594-coupled silica beads at 1:300 dilution in bead assay buffer for 3 min at RT. Silica beads were replaced with pre-warmed bead assay buffer. Real-time fluorescence intensities were measured at 37°C using a Clariostar (BMG Labtech) microplate reader at reading intervals of 2 min over a 6 h time window. Fluorescence intensities were measured at excitation/emission wavelengths 490/520 nm (DQ Green BSA) and at excitation/emission wavelengths 590/620 nm (Alexa Fluor 594). The calibration fluorophore Alexa Fluor 594 was used to normalise against phagocytic bead uptake. Plots were generated from DQ Green BSA to Alexa

Fluor 594 ratios. As negative control, BMDMs were pre-treated with 100 µg/ml leupeptin (Sigma-Aldrich) for 1h, a serine-cysteine protease inhibitor. Alternatively, BMDMs were pre-treated with 1 µM bafilomycin A1 (Sigma-Aldrich) for 15 min, an inhibitor of V-ATPases.

2.2.7.5 Coupling of BCECF-coupled silica beads

Experimental procedures were adapted from 2.2.7.1. Here, 500 µl silica beads were used for coupling. For fluorophore coupling, beads were incubated with 0.1 mg BSA and 10 µl of the 5 mg/ml stock of BCECF acid (2',7'-Bis-(2-Carboxyethyl)-5-(and-6)-Carboxyfluorescein) (Thermo Fisher Scientific) at 900 rpm for 16 h at RT on a Thermoshaker.

2.2.7.6 Phagosome pH assay

Experimental procedures were adapted from 2.2.7.4. Cells were incubated with BCECF-coupled silica beads at 1:200 dilution in bead assay buffer for 3 min at RT. Real-time fluorescence intensities were measured at 37°C using a PHERAstar Plus (BMG Labtech) microplate reader at excitation/emission wavelengths 485/520 nm with reading intervals of 1 min over a 1 h time window. As negative control, BMDMs were pre-treated with 1 µM bafilomycin A1 (Sigma-Aldrich) for 15 min. BCECF is a pH indicator with optimal fluorescence at pH 7. As phagosomal pH rapidly decreases, fluorescence intensity of the bead-coupled pH indicator BCECF decreases at 485nm/520nm.

2.2.7.7 Preparation of LPS-coated latex beads

400µl blue-dyed carboxylated polystyrene beads with a diameter of 0.93 µM (K1-080 blue, Estapor Merck Chimie SAS) were incubated with 1 ml soluble LPS from *Salmonella minnesota* R595 (1 mg/ml, Enzo Life Sciences) for 1 h at 4°C with constant rotation. LPS-coated beads were washed twice with PBS to remove unbound LPS. Beads were resuspended in 400µl PBS and stored at 4°C.

2.2.7.8 Phagosome isolation

The phagosome isolation protocol was adapted from methods described by the Trost laboratory (Dill *et al*, 2015; Trost *et al*, 2009). Bone marrow cells from both femurs of one mouse were equally divided among seven 10 cm dishes, cultured according to standard protocols (2.2.2.1) and on day 7, phagosome isolation was performed. Blue-dyed carboxylated polystyrene beads with a diameter of 0.93 µM (K1-080 blue, Estapor Merck Chimie SAS) were incubated in a sonicator bath for 20 sec. Beads were added to pre-warmed BMDM seeding medium at a final dilution of 1:50 (v/v). Culture medium was removed from 10 cm dishes, BMDMs were washed with 5 ml pre-warmed DPBS and 5 ml bead-medium mixture was added per 10 cm dish. BMDMs were incubated with beads for 0.5 h at 37°C. Cells were washed once with ice-cold DPBS to remove non-phagocytosed beads, scraped in DPBS and BMDMs from seven 10 cm dishes were collected into a 50 ml Falcon tube. Cells were centrifuged at 500×g for 3 min at 4°C and the supernatant was discarded by aspiration. The cell pellet was resuspended in 10 ml DPBS, transferred to a 15 ml Falcon tube and washed twice with ice-cold DPBS to remove any non-internalised bead particles. Cells were resuspended in 3 ml ice-cold hypotonic buffer (Table 8). Cells were centrifuged at 500×g for 3 min at 4°C, the cell pellet was resuspended in 3 ml hypotonic buffer and the cell suspension was transferred into a pre-chilled Dounce homogeniser. Cells were homogenised by approximately 10 to 15 strokes of Dounce homogenisation. Trypan blue cell staining and light microscopy was utilised to confirm a cell disruption efficiency of 90%. The cell homogenate was centrifuged at 1,000×g for 5 min at 4°C to remove nuclei and intact cells. The post-nuclear fraction containing phagosomes was diluted to 38% (w/v) sucrose content by adding the appropriate volume of 68% (w/v) sucrose solution supplemented with Pierce Protease and Phosphatase Inhibitor Mini Tablets (Thermo Fisher Scientific). All sucrose solutions contained 3 mM imidazole pH 7.4, a catalyst of sucrose hydrolysis. 1.8 ml phagosome-containing 38 % sucrose (w/v) mixture was layered above a 1 ml layer of 68% sucrose (w/v) in a SW41 Ultra-clear 13.2 ml centrifuge tube (344059, Beckman Coulter). Additionally, 2 ml 35% (w/v) sucrose, 2 ml 25 % (w/v) sucrose, and 2 ml 10% (w/v) sucrose solutions were gently layered onto the phagosome mixture. Samples were centrifuged in a SW41Ti swinging bucket rotor in an Optima™ L-90 K ultracentrifuge (Beckman Coulter) at 72,300×g for 1 h at 4°C.

The blue-coloured phagosomal fraction was gently collected from the interface of the 10% (w/v) sucrose and 25% (w/v) sucrose layers using a fine tip micro Pasteur pipette and transferred to a fresh SW41 Ultra-clear 13.2 ml centrifuge tube. The phagosomal fraction was washed with ice-cold DPBS, centrifuged at 28,400×g for 15 min at 4°C and stored at -80°C.

2.2.8 Mass spectrometry techniques

2.2.8.1 Proteomic sample preparation of phagosomes and label-free MS acquisition of phagosome proteomes

Dr Anetta Härtlova and Dr Julien Peltier (Professor Matthias Trost Lab, Newcastle University) carried out proteomic sample preparation and label-free MS acquisition of phagosome proteomes. Isolated phagosomes were lysed in 5% (w/v) SDS, 50 mM TEAB pH 7.5 (S-Trap) and sonicated. Subsequently, protein concentration of samples was determined using the BCA Protein Assay Kit (Pierce). Samples were reduced in 10 mM tris(2-carboxyethyl)phosphine for 0.5 h at RT followed by alkylation in 10 mM iodoacetamide for 0.5 h. Samples were acidified and digested on an S-trap spin column using porcine trypsin at 1:10 (Pierce) for 2 h at 47°C. Peptides were eluted in 50 mM TEAB pH 8.0, 0.2% (v/v) formic acid and 0.2% (v/v) formic acid in 50% (v/v) acetonitrile, respectively. Prior to MS acquisition, peptide samples were separated on an Ultimate 3000 RSLC system (Thermo Fisher Scientific) with a C18 PepMap, serving as a trapping column (2 cm x 100 µm ID, PepMap C18, 5 µm particles, 100 Å pore size) followed by a 50 cm EASY-Spray column (50 cm x 75 µm ID, PepMap C18, 2 µm particles, 100 Å pore size) (Thermo Scientific). Buffer A contained 0.1% (v/v) formic acid, while Buffer B contained 80% (v/v) acetonitrile and 0.1% (v/v) formic acid. Peptides were separated with a linear gradient of 1-35% (Buffer B) over 120 min followed by a step from 35-90% (v/v) acetonitrile, 0.1% (v/v) formic acid in 0.5 min at 300 nL/min and held at 90% for 4 min. The gradient was then decreased to 1% Buffer B in 0.5 min at 300 nL/min for 10 min. MS identification was performed on an Orbitrap QE HF mass spectrometer (Thermo Scientific Scientific) operated in a “TopN” data-dependent mode in positive ion mode. FullScan spectra were acquired in a range from 400 m/z to 1,500 *m/z*, at a resolution of 120,000 (at 200 m/z), with an automated gain control (AGC) of 1×10^6

and a maximum injection time of 50 ms. Charge state screening was enabled to exclude precursors with a charge state of 1. For MS/MS fragmentation, the minimum AGC was set to 5,000 and the most intense precursor ions were isolated with a quadrupole mass filter width of 1.6 *m/z* and 0.5 *m/z* offset. Precursors were subjected to higher-energy collisional dissociation (HCD) fragmentation that was performed in one-step collision energy of 25%. MS/MS fragments ions were analysed in the Orbitrap mass analyser with a 15,000 resolution at 200 *m/z*.

2.2.8.2 Proteomic sample preparation for Absolute Quantification of Ubiquitin (Ub-AQUA)

Dr Tiaan Heunis (Professor Matthias Trost Lab, Newcastle University) carried out proteomic sample preparation. Phagosomal fractions were lysed by sonication in 5% (w/v) SDS in 50 mM TEAB buffer (Sigma-Aldrich) pH 7.5 supplemented with 100 mM NEM (Sigma-Aldrich). Following protein quantification using the BCA Protein Assay Kit (Pierce Protein), 20 µg phagosomal protein was used for sample preparation by suspension trapping (S-trap) (Zougman *et al*, 2014). The manufacturer protocol was followed, with only minor modifications proposed by the supplier (ProtiFi). Samples were reduced with 5 mM TCEP (Pierce) for 15 min at 37°C. Subsequently, samples were alkylated with 10 mM NEM for 15 min at RT, while protected from light. Samples were acidified by addition of 2.5 µl 12% (v/v) phosphoric acid, followed by the addition of 160 µl S-Trap binding buffer (Table 8). Samples were applied to S-Trap mini-spin columns (ProtiFi) and centrifuged at 4,000×g for 1 min at RT. S-Trap mini-spin columns were washed five times with 150 µl S-Trap binding buffer. Porcine trypsin (Pierce) was resuspended in 25 µl 50 mM TEAB pH 8.0 and added to each sample at a 1:10 ratio of trypsin:protein. Tryptic digests were incubated for 2 h at 47°C. Peptides were eluted by applying 50 mM TEAB pH 8 to the columns, followed by centrifugation at 1,000×g for 1 min at RT. The elution step was repeated by applying 0.2% (v/v) formic acid and 0.2% (v/v) formic acid in 50% (v/v) acetonitrile, respectively. All three eluates from each sample were combined, frozen with liquid nitrogen and dried by vacuum centrifugation. Samples were reconstituted to 1 µg/ul in 5% (v/v) formic acid. On ice, reagents were combined in the following order: 15 µl HPLC-grade water, 5 µl peptide digest (5 µg), 5 µl heavy ubiquitin peptide master

mix at 100 fmol/µl, 20 µl 10% (v/v) formic acid and 5 µl 10% (v/v) hydrogen peroxide. Once combined, samples were incubated for 2 h at 60°C for oxidation to be completed. Synthetic ubiquitin peptides (Table 14) were purchased from Cambridge Research Biochemicals (CRB Discovery).

Table 14 Synthetic ubiquitin peptides

Sequence	m/z	Z
GGM(ox^2)QIFVK[$^{13}C_6{}^{15}N_2$]	460.2435	2+
GGM(ox^2)QIFVK	456.2364	2+
M(ox^2)QIFVK(GG)TLTGK[$^{13}C_6{}^{15}N_2$]	710.3914	2+
M(ox^2)QIFVK(GG)TLTGK	706.3843	2+
TLTGK(GG)TITLEVEPSDTIENVK[$^{13}C_6{}^{15}N_2$]	804.0983	3+
TLTGK(GG)TITLEVEPSDTIENVK	801.4269	3+
TITLEVEPSDTIENVK(GG)AK[$^{13}C_6{}^{15}N_2$]	1055.061	2+
TITLEVEPSDTIENVK(GG)AK	1051.054	2+
AK(GG)IQDK[$^{13}C_6{}^{15}N_2$]	412.7394	2+
AK(GG)IQDK	408.7323	2+
IQDK(GG)EGIPP[$^{13}C_5{}^{15}N$]DQQR[$^{13}C_6{}^{15}N_4$]	551.9536	3+
IQDK(GG)EGIPPDQQR	546.6129	3+
LIFAGK(GG)QLEDGR[$^{13}C_6{}^{15}N_4$]	735.9006	2+
LIFAGK(GG)QLEDGR	730.8964	2+
TLSDYNIQK(GG)ESTLHLVLR[$^{13}C_6{}^{15}N_4$]	752.0737	3+
TLSDYNIQK(GG)ESTLHLVLR	748.7376	3+
ESTESTLHLVLR[$^{13}C_6{}^{15}N_4$]	539.3182	2+
ESTESTLHLVLR	534.314	2+
TITTITLEVEPSDTIENVK[$^{13}C_6{}^{15}$N2]	898.4744	2+
TITTITLEVEPSDTIENVK	894.4673	2+

ox^2 – sulfone version of methionine

2.2.8.3 Targeted LC-MS/MS analysis of Ub-AQUA by Parallel Reaction monitoring (PRM)

Dr Tiaan Heunis (Professor Matthias Trost Lab, Newcastle University) carried out mass spectrometric analyses of Ub-AQUA by PRM. Peptides were injected on a Dionex Ultimate 3000 RSLC (Thermo Fisher Scientific) connected to a Q-Exactive HF mass spectrometer (Thermo Fisher Scientific). 50 fmol of each ubiquitin peptide

was injected during analysis, alongside 500 ng phagosome tryptic peptide digest. A direct injection LC setup was used to minimise analysis time. During the loading phase, samples were loaded using a 5 µl loop and full loop injection, with a 2.4 µl needle and an overfill ratio of 1.5. Samples were injected onto a 150 µm × 150 mm EASY-Spray LC column (Thermo Fisher Scientific) using the nano-pump and LC-MS/MS infection buffer (Table 8) at 1.5 µl/min. Following an injection volume of 6 µl after 4 min, the column oven valve was switched to bypass the loop and peptides were eluted by increasing concentrations of LC-MS/MS elution buffer using a multistep gradient. The source was heated to 320°C. Subsequently 2.5 kV was applied between the column emitter and the MS. The Q-Exactive HF was operated in PRM mode using a resolution of 15,000, AGC target of 2×10^5 and maximum injection time of 25 msec. Peptides were selected for MS/MS data acquisition using pre-set isolation windows and fragmented using HCD.

2.2.8.4 Targeted proteomic data analysis of Ub-AQUA-PRM

Dr Tiaan Heunis (Professor Matthias Trost Lab, Newcastle University) carried out analysis of Ub-AQUA-PRM raw data. Raw files from Ub-AQUA-PRM mass spectrometry were processed using Skyline-daily (MacLean *et al*, 2010). Light ubiquitin peptides were used to generate standard curves for absolute quantification. These standard curves were used to calculate the absolute concentration of endogenous ubiquitin. The Skyline application was used to automatically determine light to heavy (L/H) ratios of corresponding peptide pairs from fragment ion intensities. Log transformed L/H peptide ratios and peptide concentrations were used to generate standard curves, to determine lower limit of detection (LLOD) and lower limit of quantification (LLOQ) for each individual peptide. The coefficient of determination, R^2, was calculated based on the LLOQ of each respective peptide. An R^2 value of >0.99 was put as threshold to consider curves for determination of absolute concentration of total ubiquitin and different ubiquitin chains. Group comparisons were carried out using a Student's t-test, and multiple group comparisons were performed using an analysis variance (ANOVA) followed by a Tukey's HSD test for characterising significance of pairwise comparisons. Statistical analyses were performed in GraphPad Prism (version 8.0.1).

2.2.8.5 Tandem Mass Tag phosphoproteomics

Two independent Tandem Mass Tag (TMT) phosphoproteome experiments were performed simultaneously. In one experiment, BMDMs from WT or *Tpl2*$^{D270A/D270A}$ mice were stimulated with uncoated latex beads (K1-080 blue, Estapor Merck Chimie SAS) at a final dilution of 1:50 for 0.5 h. In a second experiment, BMDMs from WT or *Tpl2*$^{D270A/D270A}$ mice were stimulated with LPS-coated latex beads (2.2.7.7) at a final dilution of 1:300 for 0.5 h. Five mice per genotype were used as biological replicates. Cells were lysed in detergent-free phosphoproteome lysis buffer (Table 8). A TMT-based labelling approach was used to allow for quantitative comparisons between conditions. For each condition per TMT channel, 200 µg of protein material was required. Samples were reduced by addition of DTT (Sigma-Aldrich) at a final concentration of 10 mM and incubated for 25 min at 56°C. DTT acts as a reducing agent to break disulphide bridges between cysteine residues. Samples were cooled to RT and alkylated by addition of iodoacetamide (Sigma-Aldrich) at a final concentration of 20 mM. Samples were incubated for 0.5 h at RT, protected from light. Iodoacetamide acts as an alkylating agent by preventing the reformation of disulphide bridges. To prevent alkylation reactions with other residues, iodoacetamide was quenched by addition of DTT at a final concentration of 20 mM. Prior to proteolytic digestion, the concentration of urea was reduced to <2 M by addition of 50 mM HEPES pH 8.5 (J61360, Alfa Aesar). Samples were first digested with lysyl endopeptidase (125-05061, FUJIFILM Wako Pure Chemical Corporation), LysC, which cleaves C-terminal ends of lysine residues. Each sample was digested with 4 µg LysC for 2 h at 37°C. Following LysC cleavage, a second digestion step involved MS-grade trypsin (90058, Thermo Fisher Scientific), which cleaves the C-terminal ends of lysine and arginine residues. Each sample was digested with 10 µg trypsin at 37°C overnight. Nest Group C_{18} MacroSpin columns (SMMSS18V, Thermo Fisher Scientific) were used to concentrate and clean up peptides following tryptic digests. Removal of lysis and digestion buffer components is essential prior to TMT labelling. Instructions in the standard manufacturer protocol were followed. Eluted peptide solutions were frozen with liquid nitrogen and dried by vacuum centrifugation. TMT10plex Isobaric Label Reagent Sets 0.8 mg (90111, Thermo Fisher Scientific) were used for chemical mass tagging of samples. Instructions in the standard manufacturer protocol were followed, however, minor adaptations were undertaken

to accommodate peptide labelling of 200 µg samples. Samples were solubilised in 200 µl 50 mM HEPES pH 8.5 with sonication in an ultrasonic bath for 15 min. LC-MS/MS label efficiency checks were carried out on 1/200 of each sample by diluting 2 µl of each reaction to 20 µl with 0.1% (v/v) TFA in a Total Recovery glass vial (186005663CV, Waters). Upon confirmation of labelling efficiencies of >99%, samples were quenched by addition of 16 µl 5% (v/v) hydroxylamine and incubation for 15 min at RT. Following quenching, all 10 TMT-labelled samples were combined in a 5 ml LoBind Eppendorf tube (Sigma-Aldrich), frozen with liquid nitrogen and partially dried by vacuum centrifugation for 2 h to remove organic content prior to Sep-Pak clean up. Samples were diluted in 0.1% (v/v) TFA to 3 ml and neat TFA was added to the sample mixture to a final concentration of 1% (v/v) TFA, thus ensuring a pH <2.0. Sep-Pak C18 Vac cartridges with 50 mg sorbent (054955, Waters) were washed in 1.25 ml acetonitrile, followed by conditioning with 0.5 ml 50% (v/v) acetonitrile/0.5% (v/v) acetic acid and equilibration with 1.25 ml 0.1% (v/v) TFA. The sample was loaded and the cartridge was subsequently desalted with 1.25 ml 0.1% (v/v) TFA. Following a wash with 150 µl 0.5% (v/v) acetic acid, peptides were eluted with 1 ml 50% (v/v) acetonitrile/0.5% (v/v) acetic acid. To carry out a final LC-MS/MS mixing check, 5 µl of the eluate was diluted with 95 µl 0.1% (v/v) TFA in a Total Recovery glass vial. The remainder of the eluate was frozen with liquid nitrogen and dried by vacuum centrifugation. For phosphopeptide enrichment the High-Select TiO_2 phosphopeptide enrichment kit (A32993, Thermo Fisher Scientific) was used according to the manufacturer protocol. The eluate was frozen with liquid nitrogen and dried by vacuum centrifugation to remove components of the phosphopeptide elution buffer. For a second phosphopeptide enrichment step the High-Select Fe-NTA phosphopeptide enrichment kit (A32992, Thermo Fisher Scientific) was used according to the manufacturer protocol. The eluate was frozen with liquid nitrogen and dried by vacuum centrifugation since the basic pH of the elution buffer would otherwise lead to loss of phosphates on phosphopeptides. The Pierce High pH Reversed-Phase Peptide Fractionation Kit (84868, Thermo Fisher Scientific) was used according to manufacturer instructions for unlabelled native peptides. Although TMT-labelled peptides were subjected to fractionation, samples contained enriched phosphopeptides with high hydrophilicity, thus elution solutions for unlabelled native peptides were used. Fractionated phosphopeptides were frozen with liquid nitrogen and dried by vacuum centrifugation. Prior to LC-MS/MS analysis,

dried fractions were resuspended in 32 µl 0.1% (v/v) TFA with sonication for 15 min. 15 µl injections were made of each fraction with the HCD-MS2 method and the multi-stage activation Orbitrap MS3 method on a 3 h gradient run (Jiang *et al*, 2017). Samples were analysed on an Orbitrap Fusion Lumos ETD mass spectrometer (Thermo Fisher Scientific) with an Ultimate 3000 RSLCnano LC system (Thermo Fisher Scientific). Dr Helen Flynn (Mass Spectrometry Proteomics STP, The Francis Crick Institute) performed LC-MS/MS analyses and processed all raw data files in the MaxQuant bioinformatics suite.

2.2.8.6 IP-MS label free TPL-2 interactome

BMDMs from *Tpl2*$^{3xFLAG/3xFLAG}$ mice were stimulated with LPS (100 ng/ml) or TNFα (20 ng/ml) for 15 min. Unstimulated BMDMs from *Tpl2*$^{3xFLAG/3xFLAG}$ mice were seeded alongside. Biological triplicates were prepared for each condition. Cells were prepared as described (2.2.4.2 and 2.2.4.3), with the exception that Triton X-100 in the lysis buffer was reduced to 0.25% (v/v). 3xFLAG-TPL-2 was immunoprecipitated from whole cell lysates according to standard procedures (2.2.4.7), with the exception that 5 mg cell extract and 20 µg packed resin was used in each IP sample. Eluates were subjected to SDS-PAGE on a 10% Bis-Tris NuPAGE gel (Invitrogen). Gels were run until the sample buffer front migrated through approximately 10 mm of the gel. Gels were stained with colloidal Coomassie, gel regions of interest were excised and transferred to a 96-well plate. Proteins were digested using a JANUS Automated Workstation (Perkin Elmer), where procedures were conducted in 50 mM ammonium bicarbonate (Sigma-Aldrich). Gel fragments were destained in 50% (v/v) acetonitrile. Cysteine reduction was performed by addition of DTT at a final concentration of 10 mM and incubated for 25 min at 56°C. Thiols were capped via alkylation by addition of iodoacetamide at a final concentration of 55 mM for 0.5 h at RT, protected from light. Proteolysis was performed by addition of MS-grade trypsin (Thermo Fisher Scientific) at 6 ng/µl for 5 h at 37°C. Extraction of peptides was completed by using 2% (v/v) formic acid in 2% (v/v) acetonitrile, followed by 50% (v/v) acetonitrile. Peptides were chromatographically resolved on an Ultimate 3000 RSLCnano (Dionex) with an EASY-Spray column, PepMap C18, 2 µm particles, 100 Å pore size and 50 cm × 75 µm ID (Thermo Fisher Scientific). The LC-gradient was

run with a flow of 0.25 µl/min, applying 98% IP-MS buffer A and 2% IP-MS buffer B (Table 8). IP-MS buffer B was increased to 8% over 0.5 min, to 40% over 30.5 min, and further increased to 90% in 1 min and held for 10 min. Lastly, IP-MS buffer B was decreased to 2% over 1 min for the remainder of the LC-MS data acquisition. Data acquisition was conducted in real-time over 2 h using a Lumos Mass Spectrometer (Thermo Fisher Scientific) and Xcalibur software. The mass spectrometer scanned using a 200-2,000 *m/z* acquisition window. A data-dependent acquisition mode was adapted to sample the top 10 most abundant peptides with charge states 2-4 selected for MS/MS and fragmented with collision-induced dissociation, at 30% normalised collision energy. To avoid recurring sampling of identical peptides, a dynamic exclusion list was used, with a repeat count of 1, repeat duration of 20 sec, exclusion list size of 500, and exclusion duration of 20 sec. Raw data was analysed in the MaxQuant bioinformatics suite. Protein text files were uploaded into Perseus (version 1.4.0.11) for further downstream data analysis and visualisation in the form of iBAQ intensity profile plots. Dr David Frith (Mass Spectrometry Proteomics STP, The Francis Crick Institute) carried out peptide digests, performed LC-MS analyses and processed all raw data files in the MaxQuant bioinformatics suite.

2.2.9 Immunofluorescence

2.2.9.1 Antibody staining

Confocal imaging experiments were performed on 13 mm, 1.5 mm round coverslips (VWR International). BMDMs were seeded in antibiotic-free BMDM seeding medium (Table 9) at a density of 1×10^5 cells per well in a 24-well plate one day prior to the experiment. Cells were incubated with latex beads (1:50) or infected with YFP-labelled *S. aureus* at an MOI of 10 as described. After the indicated incubation time, cells were washed twice in pre-warmed PBS and fixed in formaldehyde-containing eBioscience™ IC fixation buffer (Thermo Fisher Scientific) for 10 min at RT. Cells were washed twice in PBS and permeabilised in 0.1% (v/v) Triton X-100 in PBS for 4 min at RT. Subsequently, cells were washed three times in PBS and blocked in 0.4% (w/v) gelatin from cold water fish skin (Sigma-Aldrich) in PBS for 10 min at RT. Cells were directly incubated with 0.1% (w/v) sodium borohydride pH 8.0 (Sigma-

Aldrich) for 10 min at RT. Sodium borohydride quenches residual aldehyde groups following fixation, thus yielding higher imaging resolution. Cells were washed twice in 0.4% (w/v) gelatin fish skin and incubated with primary antibody in 0.4% (w/v) gelatin fish skin for 1 h at RT. Following antibody staining, cells were washed three times in 0.4% (w/v) gelatin fish skin and incubated with secondary antibody in 0.4% (w/v) gelatin fish skin for 0.5 h at RT. Cells were washed three times in 0.4% (w/v) gelatin fish skin and stained with DAPI (Thermo Fisher Scientific) in 0.4% (w/v) gelatin fish skin at 1:1000 dilution for 15 min at RT. Lastly, cells were washed three times with 0.4% (w/v) gelatin fish skin and once in PBS. Coverslips were mounted on Corning® microscope glass slides (Merck) with one drop of Fluoromount™ Aqueous Mounting Medium (Sigma-Aldrich). Slides were incubated in the dark at RT overnight and then stored at 4°C until image acquisition. Images were acquired with a Zeiss Inverted LSM 880 AxioObserver confocal laser scanning microscope (ZEISS) using a ZEISS 40x Plan-Apochromat (numerical aperture = 1.3) DIC M27 oil immersion objective. A ZEISS 63x Plan-Apochromat (numerical aperture = 1.4) DIC UV-VIS-IR M27 oil immersion objective was used in co-localisation studies.

2.2.9.2 Cathepsin activity assay

Following latex bead stimulation or bacterial infection, cells were washed twice in pre-warmed PBS. To determine cathepsin L protease activity in macrophages, the Magic Red cathepsin L substrate (ICT942, Bio-Rad Antibodies) was used at a final dilution of 1:250 in bead assay buffer (Table 8). Cells were incubated with the Magic Red cathepsin L substrate for 1 h at 37°C. Subsequently, cells were fixed, DAPI-stained, mounted and imaged as outlined in 2.2.9.1. Fluorescence intensity of the Magic Red substrate was captured at excitation/emission wavelengths 592/628 nm.

2.2.9.3 LysoTracker Red

Following latex bead stimulation or bacterial infection, cells were washed twice in pre-warmed PBS. To label and track acidic organelles in macrophages, LysoTracker Red DND-99 (L7528, Thermo Fisher Scientific), an acidotropic red-fluorescent dye, was used at a final concentration of 100 nM in bead assay buffer (Table 8). Cells

were incubated with LysoTracker Red for 1 h at 37°C. Subsequently, cells were washed, fixed, stained with DAPI and imaged as outlined in 2.2.9.1. Fluorescence intensity of LysoTracker Red was captured at excitation/emission wavelengths 577/590 nm.

2.2.9.4 Reactive oxygen species

To detect ROS, in particular superoxides and hydroxyl radicals, a ROS Deep Red dye (ab186029, Abcam) was used. Experimental steps were followed as described in 2.2.9.3. Briefly, the ROS-reactive dye was added at a final concentration of 100 nM and incubated with cells for 1 h at 37°C. Fluorescence intensity of ROS levels was captured at excitation/emission wavelengths 650/675 nm

2.2.9.5 Image Analysis

Images were processed and analysed using ImageJ (Fiji) version 2.0.0 (National Institutes of Health, USA). Fluorescence intensities per cell were quantified by creating masks of cell outlines and determining integrated density (IntDen), the product of area and mean fluorescence intensity, for each cell. Relative fluorescence intensity was calculated by determining the ratios of integrated densities for two different markers in the same masked area. The Fiji plugin Coloc 2 was used for colocalisation studies, where parameters were set to bisectional threshold regression with a point spread function (PSF) of 3.0 and Costes randomisations adjusted to 100. Coloc 2 performs pixel intensity correlation analyses to determine Pearson correlation coefficients and Manders' coefficients (Manders *et al*, 1993; Mukaka, 2012). For all statistical analyses, only coefficients above the Coloc 2 autothreshold were selected. In LAMP1 and ubiquitin studies, the number of YFP-*S. aureus* bacteria was automatically counted by normalising the YFP fluorescence threshold across all images and determining the number of particles >0.2 µm. The percentages of YFP-fluorescent *S. aureus* phagosomes that were associated with distinct LAMP1 rings or ubiquitin puncta were quantified by analysing >100 cells including >600 bacteria per genotype from at least 40 random fields in three independent experiments. Macrophages and bacteria as well as imaging fields were

captured for all microscopy experiments in similar quantity. At least two biological controls per genotype and technical duplicates per condition were included in each experiment.

2.2.10 Statistical Analysis

Experiments throughout this thesis were independently repeated at least three times and one representative experiment is shown. Statistical analyses were performed in GraphPad Prism software (version 8.2.1). Detailed descriptions of statistical tests are outlined in figure legends. Statistical significance of data is represented by asterisks (*) corresponding to *P* value thresholds, where not significant (ns) $P > 0.05$, * $P < 0.05$, ** $P < 0.01$, *** $P < 0.001$, **** $P < 0.0001$. Error bars represent standard errors of the mean (SEM).

2.2.11 Molecular biology techniques

2.2.11.1 Plasmids

Two plasmids expressing HA-tagged NF-κB1 p105 and His_6-tagged TPL-2 were previously described in published work by the Ley laboratory. The plasmid constructs used in this study are outlined in Table 15. All new cDNA constructs were generated by the DSTT cloning team at the University of Dundee, led by Dr James C. Hastie. Newly designed cDNA constructs were sequence-verified by the DNA Sequencing Service at the College of Life Sciences, University of Dundee.

Table 15 Plasmids

Protein	Species	Vector backbone	ID	Source
3xFLAG-DMXL1^{WT} [1773-2047]	Mouse	pcDNA3.1 (Invitrogen)	DU67566	DSTT
3xFLAG-DMXL1^{SSAA} [1773-2047]	Mouse	pcDNA3.1 (Invitrogen)	DU67567	DSTT
HA-NF-κB1 p105	Human	pcDNA3.1 (Invitrogen)	N/A	Ley laboratory (Salmerón *et al*, 2001)
His_6-TPL-2	Human	pcDNA3.1 (Invitrogen)	N/A	Ley laboratory (Gantke *et al*, 2013)
3xFLAG-A20	Human	pcDNA3.1 (Invitrogen)	DU27546	DSTT
3xFLAG-ALIX	Human	pcDNA3.1 (Invitrogen)	DU53929	DSTT
3xFLAG-TSG101	Human	pcDNA3.1 (Invitrogen)	DU53924	DSTT

2.2.11.2 Plasmid transformation

Competent library efficiency *E. coli* DH5α cells (Life Technologies) were combined with 2 µl plasmid cDNA and incubated on ice for 0.5 h. Cells were heat-shocked at 42°C for 45 sec to ensure DNA uptake into competent cells. Transformed cells were incubated on ice for 2 min. Cells were incubated with 900 µl Super Optimal broth with Catabolite repression (SOC) medium (Sigma-Aldrich) for 1 h in a 37°C incubator set to 225 rpm. Cells were streaked out on LB agar plates supplemented with 100 µg/ml ampicillin (Sigma-Aldrich) for antibiotic selection. Plates were incubated for 16 h at 37°C.

2.2.11.3 Plasmid growth and isolation

One transformed bacterial colony was selected to inoculate 500 ml LB media supplemented with 100 µg/ml ampicillin. The bacterial culture was incubated for 16

h in a 37°C incubator set to 225 rpm. Following bacterial growth, the culture was pelleted by centrifugation at 3,800 rpm for 15 min at 4°C. Using a Qiagen EndoFree Plasmid Maxi Kit (Thermo Fisher Scientific) plasmid cDNA was isolated following manufacturer instructions. cDNA concentration was quantified using a NanoDrop spectrophotometer (Thermo Fisher Scientific).

2.2.11.4 RNA extraction and purification

BMDMs were seeded and stimulated or infected as outlined in the respective experiment. Cells were lysed in 350 µl Qiagen RLT lysis buffer (Thermo Fisher Scientific) supplemented with β-ME at 1:100 (v/v). RNA was extracted and purified using the Qiagen RNeasy Mini Kit (Thermo Fisher Scientific) and Qiagen RNase-free DNase set (Thermo Fisher Scientific) according to manufacturer instructions.

2.2.11.5 Real-time quantitative reserve transcription PCR (qRT-PCR)

Purified RNA was reverse transcribed to cDNA using the SuperScript VILO cDNA Synthesis Kit (Invitrogen) according to manufacturer instructions. Briefly, 200-500 ng RNA was reverse transcribed in a total reaction volume of 10 µl. cDNA was subsequently diluted in nuclease-free water and stored at 4°C. qRT-PCR was set up in MicroAmp Optical 384-well plates (Applied Biosystems). The 7 µl reaction volume in each well contained 2 µl cDNA (20-40 ng), 3.5 µl 2x TaqMan Universal PCR Master Mix (Applied Biosystems), 0.35 µl TaqMan FAM-coupled probe (Table 16), and 1.15 µl nuclease-free water. Samples were analysed on a Quantstudio 3 and 5 (Applied Biosystems) set to comparative C_T mode. *Hprt* was used as a housekeeping gene and gene expression levels were normalised to *Hprt* measurements. C_T values were used to calculate ΔC_T values and mRNA fold changes.

qRT-PCR probes

All TaqMan FAM-MGB-coupled probes were purchased from Thermo Fisher Scientific (4331182).

Table 16 FAM-MGB-coupled qRT-PCR probes

Gene target	Assay ID
Cxcl2	Mm00436450_m1
Dmxl1	Mm01261785_m1
Dmxl2	Mm00555326_m1
Hprt	Mm01545399_m1
Ifna1	Mm03030145_gH
Ifna2	Mm00833961_s1
Ifna5	Mm00833976_s1
Ifna6	Mm01703458_s1
Ifnb1	Mm00439552_s1
Il1b	Mm00434228_m1
Il6	Mm00446190_m1
Il12	Mm01288989_m1
Il23a	Mm01160011_g1
Nlrp3	Mm00840904_m1
Tnf	Mm00443260_g1
Tnfaip3	Mm00437121_m1

2.2.12 RNA sequencing

Three independent RNA sequencing (RNA-seq) experiments were performed in this thesis:

1) BMDMs from WT and *Abin2*$^{E256K/E256K}$ mice were stimulated with LPS (100 ng/ml)
2) BMDMs from WT and *Tpl2*$^{D270A/D270A}$ mice were stimulated with LPS-coated latex beads (1:300)
3) BMDMs from WT and *Tpl2*$^{D270A/D270A}$ mice were infected with *S. aureus* (MOI of 10)

RNA was extracted and purified as described in 2.2.11.4. RNA quality control was carried out using the 2100 Expert Agilent Bioanalyzer. Libraries were generated using the TruSeq RNA Library Prep Kit (Illumina) and single-end sequencing was performed using the Illumina HiSeq 2500 platform. Approximately 22 million strand-specific reads were obtained. Both the RSEM package and STAR alignment algorithm were applied for mapping and counting of sequencing reads (Li & Dewey,

2011; Dobin *et al*, 2013). Data analysis of differential gene expression was performed using the DESeq2 package within the R software package (Love *et al*, 2014). After RNA extraction and purification, all experimental stages for RNA sequencing were performed by the Advanced Sequencing Facility at The Francis Crick Institute. Analysis of RNA sequencing data was carried out by Probir Chakravarty (Bioinformatics STP, The Francis Crick Institute).

Chapter 3. Biochemical characterisation of ABIN-2

3.1 Introduction

The adaptor protein ABIN-2 was originally identified as an A20-binding protein and subsequent studies have shown its ability to interact with ubiquitin and TSG101 of the ESCRT-I complex (Webb *et al*, 2019; Banks *et al*, 2016). ABIN-2 is also an integral component of the TPL-2 complex, interacting with TPL-2 and NF-κB1 p105, which are both required to maintain ABIN-2 protein stability (Sriskantharajah *et al*, 2014; Webb *et al*, 2019).

Originally, the role of ABIN-2 in innate immunity and inflammation was investigated using overexpression systems in mammalian cell lines. Such studies showed that overexpressed ABIN-2 inhibits NF-κB activation via its ability to bind to ubiquitin (Wagner *et al*, 2008; Van Huffel *et al*, 2001). However, NF-κB activation is normal in *Abin2*$^{-/-}$ immune cells and endogenous ABIN-2 does not appear to be important for NF-κB activation. ABIN-2 is required to maintain TPL-2 stability and consequently, optimal activation of the TPL-2-ERK1/2 MAP kinase pathway is impaired in *Abin2*$^{-/-}$ immune cells. However, ABIN-2 is presumably not important for physiological activation of the TPL-2 MAP kinase pathway.

More recent studies have focused on the biological function of ABIN-2 by studying the effects of loss-of-function point mutations in *Abin2* knock-in mice. Previous *in vitro* studies have shown that *Abin2*^{D310N} point mutation abrogates ubiquitin binding (Nanda *et al*, 2018), while *Abin2*^{E256K} mutation reduces binding to A20 (Dong *et al*, 2011). Analyses of the effects of these mutations in knock-in mice demonstrated that both ubiquitin and A20 binding to ABIN-2 are critical to limit inflammation in models of inflammatory bowel disease and allergic airway inflammation, respectively. However, the underlying molecular mechanisms remain to be fully understood (Nanda *et al*, 2018; Ventura *et al*, 2018). The biological relevance of the recently discovered interaction between ABIN-2 and TSG101, which is disrupted by the Y230A point mutation in human ABIN-2, has remained unknown (Banks *et al*, 2016).

In Chapter 3 of this thesis, I set out to biochemically characterise ABIN-2 point mutations in detail. In order to decipher the physiological signalling roles of ABIN-2, it was essential to determine whether individual point mutations in ABIN-2 affect

interaction with other binding partners. Moreover, it was important to establish the effects of *Abin2* point mutations on ABIN-2 interaction with TPL-2 and p105.

Following biochemical characterisation of ABIN-2 point mutations, I investigated whether ubiquitin or A20 binding to ABIN-2 regulate innate immune signalling in primary murine macrophages. Based on the previous observation that ABIN-2 interacts with the TNF receptor and the fact that ABIN-2 associates with TPL-2, I focused these experiments on TLR4- and TNF receptor-mediated signalling pathways.

3.2 Results

3.2.1 Characterisation of *Abin2* point mutations

To establish the effects of *Abin2* point mutations on ABIN-2 interactions, I used GST-ABIN-2 WT, GST-ABIN-2^{D309N} and GST-ABIN-2^{E255K} fusion proteins. The human ABIN-2 sequence was used for generating GST-ABIN-2 fusion proteins since purified human WT and D309N ABIN-2 proteins were already available from Dundee University, which also produced GST-ABIN-2^{E255K} protein for my experiments. The D309N point mutation in human ABIN-2 corresponds to the D310N mutation in *Abin2*$^{D310N/D310N}$ mice, while the E255K point mutation in human ABIN-2 corresponds to the E256K mutation in *Abin2*$^{E256K/E256K}$ mice. In addition, Dundee University produced a human GST-ABIN-2^{Y230A} fusion protein to study the effects of ABIN-2 interaction with the ESCRT-I proteins TSG101 and ALIX on other associations.

Dong *et al*., Banks *et al.* as well as Nanda *et al*. have previously shown that *Abin2*^{E255K}, *Abin2*^{Y230A}, and *Abin2*^{D309N} mutations disrupt A20, ESCRT-I and ubiquitin binding to ABIN-2, respectively. However, the potential effects of these point mutations on ABIN-2 binding to other known interactors were not determined. Therefore, it remained unclear whether these mutations specifically impaired A20, ESCRT-I and ubiquitin binding, respectively. I performed GST pulldown experiments to characterise the effects of these three *Abin2* point mutations in detail.

Ubiquitin. GST-ABIN-2 fusion proteins were incubated with purified M1-linked ubiquitin octamers. GST-ABIN-2^{E255K} and GST-ABIN-2^{Y230A} associated with M1-linked ubiquitin octamers to a similar extent as GST-ABIN-2 WT (Figure 10A and C).

In contrast, M1-linked ubiquitin octamers did not bind to GST-ABIN-2^{D309N} (Figure 10B).

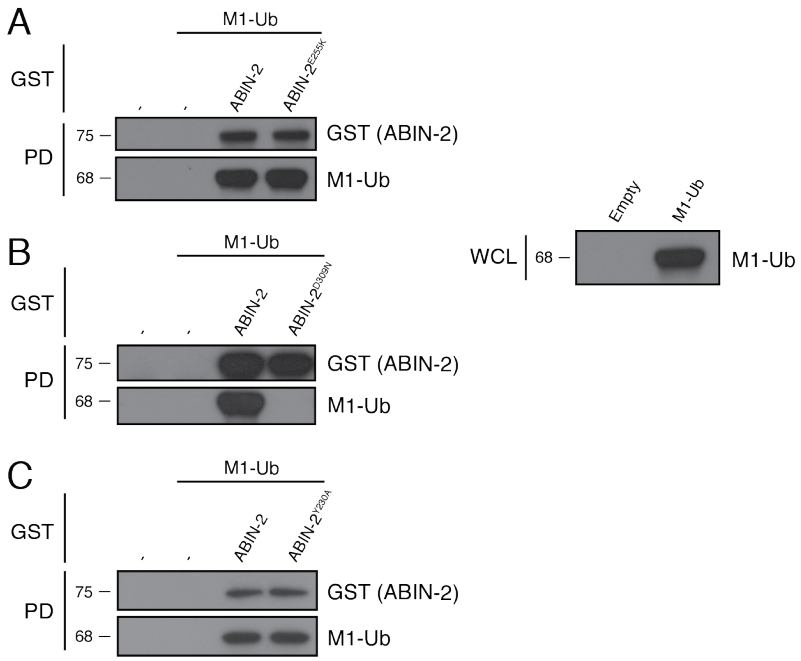

Figure 10 ABIN-2^{D309N} selectively abrogates ubiquitin binding to ABIN-2

GST pulldowns were performed with GST-ABIN-2 fusion proteins and purified M1-linked ubiquitin octamers. WCL and eluates were immunoblotted with antibodies recognising GST and M1-linked ubiquitin. (**A**) Ubiquitin octamers were separately incubated with GST-ABIN-2 WT and GST-ABIN-2^{E255K}. (**B**) Ubiquitin octamers were separately incubated with GST-ABIN-2 WT and GST-ABIN-2^{D309N}. (**C**) Ubiquitin octamers were separately incubated with GST-ABIN-2 WT and GST-ABIN-2^{Y230A}. PD, pulldown; WCL, whole cell lysate.

A20. GST-ABIN-2 fusion proteins were incubated with whole cell lysates from HEK293 cells, in which 3xFLAG-A20 was transiently overexpressed. GST-ABIN-2^{E255K} binding to 3xFLAG-A20 was reduced by 70% relative to GST-ABIN-2 WT binding to 3xFLAG-A20 (Figure 11A). However, A20 binding to neither GST-ABIN-2^{D309N} (Figure 11B) nor GST-ABIN-2^{Y230A} (Figure 11C) was impaired.

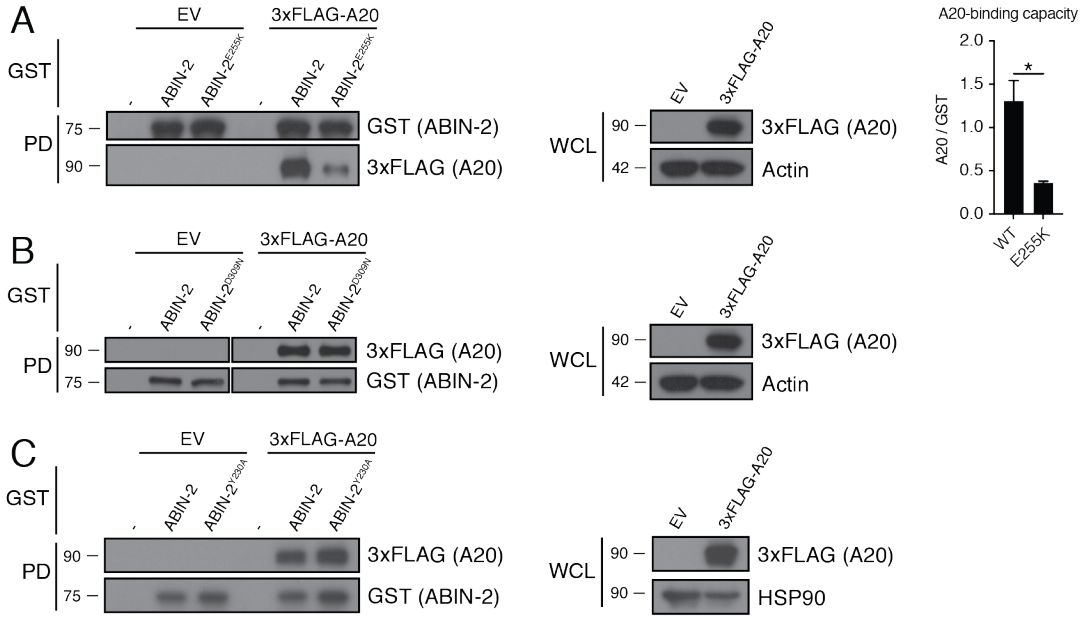

Figure 11 ABIN-2^{E255K} selectively reduces A20 binding to ABIN-2

GST pulldowns were performed with GST-ABIN-2 fusion proteins and 3xFLAG-A20. WCL and eluates were immunoblotted with antibodies recognising GST and 3xFLAG-tagged A20. (**A**) Interaction of 3xFLAG-A20 with GST-ABIN-2 WT and GST-ABIN-2^{E255K} was determined in GST pulldown assays (left). The A20-binding capacity of GST-ABIN-2 WT and GST-ABIN-2^{E255K} was quantified from three independent experiments. An unpaired two-tailed t-test was carried out, with * $P < 0.05$ (right). Error bars represent SEM. (**B**) Interaction of 3xFLAG-A20 with GST-ABIN-2 WT and GST-ABIN-2^{D309N} was determined in GST pulldown assays. (**C**) Interaction of 3xFLAG-A20 with GST-ABIN-2 WT and GST-ABIN-2^{Y230A} was determined in GST pulldown assays. EV, empty vector; PD, pulldown; WCL, whole cell lysate.

ESCRT-I. GST-ABIN-2 fusion proteins were incubated with whole cell lysates from HEK293 cells, in which either 3xFLAG-TSG101 or 3xFLAG-ALIX was transiently overexpressed. TSG101 is a core component of the ESCRT-I complex while ALIX is a critical accessory protein of ESCRT-I. Although Banks *et al.* provided evidence that *Abin2*^{Y230A} mutation impairs ALIX binding to ABIN-2, biochemical studies to show this directly were not carried out (Banks *et al*, 2016). My experiments showed that GST-ABIN-2^{E255K} and GST-ABIN-2^{D309N} bind to both TSG101 and ALIX as strongly as GST-ABIN-2 WT (Figure 12A and B). Strikingly, however, GST-ABIN-2^{Y230A} did not interact with either TSG101 or ALIX (Figure 12C).

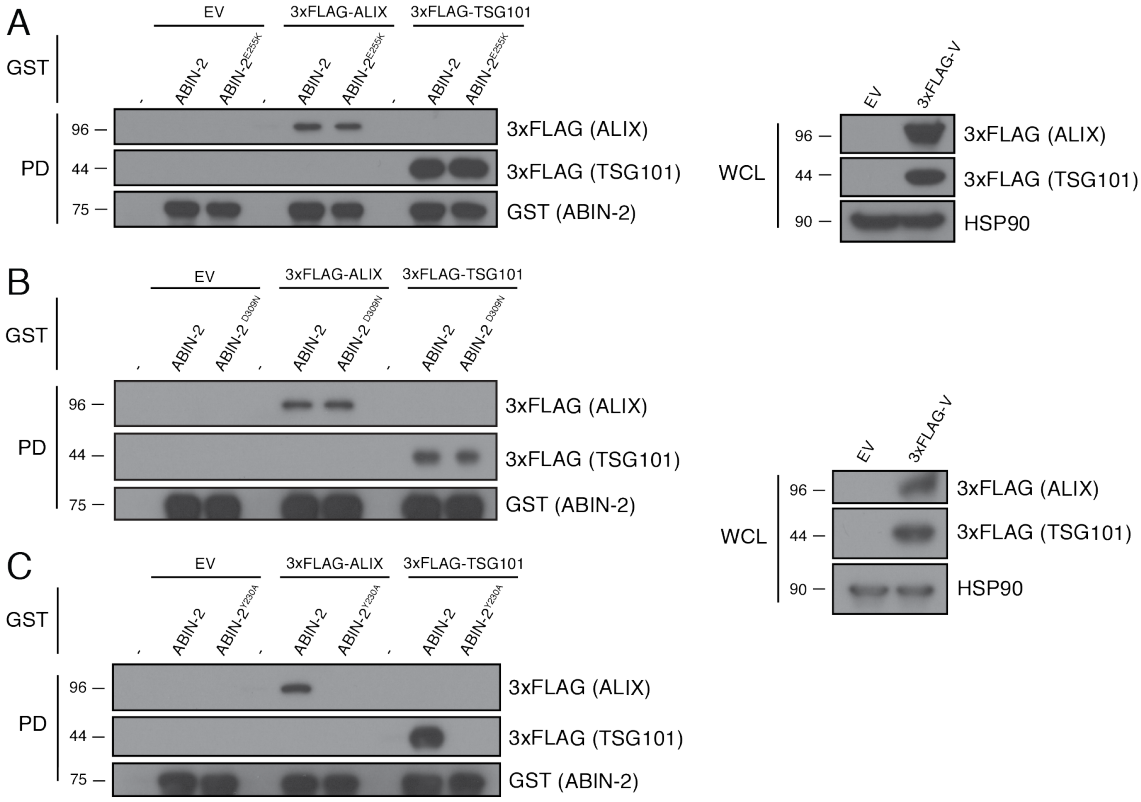

Figure 12 ABIN-2^{Y230A} selectively abrogates ESCRT-I binding to ABIN-2

GST pulldowns were performed with GST-ABIN-2 fusion proteins and 3xFLAG-TSG101 as well as 3xFLAG-ALIX. WCL and eluates were immunoblotted with antibodies recognising GST and 3xFLAG-tagged TSG101 or ALIX. (**A**) Interaction of 3xFLAG-TSG101 or 3xFLAG-ALIX with GST-ABIN-2 WT and GST-ABIN-2^{E255K} was determined in GST pulldown assays. (**B**) Interaction of 3xFLAG-TSG101 or 3xFLAG-ALIX with GST-ABIN-2 WT and GST-ABIN-2^{D309N}. (**C**) Interaction of 3xFLAG-TSG101 or 3xFLAG-ALIX with GST-ABIN-2 WT and GST-ABIN-2^{Y230A}. EV, empty vector; PD, pulldown; WCL, whole cell lysate.

TPL-2/NF-κB1 p105. As previously mentioned, in unstimulated cells ABIN-2 forms a ternary complex with TPL-2 and p105 (Lang *et al*, 2004). To investigate whether *Abin2* point mutations disrupt the interaction between ABIN-2 and TPL-2/p105 complexes, I transiently co-overexpressed His_6-TPL-2 and HA-p105 in HEK293 cells. The binding capacity of GST-ABIN-2 fusion proteins to His_6-TPL-2/HA-p105 complexes was investigated in pulldown assays. All three mutant GST-ABIN-2 proteins interacted with His_6-TPL-2/HA-p105 complexes similarly to GST-ABIN-2 WT (Figure 13).

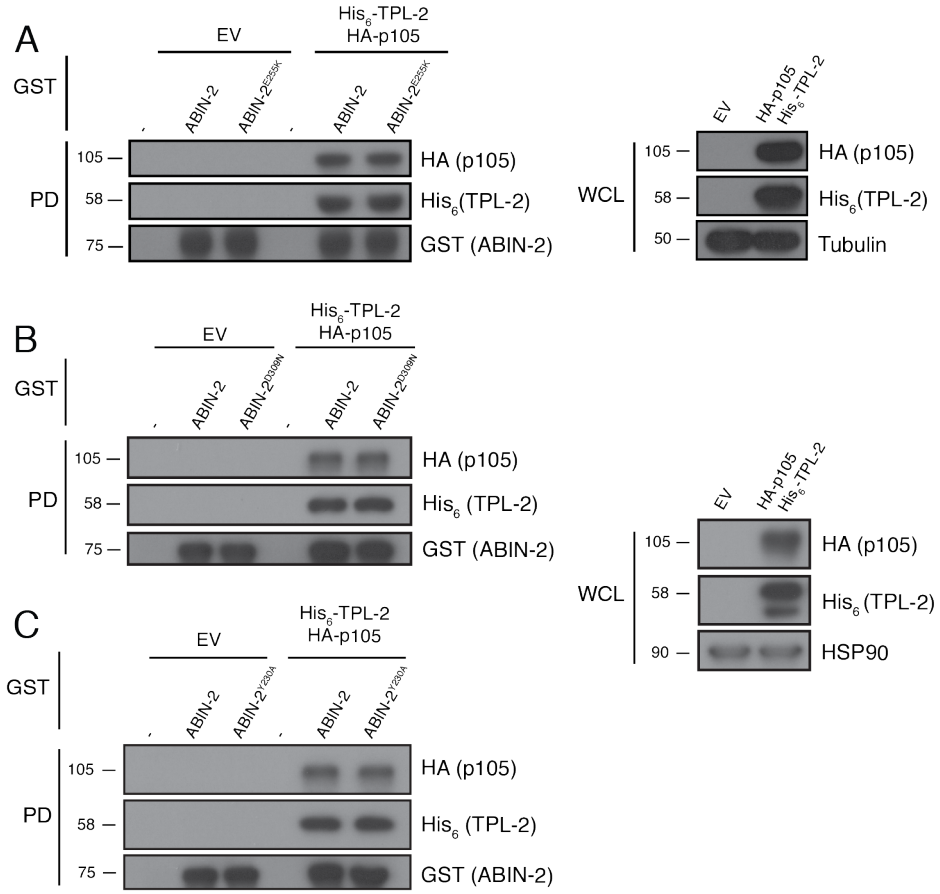

Figure 13 ABIN-2 point mutations do not impair binding to TPL-2/p105 complexes

GST pulldowns were performed with GST-ABIN-2 fusion proteins and co-overexpressed His_6-TPL-2/HA-p105. WCL and eluates were immunoblotted with antibodies recognising GST, His_6-tagged TPL-2 and HA-tagged p105. (**A**) Interaction of His_6-TPL-2/HA-p105 with GST-ABIN-2 WT and GST-ABIN-2^{E255K}. (**B**) Interaction of His_6-TPL-2/HA-p105 with GST-ABIN-2 WT and GST-ABIN-2^{D309N}. (**C**) Interaction of His_6-TPL-2/HA-p105 with GST-ABIN-2 WT and GST-ABIN-2^{Y230A}. EV, empty vector; PD, pulldown; WCL, whole cell lysate.

My pulldown studies demonstrated that *Abin2* point mutations specifically disrupted binding to the respective interaction partner, without affecting binding to other known interactors. More specifically, *Abin2*^{E255K} mutation reduced A20 binding, *Abin2*^{D309N} mutation abrogated linear ubiquitin binding, and *Abin2*^{Y230A} mutation diminished ESCRT-I binding. Moreover, none of the ABIN-2 point mutations affected the association with TPL-2/p105 complexes.

3.2.2 The role of ABIN-2 in TLR4 and TNF receptor signalling

As previously described, ABIN-2 is required for maintaining TPL-2 stability and vice versa. Since both *Abin2*$^{-/-}$ and *Tpl2*$^{-/-}$ mice are essentially TPL-2/ABIN-2 compound knockout mice, I used knock-in mouse strains, which harbour loss-of-function point mutations in *Abin2* and *Tpl2*, throughout this thesis to separately study ABIN-2 and TPL-2 functions. *Tpl2*$^{D270A/D270A}$ knock-in mice express catalytically inactive TPL-2.

In initial experiments, I determined the effects of mutations studied on steady-state TPL-2 and ABIN-2 protein expression levels. In unstimulated BMDMs from *Abin2*$^{E256K/E256K}$, *Abin2*$^{D310N/D310N}$ and *Tpl2*$^{D270A/D270A}$ knock-in mice, endogenous ABIN-2 and TPL-2 protein levels were similar to protein levels in BMDMs from WT mice (Figure 14).

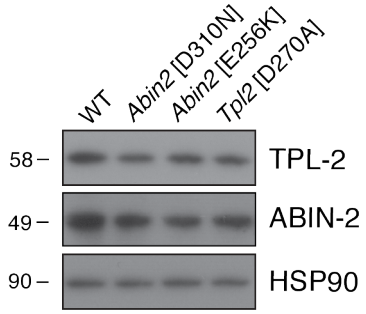

Figure 14 ABIN-2 and TPL-2 levels are normal in knock-in mouse strains
BMDMs from WT, *Abin2*$^{D310N/D310N}$, *Abin2*$^{E256K/E256K}$ and *Tpl2*$^{D270A/D270A}$ mice were lysed and cell extracts were immunoblotted with antibodies that specifically recognise TPL-2, ABIN-2 and HSP90.

To investigate whether ubiquitin and A20 binding to ABIN-2 are involved in regulating innate immune signalling in macrophages, I focused on TLR4- and TNF receptor-mediated signalling. TLR4 activation of ERK1/2 in macrophages is mediated by TPL-2 and involves dissociation of the ternary TPL-2 complex to liberate ABIN-2 (Gantke *et al*, 2012). Furthermore, proteomic studies have shown that ABIN-2 binds to the activated TNF receptor (Wagner *et al*, 2016).

To biochemically confirm ABIN-2/TNFR1 interaction, I stimulated MEFs with recombinant 3xFLAG-TNF ligand and immunoprecipitated the 3xFLAG-TNF/TNF receptor signalling complex. The unstimulated TNF receptor complex was immunoprecipitated by addition of 3xFLAG-TNF to cell extract from unstimulated

MEFs. ABIN-2 was recruited to the TNF receptor upon TNF stimulation (Figure 15), thus consistent with the findings of Wagner *et al*. Post-translational modifications of RIP1 indicated potent TNF stimulation of MEFs (Figure 15, left).

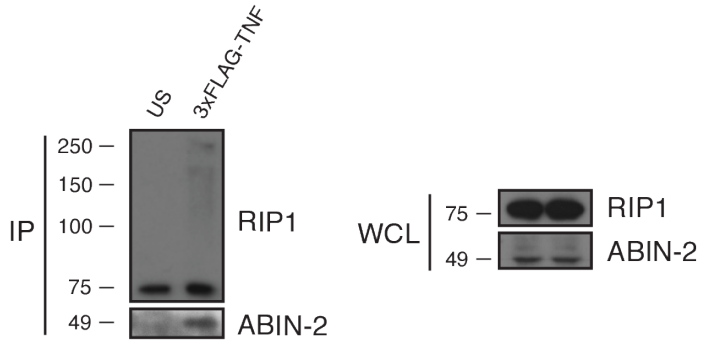

Figure 15 ABIN-2 is recruited to TNFR1 upon stimulation

MEFs were stimulated with 3xFLAG-tagged TNF at 0.5 µg/ml for 15 min. The cell extract of unstimulated MEFs was incubated with 3xFLAG-tagged TNF at 0.5 µg/ml following cell lysis. 3xFLAG-TNF/TNF receptor signalling complexes were immunoprecipitated by incubation of cell extracts with M2 Anti-FLAG Affinity Gel. Eluates (left) and WCL (right) were immunoblotted with antibodies that recognise RIP1 and ABIN-2. US, unstimulated; IP, immunoprecipitation; WCL, whole cell lysate.

I set out to test whether *Abin2*^{E256K} or *Abin2*^{D310N} mutation alter signalling downstream of TLR4 and the TNF receptor. Stimulation of BMDMs with LPS and TNFα activates TLR4 and TNF receptor signalling, respectively. Both LPS and TNFα led to strong activation of the IKK complex, as indicated by phosphorylation of p105 at S933, and activation of MAPK cascades, as indicated by ERK1/2 and p38α phosphorylation (Figure 16). Phosphorylation of ERK1 (p44) and ERK2 (p42) isoforms at activation loop residues T202 and Y204 by MEK1 and MEK2 is critical for protein kinase activation (Pagès & Pouysségur, 2004). Similarly, phosphorylation of residues T180 and Y182 in the activation loop of p38α MAP kinase by MKK3 and MKK6 is a prerequisite for kinase activation. Notably, p105, ERK1/2 as well as p38α phosphorylation in BMDMs from *Abin2*$^{E256K/E256K}$ and *Abin2*$^{D310N/D310N}$ mice was comparable to BMDMs from WT mice.

Upon LPS stimulation, autocrine JAK-STAT signalling was triggered at later time points, as indicated by STAT1 and STAT3 phosphorylation at Y701 and Y705, respectively (Figure 16A). Both phosphorylation sites promote STAT dimerisation and nuclear translocation (Ihle *et al*, 1994; Darnell *et al*, 1994). Neither *Abin2*^{E256K} nor *Abin2*^{D310N} mutation altered LPS-induced STAT1 or STAT3 phosphorylation

(Figure 16A). Besides targeting p105, the IKK complex also phosphorylates IκBα, leading to its degradation thereby liberating and activating NF-κB transcription factors. LPS- and TNFα-induced degradation of IκBα was normal in *Abin2*$^{E256K/E256K}$ and *Abin2*$^{D310N/D310N}$ BMDMs relative to WT BMDMs (Figure 16). Moreover, AKT signalling was activated following LPS and TNFα stimulation, as indicated by inducible phosphorylation of AKT at S473 and ribosomal S6 kinase p70 (p70S6K) at T389 (Figure 16). The S473 site is located in the C-terminus of AKT and its phosphorylation by the mammalian target of rapamycin (mTOR) complex 2 is required for AKT activation. AKT mediates activation of mTOR complex 1, which in turn phosphorylates p70S6K on T389, a residue in the linker domain of p70S6K, which is critical for kinase activity (Sarbassov *et al*, 2005; Pullen & Thomas, 1997). Levels of AKT S473 and p70S6K T389 phosphorylation in *Abin2*$^{E256K/E256K}$ and *Abin2*$^{D310N/D310N}$ BMDMs were comparable to WT BMDMs, suggesting that neither ubiquitin nor A20 binding to ABIN-2 regulates AKT signalling (Figure 16).

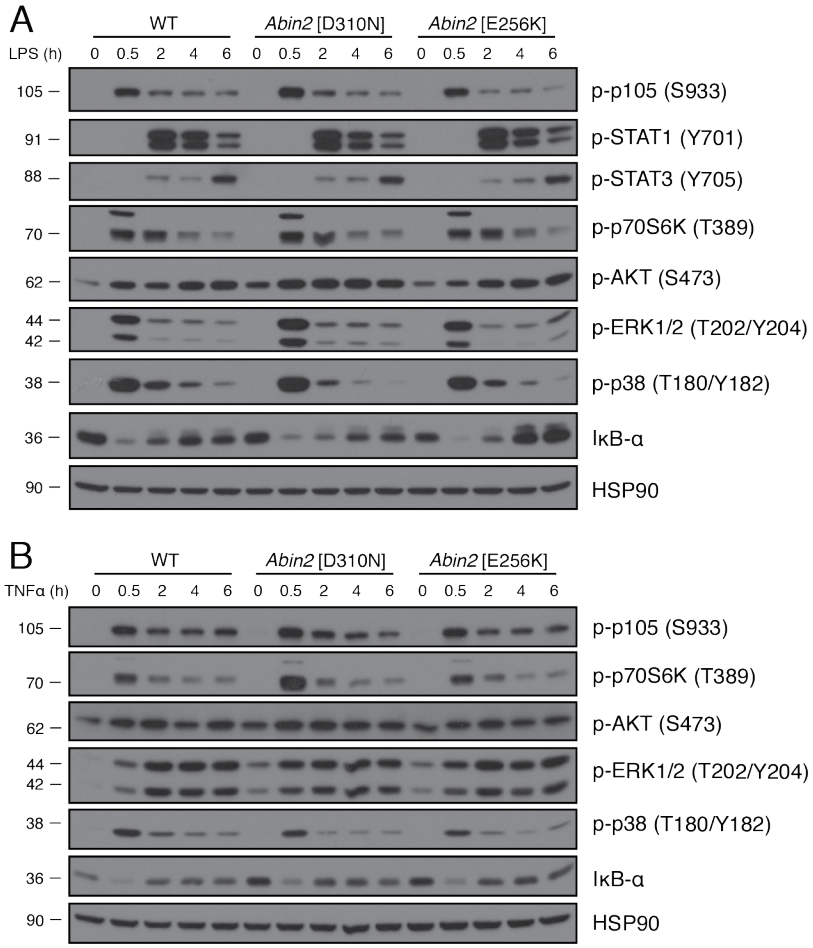

Figure 16 A20 and ubiquitin binding to ABIN-2 do not regulate TLR4 and TNFR1 signalling

BMDMs from WT, *Abin2*$^{D310N/D310N}$ and *Abin2*$^{E256K/E256K}$ mice were stimulated with (**A**) LPS (100 ng/ml) and (**B**) TNFα (20 ng/ml) for the times indicated and cell extracts were immunoblotted with the antibodies indicated. p, phospho.

In conclusion, these experiments indicated that ABIN-2 binding to ubiquitin and A20 did not alter immediate signalling events downstream of either TLR4 or TNF receptor 1.

3.2.3 Regulation of TLR4-mediated gene expression by ABIN-2/A20 complexes

Previous studies have proposed that ABIN-2 regulates gene expression by functioning as a transcriptional co-activator (Chien *et al*, 2003). Given the suggested nuclear role for ABIN-2, I therefore intended to further study whether A20 binding to ABIN-2 regulates gene expression. To investigate whether A20 binding to ABIN-2 regulates gene expression downstream of TLR4, I characterised the LPS-induced transcriptome in BMDMs from *Abin2*$^{E256K/E256K}$ mice compared to WT controls. As the LPS time course proceeded, all four biological replicates from WT and *Abin2*$^{E256K/E256K}$ mice co-migrated on the PCA plot (Figure 17A). This indicated that TLR4-mediated gene signatures in WT and *Abin2*$^{E256K/E256K}$ BMDMs were similar. All genes identified by RNA sequencing were visualised on volcano plots. At all time points, no gene sets were significantly up- or downregulated by more than 4-fold in *Abin2*$^{E256K/E256K}$ BMDMs relative to WT controls (Figure 17B). Importantly, I was unable to identify genes that were differentially regulated in *Abin2*$^{E256K/E256K}$ BMDMs in response to LPS stimulation (Figure 17B), suggesting that binding of A20 to ABIN-2 does not regulate gene expression following TLR4 activation.

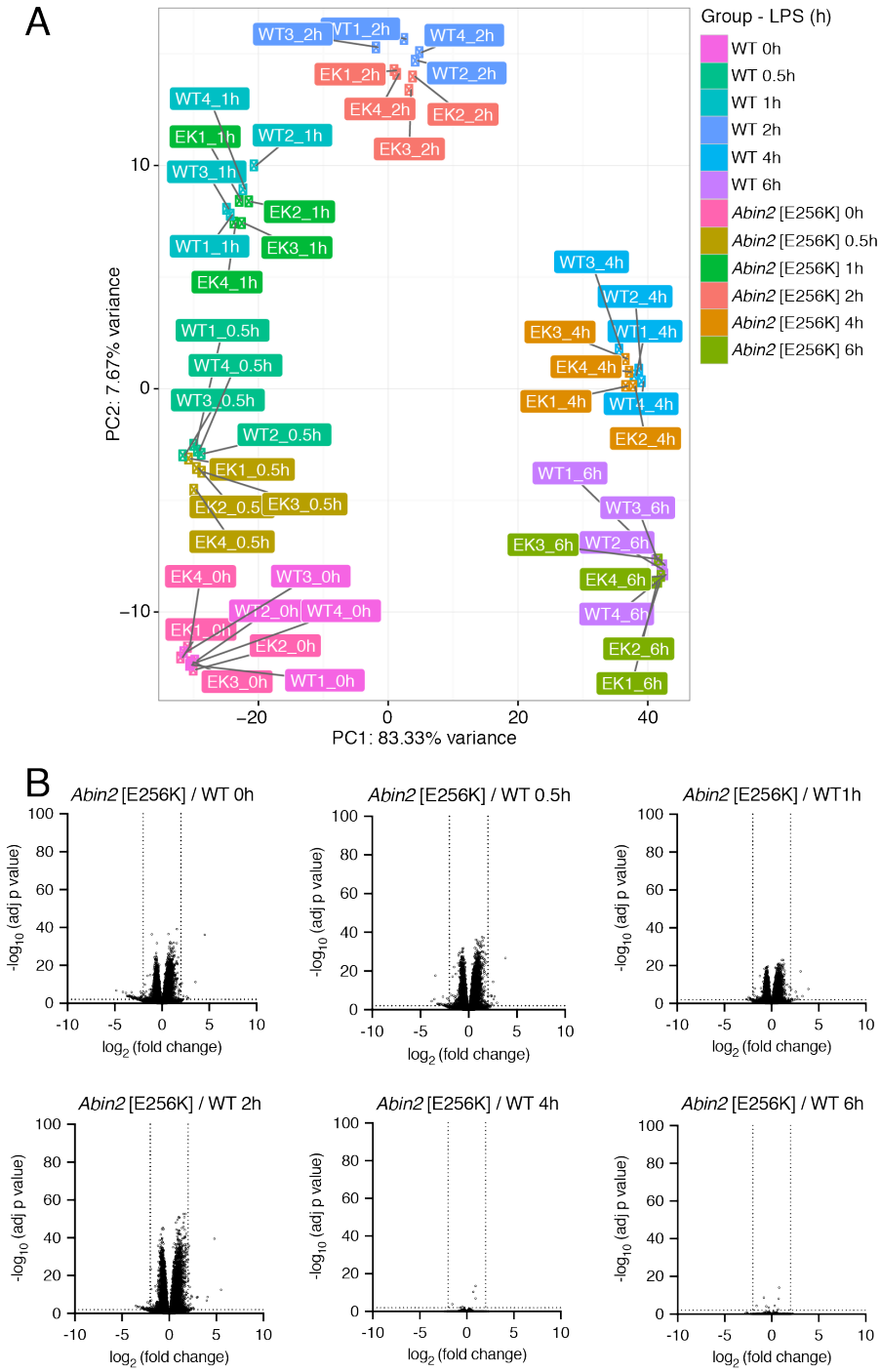

Figure 17 Regulation of gene expression by ABIN-2/A20 complexes in response to TLR4 activation

BMDMs from WT and *Abin2*$^{E256K/E256K}$ mice were stimulated with LPS (100 ng/ml) for the times indicated. Four biological replicates were included per genotype. Following BMDM lysis, RNA was extracted and purified. Libraries were generated and samples were sequenced. (**A**) Principal component analysis (PCA) comparing RNA sequencing samples. (**B**) The $\log_2$ (fold change) and -$\log_{10}$ (adjusted *P* value) was plotted for each gene that was identified by RNA sequencing. X-axis grid line at $\log_2$

(fold change) of 2 and -2; Y-axis grid line at -$\log_{10}$ (adjusted *P* value) of 2, which corresponds to a *P* value of 0.01. EK, *Abin2*^{E256K}; PC, principal component.

To confirm that *Abin2*^{E256K} mutation did not regulate expression of critical genes induced in response to LPS stimulation, I verified expression levels of selected genes by qPCR. Upon LPS stimulation, expression of the pro-inflammatory cytokines *Il1b*, *Il6*, *Il12* and *Il23a* was strongly induced. No significant differences in expression levels were detected between WT and *Abin2*^{E256K} (Figure 18). In addition, upon LPS stimulation *Ifnb1* mRNA levels in BMDMs from *Abin2*$^{E256K/E256K}$ mice were similar to BMDMs from WT mice. The *Ifnb1* gene encodes a type I IFN with important antiviral and antibacterial properties. Moreover, *Abin2*^{E256K} did not regulate expression of *Nlrp3*, which encodes the NLRP3 inflammasome that drives IL-1β production, and *Tnfaip3*, the gene encoding A20 itself (Figure 18).

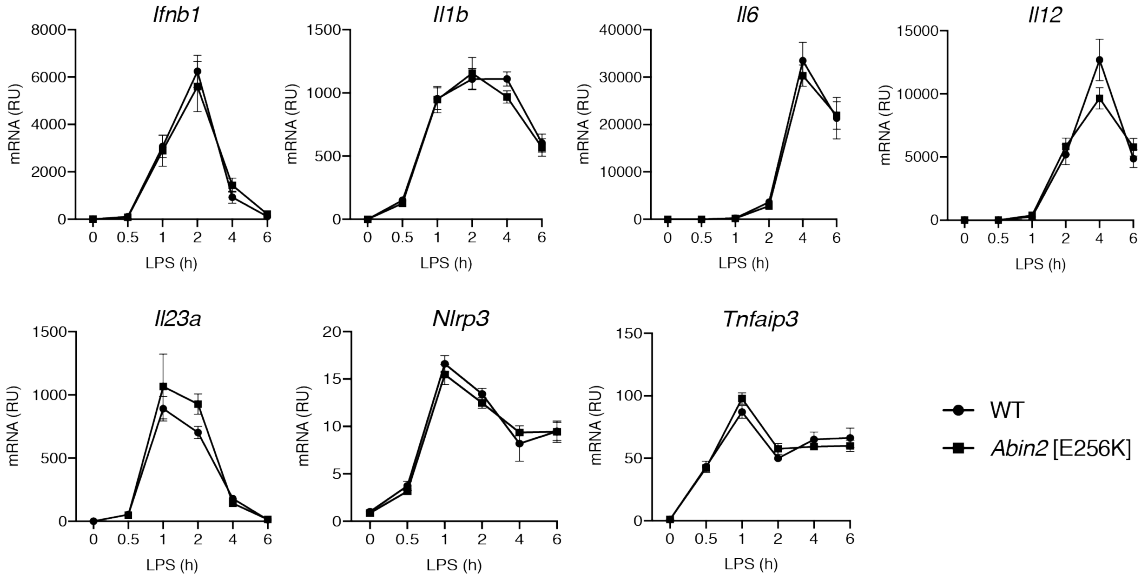

Figure 18 *Abin2*^{E256K} mutation does not regulate expression of select innate immune genes upon LPS stimulation

BMDMs from WT and *Abin2*$^{E256K/E256K}$ mice were stimulated with LPS (100 ng/ml) for the times indicated. Following BMDM lysis, RNA was purified and reverse transcribed into cDNA. Gene expression levels were quantified by qPCR using mRNA-specific TaqMan FAM-MGB-coupled probes recognising *Ifnb1*, *Il1b*, *Il6*, *Il12*, *Il23a*, *Nlrp3*, and *Tnfaip3*. Error bars represent SEM (n = 3). RU, relative units.

3.3 Conclusion

3.3.1 Specificity of *Abin2* mutation effects on ABIN-2 interactions

Since TPL-2 stabilises ABIN-2 and vice versa, it is not possible to use *Tpl2*$^{-/-}$ and *Abin2*$^{-/-}$ mice to specifically study TPL-2 and ABIN-2 function (Sriskantharajah *et al*, 2014; Papoutsopoulou *et al*, 2006). Therefore, it is essential to use TPL-2 and ABIN-2 knock-in mouse strains, which harbour loss-of-function point mutations that distinctly, and independently, block TPL-2 and ABIN-2 functions, respectively, without affecting TPL-2 or ABIN-2 stability.

I initiated my research into the biochemical characterisation of the effects of ABIN-2 mutations on ABIN-2 interactions since this knowledge is a prerequisite for any interpretation of results obtained from experiments using the respective *Abin2* knock-in mouse strains. Prior to commencing my thesis, Dong *et al*. provided experimental evidence that the human *Abin2*^{E255K} mutation reduces binding to A20 (Dong *et al*, 2011). Moreover, the Cohen laboratory showed that the human *Abin2*^{D309N} mutation disrupts ubiquitin binding to ABIN-2 (Nanda *et al*, 2018). In addition, preliminary evidence suggested that the human *Abin2*^{Y230A} mutation impairs ESCRT-I binding (Banks *et al*, 2016). ABIN-2 interacts with TPL-2/NF-κB1 p105, linear ubiquitin, the negative regulator of NF-κB A20 and ESCRT-I. My results, using purified human GST-ABIN-2 proteins, showed that *Abin2*^{E255K} mutation selectively reduced A20 binding, *Abin2*^{D309N} mutation selectively abrogated linear M1-linked ubiquitin binding, and *Abin2*^{Y230A} mutation selectively diminished TSG101 and ALIX binding to ABIN-2. None of the human *Abin2* point mutations affected the association between ABIN-2 and TPL-2/NF-κB1 p105 complexes.

The amino acid sequence between human and murine ABIN-2 shares an 86% sequence similarity and, in comparison to the human sequence, homologous point mutations in mice are shifted by one amino acid residue towards the C-terminus. Therefore, it can be confidently assumed that results obtained from interaction studies using mutant human ABIN-2 translate into biochemical interactions that occur in *Abin2* knock-in mice. The three *Abin2* knock-in mouse strains described, together with *Tpl2*$^{D270A/D270A}$, *Nfkb1*$^{SSAA/SSAA}$, and *Nfkb1*$^{SSAA/SSAA}$ *Tpl2*$^{D270A/D270A}$ mice that have

previously been characterised by the Ley laboratory provided a comprehensive repertoire of transgenic mouse strains to independently assess TPL-2 and ABIN-2 functions in innate immunity (Figure 19).

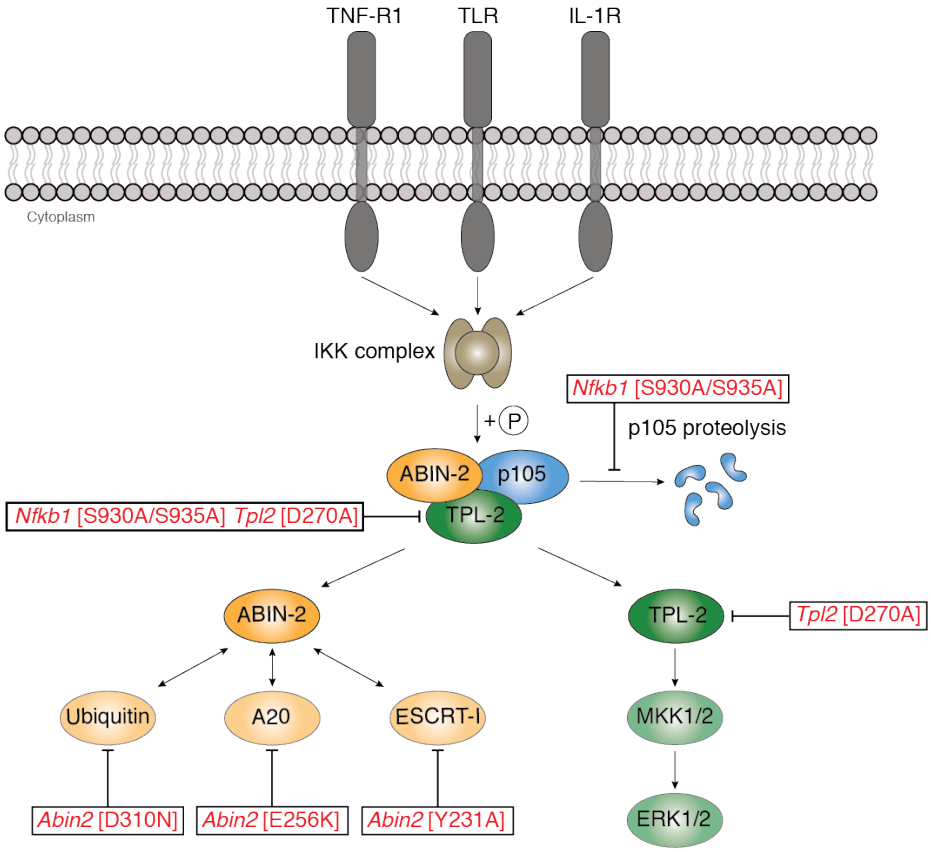

Figure 19 Genetically-modified mouse strains to decipher ABIN-2 and TPL-2 signalling

Individual mouse strains available to study the role of ABIN-2 and TPL-2 in biological processes. Knock-in mouse strains enable the independent characterisation of ABIN-2 and TPL-2 function. *Tpl2*^{D270A} mutation blocks TPL-2 catalytic activity, while *Nfkb1*^{SSAA} mutation prevents IKK-induced release of TPL-2/ABIN-2 from p105. *Abin2*^{D310N}, *Abin2*^{Y231A}, and *Abin2*^{E256K} mutation block ubiquitin, ESCRT-I (TSG101 and ALIX) and A20 binding, respectively. Boxes highlight targets of indicated mouse knock-in mutations, which block TPL-2 signalling and ABIN-2 interactions.

3.3.2 ABIN-2 is not a regulator of TLR4 or TNF receptor-mediated signalling in macrophages

Although initial overexpression studies suggested that ABIN-2 inhibits NF-κB activation, subsequent research using *Abin2*$^{-/-}$ mice showed that endogenous ABIN-2 does not regulate NF-κB signalling (Van Huffel *et al*, 2001; Papoutsopoulou *et al*, 2006). Instead of using primary cells from *Abin2*$^{-/-}$ mice, I set out to confirm these findings in primary macrophages from *Abin2*$^{E256K/E256K}$ and *Abin2*$^{D310N/D310N}$ mice. If ubiquitin and A20 binding to ABIN-2 have opposing regulatory roles, then dysregulation of signalling may not be evident in macrophages from *Abin2*$^{-/-}$ mice. However, my findings demonstrated that *Abin2*^{D310N} and *Abin2*^{E256K} mutation do not regulate NF-κB, MAP kinase or AKT signalling following TLR4 activation by LPS.

My experiments confirmed that ABIN-2 interacts with the TNF receptor upon stimulation, but neither *Abin2*^{D310N} nor *Abin2*^{E256K} mutation impaired NF-κB, MAP kinase or AKT activation upon stimulation of the TNF receptor on macrophages with TNFα. Previous experimental evidence from the Ley laboratory indicated that *Abin2*^{D310N} mutation does not significantly regulate the transcriptome in LPS-stimulated macrophages (Dr Michael Pattison, unpublished findings). Similarly, I provided evidence that *Abin2*^{E256K} mutation does not alter immune signalling in macrophages following TLR4 activation. It cannot be excluded that ABIN-2 regulates innate immune signalling in other cell types or in response to other stimuli. This hypothesis is supported by the recent discovery that ABIN-2 ubiquitin binding is important to promote IL-1β-dependent induction of cyclooxygenase 2 and secretion of PGE_2 in IMFs and MEFs (Nanda *et al*, 2018). Moreover, experiments from our laboratory indicated that A20 binding to ABIN-2 in DCs is required to dampen inflammation during HDM-induced allergic asthma and *Abin2*^{E256K} mutation increases induction of the CCL24 chemokine in DCs following HDM challenge (Ventura *et al*, 2018). These studies suggest that future research into context-specific mechanisms of ABIN-2 signalling will be important.

Chapter 4. A novel role for the TPL-2 complex in promoting phagosome maturation

4.1 Introduction

TPL-2 expression is required for effective immune responses to *C. rodentium*, decreasing bacterial burden and dissemination to the liver and spleen (Acuff *et al*, 2017b). In TPL-2-deficient mice, neutrophil recruitment to the colon during infection is impaired. Similar to macrophages, TPL-2 expression in neutrophils is critical for LPS-mediated activation of ERK1/2 and subsequent production of TNF *in vitro* (Acuff *et al*, 2017b). TPL-2 is also required for efficient killing of internalised *C. rodentium*. Importantly, phagocytic uptake of bacteria is not regulated by TPL-2 (Acuff *et al*, 2017b). The molecular mechanism by which TPL-2 promotes bacterial killing has not been established.

A recent study by the Ley laboratory using quantitative mass spectrometry revealed that TPL-2 catalytic activity may regulate intracellular vesicle trafficking. *Tpl2*^{D270A} mutation in LPS-stimulated BMDMs, which renders TPL-2 kinase catalytically inactive (Sriskantharajah *et al*, 2014), significantly reduced phosphorylation of numerous proteins involved in the regulation of vesicle trafficking, endocytosis and GTPase signalling (Pattison *et al*, 2016). Together, these findings raised the possibility that TPL-2 kinase activity may promote bacterial killing by modulating intracellular trafficking during phagosome maturation in macrophages.

In recent years, advances in mass spectrometry have provided insights into the importance of PTMs, in particular phosphorylation and ubiquitylation, on phagosomes. It has become apparent that phagosomes provide signalling platforms and that ubiquitylation plays a critical role in regulating the function of phagosomal proteins (Dean *et al*, 2019). Notably, K63-linked polyubiquitin chains are highly abundant on phagosomal membranes in macrophages (Warren *et al*, 2005; Guo *et al*, 2019). The UBAN domain of ABIN-2 interacts with K63-linked polyubiquitin chains in addition to linear polyubiquitin chains, raising the possibility that ABIN-2 may be recruited to phagosomes in a ubiquitin-dependent manner. Ubiquitylation is essential for MVB formation on phagosomes (Warren *et al*, 2005). The interplay between ubiquitylation and ESCRT complexes is required for the efficient inward budding of

MVB membranes (Lefebvre *et al*, 2018a). Furthermore, TSG101 of the ESCRT-I complex promotes maturation of autophagosomes (Doyette *et al*, 2005). Since ABIN-2 interacts with TSG101, it may suggest that ABIN-2 regulates certain aspects of ESCRT-I biology during phagocytosis. Moreover, K63-linked ubiquitin is vital to regulate stability of phagosomal proteins, including the type III PI3K complex VPS34, which drives PI(3)P production to promote phagosome maturation (Liu *et al*, 2018).

Although ABIN-2 itself has not been linked to the regulation of phagosome maturation, its ability to interact with ubiquitin and ESCRT-I, both of which have been shown to promote phagosome maturation, motivated me to investigate whether ubiquitin or TSG101 binding to ABIN-2 plays a role in phagosome biology in macrophages. In addition, preliminary experimental evidence implicating TPL-2 in vesicle trafficking encouraged me to investigate the role of TPL-2 catalytic activity in regulating phagocytosis.

4.2 Results

4.2.1 ABIN-2 ubiquitin binding and TPL-2 kinase activity induce phagosome proteolysis

To investigate the role of TPL-2 and ABIN-2 signalling in phagosome maturation, I generated BMDMs from *Tpl2*$^{D270A/D270A}$, *Abin2*$^{D310N/D310N}$, *Abin2*$^{E256K/E256K}$ knock-in and *Abin2*$^{-/-}$ knockout mice. Phagosome maturation was studied in primary macrophages since these specialised cells are professional phagocytes that efficiently internalise and degrade particles upon recognition (Uribe-Quero & Rosales, 2017). Moreover, several studies have demonstrated the importance of TPL-2 signalling in macrophages during innate immune responses (Gantke *et al*, 2012; Xu *et al*, 2018).

I first aimed to investigate whether TPL-2 or ABIN-2 regulated phagocytic uptake of fluorescently-labelled beads. Uptake of beads was similar between all genotypes (Figure 20A and B). As positive assay control, BMDMs from WT mice were pre-treated with cytochalasin D, an inhibitor of actin polymerisation (Schliwa, 1982). As expected, cytochalasin D prevented uptake of beads showing that the assay measured bead uptake and not adsorption to the outside of cells (Figure 20B).

To investigate whether the TPL-2 complex regulated phagosome maturation, I monitored bulk intra-phagosomal proteolysis using silica beads coupled to the fluorescent substrate DQ Green BSA (Yates & Russell, 2008; Russell *et al*, 2009). These beads were additionally labelled with Alexa Fluor 594, which was used to normalise phagocytic uptake. Real-time measurements demonstrated that phagosomal proteolysis was significantly reduced in *Tpl2*$^{D270A/D270A}$, *Abin2*$^{D310N/D310N}$ and *Abin2*$^{-/-}$ BMDMs compared to WT controls (Figure 20C). Notably, phagosomal proteolysis was similar in *Abin2*$^{E256K/E256K}$ BMDMs and WT BMDMs (Figure 20D). As positive assay control, BMDMs from WT mice were pre-treated with leupeptin, an inhibitor of serine-cysteine proteases, which blocked phagosomal proteolysis as expected (Libby & Goldberg, 1978) (Figure 20C). Interestingly, the degree of reduction in *Abin2*$^{-/-}$ BMDMs, which are deficient in both TPL-2 and ABIN-2, was similar to *Tpl2*$^{D270A/D270A}$ and *Abin2*$^{D310N/D310N}$ BMDMs (Figure 20C).

In addition, I coated fluorescently-labelled silica beads with soluble LPS to trigger TLR-mediated phagocytosis. Due to the large particle size, LPS-coated beads are able to interact with several TLR4 molecules on the cell surface, thereby mimicking bacterial infection and potently mediating TLR4 internalisation (Zanoni *et al*, 2011). Similarly to previous observations with uncoated beads, phagosomal proteolysis was significantly reduced in *Tpl2*$^{D270A/D270A}$, *Abin2*$^{D310N/D310N}$ and *Abin2*$^{-/-}$ BMDMs, while proteolysis remained unchanged in *Abin2*$^{E256K/E256K}$ BMDMs compared to WT controls (Figure 20E and F).

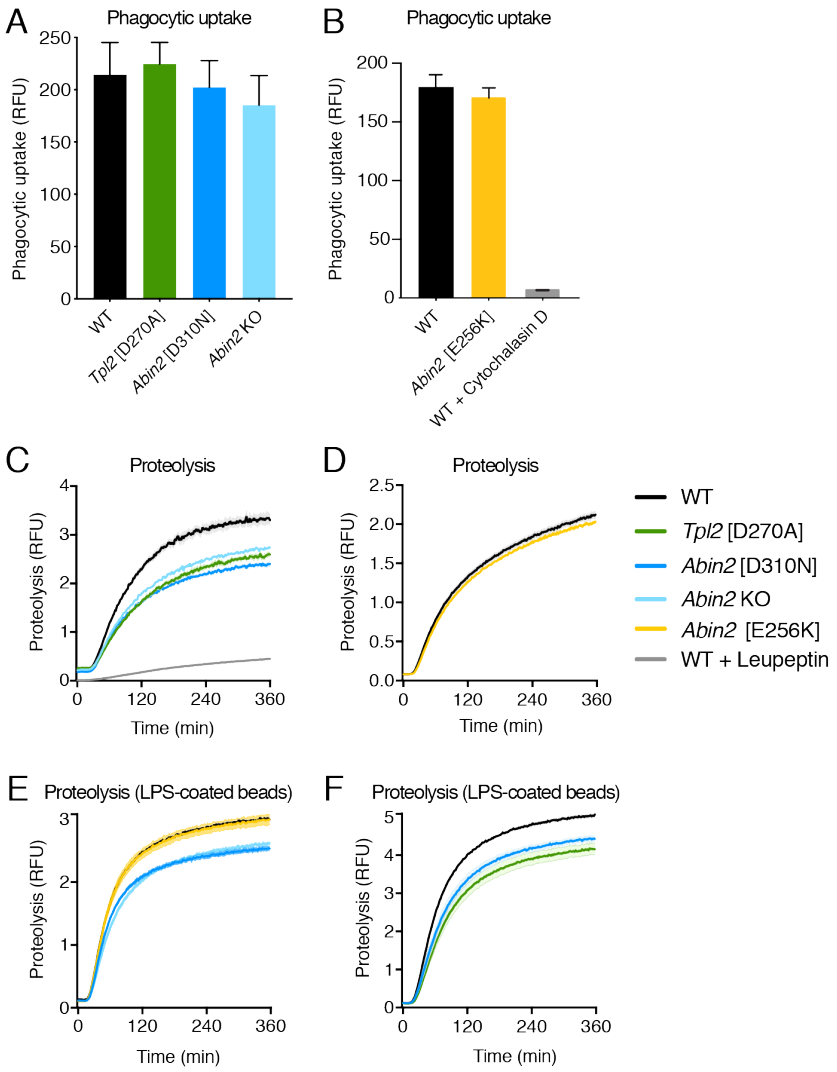

Figure 20 *Tpl2*^{D270A} and *Abin2*^{D310N} mutation impair phagosomal proteolysis

(**A-B**) Phagocytic uptake of fluorescently-labelled silica beads by BMDMs of genotypes indicated. Intracellular fluorescence was monitored 0.5 h following uptake of AF488-coupled beads by BMDMs (n = 4). As positive control, BMDMs were pre-treated with 10 µg/ml cytochalasin D for 0.5 h to inhibit actin polymerisation. Error bars represent SEM. (**C-D**) Intra-phagosomal proteolysis in BMDMs of genotypes indicated was assayed following uptake of DQ Green BSA / AF594 silica beads (n = 4). BMDMs were pre-treated with 100 µg/ml leupeptin for 1 h to inhibit serine-cysteine proteases. (**E-F**) Intra-phagosomal proteolysis in BMDMs of genotypes indicated was assayed following uptake of LPS-coated, DQ Green BSA / AF594 silica beads (n = 4). Prior to fluorescence coupling, silica beads were coated for 1 h with soluble LPS from *Salmonella minnesota* R595 (1 mg/ml). (**C-F**) Measurements were taken at reading intervals of 2 min. Shaded areas represent SEM. **** $P < 0.0001$. Paired Mann-Whitney t-test; All differences relative to WT are ****. RFU, relative fluorescence units.

Since intra-phagosomal proteolysis was impaired in *Tpl2*$^{D270A/D270A}$ and *Abin2*$^{D310N/D310N}$ BMDMs, I next used a confocal microscopy assay to monitor

cathepsin protease activation following internalisation of latex beads. Following phagocytic uptake of latex beads, BMDMs were incubated with a fluorescently-labelled cathepsin L target peptide. Thirty minutes after latex bead uptake, phagosomal cathepsin activity was significantly impaired in both *Tpl2*$^{D270A/D270A}$ and *Abin2*$^{D310N/D310N}$ BMDMs compared to WT controls (Figure 21A). Average cathepsin L activity per cell was quantified, indicating that *Tpl2*^{D270A} mutation reduced cathepsin L activation more than *Abin2*^{D310N} mutation (Figure 21B).

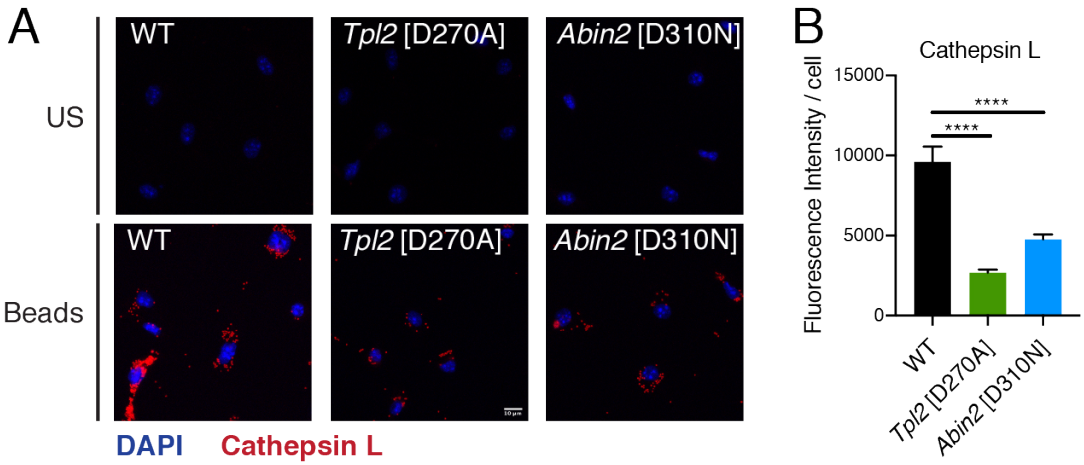

Figure 21 *Tpl2*^{D270A} and *Abin2*^{D310N} mutation reduce cathepsin activity

(**A-B**) Cathepsin activity assay in WT, *Tpl2*$^{D270A/D270A}$ and *Abin2*$^{D310N/D310N}$ BMDMs 0.5 h after uptake of latex beads. BMDMs were stained with the Magic Red cathepsin L substrate at a final dilution of 1:250 for 1 h (red). Fluorescence of the Magic Red cathepsin L substrate was monitored at ex/em 592/628 nm. (**B**) Average fluorescence intensity of the cathepsin probe per cell was quantified (n = 40-51). Error bars represent SEM. **** $P < 0.0001$. Unpaired t-test. US, unstimulated.

4.2.2 TPL-2 kinase activity promotes phagosome acidification

As phagosome maturation proceeds, the phagosomal lumen becomes increasingly acidic due to the activity of V-ATPases, which are acquired by the phagosome through fusion with endosomes and lysosomes (Kinchen & Ravichandran, 2008). I assayed intra-phagosomal acidification using silica beads, which were coupled to the pH indicator BCECF (Russell *et al*, 1995). The optimal pH for BCECF at ex/em 485/628 nm is neutral, and BCECF fluorescence continuously decreases as pH decreases. Real-time measurements demonstrated that phagosomal acidification was significantly impaired in *Tpl2*$^{D270A/D270A}$ BMDMs compared to WT controls (Figure

22A). However, neither *Abin2*^{D310N} nor *Abin2*^{E256K} mutation altered acidification, suggesting that ABIN-2 signalling did not regulate intra-phagosomal acidification (Figure 22A and B). Phagosomal acidification was significantly impaired in *Abin2*$^{-/-}$ BMDMs, phenocopying *Tpl2*^{D270A} mutation (Figure 22C). Since ABIN-2 point mutations do not block acidification, this result suggested that impaired acidification in *Abin2*$^{-/-}$ BMDMs resulted from reduced TPL-2 signalling, and not from the absence of ABIN-2 signalling. *Tpl2*^{D270A} mutation reduced phagosome acidification to a similar degree to the pre-treatment of WT BMDMs with the V-ATPase inhibitor bafilomycin A1 (Figure 22A).

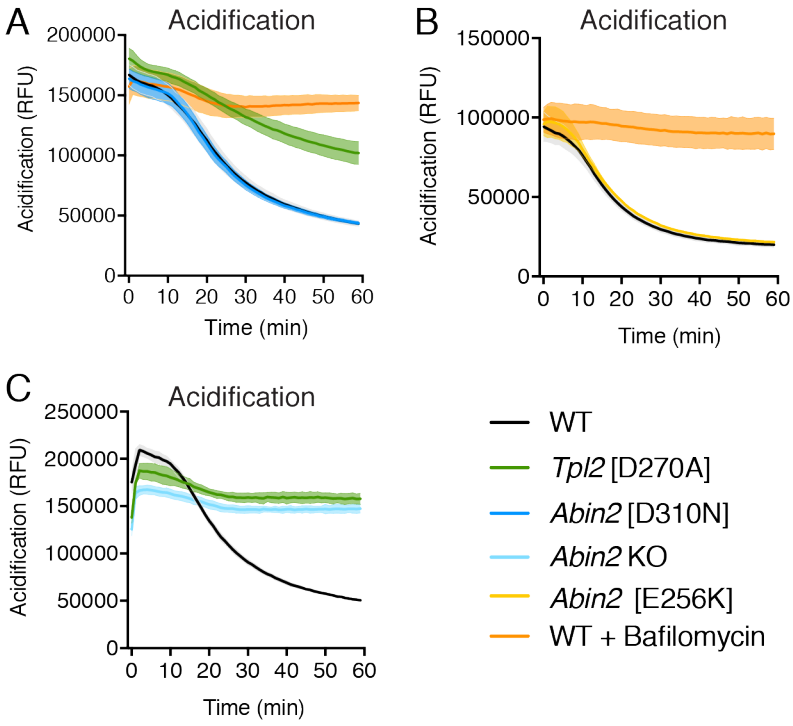

Figure 22 *Tpl2*^{D270A} mutation blocks phagosomal acidification following uptake of BCECF-coupled silica beads

(**A-C**) Intra-phagosomal acidification in BMDMs of genotypes indicated was monitored following uptake of BCECF-coupled silica beads. BMDMs were pre-treated with 1 μM bafilomycin A1 for 15 min to inhibit V-ATPases (n = 4). Measurements were taken at reading intervals of 1 min. Shaded areas represent SEM. **** $P < 0.0001$. Paired Mann-Whitney t-test; All differences relative to WT are ****. RFU, relative fluorescence units.

Next, I performed the phagosome acidification assay with LPS-coated BCECF-coupled silica beads. In accordance with my findings in Figure 22A, phagosomal

acidification was also significantly reduced following uptake of LPS-coated BCECF-coupled silica beads by *Tpl2*$^{D270A/D270A}$ BMDMs relative to WT controls (Figure 23).

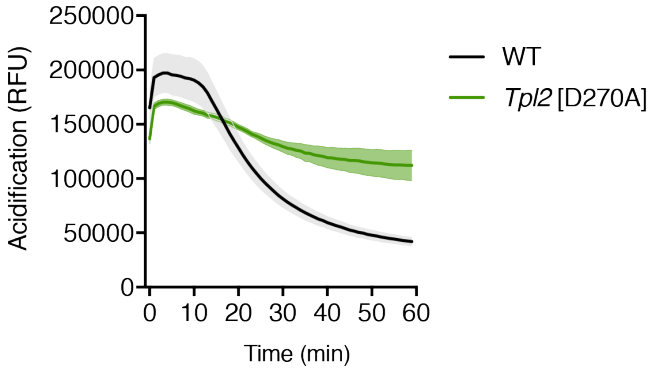

Figure 23 *Tpl2*^{D270A} mutation blocks phagosomal acidification following uptake of LPS-coated BCECF-coupled silica beads

Intra-phagosomal acidification in WT and *Tpl2*$^{D270A/D270A}$ BMDMs was monitored following uptake of LPS-coated BCECF-coupled silica beads (n = 4). Measurements were taken at reading intervals of 1 min. Shaded areas represent SEM. **** $P < 0.0001$. Paired Mann-Whitney t-test; All differences relative to WT are ****. RFU, relative fluorescence units.

To confirm the importance for TPL-2 kinase activity in promoting phagosome acidification, BMDMs from WT, *Tpl2*$^{D270A/D270A}$ and *Abin2*$^{D310N/D310N}$ mice were stimulated with latex beads and stained with LysoTracker Red, an acidotropic red-fluorescent dye that labels acidic compartments. Confocal microscopy illustrated that LysoTracker Red staining was significantly reduced in *Tpl2*$^{D270A/D270A}$ BMDMs following latex bead uptake (Figure 24A). Quantification of LysoTracker Red fluorescence intensity per cell demonstrated that *Tpl2*^{D270A} mutation reduced staining for acidic compartments by approximately 3-fold (Figure 24B). In line with previous findings that *Abin2*^{D310N} mutation did not reduce phagosome acidification following uptake of BCECF-coupled beads, LysoTracker Red staining was similar in *Abin2*$^{D310N/D310N}$ BMDMs and WT controls (Figure 24A and B).

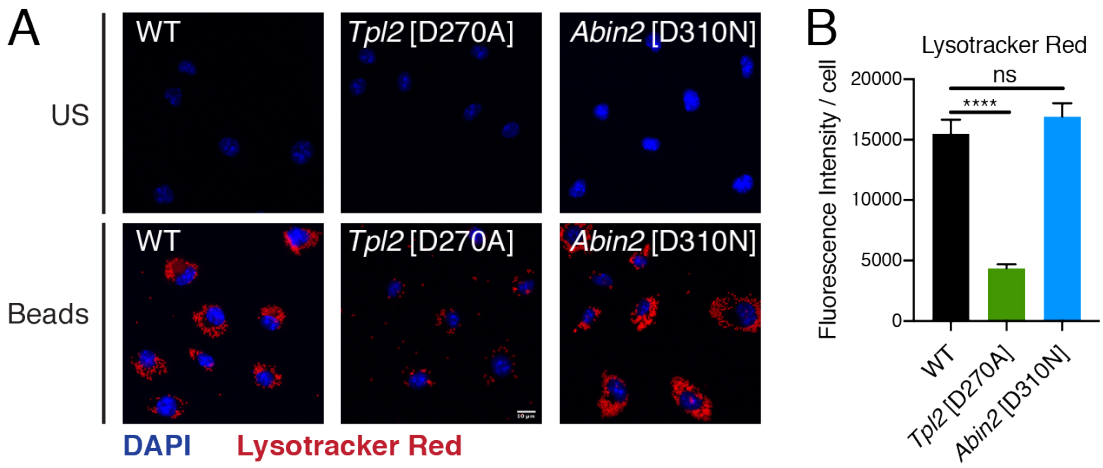

Figure 24 *Tpl2*^{D270A} mutation reduces abundance of acidic compartments following bead uptake

(**A-B**) pH assay in WT, *Tpl2*$^{D270A/D270A}$ and *Abin2*$^{D310N/D310N}$ BMDMs 0.5 h after uptake of latex beads. BMDMs were stained with the LysoTracker Red DND-99 dye at a final concentration of 100 nM for 1 h (red). Fluorescence of LysoTracker Red was monitored at ex/em 577/590 nm. (**B**) Average fluorescence intensity of the LysoTracker Red dye per cell was quantified (n = 95-126). Error bars represent SEM. **** $P < 0.0001$, not significant (ns). Unpaired t-test. US, unstimulated.

4.2.3 ABIN-2 ubiquitin binding and TPL-2 kinase activity drive ROS production upon phagocytosis

Besides maturing into a highly proteolytic and acidic vesicle, nascent phagosomes also produce ROS, a process that is driven by the NADPH oxidase. ROS production is critical for ensuring a strongly microbicidal milieu within the phagosomal lumen. To assay ROS production following phagocytic uptake of latex beads, I stained BMDMs with ROS Deep Red, a cell-permeable deep red-fluorescent dye, which reacts with superoxides and hydroxyl radicals. ROS production was significantly decreased in both *Tpl2*$^{D270A/D270A}$ and *Abin2*$^{D310N/D310N}$ BMDMs (Figure 25A and B). *Tpl2*^{D270A} mutation reduced ROS production more than *Abin2*^{D310N} mutation, possibly due to the inhibitory effects of the former mutation on phagosome acidification, which is required for ROS production (Figure 25B).

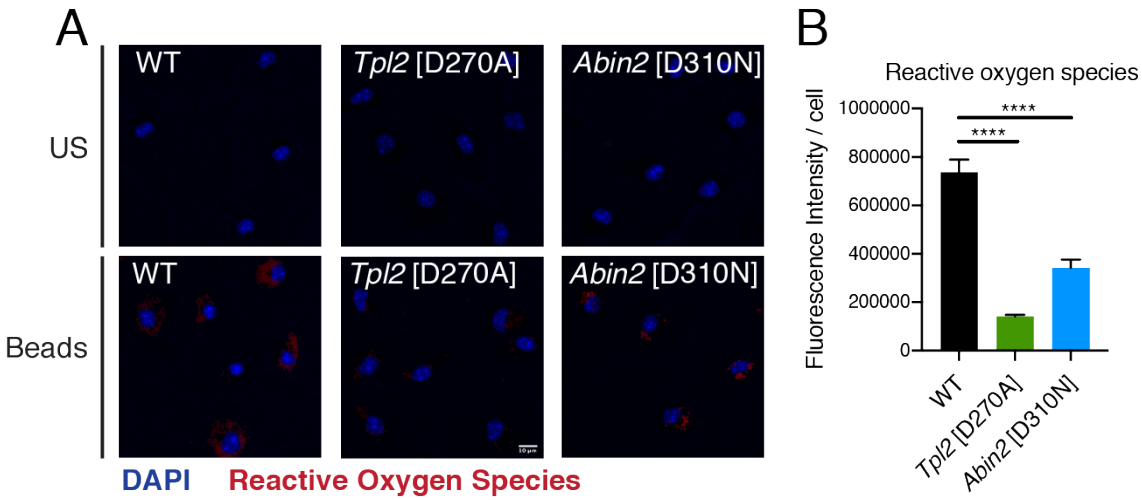

Figure 25 *Tpl2*^{D270A} and *Abin2*^{D310N} mutation reduce ROS levels following uptake of latex beads

(**A-B**) Reactive oxygen species assay in WT, *Tpl2*$^{D270A/D270A}$ and *Abin2*$^{D310N/D310N}$ BMDMs 0.5 h after uptake of latex beads. BMDMs were stained with ROS Deep Red dye at a final concentration of 100 nM for 1 h (red). Fluorescence of ROS Deep Red dye was monitored at ex/em 650/675 nm. (**B**) Average fluorescence intensity of the ROS Deep Red dye per cell was quantified (n = 80-110). Error bars represent SEM. **** $P < 0.0001$. Unpaired t-test. US, unstimulated.

4.2.4 TPL-2 induces phagosome maturation independently of MAP kinase activation

The previously identified functions of TPL-2 in innate immune responses are predominantly mediated by activation of MAP kinase cascades (Gantke *et al*, 2011a). To investigate whether TPL-2 kinase activity promoted phagosome maturation via MAP kinase activation, I used a combination of genetic and pharmacological approaches.

Following receptor-mediated activation, the IKK complex induces proteolysis of NF-κB1 p105 by dual phosphorylation of S930 and S935 in the PEST region of p105 (Lang *et al*, 2003). The Ley laboratory previously generated an NF-κB1 p105 knock-in mouse strain in which both serine residues are mutated to alanine. *Nfkb1*^{S930A,S935A} (*Nfkb1*^{SSAA}) mutation blocks IKK-induced p105 proteolysis, thereby preventing the release of TPL-2 and ABIN-2 from p105 (Sriskantharajah *et al*, 2009). TPL-2 kinase is catalytically active when present in the ternary complex, however, only free TPL-2 can activate MAP kinase signalling. Therefore, in *Nfkb1*$^{SSAA/SSAA}$ macrophages, TPL-

2 activation of ERK1/2 and p38α MAP 2-kinases is blocked following LPS stimulation (Pattison *et al*, 2016; Yang *et al*, 2012).

If TPL-2 promoted phagosome maturation via MAP kinase activation, then phagosome maturation would be impaired by *Nfkb1*^{SSAA} mutation. I therefore generated BMDMs from WT, *Nfkb1*$^{SSAA/SSAA}$ as well as *Nfkb1*$^{SSAA/SSAA}$ *Tpl2*$^{D270A/D270A}$ mice to monitor phagosomal proteolysis and acidification in silica bead assays. Phagosomal proteolysis and acidification were not reduced in *Nfkb1*$^{SSAA/SSAA}$ BMDMs compared to WT controls (Figure 26A and C). Importantly, both proteolysis and acidification were significantly impaired in compound mutant *Nfkb1*$^{SSAA/SSAA}$ *Tpl2*$^{D270A/D270A}$ BMDMs, confirming dependence of both processes on TPL-2 catalytic activity (Figure 26A and C). Inhibition of ERK1/2 phosphorylation at T202 and Y204 residues in *Nfkb1*$^{SSAA/SSAA}$ and *Nfkb1*$^{SSAA/SSAA}$ *Tpl2*$^{D270A/D270A}$ BMDMs following LPS stimulation was confirmed by immunoblotting (Figure 26B). Phosphorylation of p38α at T180 and Y182 residues, which is not fully dependent on TPL-2 activity, was only marginally reduced in *Nfkb1*$^{SSAA/SSAA}$ and *Nfkb1*$^{SSAA/SSAA}$ *Tpl2*$^{D270A/D270A}$ BMDMs following LPS stimulation (Figure 26B).

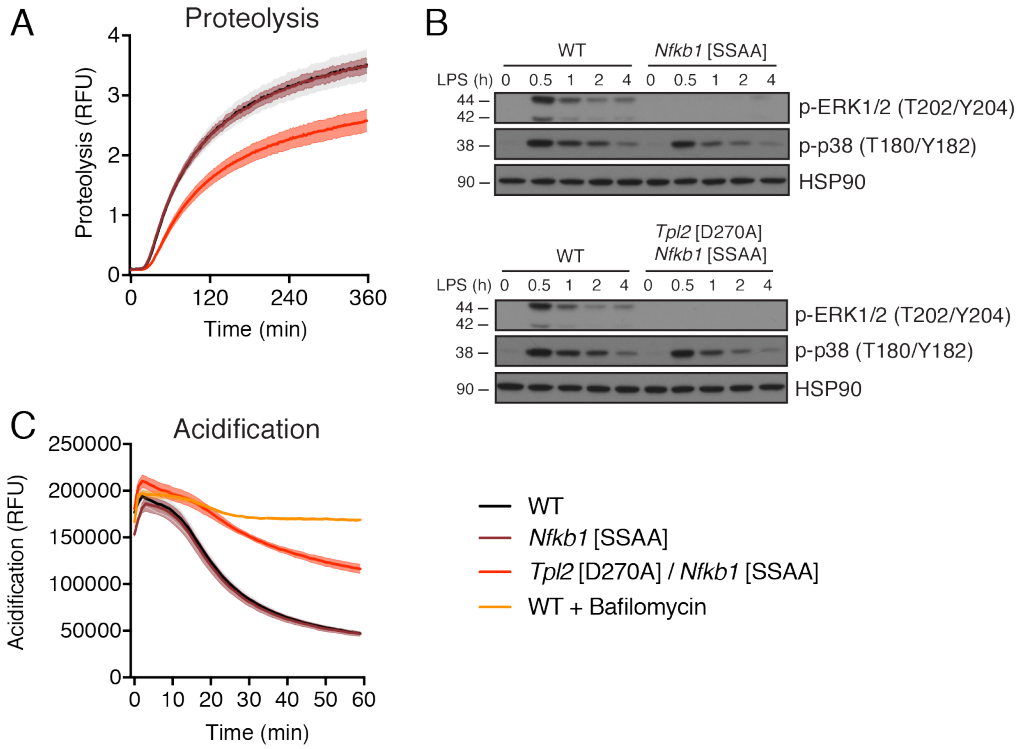

Figure 26 *Nfkb1*^{SSAA} mutation does not impair phagosomal proteolysis or acidification

(**A**) Intra-phagosomal proteolysis in WT, *Nfkb1*$^{SSAA/SSAA}$ and *Nfkb1*$^{SSAA/SSAA}$ *Tpl2*$^{D270A/D270A}$ BMDMs was monitored (n = 4). (**B**) BMDMs from WT, *Nfkb1*$^{SSAA/SSAA}$ and *Nfkb1*$^{SSAA/SSAA}$ *Tpl2*$^{D270A/D270A}$ mice were stimulated with LPS (100 ng/ml) for the times indicated. Cell extracts were immunoblotted with the antibodies indicated. (**C**) Intra-phagosomal acidification in WT, *Nfkb1*$^{SSAA/SSAA}$ and *Nfkb1*$^{SSAA/SSAA}$ *Tpl2*$^{D270A/D270A}$ BMDMs was monitored. BMDMs were pre-treated with 1 μM bafilomycin A1 for 15 min to inhibit V-ATPases (n = 4). (**A, C**) Shaded areas represent SEM. **** $P < 0.0001$. Paired Mann-Whitney t-test; All differences relative to WT are ****. p, phospho; RFU, relative fluorescence units.

To confirm that phagosome proteolysis was induced in a MAP kinase-independent manner, I separately pre-treated WT BMDMs with PD0325901 and VX-745 inhibitors, to pharmacologically inhibit ERK1/2 and p38α activation, respectively. PD0325901 is a MEK1 inhibitor, which blocks ERK1/2 activation, whereas VX-745 is a p38 inhibitor, which selectively abrogates p38α activation (Ciuffreda *et al*, 2009; Duffy *et al*, 2011). While *Tpl2*^{D270A} mutation significantly reduced phagosomal proteolysis relative to WT BMDMs, neither PD0325901 nor VX-745 pre-treatment impaired proteolysis in WT BMDMs (Figure 27A). Potent inhibition of ERK1/2 phosphorylation by PD0325901 and p38α phosphorylation by VX-745 pre-treatment following LPS stimulation was confirmed by immunoblotting (Figure 27B).

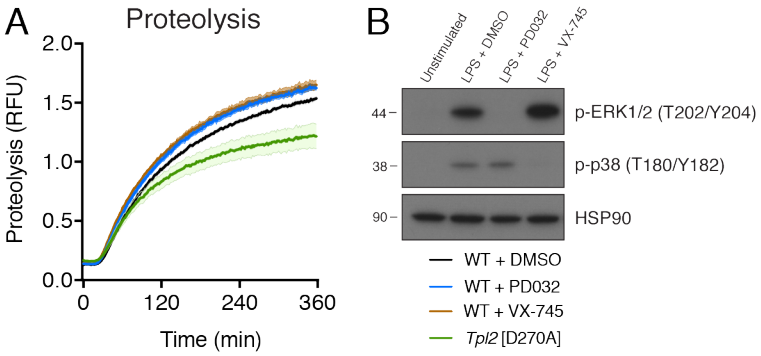

Figure 27 Pharmacological inhibition of ERK1/2 and p38α activation does not impair phagosomal proteolysis

BMDMs from WT mice were pre-treated with 0.1 μM PD0325901 (10 min) to inhibit MEK1, and pre-treated with 1 μM VX-745 (1 h) to inhibit p38α. WT BMDMs were separately pre-treated with DMSO (vehicle control). (**A**) Intra-phagosomal proteolysis in *Tpl2*$^{D270A/D270A}$, WT and inhibitor-treated BMDMs was monitored (n = 4). Shaded areas represent SEM. **** $P < 0.0001$. Paired Mann-Whitney t-test; *Tpl2*$^{D270A/D270A}$ / WT difference is ****. (**B**) WT and inhibitor-treated BMDMs were stimulated with LPS (100 ng/ml) for 0.5 h. Cell extracts were immunoblotted with the antibodies indicated. p, phospho; RFU, relative fluorescence units.

I next investigated whether combinatorial inhibition of ERK1/2 and p38α MAP kinase activation impaired phagosome maturation. BMDMs were simultaneously pre-treated with PD0325901 and VX-745. In line with genetic data, simultaneous pharmacological inhibition of ERK1/2 and p38α activity did not affect phagosome proteolysis or acidification (Figure 28A and B). Inhibition of ERK1/2 and p38α phosphorylation following LPS stimulation was confirmed by immunoblotting (Figure 28C). In contrast, TPL-2 inhibition with the small molecule inhibitor C34 significantly disrupted both phagosomal proteolysis and acidification to a similar degree as *Tpl2*^{D270A} mutation (Figure 28A and B) (Wu *et al*, 2009). A complete block in ERK1/2 activation, as well as partial reduction in p38α activation following C34 pre-treatment were confirmed by immunoblotting (Figure 28C). Phosphorylation states of ERK1/2 and p38α following C34 pre-treatment mimicked *Tpl2*^{D270A} mutation in LPS-stimulated BMDM lysates (Figure 28C). TPL-2 catalytic activity, therefore, stimulated phagosome maturation in primary mouse macrophages independently of MAP kinase activation. The inhibitory effects of C34 on phagosome maturation in WT BMDMs suggested that effects of TPL-2 catalytic activity on phagosome maturation

were induced acutely upon phagocytic uptake of beads, ruling out inhibitory effects of *Tpl2*^{D270A} mutation on macrophage generation *in vitro*.

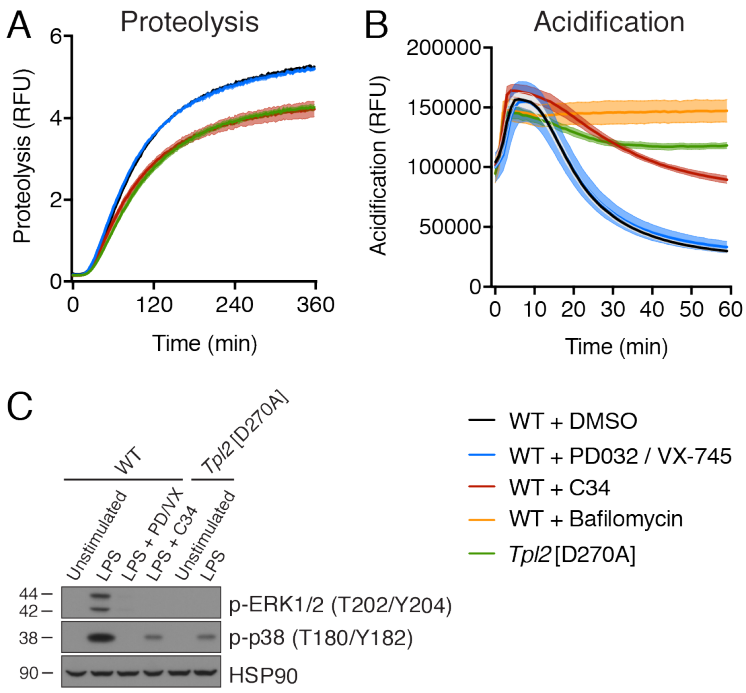

Figure 28 Pharmacological inhibition of TPL-2, but not MAP kinases, impairs phagosome maturation in BMDMs

BMDMs from WT mice were simultaneously pre-treated with 0.1 μM PD0325901 (10 min) to inhibit MEK1, and pre-treated with 1 μM VX-745 (1 h) to inhibit p38α. WT BMDMs were separately pre-treated with DMSO (vehicle control). Additionally, WT BMDMs were pre-treated with 10 μM C34 (1 h) to inhibit TPL-2. (**A**) Intra-phagosomal proteolysis in *Tpl2*$^{D270A/D270A}$, WT and inhibitor-treated BMDMs was monitored (n = 4). (**B**) Intra-phagosomal acidification in *Tpl2*$^{D270A/D270A}$, WT and inhibitor-treated BMDMs was monitored. BMDMs were pre-treated with 1 μM bafilomycin A1 for 15 min to inhibit V-ATPases (n = 4). (**A-B**) Shaded areas represent SEM. **** $P < 0.0001$. Paired Mann-Whitney t-test; All differences relative to WT are ****. (**C**) *Tpl2*$^{D270A/D270A}$, WT and inhibitor-treated BMDMs were stimulated with LPS (100 ng/ml) for 0.5 h. Cell extracts were immunoblotted with the antibodies indicated. p, phospho; RFU, relative fluorescence units.

4.2.5 TPL-2 catalytic activity promotes phagosome maturation in primary human macrophages independently of MAP kinase activation

To investigate whether the role of TPL-2 in phagosome maturation was conserved in human primary macrophages, I generated macrophages from monocytes, that were isolated from human peripheral blood. PBMCs were isolated from human blood

by density gradient centrifugation and monocytes were subsequently selected for by $CD14^+$ selection. Staining of the isolated PBMCs with APC-CD14 indicated that approximately 10% of the PBMC pool were $CD14^+$ monocytes (Figure 29A-C). Selection of $CD14^+$ mononuclear cells with CD14 MicroBeads increased the proportion of $CD14^+$ monocytes by more than 6-fold to approximately 60% (Figure 29D and F). As expected, $CD14^+$ cells were absent from the effluent following positive selection (Figure 29E). $CD14^+$ monocytes were cultured in GM-CSF to induce differentiation into primary human macrophages.

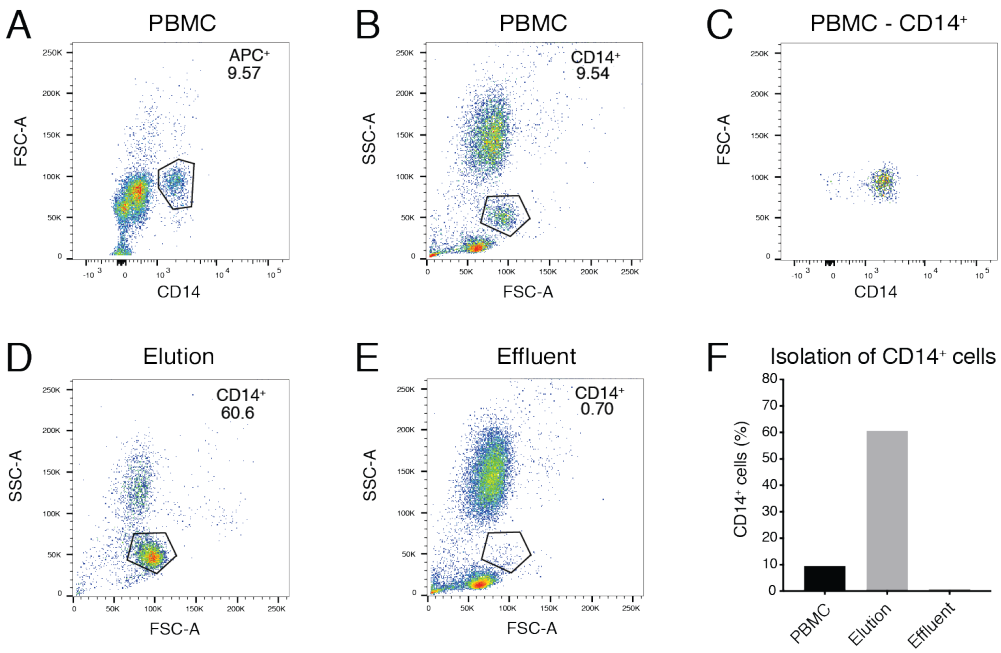

Figure 29 FACS analysis of positive selection for $CD14^+$ monocytes

(**A-C**) Human peripheral blood mononuclear cells (PBMCs) were isolated from peripheral blood by density gradient centrifugation, stained with APC-CD14 and gated for $CD14^+$ PBMCs. (**B**) Forward scatter (FSC) of the highlighted $CD14^+$ PBMC population from (A) is shown. (**D**) $CD14^+$ monocyte population in the elution following positive selection with CD14 MicroBeads. (**E**) $CD14^-$ PBMC population in the effluent following positive selection with CD14 MicroBeads. (**F**) Quantification of $CD14^+$ cells in PBMC, elution and effluent cell fractions.

Phagosome maturation in primary human macrophages was assayed as for BMDMs. C34 inhibition of TPL-2 catalytic activity significantly reduced intra-phagosomal proteolysis (Figure 30A) and acidification (Figure 30C) in primary human macrophages compared to cells pre-treated with DMSO vehicle control. In contrast, simultaneous pharmacological inhibition of ERK1/2 (PD0325901) and p38α (VX-

745) activation did not alter phagosomal proteolysis (Figure 30B) or acidification (Figure 30D). Potent inhibition of ERK1/2 and p38α activation following LPS stimulation was confirmed in primary human macrophages by immunoblotting (Figure 30E). These findings demonstrated that a role for TPL-2 catalytic activity in promoting phagosome maturation independently of MAP kinase activation was conserved between primary macrophages from both mice and humans.

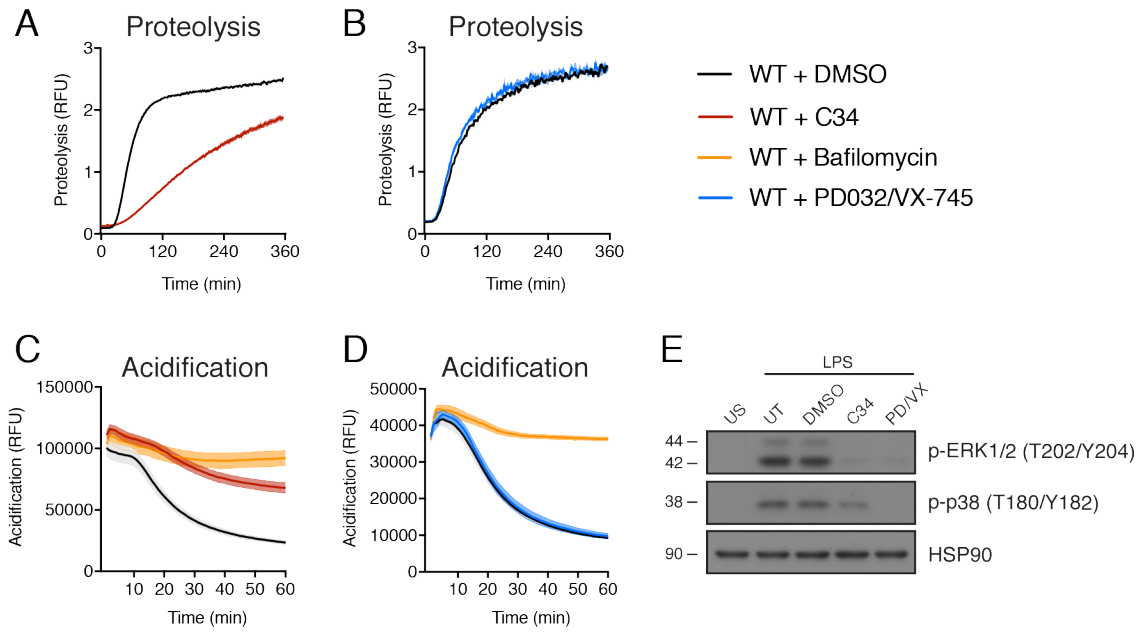

Figure 30 Pharmacological inhibition of TPL-2, but not MAP kinases, impairs phagosome maturation in primary human macrophages

Primary human macrophages were simultaneously pre-treated with 0.1 μM PD0325901 (10 min) to inhibit MEK1, and pre-treated with 1 μM VX-745 (1 h) to inhibit p38α. Human macrophages were separately pre-treated with DMSO (vehicle control). Additionally, human macrophages were pre-treated with 10 μM C34 (1 h) to inhibit TPL-2. (**A**) Intra-phagosomal proteolysis in untreated and C34-treated human macrophages was monitored (n = 4). (**B**) Intra-phagosomal proteolysis in untreated and PD0325901/VX-745-treated human macrophages was monitored (n = 4). (**C**) Intra-phagosomal acidification in untreated and C34-treated human macrophages was monitored (n = 4). (**D**) Intra-phagosomal acidification in untreated and PD0325901/VX-745-treated human macrophages was monitored (n = 4). (**C, D**) Human macrophages were pre-treated with 1 μM bafilomycin A1 for 15 min to inhibit V-ATPases. (**A-D**) Shaded areas represent SEM. **** $P < 0.0001$. Paired Mann-Whitney t-test; All differences relative to untreated macrophages are ****. (**E**) Untreated and inhibitor-treated human macrophages were stimulated with LPS (100 ng/ml) for 0.5 h. Cell extracts were immunoblotted with the antibodies indicated. US, unstimulated; UT, untreated; PD, PD0325901; VX, VX-745; p, phospho; RFU, relative fluorescence units.

4.2.6 TPL-2 and ABIN-2 regulate the protein composition of phagosomes

To further study the molecular mechanism by which TPL-2 kinase activity and ABIN-2 ubiquitin binding promote phagosome maturation, the composition of phagosomes isolated from *Tpl2*$^{D270A/D270A}$, *Abin2*$^{D310N/D310N}$, *Abin2*$^{-/-}$, and WT BMDMs following phagocytic uptake of latex beads was analysed by mass spectrometry. In total, 1552 proteins were identified by mass spectrometry on isolated phagosomes from BMDMs. Phagosome proteomes from *Tpl2*$^{D270A/D270A}$ and *Abin2*$^{-/-}$ BMDMs displayed more striking differences to WT controls than *Abin2*$^{D310N/D310N}$ BMDMs. More specifically, 169 phagosomal proteins were significantly downregulated by more than 1.5-fold by *Tpl2*^{D270A} mutation, whereas 78 and 101 phagosomal proteins were significantly downregulated by at least 1.5-fold by *Abin2*^{D310N} mutation and ABIN-2 / TPL-2 deficiency in *Abin2* $^{-/-}$ BMDMs, respectively. Gene set enrichment analysis demonstrated that several highly downregulated pathways in *Tpl2*$^{D270A/D270A}$ and *Abin2*$^{D310N/D310N}$ BMDMs compared to WT controls were implicated in vesicle-mediated transport, receptor-mediated transport as well as ion and transmembrane transport, all of which are essential processes underlying phagosome maturation (Figure 31). Importantly, the phagosome proteome from *Abin2*$^{-/-}$ BMDMs distinctly shared characteristics of both *Tpl2*$^{D270A/D270A}$ and *Abin2*$^{D310N/D310N}$ BMDMs (data not shown). In addition, contrasting enrichment scores between *Tpl2*^{D270A} and *Abin2*^{D310N} mutation indicated that TPL-2 and ABIN-2 may regulate phagosome maturation by distinct mechanisms (Figure 31).

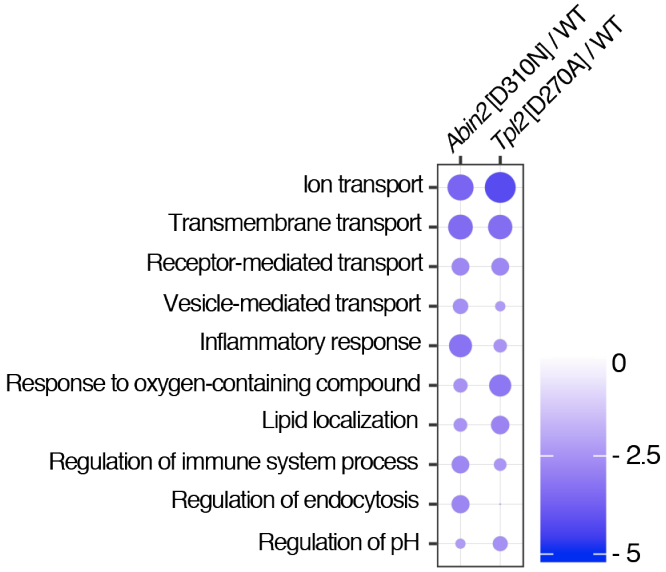

Figure 31 Biological processes downregulated by *Tpl2*^{D270A} and *Abin2*^{D310N} mutation

WT, *Tpl2*$^{D270A/D270A}$ and *Abin2*$^{D310N/D310N}$ BMDMs were incubated with latex beads for 0.5h. Latex bead phagosomes were purified from WT, *Tpl2*$^{D270A/D270A}$ and *Abin2*$^{D310N/D310N}$ BMDMs and analysed by mass spectrometry. Biological triplicates were analysed for each genotype. Gene set enrichment analysis (GSEA) of significantly downregulated biological processes in phagosomal fractions. Changes of *Tpl2*^{D270A} and *Abin2*^{D310N} phagosomes relative to WT. Dot colour; enrichment score. Dot size; statistical significance.

Selected downregulated protein hits were grouped into clusters according to molecular function. Both *Tpl2*^{D270A} and *Abin2*^{D310N} mutation resulted in reduced abundance of Rab GTPases on phagosomes. Strikingly, *Tpl2*^{D270A} mutation had a more pronounced effect on the Rab GTPases family, significantly decreasing the abundance of more than 15 distinct RAB proteins, including RAB5 and RAB7, which have key roles in regulating the maturation of phagosomes (Figure 32) (Huynh *et al*, 2007; Vieira *et al*, 2003b). The abundance of nine V-ATPase subunits was also significantly decreased on phagosomes from *Tpl2*$^{D270A/D270A}$ BMDMs compared to WT controls (Figure 32). Since V-ATPases are critical for driving low pH in the phagosome as maturation proceeds, this finding was particularly interesting given the inhibitory effect of *Tpl2*^{D270A} mutation on phagosome acidification. In contrast, *Abin2*^{D310N} mutation had no or only minimal effect on the abundance of V-ATPase subunits on phagosomes, which coincided with my previous findings that *Abin2*^{D310N} mutation did not regulate phagosomal acidification (Figure 32). In addition, abundance of four members of the LAMTOR protein complex, a key regulator of

lysosomal trafficking (Colaço & Jäättelä, 2017), was also reduced in *Tpl2*$^{D270A/D270A}$ BMDMs relative to WT controls. *Tpl2*^{D270A} mutation resulted in a strong reduction of numerous lysosomal enzymes on phagosomes, while *Abin2*^{D310N} mutation had only subtle effects on few lysosomal enzymes (Figure 32). In addition, *Tpl2*^{D270A} mutation resulted in a significant reduction of several SNARE proteins (Figure 32). Both *Tpl2*^{D270A} and *Abin2*^{D310N} mutation significantly reduced multiple cathepsins, sorting nexins, and proteins involved in ubiquitin signalling (Figure 32).

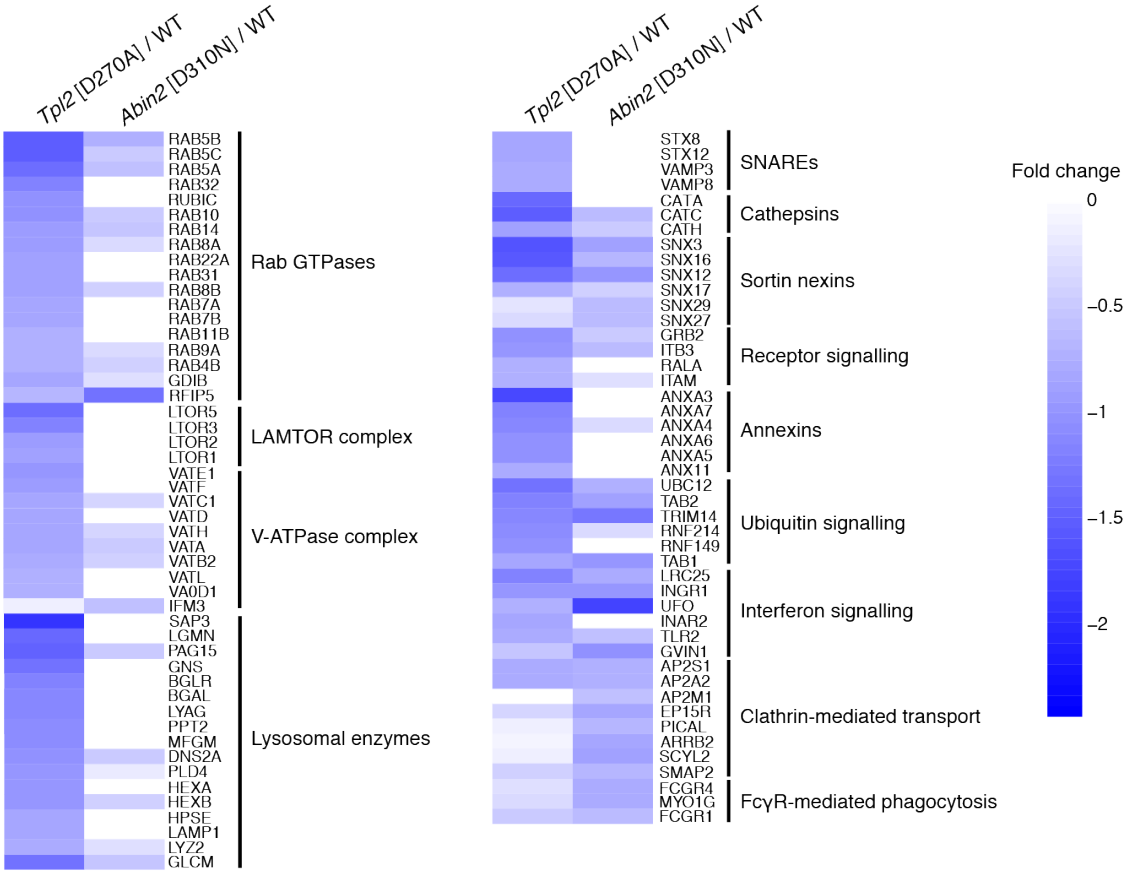

Figure 32 *Tpl2*^{D270A} and *Abin2*^{D310N} mutation reduce abundance of critical regulators of phagosome maturation

Heatmap of selected proteins that were significantly downregulated in BMDMs from *Tpl2*$^{D270A/D270A}$ and *Abin2*$^{D310N/D310N}$ mice relative to WT ($P < 0.05$). Selected hits were grouped into clusters according to their molecular functions. Fold changes are on $\log_2$ scale.

To study the effect of TPL-2 and ABIN-2 mutations on individual phagosomal proteins, I plotted protein intensities of selected hits from phagosome proteome data. Both *Tpl2*^{D270A} and *Abin2*^{D310N} mutation significantly decreased abundance of the

proteases cathepsin C and H on phagosomes (Figure 33A and B). Moreover, both mutations resulted in significantly decreased phagosomal abundance of sorting nexin-3, phospholipase D4 and galectin-9, which synergistically promote membrane recycling of maturing phagosomes (Klose *et al*, 2019; Lennartz, 2008) (Figure 33C, D and F). Notably, *Tpl2*^{D270A} and *Abin2*^{D310N} mutation reduced nitric oxide synthase-interacting protein, a regulator of NO production (Dedio *et al*, 2001) (Figure 33E). Furthermore, significant differences were detected in the abundance of proteins involved in ESCRT biology. *Abin2*^{D310N} mutation significantly reduced phagosomal levels of the charged multivesicular body protein 2B (CHMP2B). CHMP2B, an ESCRT-III component, is critical for mediating fusion of autophagosomes with lysosomes (Hyung *et al*, 2008; Metcalf & Isaacs, 2010) (Figure 33G). Besides CHMP2B, both *Tpl2*^{D270A} and *Abin2*^{D310N} mutation reduced programmed cell death protein 6 (PDCD6) levels on phagosomes. PDCD6 promotes the association between ALIX and TSG101, thus mediating an interplay between ESCRT-I and ESCRT-III complexes (Okumura *et al*, 2009) (Figure 33H).

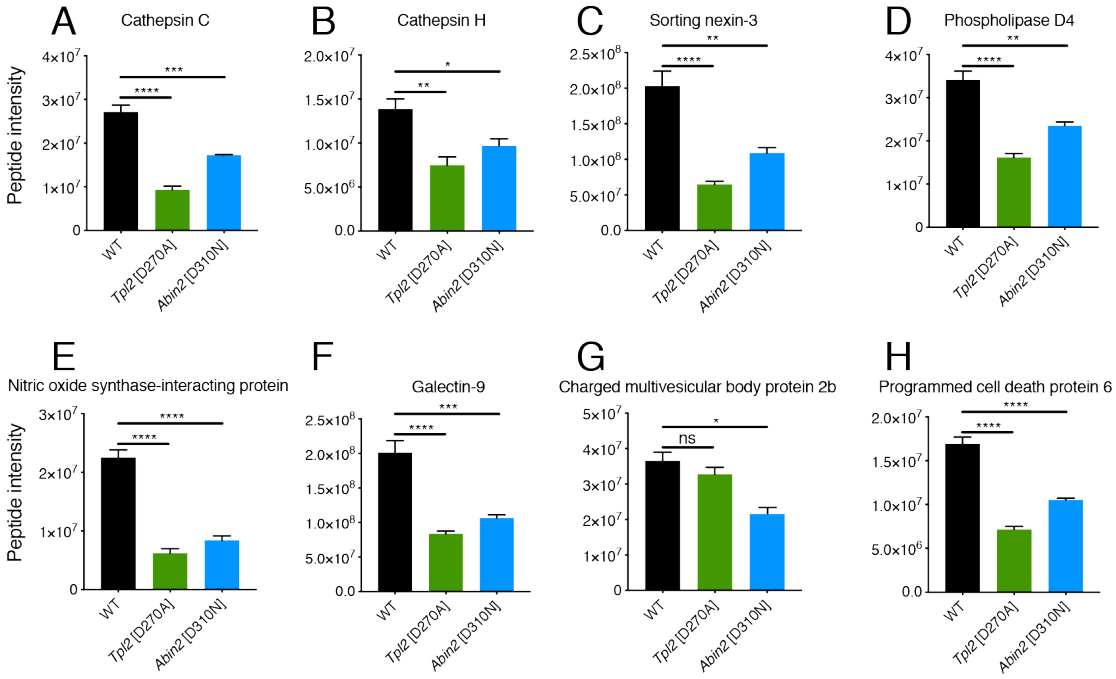

Figure 33 Selected phagosomal proteins downregulated by *Tpl2*^{D270A} and *Abin2*^{D310N} mutation

Protein intensities of selected hits from phagosomes purified from WT, *Tpl2*$^{D270A/D270A}$ and *Abin2*$^{D310N/D310N}$ BMDMs (n = 3). Data were analysed by Student's t-test. Error bars represent SEM. * $P < 0.05$, ** $P < 0.01$, *** $P < 0.001$, **** $P < 0.0001$, not significant (ns).

As previously mentioned, both *Tpl2*^{D270A} and *Abin2*^{D310N} mutation significantly decreased abundance of several Rab GTPases on phagosomes, however, *Tpl2*^{D270A} mutation had a more striking effect on the loss of numerous Rab GTPases (Figure 32 and Figure 34). More specifically, both *Tpl2*^{D270A} and *Abin2*^{D310N} mutation significantly decreased RAB5A, RAB5B, RAB5C, and RAB10 levels (Figure 34A-C and G). RAB5 and RAB10 are critical for maturation of early phagosomes (Flannagan *et al*, 2012). In addition, *Tpl2*^{D270A} mutation disrupted RAB11B binding to phagosomes, a Rab GTPase that mediates the recycling pathway from early phagosomes (Cox *et al*, 2000; Damiani *et al*, 2004) (Figure 34H). Importantly, only *Tpl2*^{D270A} reduced RAB7A, RAB7B and RAB32 levels on phagosomes (Figure 34D, E and J). Both RAB7 and RAB32 drive maturation of late phagosomes (Flannagan *et al*, 2009; Seto *et al*, 2011).

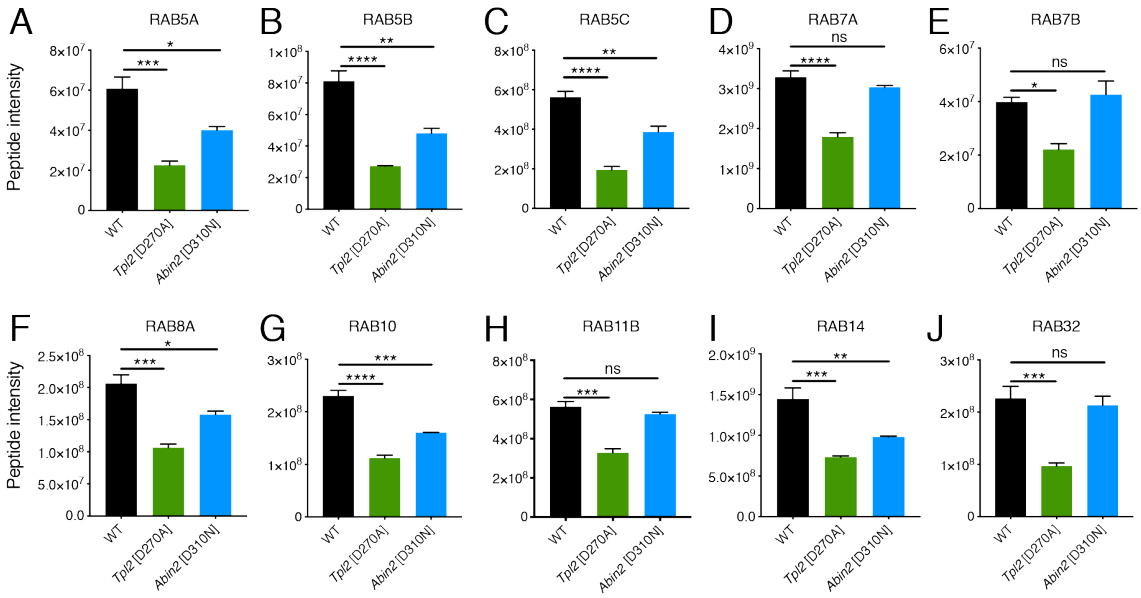

Figure 34 *Tpl2*^{D270A} and *Abin2*^{D310N} mutation decrease Rab GTPases on phagosomes

Protein intensities of selected Rab GTPases from phagosomes purified from WT, *Tpl2*$^{D270A/D270A}$ and *Abin2*$^{D310N/D310N}$ BMDMs (n = 3). Data were analysed by Student's t-test. Error bars represent SEM. * $P < 0.05$, ** $P < 0.01$, *** $P < 0.001$, **** $P < 0.0001$, not significant (ns).

As briefly outlined above, V-ATPase subunits were less abundant on phagosomes from *Tpl2*$^{D270A/D270A}$ BMDMs compared to WT controls. More specifically, *Tpl2*^{D270A} mutation resulted in significantly impaired localisation of nine V-ATPase subunits,

including V-ATPase subunits D, D1, E1 and F (Figure 35A-D). Abundance of four LAMTOR proteins, including LAMTOR1 and LAMTOR5 was also reduced (Figure 35E and F). V-ATPases and LAMTOR proteins form a multi-protein Ragulator complex on lysosomes (Colaço & Jäättelä, 2017). Process enrichment using Metacore analysis showed that *Tpl2*^{D270A}, but not *Abin2*^{D310N}, mutation significantly downregulated the abundance of phagosomal proteins, which are implicated in processes regulating phagosome acidification (Figure 35G). These observations coincided with my previous findings that TPL-2 catalytic activity, but not ABIN-2 ubiquitin binding, promoted phagosomal acidification following uptake of beads.

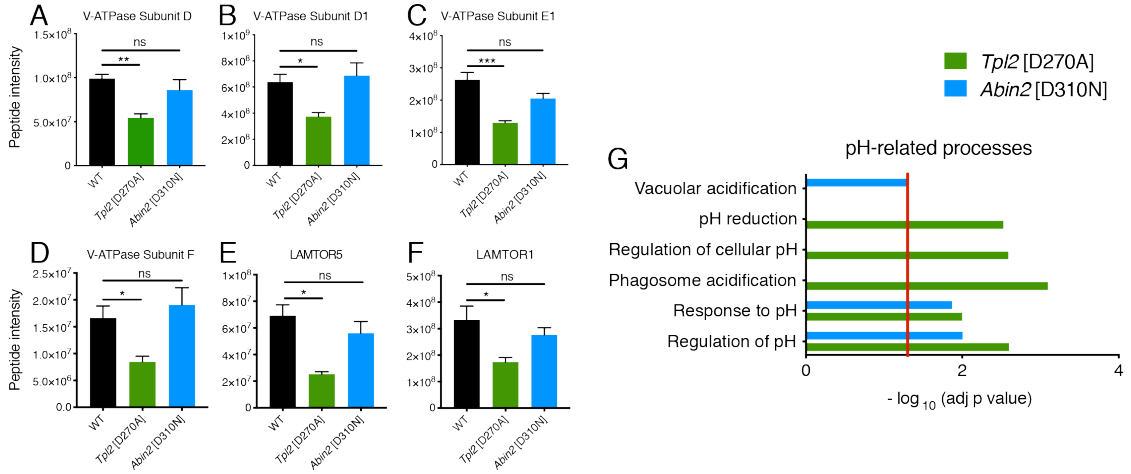

Figure 35 *Tpl2*^{D270A} mutation reduces V-ATPase abundance on phagosomes

(**A-F**) Protein intensities of V-ATPase subunits from phagosomes purified from WT, *Tpl2*$^{D270A/D270A}$ and *Abin2*$^{D310N/D310N}$ BMDMs (n = 3). Data were analysed by Student's t-test. Error bars represent SEM. * $P < 0.05$, ** $P < 0.01$, *** $P < 0.001$, not significant (ns). (**G**) Process enrichment using the Metacore database. Selected downregulated pH-related processes are shown. -log$_{10}$ of adjusted *P* values are shown. Red line represents $P = 0.05$, where processes below the red line are statistically non-significant.

Interestingly, *Abin2*^{D310N}, and to a lesser extent *Tpl2*^{D270A}, mutation significantly reduced all five core proteins of the adaptor protein-2 (AP2) complex, namely AP2A1, AP2A2, AP2B1, AP2M1 and AP2S1 (Figure 32, Figure 36A-E). Similarly, *Abin2*^{D310N} and *Tpl2*^{D270A} mutation decreased abundance of five accessory proteins of the AP2 complex, including AGFG2, EPS15L1, ITSN2, ARRB2 and PICALM (Figure 32, Figure 36F-J). The AP2 complex positively regulates phagocytosis as well as clathrin-mediated endocytosis, thus suggesting that ABIN-2, and possibly TPL-2, may be involved in this trafficking pathway (Mettlen *et al*, 2018; Chen *et al*, 2013).

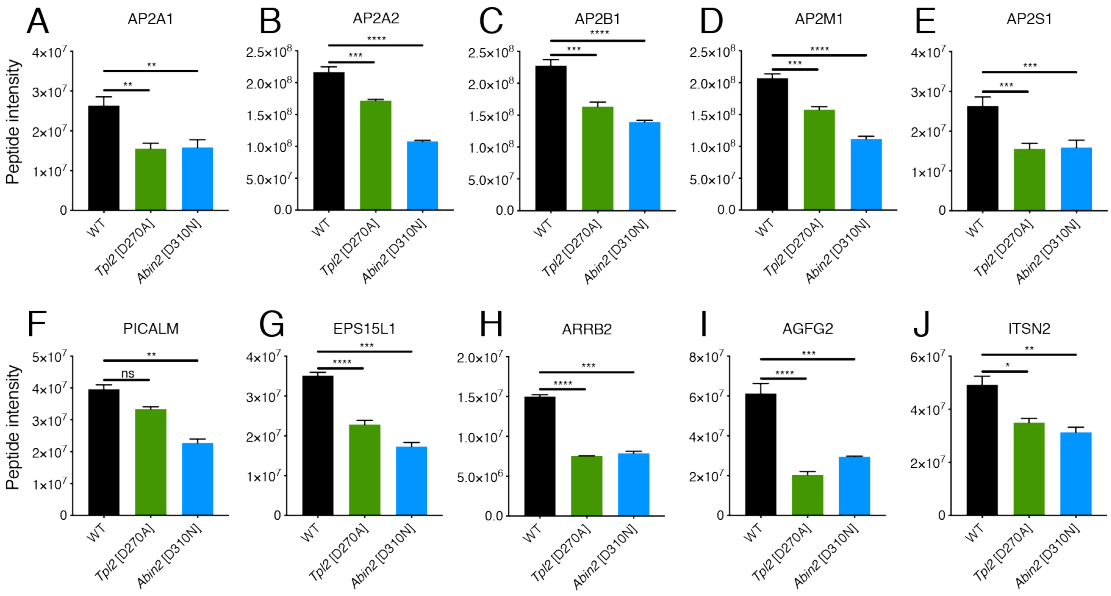

Figure 36 *Tpl2*^{D270A} and *Abin2*^{D310N} mutation reduce abundance of AP2 proteins on phagosomes

Protein intensities of AP2 proteins and AP2 complex adaptor proteins from phagosomes purified from WT, *Tpl2*$^{D270A/D270A}$ and *Abin2*$^{D310N/D310N}$ BMDMs (n = 3). Data were analysed by Student's t-test. Error bars represent SEM. * $P < 0.05$, ** $P < 0.01$, *** $P < 0.001$, **** $P < 0.0001$, not significant (ns).

To confirm that loss of TPL-2 catalytic activity and ABIN-2 ubiquitin binding reduce abundance of important phagosomal proteins, I isolated latex bead phagosomes from WT, *Tpl2*$^{D270A/D270A}$ and *Abin2*$^{D310N/D310N}$ BMDMs and immunoblotted for RAB5 and LAMP1. Both LAMP1 and RAB5 levels were significantly reduced in BMDMs from *Tpl2*$^{D270A/D270A}$ mice (Figure 37A), which was consistent with previous data from phagosome proteomics (Figure 37B). *Abin2*^{D310N} mutation also resulted in decreased abundance of LAMP1 and RAB5 on isolated phagosomes, however, reduction was not as pronounced as in *Tpl2*$^{D270A/D270A}$ BMDMs (Figure 37A). While *Abin2*^{D310N} mutation significantly reduced RAB5A levels in phagosome proteomes, its effect on LAMP1 abundance was not statistically significant (Figure 37B).

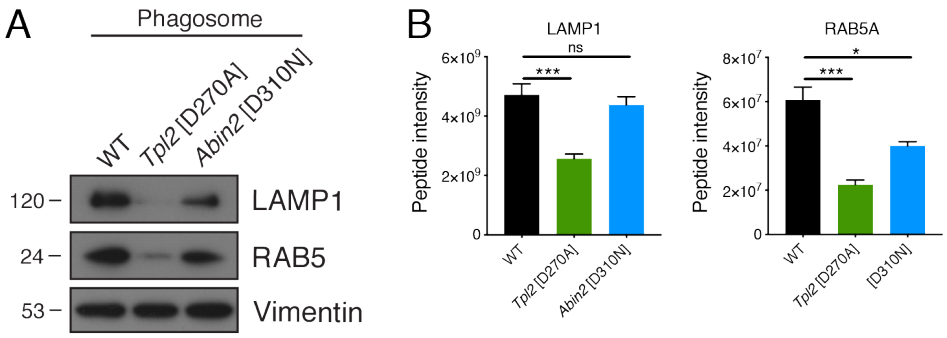

Figure 37 *Tpl2*^{D270A} and *Abin2*^{D310N} decrease LAMP1 and RAB5 protein levels on phagosomes

(**A**) WT, *Tpl2*$^{D270A/D270A}$ and *Abin2*$^{D310N/D310N}$ BMDMs were incubated with latex beads for 0.5 h. Latex bead phagosomes were purified from WT, *Tpl2*$^{D270A/D270A}$ and *Abin2*$^{D310N/D310N}$ BMDMs, lysed in sample buffer and protein concentration was determined. Phagosome isolates were boiled in sample buffer and subjected to SDS-PAGE. Immunoblots of isolated phagosomes from WT, *Tpl2*$^{D270A/D270A}$ and *Abin2*$^{D310N/D310N}$ BMDMs were probed for RAB5, LAMP1 and vimentin (loading control). Phagosomal fractions of two biological replicates were pooled. One representative experiment out of two shown (n = 2). (**B**) Protein intensities of LAMP1 and RAB5 from phagosome proteome analysis of WT, *Tpl2*$^{D270A/D270A}$ and *Abin2*$^{D310N/D310N}$ BMDMs (n = 3). Error bars represent SEM. * $P < 0.05$, *** $P < 0.001$, not significant (ns).

4.2.7 *Tpl2*^{D270A} and *Abin2*^{D310N} mutation do not affect ubiquitin abundance on phagosomes

Mass spectrometric analyses of phagosome proteomes revealed that *Tpl2*^{D270A} and *Abin2*^{D310N} mutation significantly downregulated TAB1 and TAB2 abundance on phagosomes (Figure 38A). Moreover, *Tpl2*^{D270A} and *Abin2*^{D310N} mutation significantly upregulated abundance of DUBs, namely AMSH and USP14 (Figure 38A). These observations suggested that TPL-2 kinase activity and ABIN-2 ubiquitin binding may alter the ubiquitin landscape on phagosomes. I therefore decided to quantify ubiquitin chain linkage composition of phagosomes isolated from WT, *Tpl2*$^{D270A/D270A}$ and *Abin2*$^{D310N/D310N}$ BMDMs using the Ub-AQUA-PRM assay, which was performed by Dr Tiaan Heunis from the Trost Laboratory (Newcastle University). The relative abundance of K48-, K63-, K29, and M1-linked ubiquitin remained unaltered by *Tpl2*^{D270A} and *Abin2*^{D310N} mutation (Figure 38B). Interestingly, K63-linked ubiquitin was significantly more abundant on phagosomes than M1-linked ubiquitin (Figure 38B), suggesting that ABIN-2 may be recruited to phagosomes in a K63-linked ubiquitin-dependent manner.

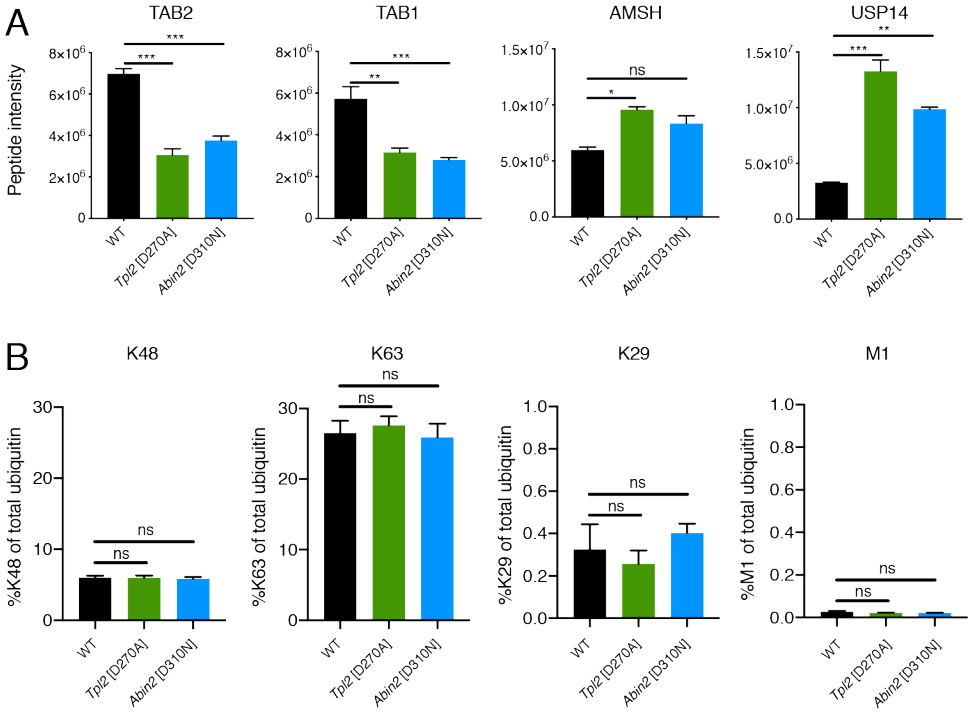

Figure 38 Ubiquitin chain abundance on isolated phagosomes from *Tpl2*$^{D270A/D270A}$ and *Abin2*$^{D310N/D310N}$ BMDMs

(**A**) Protein intensities of regulators of the ubiquitin system, including TAB2, TAB1, AMSH and USP14, which were detected on phagosomes purified from WT, *Tpl2*$^{D270A/D270A}$ and *Abin2*$^{D310N/D310N}$ BMDMs (n = 3). (**B**) Latex bead phagosomes were isolated from BMDMs. The Ub-AQUA-PRM assay was used to screen ubiquitin chain linkage composition of isolated phagosomes from WT, *Tpl2*$^{D270A/D270A}$ and *Abin2*$^{D310N/D310N}$ BMDMs. BMDMs from three mice per genotype were separately generated, stimulated, analysed and results were pooled. Data were analysed by Student's t-test. Error bars represent SEM. * $P < 0.05$, ** $P < 0.01$, *** $P < 0.001$, not significant (ns).

4.2.8 Analysis of the TPL-2-dependent phosphoproteome during phagocytosis

To further investigate the mechanism by which TPL-2 kinase activity regulated phagosome maturation, I characterised the phosphoproteome in *Tpl2*$^{D270A/D270A}$ and WT BMDMs 0.5 h after phagocytic uptake of uncoated latex beads and LPS-coated latex beads. TMT labelling and mass spectrometry were used to quantify differences in phospho-peptide abundance following induction of phagocytosis.

4.2.8.1 *Characterisation of the TPL-2-regulated phosphoproteome following phagocytic uptake of latex beads*

BMDMs from five mice per genotype were separately generated and incubated with latex beads for 0.5 h to allow phagocytic uptake. Principal component analysis of phosphoproteomes from *Tpl2*$^{D270A/D270A}$ and WT BMDMs indicated that samples from the same genotype clustered together and that phosphoproteomes of the two genotypes were different (Figure 39A).

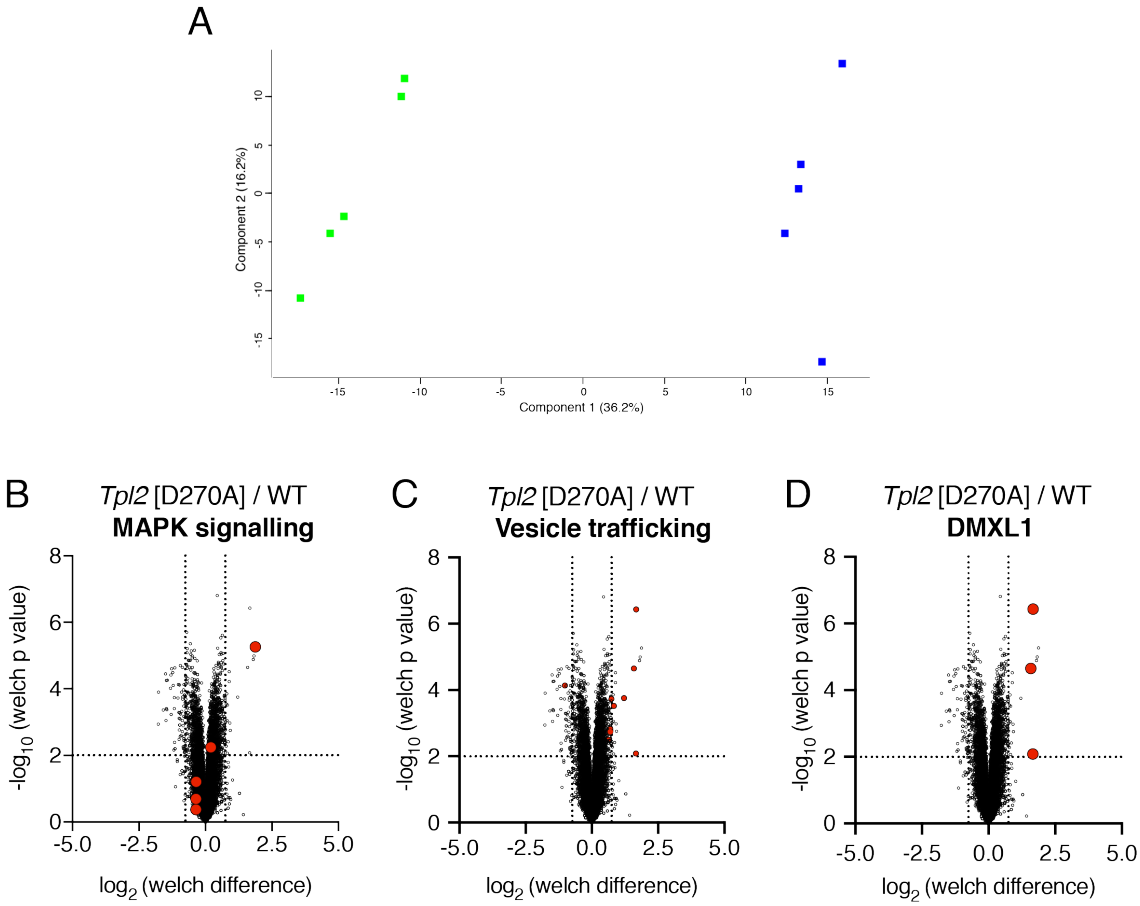

Figure 39 TPL-2-dependent phosphoproteome following uptake of latex beads

TPL-2-dependent phosphoproteome in BMDMs following phagocytosis of latex beads (0.5 h) was determined by TMT mass spectrometry. Five biological replicates were analysed per genotype, *Tpl2*$^{D270A/D270A}$ and WT (n = 5). (**A**) Principal component analysis (PCA) comparing the global phosphoproteome of all five biological replicates generated from WT and *Tpl2*$^{D270A/D270A}$ mice. (**B-D**) Volcano plots representing the significance (-$\log_{10}$ *P* values after Welch's t-test) vs. phosphorylation fold change (Welch difference ratios) between WT and *Tpl2*$^{D270A/D270A}$ BMDMs. X-axis grid line at $\log_2$ (fold change) of 1.5 and -1.5; Y-axis grid line at -$\log_{10}$ (adjusted *P* value) of 2, which corresponds to a *P* value of 0.01. (**B**) Selected phospho-sites in protein kinases of the MAPK cascade (Table 17) are highlighted in red. (**C**) Selected

phospho-sites in regulators of vesicle trafficking (Table 18) are highlighted in red. (**D**) Significantly downregulated DMXL1 phospho-sites (Table 19) are highlighted in red.

The most highly downregulated phospho-site in *Tpl2*$^{D270A/D270A}$ BMDMs compared to WT BMDMs was S141 on TPL-2 itself (Figure 39B and Table 17). S141 on TPL-2 is a known autophosphorylation site, confirming the technical soundness of the data set (Stafford *et al*, 2006; Xu *et al*, 2018). Interestingly, phosphorylation of activating sites in several kinases involved in the MAP kinase cascade, including MEK3/MEK6, ERK1 and ERK2, remained unchanged in *Tpl2*$^{D270A/D270A}$ BMDMs relative to WT controls (Figure 39B and Table 17). This was consistent with immunoblots showing that latex beads do not activate MAP kinase signalling (data not shown).

Table 17 Selected phospho-sites in MAP kinases and TPL-2 following bead uptake
Tpl2^{D270A} / WT fold changes of selected phospho-sites in protein kinases of the MAP kinase cascade were calculated from Welch difference ratios.

Protein (Gene)	Site	Fold change
MEK3 (*Map2k3*), MEK6 (*Map2k6*)	S218	0.4
TPL-2 (*Map3k8*)	S141	3.8
ERK2 (*Mapk1*)	Y185	-0.8
ERK1 (*Mapk3*)	T208	-0.8
ERK1 (*Mapk3*)	Y205	-0.6

To gain insight into molecular mechanisms by which TPL-2 kinase activity regulated phagosome maturation, I clustered significantly regulated phospho-hits according to biological processes and identified seven phospho-sites, which were involved in vesicle trafficking (Figure 39C). More specifically, six phospho-sites were significantly downregulated in *Tpl2*$^{D270A/D270A}$ compared to WT BMDMs, while one site, S692 on USP8, was significantly upregulated in *Tpl2*$^{D270A/D270A}$ BMDMs compared to WT controls (Figure 39C and Table 18). Since my previous findings indicated that TPL-2 catalytic activity is required for stable levels of Rab GTPases on phagosomes, it was of particular interest that multiple phospho-sites in three GEF proteins, namely DENND4C (S987, S1620), RAB3IL1 (S195) and RABIN8 (S272), were significantly downregulated in *Tpl2*$^{D270A/D270A}$ BMDMs compared to WT controls (Figure 39C and Table 18) (Wang *et al*, 2015; Sano *et al*, 2011; Horgan *et al*, 2013). Several phospho-sites in DENND4C, GBF1, RAB3IL1 and USP8 were not affected by *Tpl2*^{D270A}

mutation, indicating that differences in phosphorylation were not resulting from defects in protein levels.

Table 18 Selected phospho-sites in proteins implicated in vesicle trafficking following bead uptake

Tpl2^{D270A} / WT fold changes of selected phospho-sites in regulators of vesicle trafficking were calculated from Welch difference ratios.

Protein (Gene)	Site	Fold change
DENND4C (*Dennd4c*)	S987	2.4
DENND4C (*Dennd4c*)	S1620	1.4
EVI5 (*Evi5*)	S689	1.4
GBF1 (*Gbf1*)	S1290	1.6
RAB3IL1 (Rab3il1)	S195	1.4
RABIN8 (*Rab3ip*)	S272	1.2
USP8 (*Usp8*)	S692	-2

Besides the S141 autophosphorylation site on TPL-2 itself, two of the next most downregulated phospho-sites were S1903 and S1904 on DmX-like protein 1 (DMXL1) (Figure 39D). In addition, a third phosphorylation site on DMXL1, S1255, was found to be significantly downregulated in *Tpl2*$^{D270A/D270A}$ compared to WT BMDMs (Figure 39D). All three phospho-sites on DMXL1 were reduced over threefold by *Tpl2*^{D270A} mutation (Table 19). Phosphorylation of DMXL1 on S434, S915, T1373 and S1900 was not altered by *Tpl2*^{D270A} mutation indicating that TPL-2 catalytic activity did not regulate endogenous DMXL1 protein levels (data not shown).

Table 19 Significantly downregulated phospho-sites in DMXL1 following bead uptake

Tpl2^{D270A} / WT fold changes of three highly downregulated DMXL1 phospho-sites were calculated from Welch difference ratios.

Protein (Gene)	Site	Fold change
DMXL1 (*Dmxl1*)	S1903	3.4
DMXL1 (*Dmxl1*)	S1904	3.4
DMXL1 (*Dmxl1*)	S1255	3.2

A recent study showed that DMXL1, a WD40 repeat protein, interacts with the V-ATPase complex and is required for acidification of endocytic vesicles (Merkulova *et al*, 2015). This observation was particularly interesting given the inhibitory effect of *Tpl2*^{D270A} mutation on phagosomal acidification and raised the possibility that TPL-2 may promote phagosome acidification by regulating phosphorylation of DMXL1. However, these observations did not indicate whether TPL-2 may directly phosphorylate DMXL1.

4.2.8.2 Characterisation of the TPL-2-regulated phosphoproteome following phagocytic uptake of LPS-coated latex beads

Uncoated latex beads are immunologically inert and have not been shown to activate receptors of the innate immune system. I have previously shown that phagosomal proteolysis and acidification were inhibited by *Tpl2*^{D270A} mutation following phagocytic uptake of both uncoated and LPS-coated beads. Therefore, I set out to also characterise the TPL-2-dependent phosphoproteome in BMDMs following phagocytic uptake of LPS-coated beads. Similarly to the proteomic approach outlined above, BMDMs from five mice per genotype were differentiated and incubated with LPS-coated latex beads for 0.5 h. Principal component analysis illustrated that the phosphoproteome in *Tpl2*$^{D270A/D270A}$ BMDMs was significantly different from the phosphoproteome in WT BMDMs (Figure 40A). Moreover, relative percentage variance in both principal component analyses demonstrated that the phosphoproteome is more different between the two genotypes following uptake of LPS-coated, rather than uncoated, latex beads (Figure 39A and Figure 40A).

Following LPS-coated bead uptake, *Tpl2*^{D270A} mutation reduced TPL-2 autophosphorylation on S141 by more than 5-fold (Table 20). Moreover, phosphorylation of several protein kinases of the MAP kinase cascade, including MEK1, MEK2, MEK3 and MEK6 was significantly decreased in *Tpl2*$^{D270A/D270A}$ BMDMs compared to WT controls (Table 20). Previous studies have shown that TPL-2 drives ERK1/2 activation in macrophages (Gantke *et al*, 2012; Pattison *et al*, 2016), and thus these results consolidate the soundness of this proteomic data set.

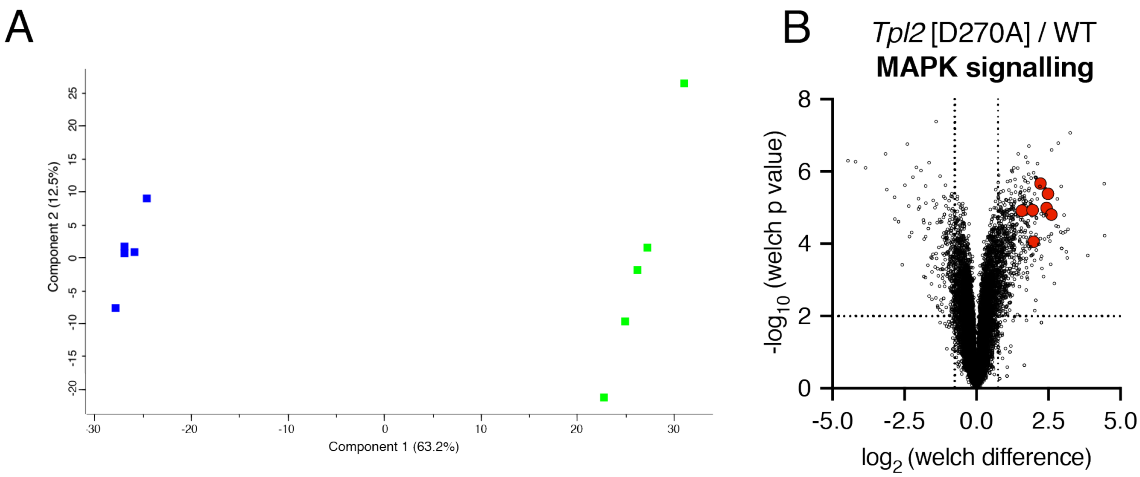

Figure 40 TPL-2-dependent phosphoproteome following uptake of LPS-coated latex beads

TPL-2-dependent phosphoproteome in BMDMs following phagocytosis of LPS-coated latex beads (0.5 h) was determined by TMT mass spectrometry. Five biological replicates were analysed per genotype, *Tpl2*$^{D270A/D270A}$ and WT (n = 5). (**A**) Principal component analysis (PCA) comparing the global phosphoproteome of all five biological replicates generated from WT and *Tpl2*$^{D270A/D270A}$ mice. (**B**) Volcano plot representing the significance (-$\log_{10}$ *P* values after Welch's t-test) vs. phosphorylation fold change (Welch difference ratios) between WT and *Tpl2*$^{D270A/D270A}$ BMDMs. X-axis grid line at $\log_2$ (fold change) of 1.5 and -1.5; Y-axis grid line at -$\log_{10}$ (adjusted *P* value) of 2, which corresponds to a *P* value of 0.01. Selected phospho-sites in protein kinases of the MAPK cascade (Table 20) are highlighted in red.

Table 20 Selected phospho-sites in MAP kinases and TPL-2 following uptake of LPS-coated beads

Tpl2^{D270A} / WT fold changes of selected phospho-sites in protein kinases of the MAP kinase cascade were calculated from Welch difference ratios.

Protein (Gene)	Site	Fold change
MEK1 (*Map2k1*), MEK2 (*Map2k2*)	S222	4.8
MEK3 (*Map2k3*), MEK6 (*Map2k6*)	S218	4.4
TPL-2 (*Map3k8*)	S141	5.2
ERK2 (*Mapk1*)	Y185	5
ERK1 (*Mapk3*)	T208	4
ERK1 (*Mapk3*)	T199	3.2
ERK1 (*Mapk3*)	Y205	4

To further investigate the signalling pathways underlying TPL-2 regulation following phagocytic uptake of LPS-coated beads, a Metacore pathway analysis was performed for phospho-sites significantly regulated by *Tpl2*^{D270A} mutation. As expected, several biological pathways involved in innate immune regulation, including negative feedback regulation of MAPK pathways, were upregulated in *Tpl2*$^{D270A/D270A}$ BMDMs compared to WT controls (Figure 41). In line with previous studies into the role of TPL-2 biology, numerous phospho-hits involved in TLR signalling cascades were downregulated in the absence of TPL-2 catalytic activity (Figure 41). Interestingly, *Tpl2*^{D270A} mutation significantly downregulated vesicle-mediated transport, membrane trafficking and mTOR signalling pathways (Figure 41). Since these biological pathways are implicated in the regulation of phagosome maturation, I decided to investigate these phospho-hits in more detail.

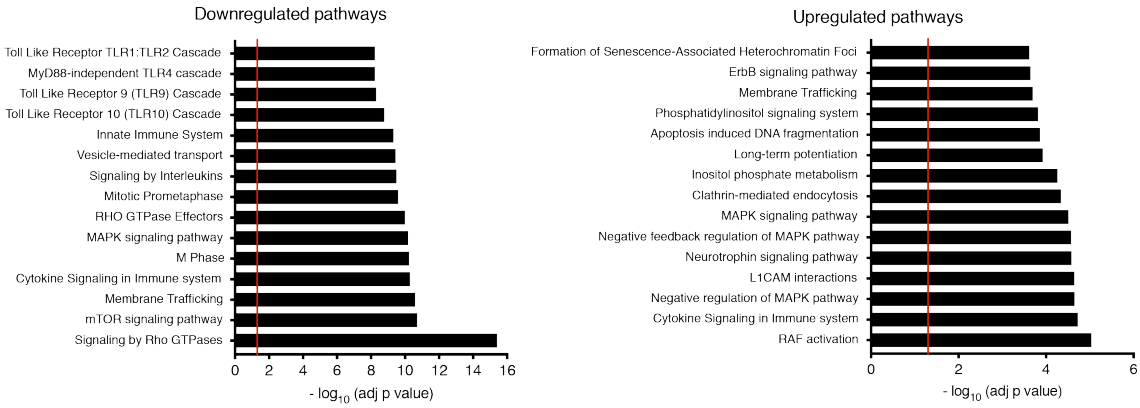

Figure 41 Biological pathways regulated by *Tpl2*^{D270A} mutation following uptake of LPS-coated beads

Pathway enrichment using the Metacore database. 15 selected downregulated and upregulated pathways in *Tpl2*$^{D270A/D270A}$ BMDMs compared to WT BMDMs were plotted. -$\log_{10}$ of adjusted *P* values are shown. Red line represents *P* = 0.05, where pathways below the red line are statistically non-significant.

A total of 21 phospho-sites in proteins that regulate vesicle trafficking were strongly regulated by *Tpl2*^{D270A} mutation. While 19 phospho-sites were downregulated by *Tpl2*^{D270A} mutation, phospho-sites in two GAP proteins (ARHGAP25 and ARHGAP39) were significantly upregulated in *Tpl2*$^{D270A/D270A}$ BMDMs compared to WT controls (Figure 42A and Table 21).

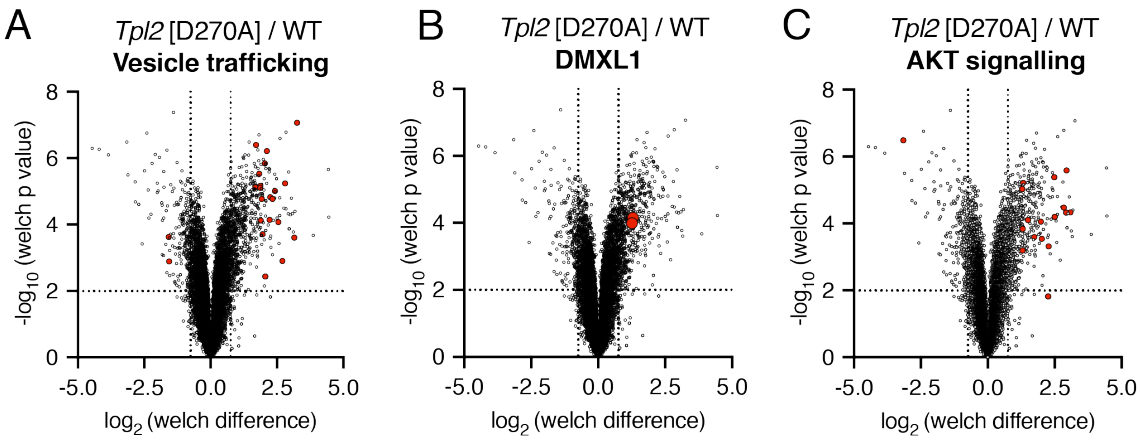

Figure 42 TPL-2-dependent phosphoproteome following uptake of LPS-coated latex beads

TPL-2-dependent phosphoproteome in BMDMs following phagocytosis of LPS-coated latex beads (0.5 h) was determined by TMT mass spectrometry. Five biological replicates were analysed per genotype, *Tpl2*$^{D270A/D270A}$ and WT (n = 5). Volcano plots representing the significance (-$\log_{10}$ *P* values after Welch's t-test) vs. phosphorylation fold change (Welch difference ratios) between WT and *Tpl2*$^{D270A/D270A}$ BMDMs. X-axis grid line at $\log_2$ (fold change) of 1.5 and -1.5; Y-axis grid line at -$\log_{10}$ (adjusted *P* value) of 2, which corresponds to a *P* value of 0.01. (**A**) Selected phospho-sites in regulators of vesicle trafficking (Table 21) are highlighted in red. (**B**) Significantly downregulated DMXL1 phospho-sites (Table 22) are highlighted in red. (**C**) Selected phospho-sites in regulators of AKT-mTOR signalling (Table 23) are highlighted in red.

Selected phospho-sites in vesicle trafficking proteins were downregulated by more than 3-fold in *Tpl2*$^{D270A/D270A}$ BMDMs. Phospho-hits of particular interest included MRCKB (S970), a protein kinase regulating cytoskeletal reorganisation (Unbekandt & Olson, 2014), and multiple phospho-sites in FAM21 (S866, S873, S867), a core component of the WASH complex, which activates the Arp2/3 complex that mediates phagosome formation (Ryder *et al*, 2013) (Table 21). Moreover, *Tpl2*^{D270A} mutation reduced phosphorylation of ARHGEF7 (S516), a GEF protein for a number of GTPases, including LRRK2 and RAC1 (Haebig *et al*, 2010) (Table 21). In addition, RAB11FIP5 phosphorylation on S1212 and S1214 was reduced in the absence of TPL-2 catalytic activity. RAB11FIP5 is a RAB11 effector that mediates cargo transport via recycling endosomes to phagosomes (Eaton & Martin-Belmonte, 2014; Boulais *et al*, 2010). Interestingly, *Tpl2*^{D270A} mutation reduced phosphorylation of CCT2 and OXR1 on S260 and S194, respectively (Table 21). Both CCT2 and OXR1 have been shown to interact with the V-ATPase complex (Merkulova *et al*, 2015).

Table 21 Selected phospho-sites in proteins implicated in vesicle trafficking following uptake of LPS-coated beads

Tpl2^{D270A} / WT fold changes of selected phospho-sites in regulators of vesicle trafficking were calculated from Welch difference ratios.

Protein (Gene)	Site	Fold change
HRBL (*Agfg2*)	S160	3.8
ARHGAP25 (*Arhgap25*)	T441	-3.2
ARHGAP39 (Arhgap39)	S301	-3.2
ARHGEF7 (*Arhgef7*)	S516	3.4
CCT2 (*Cct2*)	S260	4
MRCKB (*Cdc42bpb*)	S970	4.8
FAM21 (*Fam21*)	S866	6.4
FAM21 (*Fam21*)	S873	5.2
FAM21 (*Fam21*)	S867	6.6
ESE1 (*Itsn1*)	S932	3.8
MACF1 (*Macf1*)	S1378	4.4
OXR1 (*Oxr1*)	S194	4
RAB11FIP5 (*Rab11fip5*)	S1212	4.6
RAB11FIP5 (*Rab11fip5*)	S1214	4.2
RAB3GAP (*Rab3gap1*)	S538	3.6
RAB3GAP (*Rab3gap1*)	S536	3.4
RANBP2 (*Ranbp2*)	T2341	5.4
SNAP23 (*Snap23*)	T123	4.2
TOM1 (*Tom1*)	S160	3.8
TRAPPC12 (*Trappc12*)	S114	4.6
WDFY4 (*Wdfy4*)	S3088	3.8

As previously outlined, two of the most downregulated phospho-sites following phagocytic uptake of latex beads were S1903 and S1904 on DMXL1. Following uptake of LPS-coated beads, *Tpl2*^{D270A} mutation also reduced both S1903 and S1904 phosphorylation on DMXL1 by 2.6-fold compared to WT controls (Figure 42B and Table 22). Phosphorylation of DMXL1 on S915, S916, S1283, S572 and S1896 were unaffected by *Tpl2*^{D270A} mutation, indicating that TPL-2 did also not regulate DMXL1 protein levels following uptake of LPS-coated beads (data not shown).

Table 22 Significantly downregulated phospho-sites in DMXL1 following uptake of LPS-coated beads

Tpl2^{D270A} / WT fold changes of two highly downregulated DMXL1 phospho-sites were calculated from Welch difference ratios.

Protein (Gene)	Site	Fold change
DMXL1 (*Dmxl1*)	S1903	2.6
DMXL1 (*Dmxl1*)	S1904	2.6

Next, I analysed the TPL-2-regulated phospho-hits implicated in mTOR/AKT signalling, since the mTOR/AKT signalling pathway was the second most downregulated biological pathway in *Tpl2*$^{D270A/D270A}$ BMDMs. Among the 17 significantly regulated phospho-sites, 16 sites were downregulated, and one phospho-site was upregulated in *Tpl2*$^{D270A/D270A}$ BMDMs compared to WT controls (Figure 42C and Table 23). Strikingly, phosphorylation of T964 in SHIP-1, a phosphatase that negatively regulates AKT signalling, was upregulated by *Tpl2*^{D270A} mutation by more than 6-fold (Table 23) (Edimo *et al*, 2012). Interestingly, phosphorylation of five sites in eukaryotic initiation factors (EIFs), namely EIF2B (S522), EIF3B (S123) and EIF4B (S16, T18, T27), were reduced in *Tpl2*$^{D270A/D270A}$ BMDMs by more than 4-fold (Table 23). Activation of EIFs via the mTOR/AKT signalling axis is critical for initiation of eukaryotic translation (Holz *et al*, 2005; Roux & Topisirovic, 2018). In addition, loss of TPL-2 catalytic activity led to decreased phosphorylation of tuberous sclerosis proteins (TSC) 1 and 2 on S1035 and S1805, respectively (Table 23). The heterodimeric TSC1/2 complex regulates mTORC1 activity (Huang & Manning, 2008). *Tpl2*^{D270A} mutation also reduced phosphorylation of RSK2 (RPS6KA3) on T577 by almost 6-fold, a site that was previously shown to be phosphorylated by MAP kinases following LPS stimulation (Zaru *et al*, 2015) (Table 23). Notably, only BRAF (S134), FOS (S362), GAB2 (T315), ITPKB (T32), ERK1 (T208) and ERK2 (Y185) were significantly downregulated by *Tpl2*^{D270A} mutation following stimulation with soluble LPS (Pattison *et al*, 2016), indicating that the majority of phospho-sites on regulators of AKT-mTOR signalling were only regulated by TPL-2 catalytic activity in response to uptake of LPS-coated beads.

Table 23 Significantly regulated phospho-sites in proteins of the mTOR signalling pathway following uptake of LPS-coated beads

Tpl2^{D270A} / WT fold changes of selected phospho-sites in regulators of AKT-mTOR signalling were calculated from Welch difference ratios.

Protein (Gene)	Site	Fold change
BRAF (*Braf*)	S134	2.6
EIF2B (*Eif2b*)	S522	4
EIF3B (*Eif3b*)	S123	4.6
EIF4B (*Eif4b*)	T18	6.2
EIF4B (*Eif4b*)	S16	5.8
EIF4B (*Eif4b*)	T27	5.6
FOS (*Fos*)	S362	4.6
GAB2 (*Gab2*)	T315	3.4
SHIP-1 (*Inpp5d*)	T964	-6.4
ITPKB (*Itpkb*)	T32	5
KLC1 (*Klc1*)	S513	2.6
ERK2 (*Mapk1*)	Y185	5
ERK1 (*Mapk3*)	T208	4
RPS6KA3 (*Rps6ka3*)	T577	5.8
TSC1 (*Tsc1*)	S1035	2.6
TSC2 (*Tsc2*)	S1805	3
ULK1 (*Ulk1*)	S622	2.6

4.2.9 TPL-2 promotes phosphorylation of DMXL1 following phagocytosis

Following phagocytic uptake of beads, S1903 and S1904 on DMXL1 were among the three most highly downregulated phospho-sites in *Tpl2*$^{D270A/D270A}$ BMDMs compared to WT controls. Moreover, these two phosphorylation sites were also strongly downregulated by *Tpl2*^{D270A} mutation following phagocytic uptake of LPS-coated beads. Since DMXL1 is a component of the V-ATPase complex, which is critical for acidification of endosomes, I investigated whether TPL-2 inducibly regulated the phosphorylation of DMXL1 following phagocytic uptake of beads (Merkulova *et al*, 2015). A phospho-S1903 DMXL1-peptide antibody was generated and I used immunoblotting to validate the proteomic results. Phagocytic uptake of uncoated latex beads and LPS-coated latex beads by WT BMDMs induced the phosphorylation of DMXL1 on S1903 (Figure 43). Importantly, phosphorylation of

DMXL1 on S1903 was blocked in *Tpl2*$^{D270A/D270A}$ BMDMs following uptake of latex beads (Figure 43A). In addition, phosphorylation of DMXL1 on S1903 was reduced by *Tpl2*^{D270A} mutation following uptake of LPS-coated latex beads (Figure 43B).

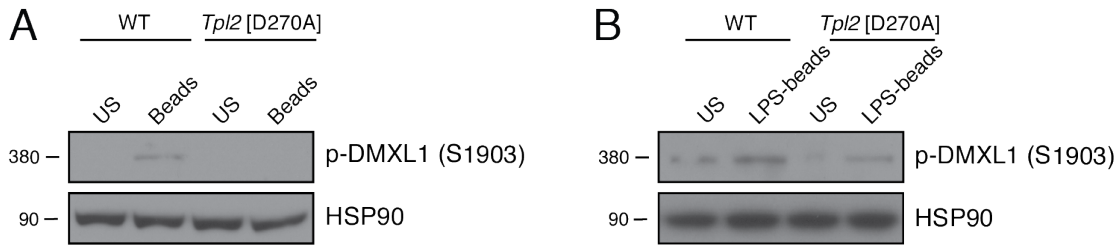

Figure 43 TPL-2 catalytic activity promotes DMXL1 phosphorylation on S1903 upon phagocytosis

WT and *Tpl2*$^{D270A/D270A}$ BMDMs were incubated with (**A**) latex beads (1:50) or (**B**) LPS-coated latex beads (1:300) for 0.5 h. Cell extracts were immunoblotted for phospho-DMXL1 (S1903) and HSP90. Immunoblot analysis of cell extracts from BMDMs stimulated with LPS-coated beads representative of two independent experiments (n = 2). US, unstimulated; beads, uncoated latex beads, LPS-beads, LPS-coated latex beads, p, phospho.

Since DMXL1 is a V-ATPase regulatory protein, these findings raised the possibility that TPL-2 may induce phagosome maturation by promoting phosphorylation of DMXL1 on S1903. Previous studies have investigated the role of DMXL1 in vesicle acidification in a kidney cell line using siRNA-mediated knockdown (Merkulova *et al*, 2015). I used immortalised BMDMs from WT mice to investigate whether DMXL1 induces phagosome maturation, and in particular phagosome acidification, in macrophages.

Prior to investigating DMXL1 function, I initially determined whether TPL-2 catalytic activity was required for phagosome maturation in iBMDMs similar to primary BMDMs. Pre-treatment of iBMDMs with C34 TPL-2 inhibitor significantly impaired phagosomal proteolysis (Figure 44A). In addition, pre-treatment of iBMDMs with C34 also significantly reduced phagosomal acidification (Figure 44B). Similar to primary BMDMs, C34 pre-treatment of iBMDMs abrogated ERK1/2 phosphorylation on T202/Y204 upon TLR4 activation (Figure 44C), indicating potent TPL-2 inhibition. These results indicated that TPL-2 catalytic activity induced phagosome maturation in immortalised macrophages similar to effects observed in primary BMDMs.

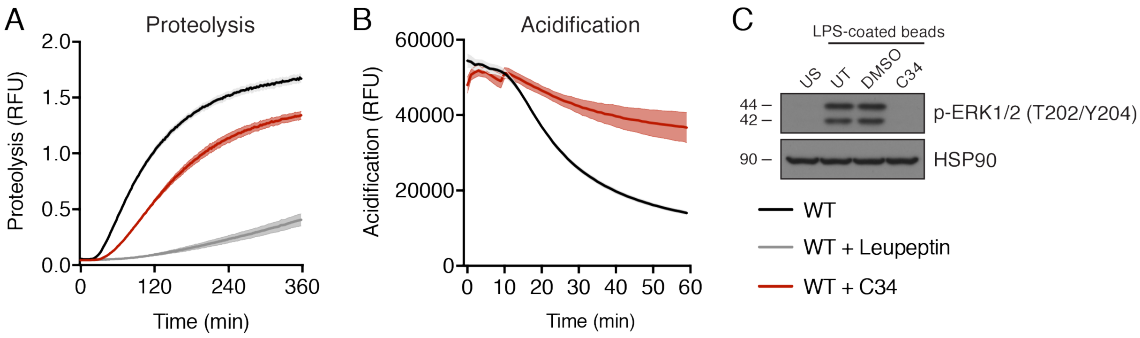

Figure 44 TPL-2 catalytic activity induces phagosome maturation in iBMDMs

(A) Intra-phagosomal proteolysis of DQ Green BSA / AF594 latex beads in iBMDMs pre-treated with 10 μM C34 TPL-2 inhibitor for 1 h (n = 4). iBMDMs were pre-treated with 100 μg/ml leupeptin for 1 h to inhibit serine-cysteine proteases. (**B**). Intra-phagosomal acidification of BCECF-coupled latex beads in iBMDMs pre-treated with 10 μM C34 TPL-2 inhibitor for 1 h (n = 4). (**A-B**) iBMDMs were separately pre-treated with DMSO (vehicle control). Shaded areas represent SEM. **** $P < 0.0001$. Paired Mann-Whitney t-test; All differences relative to WT are ****. (**C**) iBMDMs were pre-treated with 10 μM C34 TPL-2 inhibitor for 1 h and stimulated with LPS-coated latex beads (1:300) for 0.5h. Cell extracts were immunoblotted for p-ERK1/2 and HSP90. iBMDMs were separately pre-treated with DMSO (vehicle control). RFU, relative fluorescence units; US, unstimulated; UT, untreated.

To investigate whether DMXL1 was required to promote phagosome maturation in iBMDMs, I knocked down *Dmxl1* mRNA using *Dmxl1* siRNA oligonucleotides. *Dmxl1* mRNA levels were reduced by over 90% following transfection of *Dmxl1* siRNA (Figure 45C). Phagosome proteolysis was monitored using DQ Green BSA latex beads. DMXL1 knockdown significantly reduced phagosome proteolysis compared to untransfected WT iBMDMs, and WT iBMDMs that were transfected with a non-targeting siRNA pool (Figure 45A). Furthermore, following uptake of BCECF latex beads, phagosome acidification was significantly decreased compared to iBMDMs transfected with a non-targeting siRNA pool (Figure 45B). These findings that DMXL1 promoted phagosomal proteolysis were in line with previous studies suggesting that V-ATPase-mediated phagosomal acidification is involved in promoting phagosomal proteolysis (Kinchen & Ravichandran, 2008; Lennon-Duménil *et al*, 2002). DMXL2, a DMXL1 homologue, has previously been implicated in endosome maturation by associating with V-ATPases (Tuttle *et al*, 2014). I therefore tested whether DMXL2, similarly to DMXL1, induces phagosome maturation in macrophages. However, DMXL2 depletion by over 90% (Figure 45F) did not impair phagosomal proteolysis (Figure 45D) or phagosomal acidification

(Figure 45E), suggesting that DMXL2 does not regulate phagosome maturation in macrophages. Importantly, targeting *Dmxl1* or *Dmxl2* mRNA for degradation did not downregulate mRNA levels of *Dmxl2* or *Dmxl1*, respectively (Figure 45C and F).

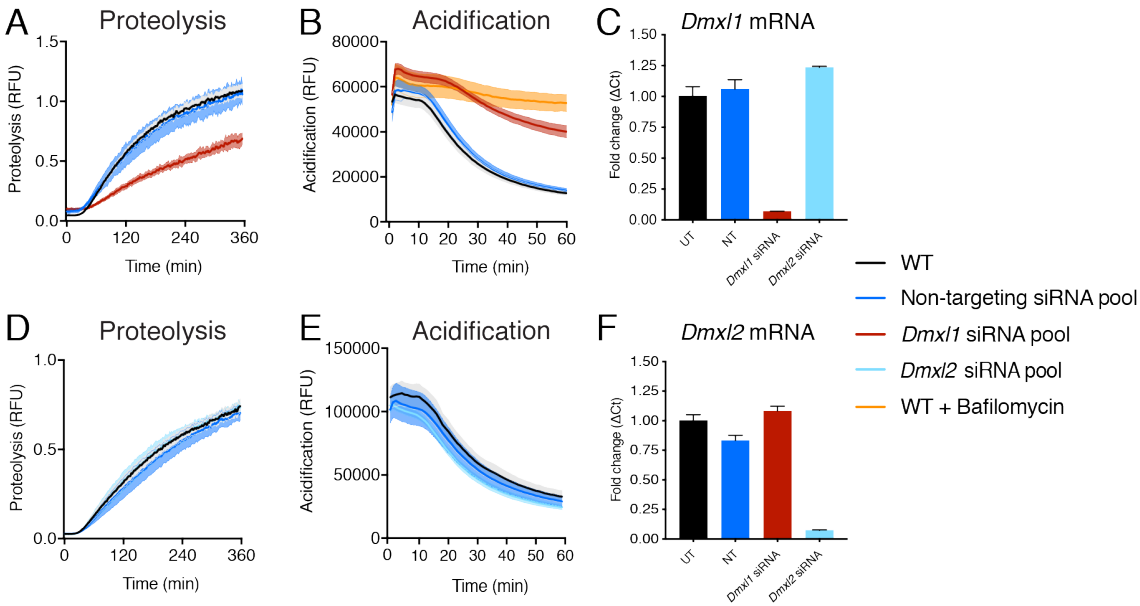

Figure 45 Knockdown of *Dmxl1*, but not *Dmxl2*, impairs phagosome maturation in iBMDMs

Dmxl1 (A-C) and *Dmxl2* (D-F) were knocked down in WT iBMDMs by RNA interference using a SMARTpool ON-TARGETplus siRNA (50 nM) for 48 h. Transfection of iBMDMs with ON-TARGETplus non-targeting pool (50 nM) for 48 h functioned as siRNA control. (**A**) Intra-phagosomal proteolysis in DMXL1 knockdown iBMDMs was assayed following uptake of DQ Green BSA / AF594 silica beads (n = 4). (**B**) Intra-phagosomal acidification in DMXL1 knockdown iBMDMs was monitored following uptake of BCECF-coupled silica beads. Untransfected iBMDMs were pre-treated with 1 µM bafilomycin A1 for 15 min to inhibit V-ATPases (n = 4). (**C**) qRT-PCR analysis of RNA extracted from iBMDMs was used to check the efficiency of *Dmxl1* knockdown (A-B). *Dmxl1* mRNA levels were normalised to *Hprt* mRNA levels and fold changes calculated (ΔC_t values) (n = 4). (**D**) Intra-phagosomal proteolysis in DMXL2 knockdown iBMDMs was assayed following uptake of DQ Green BSA / AF594 silica beads (n = 4). (**E**) Intra-phagosomal acidification in DMXL2 knockdown iBMDMs was monitored following uptake of BCECF-coupled silica beads. (**F**) qRT-PCR analysis of RNA extracted from iBMDMs was used to check the efficiency of *Dmxl2* knockdown (D-E). *Dmxl2* mRNA levels were normalised to *Hprt* mRNA levels and fold changes calculated (ΔC_t values) (n = 4). Error bars and shaded areas represent SEM. **** $P < 0.0001$. (**A, B, D, E**) Paired Mann-Whitney t-test; All differences relative to WT are ****. RFU, relative fluorescence units; UT, untransfected; NT, non-targeting siRNA pool.

To investigate whether TPL-2 regulation of DMXL1 phosphorylation controls phagosome maturation, I transfected DMXL1-deficient iBMDMs with an expression

plasmid encoding a 274 amino acid DMXL1 fragment (DMXL1 [1773-2047]), which contained the two previously identified TPL-2-regulated phosphorylation sites, S1903 and S1904. Strikingly, expression of 3xFLAG-DMXL1^{WT}[1773-2047] significantly rescued impaired phagosomal proteolysis (Figure 46A) and phagosomal acidification (Figure 46B), which was reduced by DMXL1 knockdown (Figure 46A and B). Importantly, expression of 3xFLAG-DMXL1^{SSAA}[1773-2047], in which serines 1903 and 1904 were replaced with alanines, did not rescue phagosomal proteolysis or acidification (Figure 46A and B). Knockdown of full-length *Dmxl1* was more than 90% efficient in all three conditions, regardless of co-transfection with 3xFLAG expression plasmids (Figure 46C). In addition, I confirmed by immunoblotting that expression levels of 3xFLAG-DMXL1^{WT}[1773-2047] and 3xFLAG-DMXL1^{SSAA}[1773-2047] were similar (Figure 46D). Overall, these findings indicated that TPL-2 induced phagosome maturation, in particular phagosome acidification, in macrophages by mediating the phosphorylation of the V-ATPase binding protein DMXL1 on S1903/S1904.

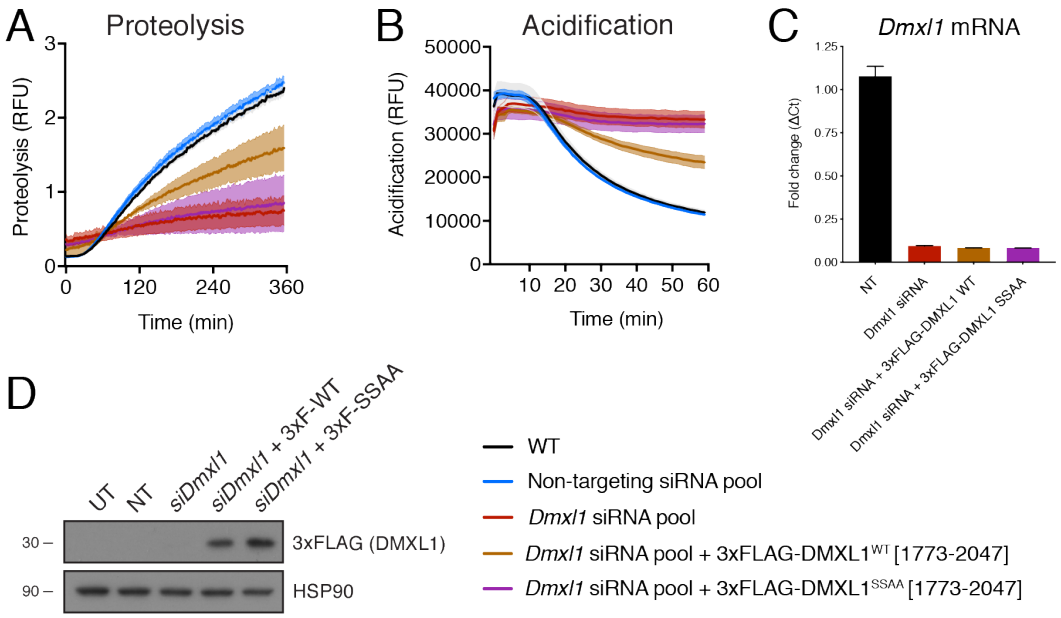

Figure 46 Phosphorylation of DMXL1 on S1903/S1904 regulates phagosome maturation

Simultaneous with siRNA-mediated *Dmxl1* knockdown, iBMDMs were co-transfected with plasmids expressing either 3xFLAG-DMXL1^{WT}[1773-2047] or 3xFLAG-DMXL1^{SSAA}[1773-2047]. (**A**) Intra-phagosomal proteolysis in DMXL1 knockdown iBMDMs was assayed following uptake of DQ Green BSA / AF594 silica beads (n = 4). (**B**) Intra-phagosomal acidification in DMXL1 knockdown iBMDMs was monitored following uptake of BCECF-coupled silica beads (n = 4). (**C**) qRT-PCR

analysis of RNA extracted from iBMDMs was used to check the efficiency of *Dmxl1* knockdown in cells expressing either 3xFLAG-DMXL1^{WT}[1773-2047] or 3xFLAG-DMXL1^{SSAA}[1773-2047] (n = 4). *Dmxl1* mRNA levels were normalised to *Hprt* mRNA levels and fold changes calculated (ΔC_t values). (**D**) Expression levels of 3xFLAG-DMXL1 were analysed by immunoblotting. Following 48 h *Dmxl1* knockdown and co-transfection of plasmids, iBMDMs were lysed and cell extracts were probed with an antibody recognising the 3xFLAG-tag. Error bars and shaded areas represent SEM. **** $P < 0.0001$, not significant (ns). Panels (A,B) Paired Mann-Whitney t-test. All differences relative to WT are ****. RFU, relative fluorescence units; UT, untransfected; NT, non-targeting siRNA pool; SSAA, S1903A/S1904A.

4.2.10 TPL-2 promotes AKT signalling following phagocytosis

I previously showed using TMT phosphoproteomics that *Tpl2*^{D270A} mutation reduced phosphorylation of several proteins in the AKT signalling pathway. The importance of the PI3K-AKT signalling axis in regulating phagosome maturation has been extensively studied by others (Thi & Reiner, 2012). Moreover, previous studies showed that in LPS-stimulated BMDMs from TPL-2 knockout mice, phosphorylation of multiple signalling proteins in the AKT pathway, including AKT itself, p70S6K, S6 and 4EBP1, was reduced compared to WT controls (López-Peláez *et al*, 2011; López-Pelaéz *et al*, 2012). I therefore investigated whether TPL-2 promoted phagosome maturation by activating PI3K-AKT signalling following phagocytic uptake of latex beads.

First, I intended to confirm the TPL-2-dependent activation of AKT following LPS stimulation. I stimulated *Tpl2*$^{D270A/D270A}$ BMDMs and WT BMDMs with soluble LPS, however, neither mTOR complex 2 (mTORC2)-mediated S473 nor phosphatidyl-inositide-dependent kinase 1 (PDK1)-mediated T308 phosphorylation on AKT were regulated by *Tpl2*^{D270A} mutation (Figure 47A). As expected, *Tpl2*^{D270A} mutation abrogated ERK1/2 phosphorylation on T202/Y204 following LPS stimulation (Figure 47A).

Next, I investigated whether TPL-2 catalytic activity regulated AKT signalling following phagocytic uptake of LPS-coated latex beads. In contrast to soluble LPS that predominately signals from the plasma membrane, LPS-coated beads are more efficiently phagocytised and potently activate endosomal signalling (Zanoni *et al*, 2011). Interestingly, AKT phosphorylation at S473 and T308 was strongly reduced

in *Tpl2*$^{D270A/D270A}$ BMDMs compared to WT controls following phagocytic uptake of LPS-coated beads (Figure 47B). In addition, phosphorylation of p70S6K at T389 and S6 at S240/S244 was decreased by *Tpl2*^{D270A} mutation (Figure 47B). Moreover, phosphorylation of the AKT downstream target 4EBP1 at T37/T46 was reduced in *Tpl2*$^{D270A/D270A}$ BMDMs following phagocytosis of LPS-coated beads (Figure 47B). While p38α phosphorylation at T180/Y182 remained unaffected, ERK1/2 phosphorylation at T202/Y204 was dramatically reduced in *Tpl2*$^{D270A/D270A}$ BMDMs (Figure 47B).

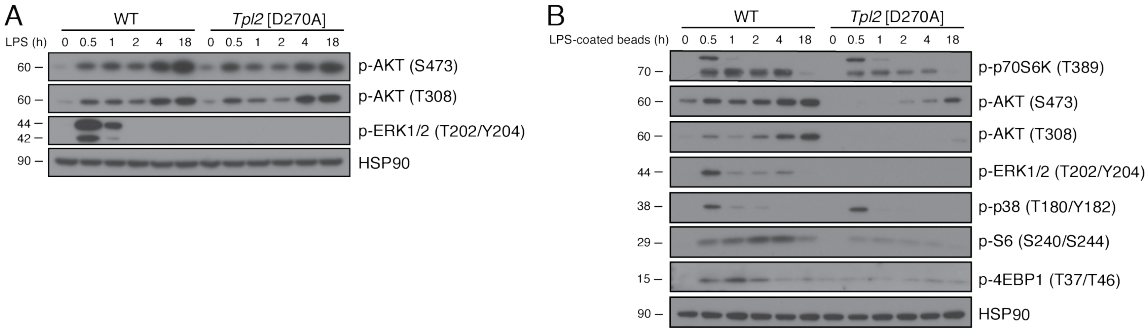

Figure 47 *Tpl2*^{D270A} mutation impairs AKT signalling following uptake of LPS-coated latex beads

BMDMs from WT and *Tpl2*$^{D270A/D270A}$ mice were stimulated with (**A**) LPS (100 ng/ml) and (**B**) LPS-coated latex beads (1:300) for the times indicated and cell extracts were immunoblotted with the antibodies indicated. p, phospho.

As TPL-2 catalytic activity promoted AKT activation following uptake of LPS-coated latex beads, I subsequently tested whether AKT signalling was reduced by *Abin2*^{D310N} mutation. Phosphorylation of AKT at S473, p70S6K at T389, and S6 at S240/S244 was comparable to WT controls following phagocytic uptake of LPS-coated latex beads (Figure 48).

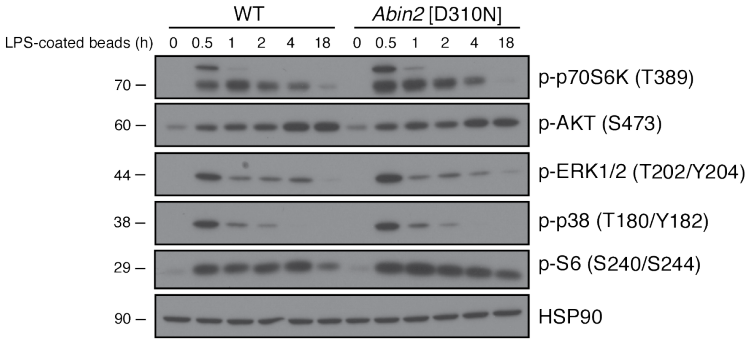

Figure 48 *Abin2*^{D310N} mutation does not regulate AKT signalling following uptake of LPS-coated latex beads

BMDMs from WT and *Abin2*$^{D310N/D310N}$ mice were stimulated with LPS-coated latex beads (1:300) for the times indicated and cell extracts were immunoblotted with the antibodies indicated. p, phospho.

Overall, my findings suggested that TPL-2 catalytic activity promotes AKT activation following phagocytic uptake of LPS-coupled latex beads, but not following stimulation with soluble LPS. Since TPL-2 induced phagosome maturation not only following uptake of LPS-coated beads, but also upon phagocytosis of uncoated beads, I decided to incubate BMDMs with uncoated latex beads and monitored AKT activation by immunoblotting. Phagocytic uptake of latex beads by BMDMs induced a subtle, but consistent increase in phosphorylation of p70S6K at T389, AKT at S473, and S6 at S240/S244 (Figure 49A). It is important to note that AKT signalling was more strongly activated upon phagocytic uptake of LPS-coated beads than following uptake of uncoated latex beads (Figure 47C and Figure 49A). Interestingly, phosphorylation of AKT at S473 as well as downstream phosphorylation of p70S6K and S6 was reduced in *Tpl2*$^{D270A/D270A}$ BMDMs compared to WT controls upon uptake of latex beads (Figure 49B-D). These findings indicated that, despite weak induction of AKT signalling, TPL-2 catalytic activity promoted AKT activation following uptake of uncoated latex beads.

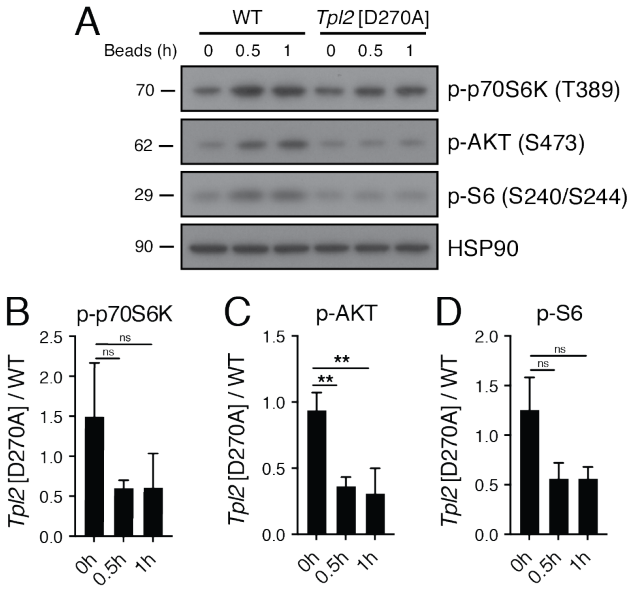

Figure 49 *Tpl2*^{D270A} mutation reduces AKT activation following phagocytic uptake of latex beads

(**A**) BMDMs from WT and *Tpl2*$^{D270A/D270A}$ mice were stimulated with latex beads (1:50) for the times indicated and cell extracts were immunoblotted with the antibodies indicated. Phosphorylation of (**B**) p70S6K at T389, (**C**) AKT at S473, and (**D**) S6 at S240/244 was quantified from three independent experiments and ratios between *Tpl2*$^{D270A/D270A}$ BMDMs and WT BMDMs were plotted (n = 3). An unpaired two-tailed t-test was carried out, with ** $P < 0.01$, not significant (ns). p, phospho.

4.2.11 AKT signalling induces phagosome maturation

Having established that TPL-2 mediates AKT activation following latex bead uptake, I investigated whether AKT signalling induces phagosome maturation in primary macrophages. Here, I pre-treated BMDMs with the AKT inhibitor Akti-1/2 and subsequently monitored phagosomal proteolysis and acidification using silica beads coupled to the fluorescent substrate DQ Green BSA and the pH sensor BCECF, respectively. Real-time measurements demonstrated that phagosomal proteolysis was significantly reduced in WT BMDMs that were pre-treated with Akti-1/2 (Figure 50A). As expected, *Tpl2*^{D270A} mutation significantly decreased phagosomal proteolysis, but interestingly AKT inhibition by Akti-1/2 impaired proteolysis more strongly than *Tpl2*^{D270A} mutation (Figure 50A). Moreover, real-time measurements demonstrated that phagosomal acidification was significantly blocked in Akti-1/2-treated WT BMDMs (Figure 50B). The inhibitory effect of AKT blockage on phagosomal acidification was more pronounced than the defect caused by *Tpl2*^{D270A}

mutation (Figure 50B). Strikingly, Akti-1/2 pre-treatment abrogated phagosomal acidification similar to bafilomycin A1 pre-treatment (Figure 50B). Immunoblotting confirmed that Akti-1/2 pre-treatment potently inhibited AKT activation, indicated by a strong reduction in phosphorylation of p70S6K (T389), AKT itself (S473), and S6 (S240/S244) in BMDMs following stimulation with LPS-coated latex beads (Figure 50C).

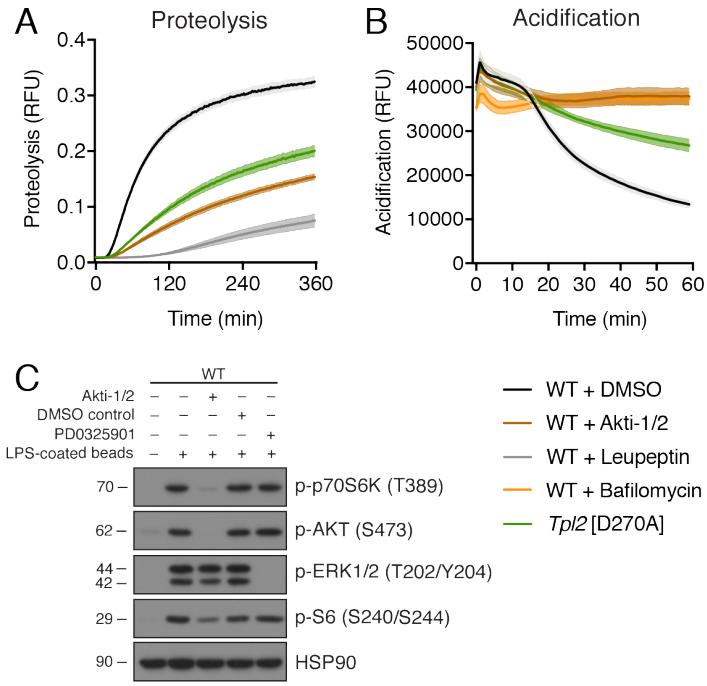

Figure 50 AKT inhibition by Akti-1/2 impairs phagosomal proteolysis and acidification

BMDMs were pre-treated with 10 µM Akti-1/2 for 1 h to inhibit AKT. BMDMs were separately pre-treated with DMSO (vehicle control). (**A**) Intra-phagosomal proteolysis in WT, Akti-1/2-treated BMDMs and *Tpl2*$^{D270A/D270A}$ BMDMs was monitored. BMDMs were pre-treated with 100 µg/ml leupeptin for 1 h to inhibit serine-cysteine proteases (n = 4). (**B**) Intra-phagosomal acidification in WT, Akti-1/2-treated BMDMs and *Tpl2*$^{D270A/D270A}$ BMDMs was monitored. BMDMs were pre-treated with 1 µM bafilomycin A1 for 15 min to inhibit V-ATPases (n = 4). (**C**) BMDMs were pre-treated with Akti-1/2 and stimulated with LPS-coated latex beads (1:300) for 0.5 h. Cell extracts were immunoblotted with the antibodies indicated. BMDMs were also pre-treated with 0.1 µM PD0325901 for 10 min to inhibit MEK1. Shaded areas represent SEM. **** $P < 0.0001$, not significant (ns). Paired Mann-Whitney t-test; All differences relative to WT are ****. p, phospho; RFU, relative fluorescence units.

To pharmacologically confirm the importance of AKT signalling in driving phagosome maturation, I pre-treated BMDMs with AZD8055, an mTOR inhibitor that potently blocks mTORC1 and also mTORC2 upstream of AKT. Similarly to my previous

findings with Akti-1/2, AZD8055 pre-treatment significantly reduced phagosomal proteolysis (Figure 51A) and phagosomal acidification (Figure 51B) compared to vehicle-treated WT BMDMs. I confirmed the inhibitory effect of AZD8055 on AKT signalling by immunoblotting, which showed that AZD8055 strongly reduced phosphorylation of p70S6K (T389), AKT itself (S473), S6 (S240/S244), and 4EBP1 (T37/46) in BMDMs following stimulation with LPS-coated latex beads (Figure 51C). As previously shown, *Tpl2*^{D270A} mutation impaired AKT signalling following uptake of LPS-coated latex beads (Figure 51C).

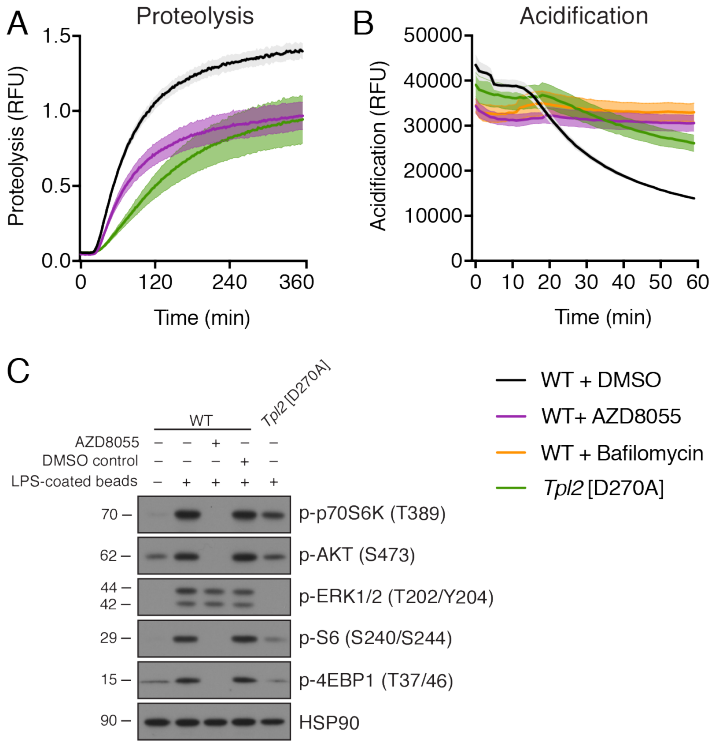

Figure 51 mTOR inhibition by AZD8055 impairs phagosomal proteolysis and acidification

BMDMs were pre-treated with 1 µM AZD8055 for 1 h to inhibit mTOR. BMDMs were separately pre-treated with DMSO (vehicle control). (**A**) Intra-phagosomal proteolysis in WT, AZD8055-treated BMDMs and *Tpl2*$^{D270A/D270A}$ BMDMs was monitored (n = 4). (**B**) Intra-phagosomal acidification in WT, AZD8055-treated BMDMs and *Tpl2*$^{D270A/D270A}$ BMDMs was monitored. BMDMs were pre-treated with 1 µM bafilomycin A1 for 15 min to inhibit V-ATPases (n = 4). (**C**) *Tpl2*$^{D270A/D270A}$ and AZD8055-treated WT BMDMs were stimulated with LPS-coated latex beads (1:300) for 0.5 h. Cell extracts were immunoblotted with the antibodies indicated. Shaded areas represent SEM. **** $P < 0.0001$, not significant (ns). Paired Mann-Whitney t-test; All differences relative to WT are ****. p, phospho; RFU, relative fluorescence units.

Next, I used RNA interference to deplete AKT in immortalised macrophages. Depletion of *Akt* mRNA significantly reduced phagosomal proteolysis compared to iBMDMs transfected with a non-targeting siRNA pool (Figure 52A). Furthermore, AKT knockdown abrogated phagosomal acidification (Figure 52B). Western blotting confirmed that siRNA-mediated knockdown of *Akt* mRNA almost fully depleted endogenous AKT levels (Figure 52C). These findings, together with studies using AKT inhibitors, showed that AKT was required for promoting phagosome proteolysis and acidification in macrophages. This was consistent with previous studies indicating that PI3K-dependent activation of AKT promotes phagosomal acidification (Rupper *et al*, 2001; Marjuki *et al*, 2011; Liberman *et al*, 2014). Taken together, these findings indicated that pharmacological inhibition and depletion of AKT phenocopies loss of TPL-2 catalytic activity following phagocytic uptake of beads.

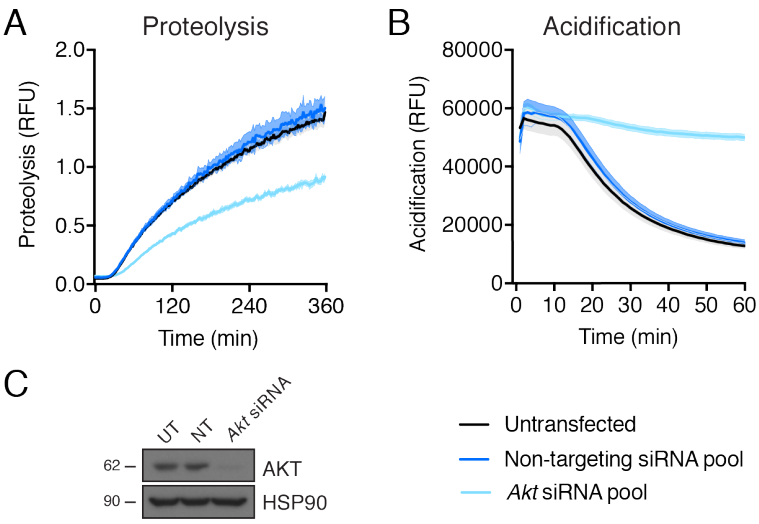

Figure 52 AKT knockdown impairs phagosome maturation in iBMDMs

Akt was knocked down in WT iBMDMs by RNA interference using a SMARTpool ON-TARGETplus siRNA (50 nM) for 48 h. Transfection of iBMDMs with ON-TARGETplus non-targeting pool (50 nM) for 48 h functioned as siRNA control. (**A**) Intra-phagosomal proteolysis in AKT knockdown iBMDMs was assayed following uptake of DQ Green BSA / AF594 silica beads (n = 4). (**B**) Intra-phagosomal acidification in AKT knockdown iBMDMs was monitored following uptake of BCECF-coupled silica beads (n = 4). (**C**) Cell extracts from untransfected and *Akt* siRNA-transfected iBMDMs were immunoblotted for AKT to confirm AKT knockdown. Shaded areas represent SEM. **** $P < 0.0001$. Paired Mann-Whitney t-test; All differences relative to WT are ****. RFU, relative fluorescence units; UT, untransfected; NT, non-targeting siRNA pool.

4.2.12 TPL-2-dependent transcriptome following phagocytic uptake of LPS-coated latex beads

The regulation of gene expression by TPL-2 following LPS stimulation of macrophages has been extensively studied in previous studies (Bandow *et al*, 2012; Eliopoulos *et al*, 2002) and more recently by the Ley laboratory (unpublished findings). My findings here suggested that TPL-2-mediated signalling pathways in response to LPS stimulation and phagocytic uptake of LPS-coated latex beads were different. I therefore characterised the transcriptome in *Tpl2*$^{D270A/D270A}$ BMDMs following stimulation with LPS-coated latex beads. Principal component analysis indicated that upon phagocytic uptake of LPS-coated beads, the global transcriptome of WT and *Tpl2*$^{D270A/D270A}$ BMDMs was significantly different (Figure 53A). In addition, volcano plots illustrated that as time proceeded, LPS-coated beads had an increasingly significant impact on the transcriptomic differences between WT and *Tpl2*$^{D270A/D270A}$ BMDMs (Figure 53B-E). Interestingly, volcano plots also suggested that the number of genes significantly downregulated by *Tpl2*^{D270A} was greater than the number of significantly upregulated genes compared to WT controls (Figure 53B-E).

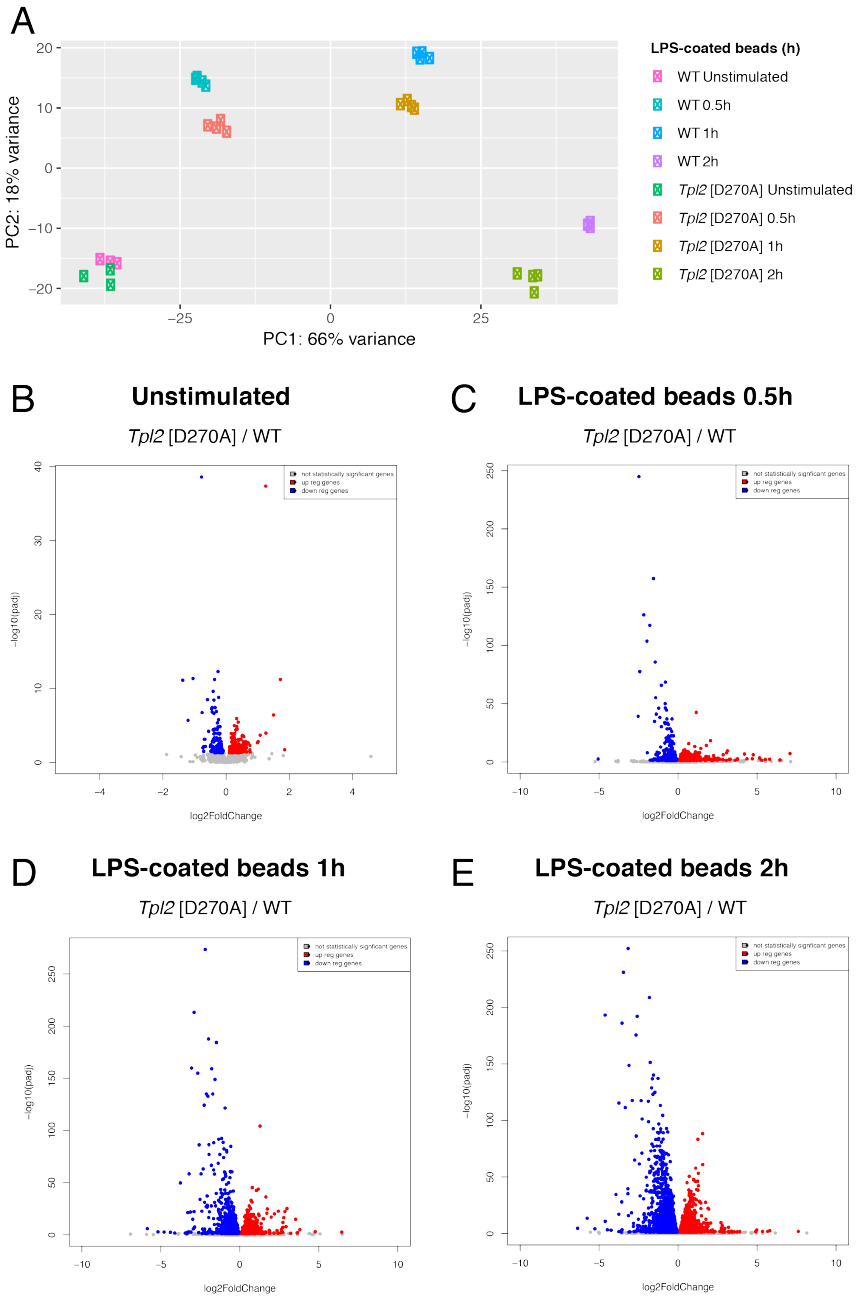

Figure 53 TPL-2-dependent transcriptome following phagocytic uptake of LPS-coated latex beads

BMDMs from WT and *Tpl2*$^{D270A/D270A}$ mice were stimulated with LPS-coated latex beads (1:300) for the times indicated. Four biological replicates were included per genotype. Following BMDM lysis, RNA was extracted and purified. Libraries were generated and samples were sequenced. (**A**) Principal component analysis (PCA) comparing RNA sequencing samples. (**B-E**) The $\log_2$ (fold change) and $-\log_{10}$ (adjusted *P* value) was plotted for each gene that was identified by RNA sequencing. Genes significantly upregulated ($P < 0.05$) by *Tpl2*^{D270A} mutation are highlighted in red, genes significantly downregulated ($P < 0.05$) by *Tpl2*^{D270A} mutation are highlighted in blue. Not statistically significant genes are shown in grey. PC, principal component.

The most strongly upregulated processes in *Tpl2*$^{D270A/D270A}$ BMDMs following uptake of LPS-coated beads were linked to interferon signalling (Figure 54A). In contrast, processes downregulated by *Tpl2*^{D270A} mutation included cytoskeletal regulation, NF-κB signalling as well as MAPK and JAK/STAT signalling (Figure 54B).

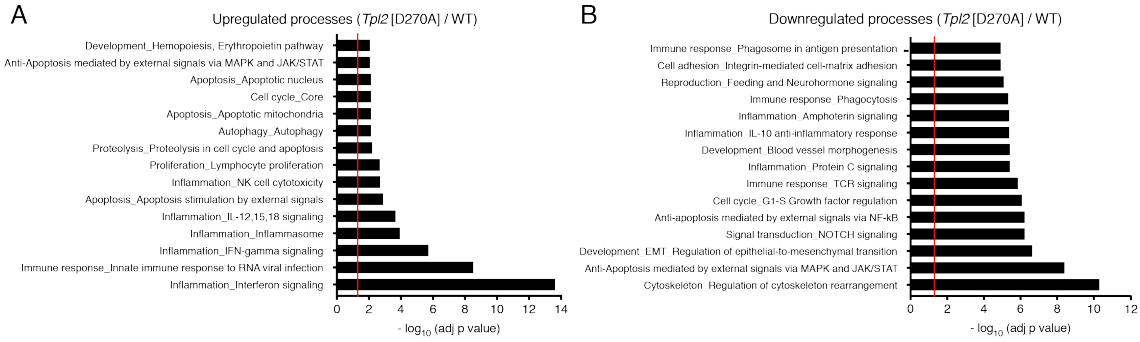

Figure 54 Selected up- and downregulated processes in the TPL-2-dependent transcriptome following uptake of LPS-coated beads

Process enrichment using the Metacore database on transcriptomic changes following incubation of BMDMs with LPS-coated latex beads for 1h. 15 selected (**A**) upregulated and (**B**) downregulated processes in *Tpl2*$^{D270A/D270A}$ BMDMs compared to WT BMDMs were plotted. -$\log_{10}$ of adjusted *P* values are shown. Red line represents *P* = 0.05, where processes below the red line are statistically non-significant.

It has previously been established that TPL-2 negatively regulates IFNβ production in macrophages (Kaiser *et al*, 2009). Upon stimulation of BMDMs with soluble LPS, *Tpl2*^{D270A} mutation strongly increased *Ifnb1* expression (Figure 55F), but expression of other type I interferons remained unchanged (Dr Michael Pattison and Dr Louise Blair, unpublished results) (Figure 55A-E). Since interferon signalling was strongly upregulated in *Tpl2*$^{D270A/D270A}$ BMDMs following uptake of LPS-coated beads, I further investigated expression levels of type I interferons. Relative expression values from RNA sequencing demonstrated that *Tpl2*^{D270A} mutation significantly increased expression of several *Ifna* genes, including *Ifna1* (Figure 55G), *Ifna2* (Figure 55H), *Ifna4* (Figure 55I), *Ifna5* (Figure 55J), and *Ifna6* (Figure 55K). As expected, *Tpl2*^{D270A} mutation significantly increased *Ifnb1* expression (Figure 55L).

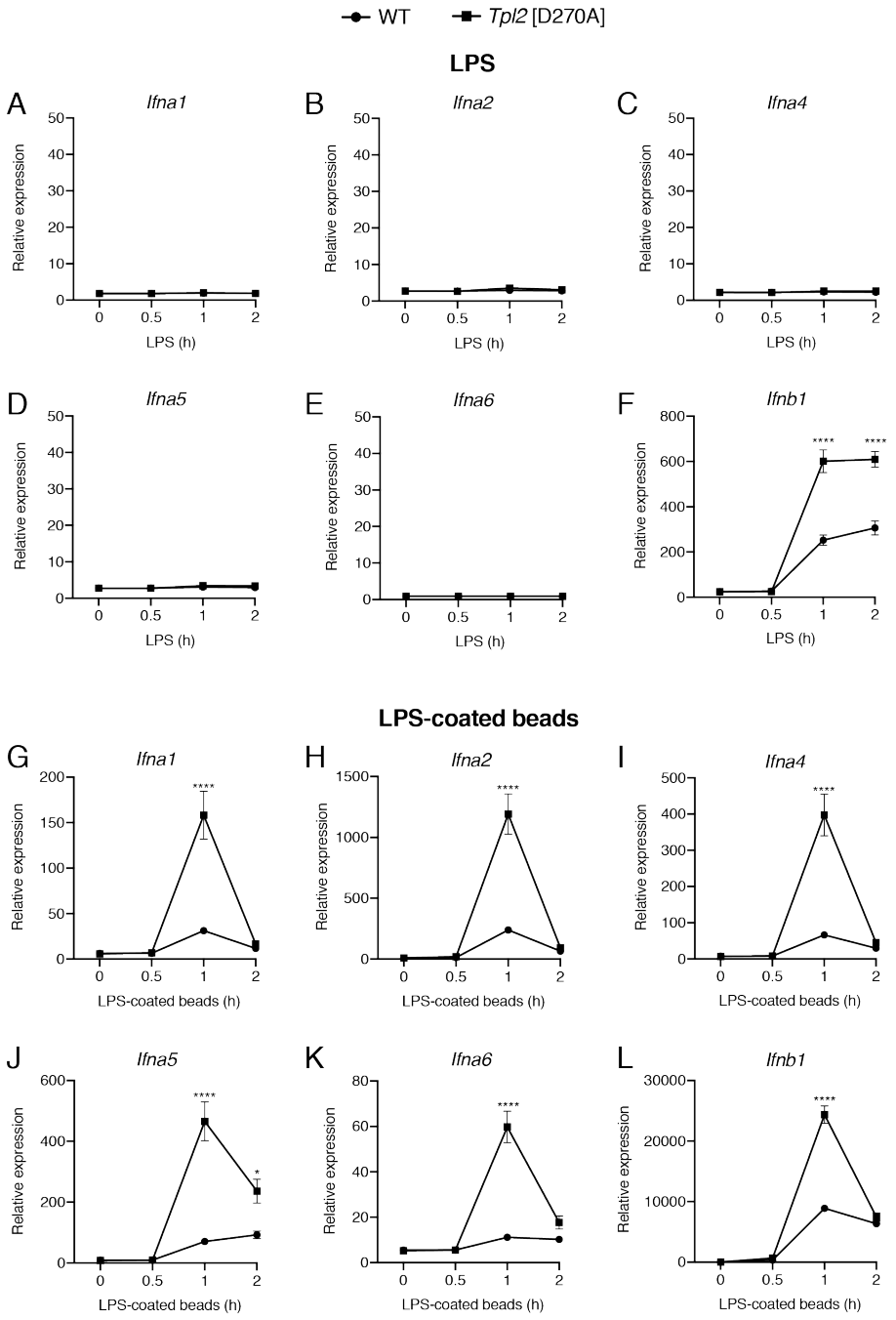

Figure 55 Relative expression of type I interferon genes in WT and *Tpl2*$^{D270A/D270A}$ BMDMs following LPS stimulation and uptake of LPS-coated beads

Relative expression values of selected type I interferon genes following (**A-F**) LPS stimulation and (**G-L**) uptake of LPS-coated latex beads. (**A-F**) Relative expression values originate from an RNA sequencing experiment that was carried out by Dr Michael Pattison. BMDMs from WT and *Tpl2*$^{D270A/D270A}$ mice were stimulated with soluble LPS (100 ng/ml) for the times indicated. (**G-L**) Relative expression values from RNA sequencing (data from Figure 53). Relative expression values were calculated from normalised RNA sequencing data (n = 3-6). Data were analysed by a two-way ANOVA. Error bars represent SEM. * $P < 0.05$, **** $P < 0.0001$.

To confirm expression changes in *Tpl2*$^{D270A/D270A}$ BMDMs, I incubated BMDMs with LPS-coated beads and analysed purified RNA using qRT-PCR. *Tpl2*^{D270A} mutation significantly downregulated expression of numerous inflammatory mediators, including *Cxcl2* (Figure 56A), *Tnf* (Figure 56B), *Il1b* (Figure 56C) and *Il6* (Figure 56D), which coincided with previous observations of TPL-2 promoting gene expression of pro-inflammatory genes following LPS stimulation. Moreover, expression of *Ifnb1* was strongly induced by *Tpl2*^{D270A} mutation 1 h after uptake of LPS-coated beads (Figure 56E). Interestingly, in line with findings from my RNA sequencing studies, mRNA expression of *Ifna1*, *Ifna2*, *Ifna5*, and *Ifna6* were significantly increased in *Tpl2*$^{D270A/D270A}$ BMDMs compared to WT controls. Overall, these experiments revealed that TPL-2 regulates gene expression of several *Ifna* genes following uptake of LPS-coated latex beads.

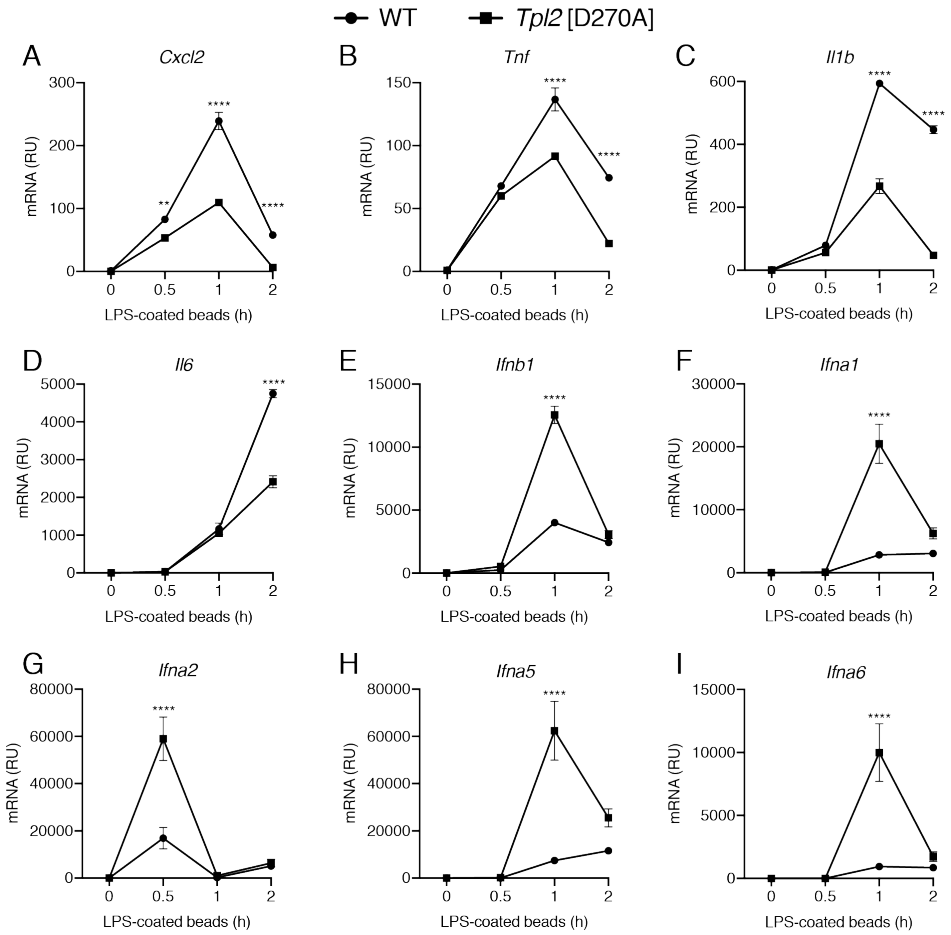

Figure 56 Expression levels of cytokines and type I interferon genes in *Tpl2*$^{D270A/D270A}$ BMDMs following uptake of LPS-coated beads

BMDMs from WT and *Tpl2*$^{D270A/D270A}$ mice were stimulated with LPS-coated latex beads (1:300) for the times indicated. Following BMDM lysis, RNA was purified and reverse transcribed into cDNA. Gene expression levels were quantified by qPCR using mRNA-specific TaqMan FAM-MGB-coupled probes recognising *Cxcl2*, *Tnf*, *Il1b*, *Il6*, *Ifnb1*, *Ifna1*, *Ifna2*, *Ifna5* and *Ifna6*. Error bars represent SEM (n = 3). An unpaired two-tailed t-test was carried out, with ** $P < 0.01$, **** $P < 0.0001$. RU, relative units.

4.2.13 TPL-2 interacts with the endosomal protein EEA1 following LPS stimulation

To characterise the interactome of endogenous TPL-2 in primary macrophages, the Ley laboratory generated *Tpl2*$^{3xFLAG/3xFLAG}$ knock-in mice, which express N-terminally 3xFLAG-tagged TPL-2. I decided to investigate the interactome of TPL-2 in response to LPS and TNFα. *Tpl2*$^{3xFLAG/3xFLAG}$ BMDMs were strongly activated by LPS and TNFα as indicated by inducible phosphorylation of ERK1/2 and p38α at T202/Y204 and T180/Y182, respectively (Figure 57A, left). Endogenous 3xFLAG-tagged TPL-2 was expressed in unstimulated *Tpl2*$^{3xFLAG/3xFLAG}$ BMDMs, and 3xFLAG-TPL-2 levels decreased upon LPS and TNFα stimulation as TPL-2 was liberated from the ternary complex, and thus less stable (Figure 57A, right). Moreover, a mobility shift of the 3xFLAG-TPL-2 band was observed upon stimulation, suggesting inducible phosphorylation of TPL-2 (Figure 57A, right). Importantly, 3xFLAG-TPL-2 was efficiently immunoprecipitated and fully depleted from cell extracts using M2 Anti-FLAG Affinity Gel (Figure 57A, right). BMDMs from three *Tpl2*$^{3xFLAG/3xFLAG}$ mice were separately cultured, treated, analysed by mass spectrometry and peptide intensities were averaged. As expected, upon LPS stimulation, TPL-2 interacted with proteins involved in pathways underlying the immune system, including cytokine signalling, MAPK as well as NF-κB signalling and antigen presentation (Figure 57B).

Table 24 TPL-2-interacting proteins upon LPS stimulation

The ten most significantly upregulated TPL-2-interacting proteins were calculated from LPS-stimulated / unstimulated peptide intensities.

Protein	Gene
RB1-inducible coiled-coil protein 1	*Rb1cc1*
Putative Polycomb group protein ASXL1	*Asxl1*
Cadherin-20	*Cdh20*
Prelamin-A/C;Lamin-A/C	*Lmna*
Amphoterin-induced protein 1	*Amigo1*
Ran-binding protein 10	*Ranbp10*
Early endosome antigen 1	*Eea1*
Nesprin-1	*Syne1*
Protein phosphatase 1B	*Ppm1b*
Sarcoplasmic/endoplasmic reticulum calcium ATPase 2	*Atp2a2*

Interestingly, LPS also induced the association of TPL-2 with proteins implicated in vesicle-mediated transport and membrane trafficking (Figure 57B). As expected, mass spectrometric data indicated that TPL-2 dissociated from both ABIN-2 and p105 (Figure 57C) (Gantke *et al*, 2011b). Interestingly, increased abundance of EEA1 peptides was detected upon LPS stimulation, whereas no EEA1-specific peptides were detected following TNFα stimulation (Figure 57C). These findings suggested that TPL-2 interacts with the endosomal protein EEA1 upon LPS stimulation.

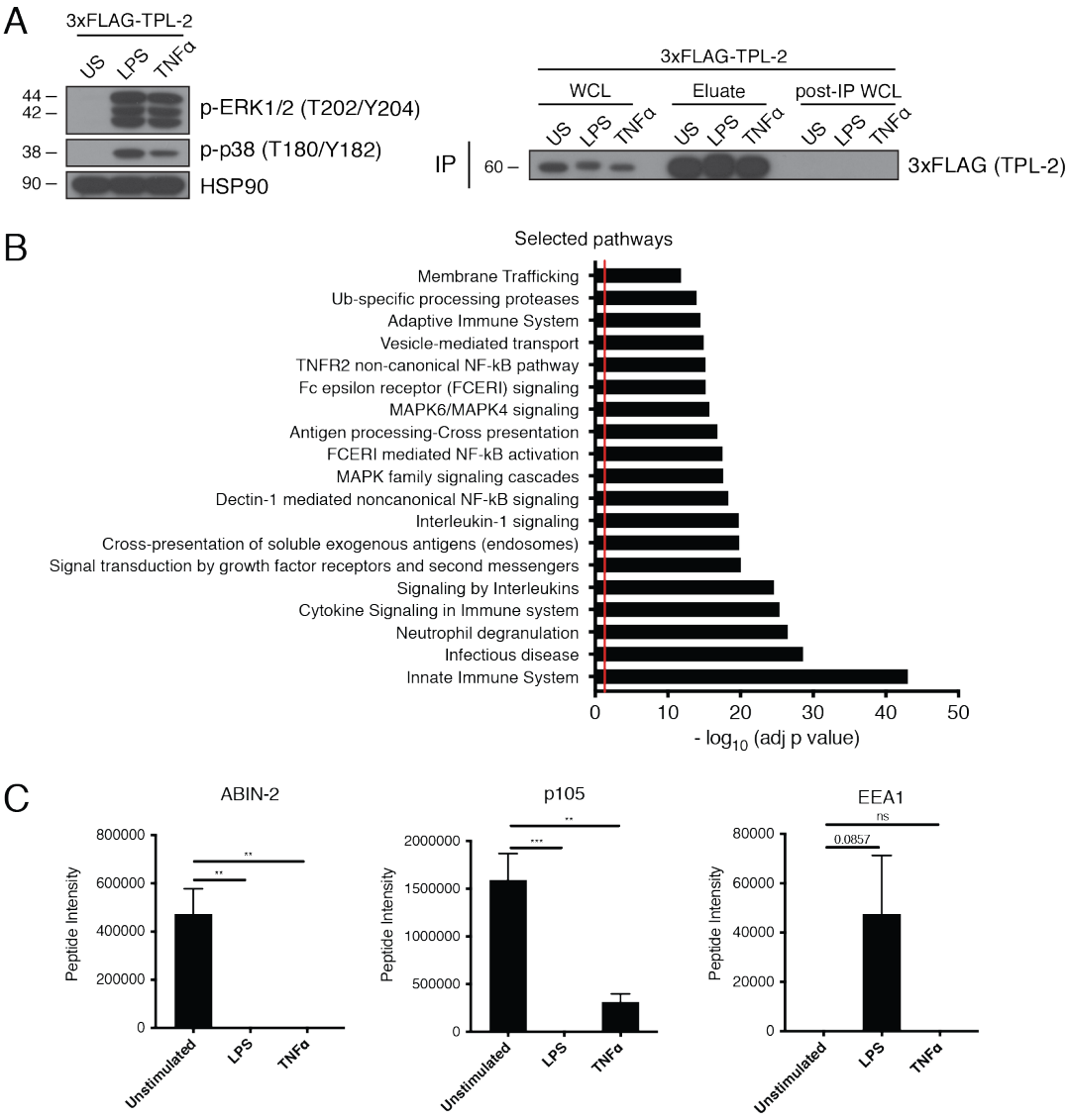

Figure 57 TPL-2 interactome following LPS and TNFα stimulation

BMDMs from *Tpl2*$^{3xFLAG/3xFLAG}$ mice were stimulated with LPS (100 ng/ml) and TNFα (20 ng/ml) for 15 min. 3xFLAG-TPL-2 interactors were immunoprecipitated by incubation of cell extracts with M2 Anti-FLAG Affinity Gel. TPL-2-interacting proteins were identified by label-free immunoprecipitation (IP) mass spectrometry (MS). Three biological replicates were analysed per genotype, *Tpl2*$^{3xFLAG/3xFLAG}$ and WT (n = 3). (**A**) Cell extracts from *Tpl2*$^{3xFLAG/3xFLAG}$ BMDMs were immunoblotted with the antibodies indicated (left). Cell extracts, eluates as well as post-IP cell extracts following immunoprecipitation with M2 Anti-FLAG Affinity Gel were immunoblotted with a 3xFLAG-specific antibody (right). (**B**) Pathway enrichment of TPL-2 interactors that were detected upon LPS stimulation using the Metacore database. 19 selected biological pathways were plotted. -log$_{10}$ of adjusted *P* values are shown. Red line represents *P* = 0.05, where pathways below the red line are statistically non-significant. (**C**) Peptide intensities of selected TPL-2-interacting proteins, ABIN-2, p105 and EEA1, were plotted (n = 3). An unpaired two-tailed t-test was carried out, with ** *P* < 0.01, *** *P* < 0.001, not significant (ns). Error bars represent SEM. IP, immunoprecipitation; US, unstimulated; WCL, whole cell extract; p, phospho.

To confirm inducible binding of TPL-2 to EEA1 following LPS stimulation, I stimulated BMDMs from *Tpl2*$^{3xFLAG/3xFLAG}$ and WT control mice with LPS for 15 min, immunoprecipitated 3xFLAG-TPL-2 and immunoblotted against endogenous EEA1. Firstly, EEA1 protein levels were comparable between WT and *Tpl2*$^{3xFLAG/3xFLAG}$ BMDMs and EEA1 levels were unaffected by LPS stimulation (Figure 58A). As previously described, protein stability of p105, ABIN-2 and 3xFLAG-TPL-2 was reduced following LPS stimulation (Figure 58A). While 3xFLAG-TPL-2 did not interact with endogenous EEA1 in unstimulated BMDMs, EEA1 was recruited to 3xFLAG-TPL-2 following LPS stimulation (Figure 58B). As outlined above, interactions between TPL-2 and p105 as well as ABIN-2 were disrupted following LPS stimulation (Figure 58B).

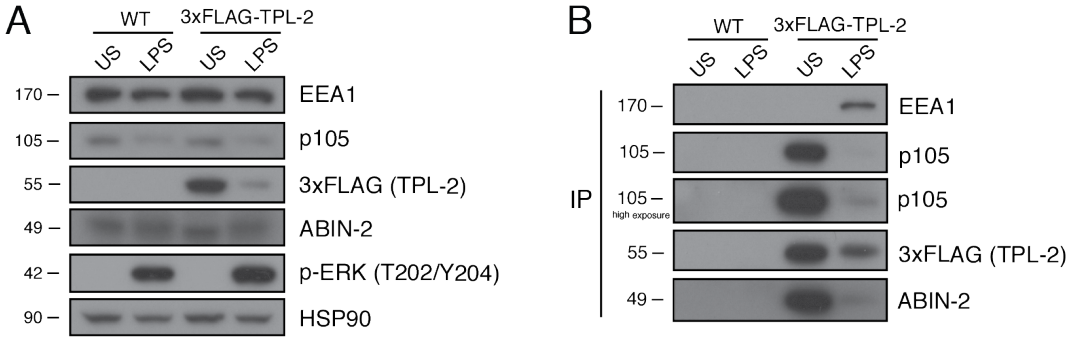

Figure 58 TPL-2 interacts with EEA1 upon LPS stimulation

BMDMs from *Tpl2*$^{3xFLAG/3xFLAG}$ and WT control mice were stimulated with LPS (100 ng/ml) for 15 min. (**A**) Cell extracts were immunoblotted with the antibodies indicated. (**B**) 3xFLAG-TPL-2 interactors were immunoprecipitated by incubation of cell extracts with M2 Anti-FLAG Affinity Gel. Eluates were immunoblotted with the antibodies indicated. US, unstimulated; IP, immunoprecipitation; p, phospho.

4.2.14 ESCRT-I binding to ABIN-2 promotes phagosomal proteolysis

Banks *et al.* discovered that the Y230A mutation in human ABIN-2 disrupts binding to TSG101 of ESCRT-I. I confirmed these results in pulldown assays (Figure 12) and we thus decided to generate a novel mouse strain, *Abin2*$^{Y231A/Y231A}$ mice, in which ABIN-2 is unable to interact with ESCRT-I. As the murine amino acid sequence is shifted by one residue, the human Y230 site is equivalent to Y231 in mice. Since ESCRT-I has been linked to endosome formation, I investigated whether ESCRT-I binding to ABIN-2 regulated phagosome maturation (Lefebvre *et al*, 2018b). Interestingly, *Abin2*^{Y231A} mutation significantly reduced phagosomal proteolysis

relative to WT control BMDMs (Figure 59A). However, phagosomal acidification in *Abin2*$^{Y231A/Y231A}$ BMDMs was normal (Figure 59B). These results indicated that ESCRT-I binding to ABIN-2 regulated phagosome maturation in a similar way as ubiquitin binding. To determine whether TPL-2-dependent MAP kinase signalling was regulated by ABIN-2/TSG101 binding, I stimulated *Abin2*$^{Y231A/Y231A}$ BMDMs with LPS. MAP kinase activation of ERK1/2 and p38α, as well as p105 phosphorylation remained unchanged by *Abin2*^{Y231A} mutation (Figure 59C), consistent with similar experiments with *Abin2*^{D310N} and *Abin2*^{E256K} mutations showing that ABIN-2 did not regulate TPL-2 activation of MAP kinase pathways (Figure 16).

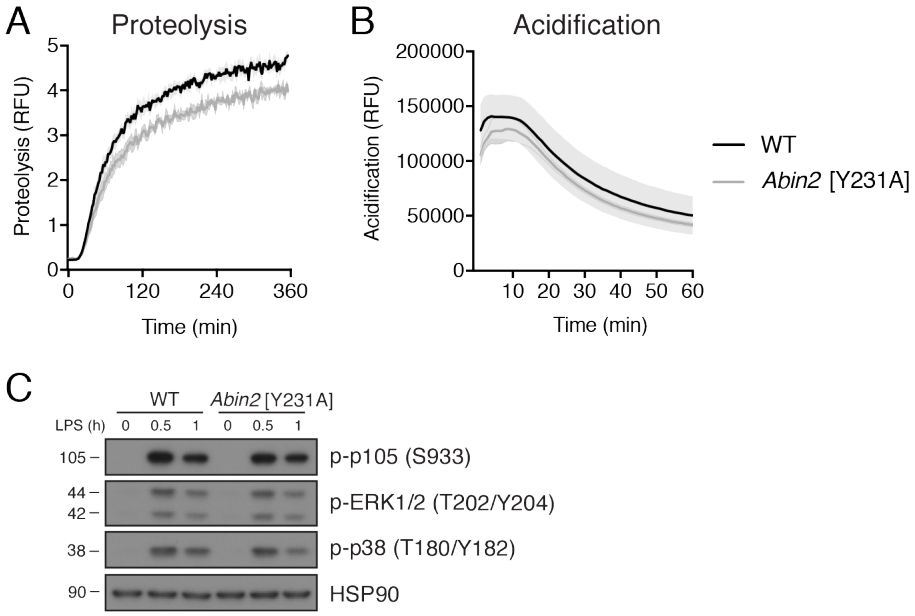

Figure 59 *Abin2*^{Y231A} mutation impairs phagosomal proteolysis while acidification remains unaffected

(**A**) Intra-phagosomal proteolysis in BMDMs of *Abin2*$^{Y231A/Y231A}$ and WT control mice was assayed following uptake of DQ Green BSA / AF594 silica beads (n = 4). (**B**) Intra-phagosomal acidification in BMDMs of *Abin2*$^{Y231A/Y231A}$ and WT control mice was monitored following uptake of BCECF-coupled silica beads (n = 4). (**C**) BMDMs from WT and *Abin2*$^{Y231A/Y231A}$ mice were stimulated with LPS (100ng/ml) for the times indicated and cell extracts were immunoblotted with the antibodies indicated. Shaded areas represent SEM. **** $P < 0.0001$. Paired Mann-Whitney t-test; All differences relative to WT are ****. RFU, relative fluorescence units; p, phospho.

Although ESCRT-I function in endocytosis and autophagy has been studied in detail (Lefebvre *et al*, 2018b; Metcalf & Isaacs, 2010), its role in phagosome maturation in macrophages has not been extensively studied. I therefore knocked down TSG101, the core component of ESCRT-I, in immortalised BMDMs to determine whether

ESCRT-I regulated phagosome maturation in macrophages. TSG101 knockdown dramatically reduced phagosomal proteolysis in iBMDMs relative to control cells, untreated or transfected with a non-targeting siRNA (Figure 60A). Interestingly, TSG101 knockdown did not impair phagosomal acidification (Figure 60B), despite pronounced depletion of TSG101 protein levels (Figure 60C). These findings indicated that TSG101 knockdown phenocopies the effect of *Abin2*^{Y231A} mutation on phagosome maturation.

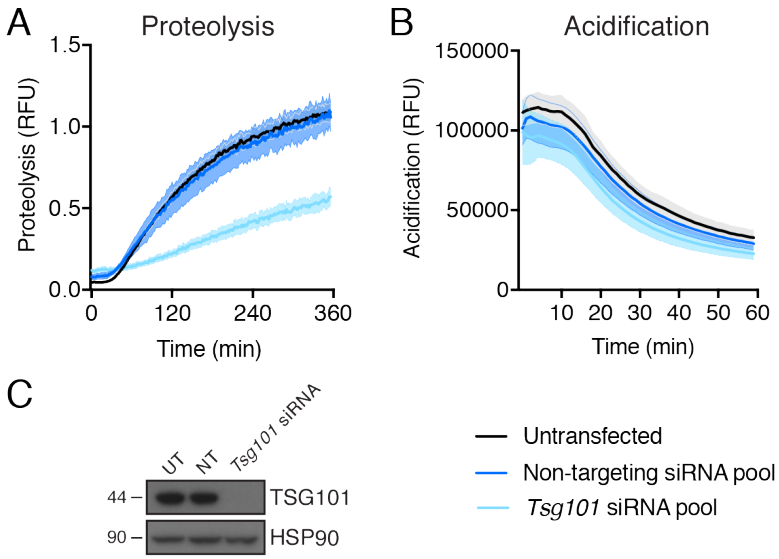

Figure 60 TSG101 knockdown reduces phagosomal proteolysis

Tsg101 was knocked down in WT iBMDMs by RNA interference using a SMARTpool ON-TARGETplus siRNA (50 nM) for 48 h. Transfection of iBMDMs with ON-TARGETplus non-targeting pool (50 nM) for 48 h functioned as siRNA control. (**A**) Intra-phagosomal proteolysis in TSG101 knockdown iBMDMs was assayed following uptake of DQ Green BSA / AF594 silica beads (n = 4). (**B**) Intra-phagosomal acidification in TSG101 knockdown iBMDMs was monitored following uptake of BCECF-coupled silica beads (n = 4). (**C**) Cell extracts from untransfected and *Tsg101* siRNA-transfected iBMDMs were immunoblotted for TSG101 to confirm TSG101 knockdown. Shaded areas represent SEM. **** $P < 0.0001$. Paired Mann-Whitney t-test; All differences relative to WT are ****. RFU, relative fluorescence units; UT, untransfected; NT, non-targeting siRNA pool.

4.3 Conclusion

Defining the molecular mechanisms by which macrophages regulate phagocytosis and phagosome maturation is critical to understand innate immune responses. The data presented in this chapter identified TPL-2 and ABIN-2 as positive regulators of phagosome maturation (Figure 61). Specifically, using loss-of-function point mutations, I showed that TPL-2 kinase activity and ubiquitin binding to ABIN-2 are critical to promote phagosome maturation.

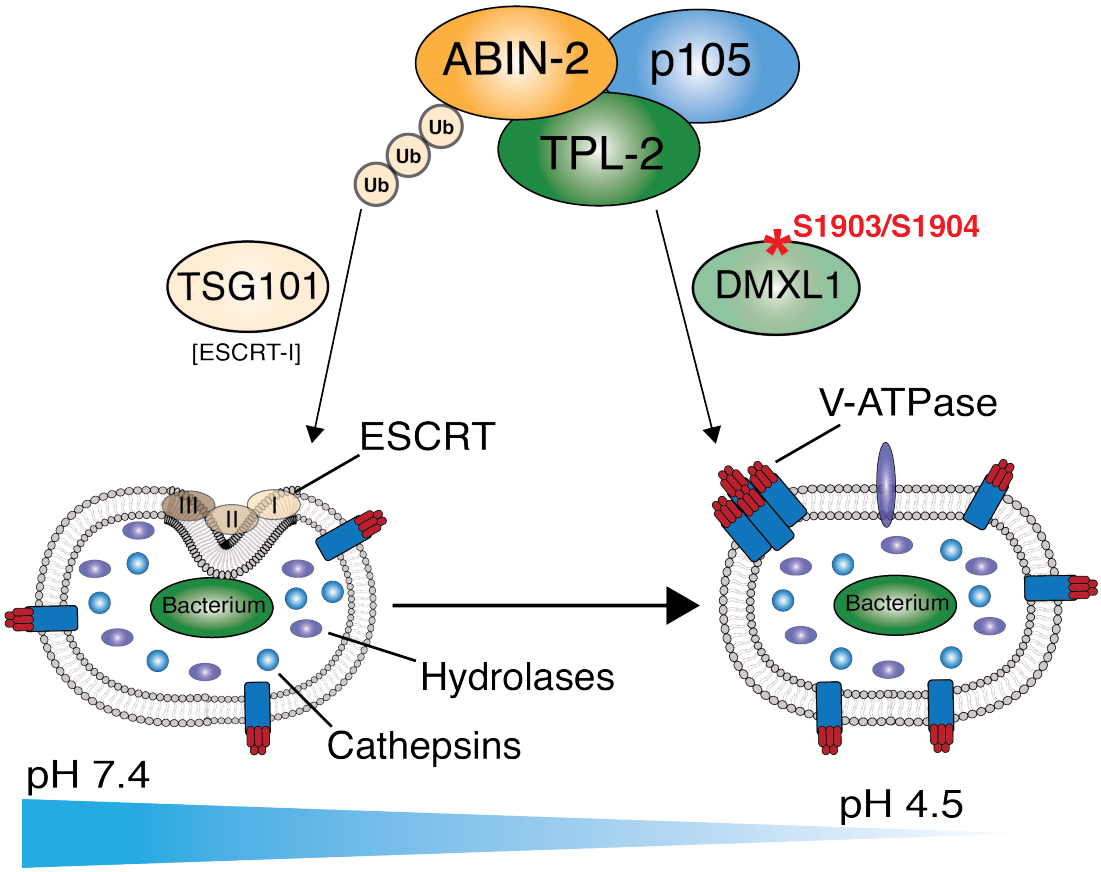

Figure 61 TPL-2 and ABIN-2 promote phagosome maturation in macrophages

Both TPL-2 and ABIN-2 are positive regulators of phagosome maturation, however, findings indicate that TPL-2 and ABIN-2 promote maturation of phagosomes via distinct pathways. TPL-2 catalytic activity promotes phagosomal proteolysis and acidification via phosphorylation of DMXL1, a V-ATPase-interacting protein. TPL-2-mediated phosphorylation of DMXL1 at S1903/1904 promotes phagosome maturation. In contrast, ABIN-2 ubiquitin binding promotes phagosomal proteolysis, but not phagosomal acidification. Ubiquitin binding to ABIN-2 is important for optimal activity of hydrolases, including cathepsin, within maturing phagosomes. Moreover, binding of TSG101, an ESCRT-I protein, to ABIN-2 mediates phagosomal proteolysis.

4.3.1 Bead particles trigger scavenger receptor-mediated phagocytosis

I provided evidence that the initial stage of phagocytosis, phagocytic uptake of particles, was not regulated by TPL-2 or ABIN-2. As phagosome formation at the plasma membrane was not reduced in *Tpl2*$^{D270A/D270A}$ and *Abin2*$^{D310N/D310N}$ macrophages, any downstream defects in phagosome maturation were not simply a consequence of impaired particle internalisation. The silica and latex beads used in biochemical assays in this chapter are non-opsonised particles, which have been extensively used to study phagocytosis as they accurately model the natural physiology of particle-macrophage interactions (Sulahian *et al*, 2008). Similar to microbes that simultaneously interact with several receptors on phagocytes, silica beads associate with multiple scavenger receptors on macrophages to trigger phagocytic uptake (Sulahian *et al*, 2008; Palecanda *et al*, 1999). Silica beads have been shown to interact with macrophage receptor with collagenous structure (MARCO), a class A scavenger receptor on macrophages, to trigger phagocytosis (Palecanda *et al*, 1999). Therefore, it can be assumed that non-opsonised beads used in my experiments were internalised by scavenger receptor-mediated phagocytosis.

4.3.2 ABIN-2 induces phagosome maturation

This thesis provides, for the first time, experimental evidence that M1- and/or K63-linked ubiquitin binding to the UBAN domain in ABIN-2 positively regulates phagosome maturation in macrophages. The initial evidence that ABIN-2 ubiquitin binding promoted phagosome maturation came from an assay monitoring bulk intra-phagosomal proteolysis in macrophages following uptake of fluorescently-labelled silica beads. *Abin2*^{D310N} mutation was found to reduce phagosomal proteolysis and decreased levels of active cathepsin L, a phagosomal protease, following uptake of silica and latex beads, respectively (Yates *et al*, 2005). Moreover, phagosomal proteolysis was also impaired by *Abin2*^{D310N} mutation following uptake of LPS-coated beads. TLR4 activation triggers phagocytosis via a Cdc42-Rac signalling axis, which leads to actin polymerisation and thus formation of the phagocytic cup (Kong & Ge, 2008). Moreover, TLR4 activates the PI3K pathway, which contributes to actin polymerisation and mediates expression of scavenger receptors (Wang *et al*, 2018).

As the mechanism by which LPS-coated beads trigger phagocytosis is different to how uncoated beads mediate internalisation, my results suggested that the role for ABIN-2 in promoting phagosome maturation in macrophages is not exclusive to signalling downstream of a single class of receptor.

I observed that ABIN-2 ubiquitin binding did not regulate phagosomal pH, however, *Abin2*^{D310N} mutation reduced ROS production following phagocytic uptake of latex beads. NOX2, which drives ROS production, is rapidly recruited from vesicles of endosomal and lysosomal compartments to phagosomes following phagocytosis (Savina *et al*, 2006; Jancic *et al*, 2007). Although my findings demonstrated that ABIN-2 induces ROS production independently of any effects on phagosomal acidification, the underlying molecular mechanism by which ABIN-2 ubiquitin binding promotes ROS production remains to be fully understood. Ubiquitin binding to ABIN-2 may be involved in localising NOX2-containing endosomes to maturing phagosomes (Jancic *et al*, 2007).

Analysis of the protein composition of *Abin2*$^{D310N/D310N}$ phagosomes revealed that ABIN-2 reduced abundance of RAB5 on phagosomes. Lys63-linked ubiquitin localises Rabex-5, a RAB5 GEF protein, to phagosomal membranes and ubiquitin binding to Rabex-5 enhances its nucleotide exchange activity, thereby stimulating RAB5 activation on endosomes and early phagosomes (Lauer *et al*, 2019). The ability of ABIN-2 to bind K63-linked chains is likely to be critical as K63-linked polyubiquitin chains are highly abundant on phagosomes (Guo *et al*, 2019). In recent years the importance of ubiquitin in regulating phagosome function and phagosomal signalling has become apparent (Dean *et al*, 2019). ABIN-2 may acts as a phagosomal ubiquitin receptor to recruit K63-linked ubiquitylated proteins, such as Rabex-5, to the phagosome. It is important to note that I did not detect ABIN-2 itself in the phagosome proteome of macrophages following uptake of latex beads. However, it is possible that ABIN-2 only transiently interacts with phagosomes via weak interactions. Future immunofluorescence assays using GFP-tagged ABIN-2 in immortalised macrophages will reveal whether ABIN-2 is localised to phagosomes over the course of the maturation process.

I have demonstrated that TPL-2 catalytic activity drives phagosomal proteolysis and acidification in human monocyte-derived macrophages. To determine whether ubiquitin binding to ABIN-2 also mediates phagosome maturation in human macrophages, using CRISPR/Cas9 gene editing to introduce the *Abin2*^{D309N} point mutation in human-induced pluripotent stem cells and monitoring phagosome maturation will provide further insights.

4.3.3 A role for ABIN-2 in the interplay between ubiquitin and ESCRT during phagosome maturation

Besides demonstrating that ubiquitin binding to ABIN-2 is required to promote phagosome maturation, I provided evidence that ESCRT-I binding to ABIN-2 is required to mediate phagosomal proteolysis following uptake of silica beads. The *Abin2*$^{Y231A/Y231A}$ mouse strain was generated by our laboratory to study the biological relevance of ESCRT-I binding to ABIN-2 and became available towards the final stages of this thesis. Therefore, the number of experiments to investigate the effects of *Abin2*^{Y231A} mutation on phagosome maturation was rather limited and this important question warrants further attention in the future.

Biochemical analyses in chapter three showed that *Abin2*^{Y231A} mutation abrogated TSG101 and ALIX binding. Importantly, knockdown of TSG101 in macrophages phenocopied the effect of *Abin2*^{Y231A} mutation on phagosomal proteolysis, which was consistent with binding of TSG101 to ABIN-2 being critical to induce phagosome maturation. It is important to note that although *Abin2*^{Y231A} mutation significantly reduced phagosomal proteolysis, the magnitude by which *Abin2*^{Y231A} mutation reduced proteolysis was not as pronounced as the effect of *Abin2*^{D310N} mutation. In future research, it will be important to characterise the proteome of latex bead phagosomes isolated from *Abin2*$^{Y231A/Y231A}$ BMDMs to gain molecular insights into the mechanism by which *Abin2*^{Y231A} mutation regulates phagosome proteolysis. It may also be of interest to investigate whether ubiquitin and ESCRT-I binding to ABIN-2 act cooperatively to promote phagosomal proteolysis. To study this, *Abin2*$^{-/-}$ immortalised macrophages will be reconstituted with *Tpl2* and a compound mutant of *Abin2* harbouring both *Abin2*^{Y231A} and *Abin2*^{D310N} mutation.

As phagosomal abundance of the ESCRT-III protein CHMP2B was significantly reduced by *Abin2*^{D310N} mutation, it suggests that an interplay between ubiquitin and ESCRT may exist (Hyung *et al*, 2008; Metcalf & Isaacs, 2010). This hypothesis was supported by the observation that *Abin2*^{D310N} mutation reduced phagosomal levels of PDCD6, which promotes the association of ALIX and TSG101 of the ESCRT-I complex (Okumura *et al*, 2009) and bridges ESCRT-III and ESCRT-I complexes (Tanner *et al*, 2016; Tarabykina *et al*, 2000; Jia *et al*, 2001). ESCRT-0, -I and -II all contain UBDs (Shields & Piper, 2011). In particular, both ESCRT-I and its accessory protein ALIX, which bind to ABIN-2, are ubiquitylated (Chung *et al*, 2008; Sette *et al*, 2010). As previously outlined, ESCRT-0 contains UBDs in its two complex components, namely Hrs and STAM1/2, which allow ESCRT-0 to associate with ubiquitylated cargo-enriched endosomes (Henne *et al*, 2011). These UBDs in ESCRT-0 are essential to recruit ESCRT-I. ABIN-2 may have a similar targeting function to ESCRT-0, whereby ABIN-2 binds to ubiquitylated cargo on phagosomal membranes via its UBAN domain and subsequently recruits ESCRT-I to the phagosomal membrane. To decipher the molecular mechanism by which ABIN-2 regulates ESCRT-I signalling during phagosome maturation, it will be of interest to study the localisation of GFP-tagged ESCRT proteins, including TSG101 and CHMP2B, in WT, *Abin2*$^{D310N/D310N}$ and *Abin2*$^{Y231A/Y231A}$ iBMDMs using confocal microscopy. If ABIN-2 regulated recruitment of ESCRT complexes to phagosomes, co-localisation of GFP-tagged ESCRT proteins with phagosomal markers, including EEA1 and LAMP1, will be disrupted by ABIN-2 point mutations.

4.3.4 How does ABIN-2 regulate phagosome maturation?

Loss of ubiquitin binding significantly reduced protein levels of all five core proteins of the AP2 complex, as well as abundance of five AP2 complex accessory proteins, including AGFG2, EPS15L1, ITSN2, ARRB2 and PICALM. The AP2 complex has been extensively studied in the context of clathrin-mediated endocytosis, whereby assembly of the AP2 complex is required for progression of the endocytic pathway (Mettlen *et al*, 2018; Sanger *et al*, 2019). *Abin2*^{D310N} mutation also decreased phagosomal levels of several sorting nexins, including SNX3, SNX12, SNX16,

SNX17, SNX27 and SNX29. The AP2 complex promotes phagosomal association of sorting nexins and dynamin, thereby inducing phagosome maturation following uptake of apoptotic cells in *Caenorhabditis elegans* (Chen *et al*, 2013). Ubiquitylation plays an important role in sorting cargo for AP2-mediated transport (Traub & Lukacs, 2007). Epidermal growth factor receptor substrate 15-like 1, EPS15L1, contains UBDs and recognises endocytic sorting signals, thereby linking ubiquitylated cargo to the clathrin-dependent endocytic pathways that are mediated by the AP2 complex (Traub & Lukacs, 2007). These observations raise the possibility that ABIN-2 may function as a receptor to target ubiquitylated cargo for AP2-mediated transport to the phagosomal membrane. Therefore, loss of ABIN-2 ubiquitin binding may result in reduced AP2 and AP2 accessory proteins as well as decreased abundance of sorting nexins.

To investigate this potential role and to further understand how ABIN-2 regulates phagosome maturation, characterisation of the ABIN-2 interactome will provide further insight. Our laboratory has recently generated *Abin2*$^{StrepII/StrepII}$ mice. Pulldowns of StrepII-ABIN-2 from *Abin2*$^{StrepII/StrepII}$ BMDMs following uptake of latex beads and subsequent MS analysis will identify ABIN-2-interacting proteins. Identification of AP2 proteins and sorting nexins would strengthen the speculative hypothesis that ABIN-2 promotes AP2-mediated transport of ubiquitylated cargo to phagosomes.

4.3.5 TPL-2 stimulates phagosome maturation

The regulation of MAP kinase signalling in macrophages by TPL-2 during the innate immune response has been extensively studied (Gantke *et al*, 2012). TPL-2 is critical for the activation of ERK1/2 MAP kinases via MEK1/2 downstream of several TLRs, including TLR4 (Banerjee *et al*, 2006). TPL-2 also activates p38 MAP kinases via MEK3 and MEK6 (Senger *et al*, 2017; Pattison *et al*, 2016). Importantly, TPL-2 induces production of TNF in an IKK-independent manner, which suggests that TPL-2 activates additional, yet unknown, downstream targets besides MAP 2-kinases during innate immune responses in macrophages (Yang *et al*, 2012; Pattison *et al*, 2016).

In this chapter, using pharmacological and genetic approaches, I demonstrated that TPL-2 kinase activity induced phagosome maturation. More specifically, I showed that TPL-2 catalytic activity drives phagosome proteolysis and acidification upon phagocytic uptake of silica beads. TPL-2 also promoted phagosomal proteolysis and acidification following the uptake of LPS-coated beads. TLR4 activation contributes to phagocytosis via a Cdc42-Rac signalling axis, which leads to actin polymerisation and thus formation of the phagocytic cup (Kong & Ge, 2008). Moreover, TLR4 activates the PI3K pathway, which regulates actin polymerisation and mediates expression of scavenger receptors (Wang *et al*, 2018). Although TLR4 is not a classical phagocytic receptor, TLR4 regulates the rate of phagocytosis by accelerating phagosome maturation in macrophages (Blander & Medzhitov, 2004; Dill *et al*, 2015). TLR4 deficiency impairs maturation of *E. coli*-containing phagosomes in macrophages (Blander & Medzhitov, 2004). My findings suggested that the role for TPL-2 in stimulating phagosome proteolysis and acidification in macrophages is also important when TLR4 contributes to the induction of phagosome maturation.

4.3.6 TPL-2 induces DMXL1 phosphorylation to induce phagosome acidification

Importantly, I provided pharmacological and genetic evidence that TPL-2 catalytic activity drives phagosome maturation, both proteolysis and acidification, independently of MAP kinase activation. The identification of this novel, MAP kinase-independent, pathway downstream of TPL-2 implied that yet uncharacterised non-MAP 2-kinase substrates for TPL-2 exist in macrophages.

Analysis of the phosphoproteome following phagocytic uptake of latex beads identified that TPL-2 kinase activity was required for phosphorylation of DMXL1 at S1903 and S1904. Recent studies identified DMXL1 as a V-ATPase-interacting protein, which promotes V-ATPase-mediated acidification of vesicles in a kidney cell line (Merkulova *et al*, 2015). RNAi knockdown experiments presented herein indicated that DMXL1 induces phagosomal proteolysis and acidification in

macrophages following phagocytic uptake of latex beads. Impaired phagosomal acidification in DMXL1-deficient macrophages was rescued by expression of a DMXL1 fragment that contained the S1903/S1904 phosphorylation sites. These findings suggested that TPL-2-dependent DMXL1 phosphorylation at S1903 and S1904 mediates V-ATPase-induced phagosomal acidification. Since DMXL1 phosphorylation at S1903 by TPL-2 was induced following internalisation of latex beads, it suggests that scavenger receptors (Sulahian *et al*, 2008) trigger TPL-2-dependent DMXL1 phosphorylation during phagocytosis. Whether TPL-2 directly phosphorylates DMXL1 or indirectly promotes DMXL1 phosphorylation via a yet unknown downstream protein kinase remains to be elucidated. The phosphorylation sequence at S1903 does not share similarities with the proline-directed kinase motif targeted by MAP kinases, which is consistent with my observations (Roux & Blenis, 2004). The target sequence at S1903 suggests involvement of AMP-activated protein kinases, cyclic AMP-activated protein kinase or protein kinase C, however, further biochemical analyses will be essential to consolidate whether any of these kinases, TPL-2 itself or another protein kinase phosphorylates DMXL1 at S1903 during phagosome maturation in a TPL-2-dependent manner.

The multimeric V-ATPase complex consists of two distinct protein subcomplexes. The peripheral membrane subcomplex, called V_1 complex, is responsible for ATP hydrolysis, while the integral membrane subcomplex, called V_0 complex, forms the proton pore in the phagosomal membrane (Beyenbach & Wieczorek, 2006). The V-ATPase complex is regulated by the reversible association of V_0 and V_1 subcomplexes, whereby release of V_1 into the cytosol prevents V-ATPase-mediated proton transport (Parra & Kane, 1998). Notably, DMXL1 has a homologue called DMXL2 (also known as Rabconnectin-3), which interacts with the cytosolic V_1 subcomplex of the V-ATPase and promotes its association with the membrane-anchored V_0 subcomplex to form a catalytically active V_0 / V_1 V-ATPase complex (Nagano *et al*, 2002; Sethi *et al*, 2010). My knockdown experiments in iBMDMs showed that DMXL1, but not DMXL2, regulates phagosome maturation following bead internalisation. However, given the structural similarity between DMXL1 and DMXL2, it is likely that DMXL1 also regulates V-ATPase assembly. My findings raise the possibility that TPL-2 catalytic activity induces phagosome acidification in macrophages by promoting V-ATPase assembly via phosphorylation of DMXL1. To

experimentally address this hypothesis, V_0- and V_1-specific antibodies will be used in pulldown experiments to test whether DMXL1 phosphorylation mediates the assembly of V_0 / V_1 V-ATPase subcomplexes to form a catalytically active V-ATPase complex. As *Nfkb1*^{SSAA} mutation did not impair phagosome maturation, TPL-2 may drive DMXL1 phosphorylation while complexed with ABIN-2 and NF-κB1 p105 (Pattison *et al*, 2016; Yang *et al*, 2012). However, it remains possible that phosphorylation sites in p105 other than S930 and S935, which are phosphorylated by the IKK complex, induce p105 degradation following internalisation of latex beads, thereby releasing TPL-2 from the ternary complex to phosphorylate DMXL1.

4.3.7 Endosomal activation of AKT signalling by TPL-2 promotes phagosome maturation

Analysis of the phosphoproteome following phagocytic uptake of LPS-coated latex beads demonstrated that TPL-2 kinase activity was required for phosphorylation of several proteins involved in AKT signalling. Importantly, I observed TPL-2-dependent activation of the PI3K-AKT-mTOR signalling axis following macrophage uptake of LPS-coated beads, but not following macrophage stimulation with soluble LPS. Since PI3K-AKT-mTOR pathway activation by TPL-2 was induced following internalisation of LPS-coated latex beads, this suggests that internalised TLR4 triggers TPL-2-dependent AKT activation from phagosomes following phagocytic uptake (Zanoni *et al*, 2011).

The PI3K-AKT signalling axis has been extensively studied and critical roles for PI3K and AKT have been described in regulating Rab GTPases and phagosomal acidification during phagosome maturation (Thi & Reiner, 2012). VPS34 PI3K has been shown to regulate the RAB5 GTPase by acting as a GAP to mediate RAB5 dissociation from early phagosomes to promote phagosome maturation (Vieira *et al*, 2003b; Chamberlain *et al*, 2004). Moreover, VPS34 PI3K is a critical RAB5 effector, generating PI(3)P to recruit EEA1 to early phagosomes (Araki *et al*, 1996; Vieira *et al*, 2001). Besides driving maturation of early phagosomes, PI3K also induces maturation of late phagosomes by targeting HOPS and SNARE complexes to the phagosomal membrane (Thi & Reiner, 2012). PI3K-AKT signalling is known to

promote vesicle acidification. In epithelial cells active AKT directly binds to subunit E of the V_1 subcomplex of the V-ATPase complex and drives V-ATPase-dependent endosomal acidification during rotavirus infection (Soliman *et al*, 2018). Although the molecular mechanism has not been fully elucidated, association of active AKT with the V_1 subcomplex presumably mediates interaction with the V_0 subcomplex to form an active V-ATPase (Soliman *et al*, 2018). In dendritic cells, V-ATPase assembly and activity are also regulated by PI3K-AKT-mTOR signalling (Liberman *et al*, 2014). During influenza infection, acidification of endosomes is essential for the viral life cycle as low pH accelerates the fusion of the viral coat with the endosomal membrane, thereby facilitating entry of viral nucleic acids into the host cell (Kohio & Adamson, 2013; Marjuki *et al*, 2011; Ochiai *et al*, 1995). Studies have shown that increased endosomal acidification during viral infection in epithelial cells, which is a prerequisite for viral fusion, is PI3K-dependent (Marjuki *et al*, 2011).

I demonstrated the importance of AKT in phagosome maturation (proteolysis and acidification) by siRNA-mediated depletion of AKT protein levels in iBMDMs and pharmacological inhibition of AKT and mTOR in BMDMs. Blocking AKT signalling phenocopied the effect of *Tpl2*^{D270A} mutation in macrophages. Previous studies showed that the PI3K complex is recruited to TLR4 upon stimulation and it is, therefore, possible that TPL-2 activates PI3K signalling at the receptor (Laird *et al*, 2009). While López-Peláez *et al*. have previously suggested that TPL-2 activates PI3K-AKT signalling following stimulation with soluble LPS, findings presented here strongly suggest that TPL-2 catalytic activity only regulates AKT from endosomes following phagocytic uptake of LPS-coated beads (López-Peláez *et al*, 2011).
Here I showed that phagosomal acidification following uptake of LPS-coated latex beads by macrophages was induced by AKT-mTOR signalling. While LPS-coated beads strongly activated AKT signalling, immunoblotting indicated that uncoated latex beads only minimally induced activation of the AKT pathway. These findings, therefore, suggest that phagosome maturation downstream of TLR-mediated phagocytosis following uptake of LPS-coated latex beads may be regulated differently to scavenger receptor-mediated phagocytosis that results from internalisation of uncoated latex beads. However, the possibility remains that low levels of AKT activation induced by uncoated latex beads may be sufficient to promote phagosome maturation. Importantly, analyses implied that TPL-2-

dependent AKT activation following uptake of LPS-coated beads was involved in inducing both early (proteolysis) and late (acidification) stages of phagosome maturation.

In this chapter, I provided evidence that TPL-2 catalytic activity promotes phagosome maturation via DMXL1 and AKT signalling. Further experiments will be needed to determine whether TPL-2 regulates two distinct signalling pathways controlling phagosome maturation, or whether DMXL1 and AKT are part of the same signalling pathway. More specifically, it will be essential to study whether pharmacological inhibition of AKT activity impairs DMXL1 phosphorylation at S1903 following uptake of uncoated or LPS-coated latex beads. Since both DMXL1 and AKT directly associate with the V-ATPase complex, AKT may directly phosphorylate DMXL1 on phagosomes (Merkulova *et al*, 2015; Soliman *et al*, 2018).

4.3.8 Endosomal activation of type I interferon expression

In addition to its stimulatory effects on phagosome maturation, TPL-2 suppressed mRNA expression of multiple type I IFN genes following incubation of macrophages with LPS-coated beads, including *Ifna1*, *Ifna2*, *Ifna5* and *Ifna6*. TPL-2 catalytic activity suppressed *Ifnb1* mRNA expression in response to both soluble LPS (Dr Michael Pattison, unpublished findings) and LPS-coated beads. However, transcriptomic analyses by Dr Michael Pattison demonstrated that TPL-2 does not regulate *Ifna* genes following stimulation with soluble LPS. Together these results suggested that TPL-2 catalytic activity only inhibits the expression of *Ifna* genes induced by endosomal TLR4 signalling (Zanoni *et al*, 2011) and not by TLR4 signalling from the plasma membrane. Previous studies have shown that TRAM-TRIF-dependent signalling downstream of endosomal TLR4 is critical in regulating the expression of type I interferons (Kagan *et al*, 2008b). It will be interesting in future studies to determine whether TPL-2 regulates *Ifna* gene expression via modulation of TRAM-TRIF-mediated signalling.

TPL-2 inhibition of type I IFN gene expression, including IFNα, is important for effective innate immune responses in mice to *Listeria monocytogenes* and

Mycobacteria tuberculosis (McNab *et al*, 2013; Mielke *et al*, 2009). Findings in this chapter propose, for the first time, that TPL-2 plays an important role in suppressing TLR4-induced IFNα production from endosomal compartments. Additional experiments in chapter five further investigate the role of TPL-2 in regulating *Ifna* expression following bacterial infection of macrophages.

Chapter 5. TPL-2 and ABIN-2 promote killing of Gram-positive and Gram-negative bacteria

5.1 Introduction

Phagosome maturation in macrophages is essential for killing of internalised bacteria and is an indispensable early process in innate immune responses (Kinchen & Ravichandran, 2008). In this thesis, I have established that TPL-2 kinase activity and ABIN-2 ubiquitin binding promote phagosome maturation in primary macrophages. Therefore, I decided to investigate whether TPL-2 and ABIN-2 promote killing of bacteria in macrophages upon infection.

Previous studies have shown that TPL-2 is required for efficient innate immune responses to several bacterial species, including *C. rodentium*, *L. monocytogenes* and *M. tuberculosis* (Acuff *et al*, 2017b, 2017a; McNab *et al*, 2013; Mielke *et al*, 2009). To date, the importance of TPL-2 in promoting bacterial clearance has largely been attributed to its ability to regulate gene expression. TPL-2 deficiency has been shown to impair neutrophil killing of *C. rodentium* but the underlying mechanism for this defect is not known. The analysis of *Tpl2*$^{-/-}$ mice in these studies also did not distinguish between the effects of TPL-2 and/or ABIN-2 deficiency. My results with latex beads raised the possibility that TPL-2 expression might regulate innate immune responses by promoting phagosome maturation in macrophages due to inhibition of TPL-2 and/or ABIN-2 signalling.

I investigated the regulation of bacterial killing in macrophages by TPL-2 and ABIN-2 using Gram-negative and Gram-positive bacterial species since TPL-2 has previously been implicated in regulating innate immunity in response to both classes of bacteria. In addition, I aimed at studying the immune function of TPL-2 and ABIN-2 during infection of both extracellular and intracellular bacteria since microbes belonging to the two categories differentially regulate the host immune response. More specifically, extracellular bacteria frequently attempt to block phagocytic uptake by immune cells or kill phagocytes prior to engulfment (Kaufmann & Dorhoi, 2016). In contrast, intracellular bacteria are efficiently phagocytosed but have evolved

complex mechanisms to block phagosome maturation and intracellular killing. The distinct phagocyte-bacteria interactions between bacterial species raised the possibility that the requirements for TPL-2 and ABIN-2 in macrophage killing of microbes might differ for distinct bacterial species.

5.2 Results

5.2.1 TPL-2 and ABIN-2 promote macrophage killing of *Escherichia coli*

To investigate whether TPL-2 and ABIN-2 promote killing of Gram-negative extracellular *E. coli* in primary macrophages, I infected BMDMs with GFP-labelled *E. coli*. Phagocytic uptake of *E. coli* into BMDMs in *Tpl2*$^{D270A/D270A}$ and *Abin2*$^{D310N/D310N}$ BMDMs was similar to WT control cells (Figure 62A). Notably, both *Tpl2*^{D270A} and *Abin2*^{D310N} mutation significantly increased bacterial burden of *E. coli* in BMDMs 0.5 h post-infection (Figure 62B). Importantly, the degree by which *Tpl2*^{D270A} and *Abin2*^{D310N} mutation impaired bacterial killing of *E. coli* was comparable to that detected by pre-treatment of WT BMDMs with the V-ATPase inhibitor bafilomycin A1 (Figure 62B), which has pronounced inhibitory effects on phagosome maturation (Bidani *et al*, 2000; Yoshimori *et al*, 1991).

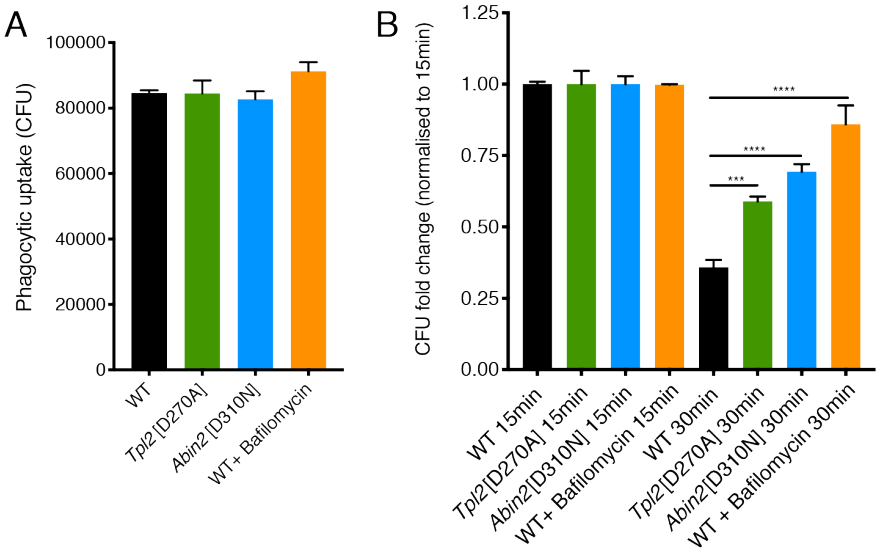

Figure 62 *Tpl2*^{D270A} and *Abin2*^{D310N} mutation impair macrophage killing of *E. coli*

BMDMs of the indicated genotypes were infected with GFP-*E. coli* (MOI 10) for 15 min. As a control, WT cells were pre-treated with 1 µM bafilomycin A1 for 0.5 h to block acidification of phagosomes. Two biological replicates were analysed per

genotype, each biological replicate was seeded in triplicates and plated in duplicates, thus providing 12 measurements per condition. (**A**) Phagocytic uptake (CFU) of GFP-labelled *E. coli* into BMDMs of indicated genotypes 15 min post-infection (n = 12). (**B**) *E. coli* CFU were assessed at 0.5 h after infection and normalised to CFU at 15 min (n = 12). Data were analysed by a one-way ANOVA. Error bars represent SEM. *** $P < 0.001$, **** $P < 0.0001$.

5.2.2 TPL-2 promotes macrophage killing of *Citrobacter rodentium*

C. rodentium is a Gram-negative mouse-restricted pathogen of extracellular nature (Collins *et al*, 2014). During infection, *C. rodentium* colonises the intestinal mucosa, where it causes the formation of attaching and effacing (A/E) lesions (Deng *et al*, 2003). *C. rodentium* infection is widely used as a mouse model to investigate human intestinal diseases, including ulcerative colitis and Crohn's disease (Higgins *et al*, 1999; Collins *et al*, 2014).

TPL-2 is required for optimal clearance of *C. rodentium* (Acuff *et al*, 2017b, 2017a). Studies showed that $Tpl2^{-/-}$ mice infected with *C. rodentium* experience increased bacterial burden, however, since $Tpl2^{-/-}$ mice are deficient in both TPL-2 and ABIN-2, I investigated whether the increased bacterial burden in $Tpl2^{-/-}$ mice was indeed due to the lack of TPL-2 signalling, a consequence of ABIN-2 deficiency or both.

BMDMs were infected with GFP-labelled *C. rodentium*. In line with results obtained using *E. coli*, phagocytic uptake of *C. rodentium* into BMDMs was not disrupted in $Tpl2^{D270A/D270A}$ and $Abin2^{D310N/D310N}$ BMDMs (Figure 63A). However, $Tpl2^{D270A}$ mutation significantly reduced killing of *C. rodentium* 1 h, 2 h and 3 h post-infection to a similar degree as pre-treatment of WT BMDMs with bafilomycin A1 (Figure 63B). Interestingly, bacterial killing in $Abin2^{D310N/D310N}$ BMDMs at all time points was normal compared to WT cells (Figure 63B). These observations suggested that TPL-2 catalytic activity, but not ABIN-2 ubiquitin binding, was required for efficient killing of *C. rodentium*.

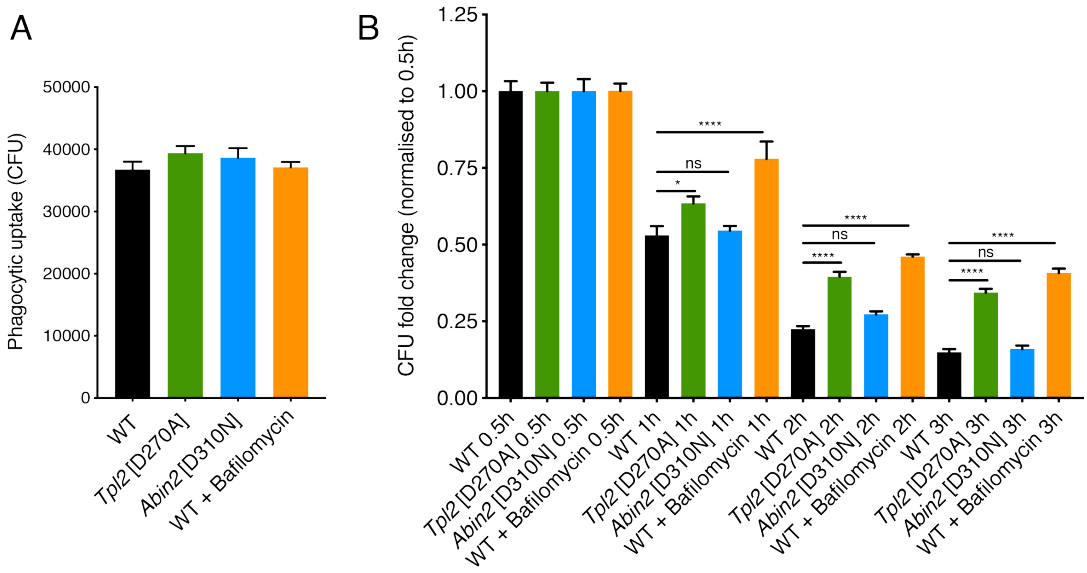

Figure 63 *Tpl2*^{D270A} mutation impairs macrophage killing of *C. rodentium*

BMDMs of the indicated genotypes were infected with GFP-*C. rodentium* (MOI 2) for 0.5 h. As a control, WT cells were pre-treated with 1 μM bafilomycin A1 for 0.5 h to block acidification of phagosomes. Two biological replicates were analysed per genotype, each biological replicate was seeded in triplicates and plated in duplicates, thus providing 12 measurements per condition. (**A**) Phagocytic uptake (CFU) of GFP-labelled *C. rodentium* into BMDMs of indicated genotypes 0.5 h post-infection (n = 12). (**B**) *C. rodentium* CFU were assessed at 1 h, 2 h and 3 h after infection and normalised to CFU at 0.5 h (n = 12). Data were analysed by a one-way ANOVA. Error bars represent SEM. * $P < 0.05$, **** $P < 0.0001$, not significant (ns).

To investigate whether reduced bacterial killing in *Tpl2*$^{D270A/D270A}$ BMDMs was due to a block in phagosome maturation, I assayed phagosomal acidification following *C. rodentium* infection. *Tpl2*$^{D270A/D270A}$ and *Abin2*$^{D310N/D310N}$ BMDMs were infected with GFP-*C. rodentium* and stained with LysoTracker Red (Figure 64A). *Tpl2*^{D270} mutation significantly reduced the percentage of LysoTracker Red^{+} phagosomes containing GFP-*C. rodentium*, whereas LysoTracker Red staining in infected *Abin2*$^{D310N/D310N}$ BMDMs was comparable to WT cells (Figure 64A and B). These findings suggested that TPL-2 drives *C. rodentium* clearance by promoting phagosome acidification.

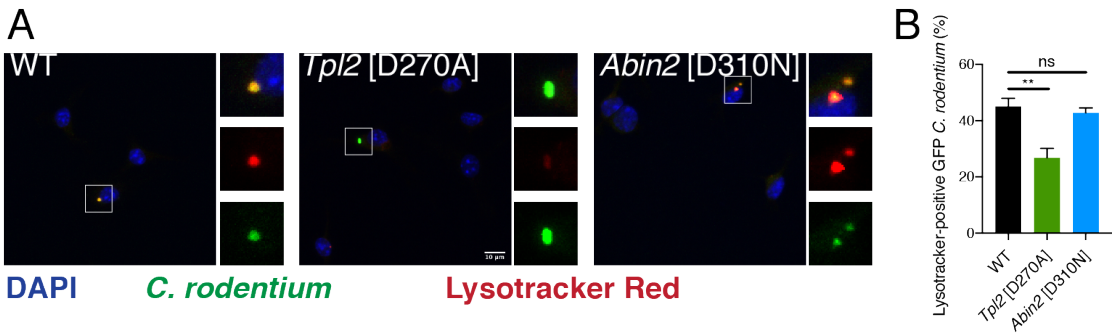

Figure 64 *Tpl2*^{D270A} mutation impairs acidification of *C. rodentium* phagosomes

BMDMs of the indicated genotypes were infected with GFP-*C. rodentium* (MOI 2) for 0.5 h. (**A-B**) pH assay in WT, *Tpl2*$^{D270A/D270A}$ and *Abin2*$^{D310N/D310N}$ BMDMs 0.5 h after infection with GFP-*C. rodentium*. BMDMs were stained with the LysoTracker Red DND-99 dye at a final concentration of 100nM for 1 h (red). Fluorescence of LysoTracker Red was monitored at ex/em 577/590 nm. (**B**) Quantification of LysoTracker Red co-localisation with GFP-*C. rodentium* from panel (A) (n = 12). Data were analysed by an Unpaired t-test. Error bars represent SEM. ** $P < 0.01$, not significant (ns).

5.2.3 TPL-2 and ABIN-2 promote macrophage killing of *Staphylococcus aureus*

I next investigated whether TPL-2 and ABIN-2 regulate phagosome maturation following *S. aureus* infection. *S. aureus* is a Gram-positive extracellular bacterium, which is pathogenic in humans and has wide-ranging implications in disease (Hassoun *et al*, 2017). Firstly, WT BMDMs were infected with YFP-labelled *S. aureus* and analysed by flow cytometry to confirm efficient infection of primary macrophages with bacteria. Within one hour of infection, 26% of BMDMs were infected with YFP-*S. aureus* and infection rates further increased to 56% within 2 h and 3 h post-infection, respectively (Figure 65). This observation confirmed that an MOI of 10 was appropriate to further study the function of TPL-2 and ABIN-2 in the context of *S. aureus* infection.

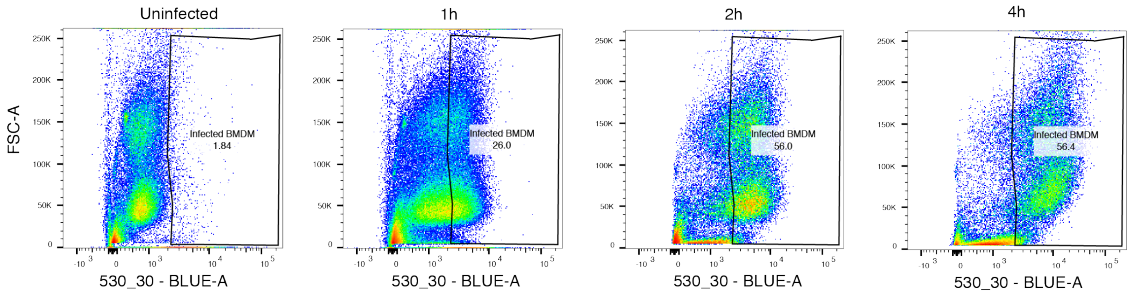

Figure 65 Infection of primary macrophages with YFP-labelled *S. aureus*

BMDMs from WT mice were infected with YFP-*S. aureus* (MOI 10) for the times indicated. Cells were harvested, analysed by flow cytometry and infection efficiencies were quantified. BMDMs were gated according to fluorescence at 530 nm, the optimal emission wavelength of YFP. YFP^{high} BMDMs were selected to calculate infection rates.

Initial experiments established the optimal time point for CFU assays. I infected BMDMs from WT mice with YFP-*S. aureus* for 8 h and 24 h, respectively. BMDMs cleared approximately 50% of internalised bacteria 8 h post-infection while <10% of bacteria remained by 24h. Consequently, I selected the 8 h time point for subsequent CFU measurements following *S. aureus* infections (Figure 66C).

To study whether TPL-2 and ABIN-2 regulated *S. aureus* clearance, I infected BMDMs from WT, *Tpl2*$^{D270A/D270A}$, *Abin2*$^{D310N/D310N}$ and *Abin2*$^{E256K/E256K}$ mice with YFP-labelled *S. aureus*. Phagocytic uptake of *S. aureus* into BMDMs was similar in *Tpl2*$^{D270A/D270A}$, *Abin2*$^{D310N/D310N}$ and *Abin2*$^{E256K/E256K}$ BMDMs relative to WT control cells (Figure 66A). However, both *Tpl2*^{D270A} and *Abin2*^{D310N} mutation significantly impaired bacterial killing of *S. aureus* in BMDMs 8 h post-infection (Figure 66D). It is important to note that the degree by which *Tpl2*^{D270A} and *Abin2*^{D310N} mutation impaired *S. aureus* clearance was similar to that detected by bafilomycin A1 pre-treatment of WT cells, suggesting that the inhibitory effects of these mutations are likely to be physiologically relevant *in vivo* (Figure 66D). *S. aureus* bacteria were killed in *Abin2*$^{E256K/E256K}$ BMDMs similar to WT cells, indicating that A20 binding to ABIN-2 was not involved in regulating *S. aureus* killing (Figure 66E). Consistent with CFU assays, the fluorescence intensity of YFP^{+} *S. aureus* per cell was significantly higher in *Tpl2*$^{D270A/D270A}$ and *Abin2*$^{D310N/D310N}$ BMDMs compared to WT controls (Figure 66F).

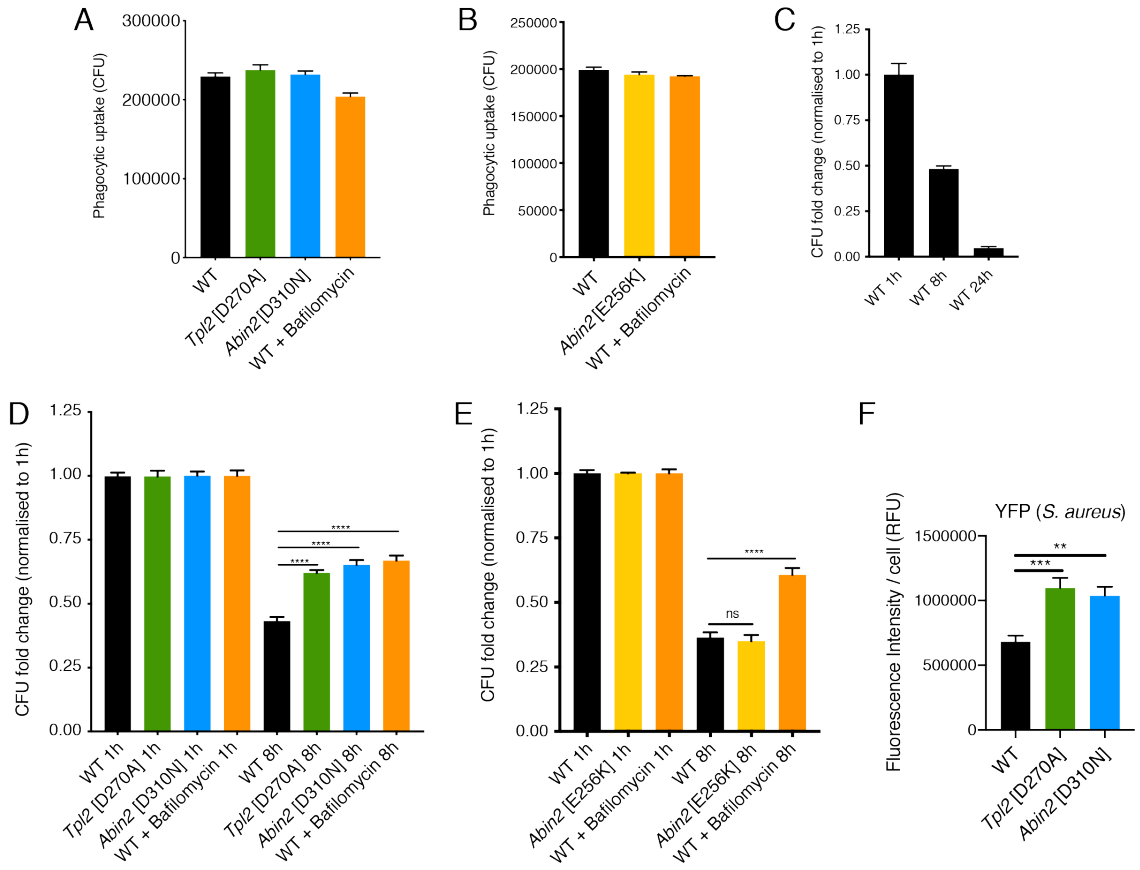

Figure 66 *Tpl2*^{D270A} and *Abin2*^{D310N} mutation impair macrophage killing of *S. aureus*

BMDMs of the indicated genotypes were infected with YFP-*S. aureus* (MOI 10) for 0.5 h. As a control, WT cells were pre-treated with 1 µM bafilomycin A1 for 0.5 h to block acidification of phagosomes. Two biological replicates were analysed per genotype, each biological replicate was seeded in triplicates and plated in duplicates, thus providing 12 measurements per condition. (**A-B**) Phagocytic uptake (CFU) of YFP-labelled *S. aureus* into BMDMs of the indicated genotypes 1 h post-infection (n = 12). (**C-E**) *S. aureus* CFU were assessed at 8 h or 24 h after infection and normalised to CFU at 1 h (n = 12). (**F**) BMDMs of the indicated genotypes were infected with YFP-*S. aureus* (MOI 10) for 1 h and analysed by confocal microscopy. Quantification of YFP-*S. aureus* average fluorescence intensity per cell (n = 66-85). Data were analysed by a one-way ANOVA. Error bars represent SEM. ** $P < 0.01$, *** $P < 0.001$, **** $P < 0.0001$, not significant (ns).

5.2.3.1 S. aureus infection induces pyroptosis of macrophages independently of TPL-2 and ABIN-2

Bafilomycin A1 has substantial inhibitory effects on phagosome maturation by blocking acidification and proteolytic activation (Yamamoto *et al*, 1998; Ip *et al*, 2010), however bafilomycin A1 pre-treatment only partially reduced bacterial clearance by BMDMs. This suggested that BMDMs employed a phagosome-independent

mechanism to kill internalised *S. aureus*. This killing mechanism was likely due to the escape of *S. aureus* bacteria from phagosomes or by injection of pore-forming toxins into the cytosol, which in turn activates the inflammasome and induces pyroptosis (Seilie & Wardenburg, 2017). I therefore analysed cytosolic lactate dehydrogenase (LDH) levels upon *S. aureus* infection as a readout for pyroptotic cell death. *S. aureus* infection decreased BMDM viability, however, this was unaltered by *Tpl2*^{D270A} or *Abin2*^{D310N} mutation, as indicated by comparable levels of released LDH at 8 h and 24 h post *S. aureus* infection (Figure 67A). Moreover, immunoblotting against the gasdermin D p30 proteolytic fragment indicated that *S. aureus* infection induced similar levels of pyroptosis in WT, *Tpl2*$^{D270A/D270A}$ and *Abin2*$^{D310N/D310N}$ BMDMs (Figure 67B). These findings suggested that *S. aureus*-induced pyroptosis as alternative macrophage killing mechanism was mediated independently of TPL-2 catalytic activity and ABIN-2 ubiquitin binding.

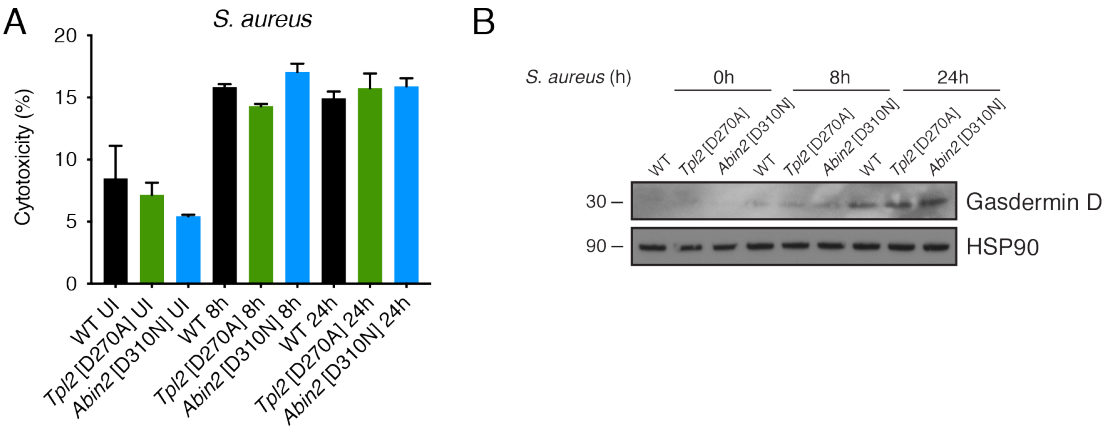

Figure 67 *Tpl2*^{D270A} and *Abin2*^{D310N} mutation do not impair pyroptosis upon *S. aureus* infection

BMDMs of the indicated genotypes were infected with YFP-*S. aureus* (MOI 10) for the times indicated. (**A**) Pyroptotic cell death following S. aureus infection was assayed by quantifying LDH release from the cytosol of BMDMs 8 h and 24 h post-infection. Supernatants were incubated with the cytotoxicity detection kit for 0.5 h and LDH levels were quantified by measuring absorbance at 490 nm (n = 4). (**B**) Cell extracts from WT, *Tpl2*$^{D270A/D270A}$ and *Abin2*$^{D310N/D310N}$ BMDMs following *S. aureus* infection were immunoblotted for the gasdermin D p30 cleavage product. UI, uninfected.

5.2.3.2 *Tpl2*^{D270A} *and Abin2*^{D310N} *mutation impair maturation of S. aureus phagosomes*

Having established that TPL-2 and ABIN-2 were required for efficient killing of internalised *S. aureus*, I next investigated whether TPL-2 and ABIN-2 regulated phagosome maturation following phagocytic uptake of *S. aureus*. I monitored phagosomal proteolysis using a labelled cathepsin L peptide substrate and confocal microscopy. Consistent with previous results using latex beads, both *Tpl2*^{D270A} and *Abin2*^{D310N} mutation significantly decreased total levels of active cathepsin L per YFP^{+} cell (Figure 68A and B). Moreover, the percentages of cathepsin L^{+} *S. aureus* phagosomes in *Tpl2*$^{D270A/D270A}$ and *Abin2*$^{D310N/D310N}$ BMDMs were significantly reduced relative to WT BMDMs (Figure 68C).

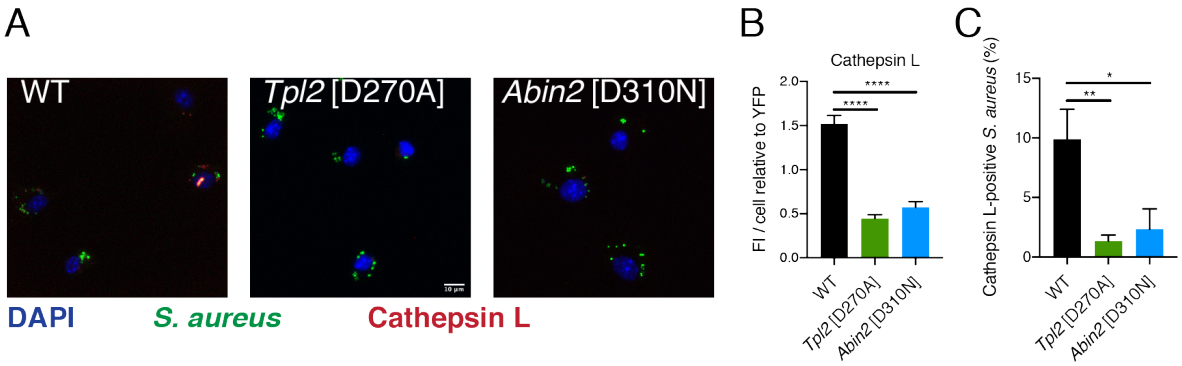

Figure 68 *Tpl2*^{D270A} and *Abin2*^{D310N} mutation reduce cathepsin activity in *S. aureus* phagosomes

BMDMs of the indicated genotypes were infected with YFP-*S. aureus* (MOI 10) for 1 h. BMDMs were stained with the Magic Red cathepsin L substrate at a final dilution of 1:250 for 1 h (red). Fluorescence of the Magic Red cathepsin L substrate was monitored at ex/em 592/628 nm. (**A**) Representative images of YFP^{+} BMDMs labelled with Magic Red cathepsin L substrate (red) and DAPI (nuclear stain). (**B**) Quantification of Magic Red cathepsin L staining from panel (A). Average fluorescence intensity of Magic Red cathepsin L substrate per cell relative to fluorescence intensity of YFP-*S. aureus* (n = 26-29). (**C**) Quantification of Magic Red cathepsin L staining co-localised with YFP-*S. aureus* from panel (A) (n = 26-29). Error bars represent SEM. * $P < 0.05$, ** $P < 0.01$, **** $P < 0.0001$. Unpaired t-test.

Phagosomal acidification was assayed following *S. aureus* internalisation by LysoTracker Red staining and confocal microscopy. *Tpl2*^{D270A} mutation significantly reduced the fluorescence intensity for LysoTracker Red per YFP^{+} cell (Figure 69A and B). Moreover, the percentage of LysoTracker Red^{+} *S. aureus* phagosomes was

significantly decreased (Figure 69C). In contrast, *Abin2*^{D310N} mutation did not significantly decrease fluorescence intensity for LysoTracker Red per YFP^{+} cell or the percentage of LysoTracker Red^{+} phagosomes containing *S. aureus* (Figure 69B and C). These results coincided with my previous observations using latex beads, where TPL-2, but not ABIN-2, promoted phagosomal acidification.

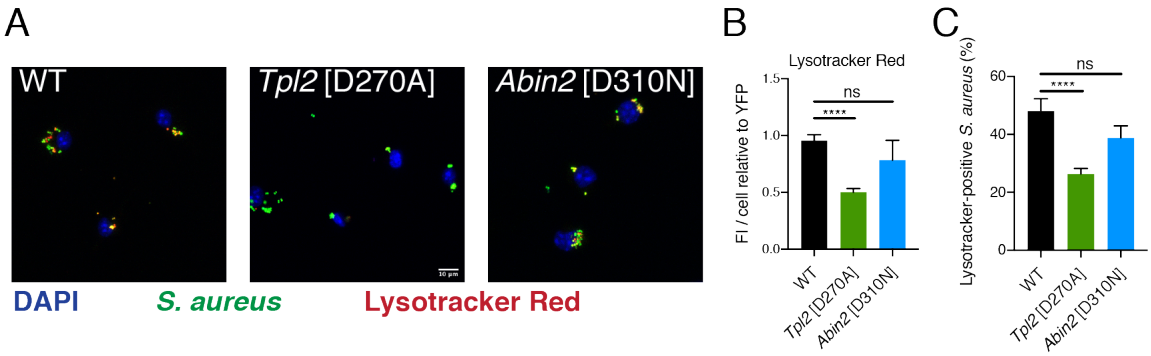

Figure 69 *Tpl2*^{D270A} mutation impairs acidification of *S. aureus* phagosomes

BMDMs of the indicated genotypes were infected with YFP-*S. aureus* (MOI 10) for 1 h. BMDMs were stained with the LysoTracker Red DND-99 dye at a final concentration of 100 nM for 1 h (red). Fluorescence of LysoTracker Red was monitored at ex/em 577/590 nm. (**A**) Representative images of YFP^{+} BMDMs labelled with LysoTracker Red DND-99 dye (red) and DAPI (nuclear stain). (**B**) Quantification of LysoTracker Red signal from panel (A). Average fluorescence intensity of LysoTracker Red per cell relative to fluorescence intensity of YFP-*S. aureus* (n = 66-98). (**C**) Quantification of LysoTracker Red co-localisation with YFP-*S. aureus* from panel (A) (n = 66-98). Error bars represent SEM. **** $P < 0.0001$, not significant (ns). Unpaired t-test.

The effects of TPL-2 catalytic activity and ABIN-2 ubiquitin binding on phagosome maturation were also investigated using specific markers of the maturation process. EEA1 is a marker of early endosomes, which is acquired by early phagosomes and mediates docking and fusion events with compartments of the endosomal pathway (McBride *et al*, 1999; Collins *et al*, 2002). Co-localisation of YFP-*S. aureus* with EEA1 was significantly reduced in BMDMs from *Tpl2*$^{D270A/D270A}$ mice compared to WT controls (Figure 70A and B). This observation was particularly interesting since earlier results from immunoprecipitation studies showed that 3xFLAG-TPL-2 interacted with endogenous EEA1 upon LPS stimulation. In contrast, co-localisation of EEA1 with YFP-*S. aureus* in *Abin2*$^{D310N/D310N}$ BMDMs was comparable to WT BMDMs (Figure 70A and B).

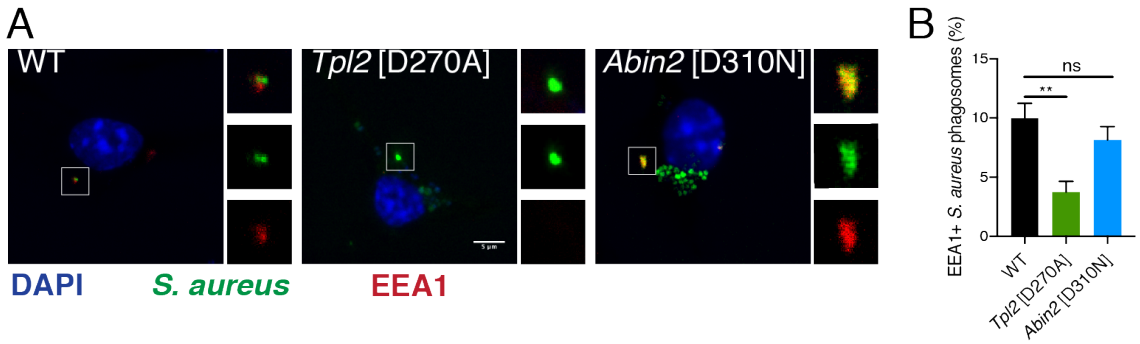

Figure 70 *Tpl2*^{D270A} mutation reduces co-localisation of YFP-*S. aureus* with EEA1

BMDMs of the indicated genotypes were infected with YFP-*S. aureus* (MOI 10) for 1 h. BMDMs were stained with an anti-EEA1 antibody at a final concentration of 1:200, followed by incubation with a secondary Alexa Fluor 647 that cross-reacts with the anti-EEA1 antibody (red). (**A**) Representative images of YFP^{+} BMDMs labelled with anti-EEA1-AF647 (red) and DAPI (nuclear stain). (**B**) Quantification of EEA1^{+} *S. aureus*-containing phagosomes from panel (A) (n = 27). Error bars represent SEM. ** $P < 0.01$, not significant (ns). Unpaired t-test.

I also investigated the effect of *Tpl2*^{D270A} and *Abin2*^{D310N} mutation on staining for LAMP1, a membrane protein on late phagosomes that facilitates RAB7 recruitment to drive phagosome maturation (Huynh *et al*, 2007; Binker *et al*, 2007). Co-localisation of YFP-*S. aureus* with LAMP1 was significantly reduced in both *Tpl2*$^{D270A/D270A}$ and *Abin2*$^{D310N/D310N}$ BMDMs relative to WT controls (Figure 71A and B). It is important to note that the percentage decrease of LAMP1^{+} *S. aureus* phagosomes was more pronounced in *Tpl2*$^{D270A/D270A}$ BMDMs relative to *Abin2*$^{D310N/D310N}$ BMDMs (Figure 71B).

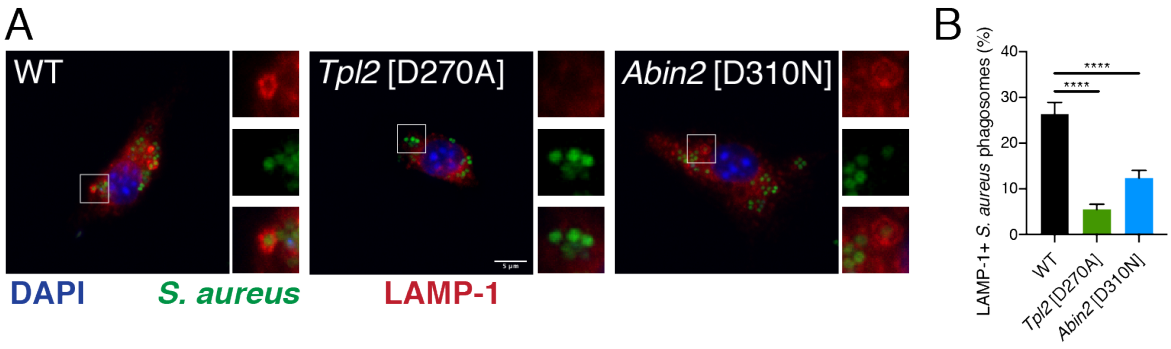

Figure 71 *Tpl2*^{D270A} and *Abin2*^{D310N} mutation reduce co-localisation of YFP-*S. aureus* with LAMP1

BMDMs of the indicated genotypes were infected with YFP-*S. aureus* (MOI 10) for 1 h. BMDMs were stained with an anti-LAMP1 antibody at a final concentration of 1:200, followed by incubation with a secondary Alexa Fluor 594 antibody that cross-

reacts with the anti-LAMP1 antibody (red). (**A**) Representative images of YFP$^+$ BMDMs labelled with anti-LAMP1-AF594 (red) and DAPI (nuclear stain). (**B**) Quantification of LAMP1$^+$ *S. aureus* phagosomes from panel (A) (n = 25). Error bars represent SEM. **** $P < 0.0001$. Unpaired t-test.

It is well established that following invasion, *S. aureus* itself becomes ubiquitylated (Neumann *et al*, 2016). Ubiquitylated *S. aureus* is subsequently recognised by ubiquitin-binding proteins, including sequestosome 1 (SQSTM1, p62) (Neumann *et al*, 2016). SQSTM1 strongly binds K63-linked ubiquitin chains and mediates phagosome formation (Neumann *et al*, 2016; Seibenhener *et al*, 2004). Since loss of ubiquitin binding to ABIN-2 disrupted the maturation of *S. aureus* phagosomes, I postulated that ABIN-2 may function as a ubiquitin-binding protein recognising ubiquitylated *S. aureus* following invasion. Moreover, previous studies and my findings presented here demonstrated that K63-linked ubiquitin chains are highly abundant on phagosomal membranes in macrophages (Figure 38) (Guo *et al*, 2019).

I visualised the co-localisation of ubiquitin with YFP-*S. aureus* by confocal microscopy. Upon *S. aureus* infection, distinct ubiquitin puncta co-localised with YFP-*S. aureus* in BMDMs from WT and *Tpl2*$^{D270A/D270A}$ mice (Figure 72A). Notably, the percentage of ubiquitin$^+$ *S. aureus* phagosomes was significantly decreased by *Abin2*^{D310N} mutation (Figure 72B).

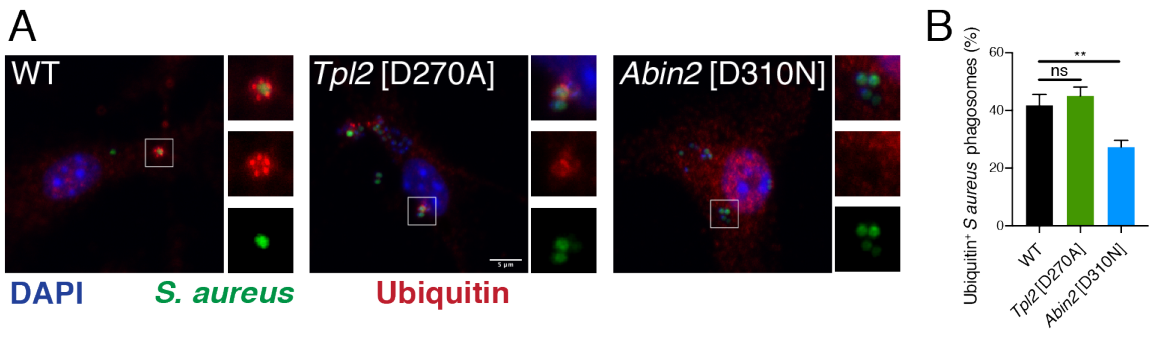

Figure 72 *Abin2*^{D310N} mutation reduces co-localisation of YFP-*S. aureus* with ubiquitin

BMDMs of the indicated genotypes were infected with YFP-*S. aureus* (MOI 10) for 1 h. BMDMs were stained with an anti-ubiquitin antibody at a final concentration of 1:200, followed by incubation with a secondary Alexa Fluor 647 antibody that cross-reacts with the anti-ubiquitin antibody (red). (**A**) Representative images of YFP$^+$ BMDMs labelled with anti-ubiquitin-AF647 (red) and DAPI (nuclear stain). (**B**)

Quantification of ubiquitin^{+} *S. aureus* phagosomes from panel (A) (n = 46). Error bars represent SEM. ** $P < 0.01$. Unpaired t-test.

5.2.3.3 TPL-2 negatively regulates type I IFN expression after S. aureus infection

Phagocytosis is required for *S. aureus* to induce MyD88-dependent production of TNF and IL-6 by macrophages (Ip *et al*, 2010). It has been proposed that TLR-dependent cytokine production requires delivery of bacteria to acidic phagosomes to liberate cryptic bacterial ligands that initiate responses from the vacuole (Ip *et al*, 2010). This raised the question of whether TPL-2 activated MAP kinase signalling from the cell surface following macrophage infection with *S. aureus* or signalled from phagosomes following internalisation.

Initial experiments demonstrated that activation of ERK1/2 in BMDMs by *S. aureus* was blocked by *Tpl2*^{D270A} mutation (Figure 73A). To investigate the role of *S. aureus* internalisation in ERK1/2 activation, WT BMDMs were pre-treated with cytochalasin D to block phagocytic uptake prior to infection. Immunoblotting revealed that *S. aureus* strongly activated ERK1/2 at early time points in the presence or absence of cytochalasin D (Figure 73B). This suggested that the initial activation of the TPL-2-ERK1/2 MAP kinase signalling pathway by *S. aureus* was mediated by TLR2 dimers at the macrophage plasma membrane and did not require phagocytic uptake. At later time points, ERK1/2 activation was partially reduced by *Tpl2*^{D270A} mutation, consistent with TPL-2 activation by TLR9 on phagosomes after *S. aureus* internalisation (Zhang *et al*, 2012) (Figure 73B). As a positive control for potent inhibition of actin polymerisation by cytochalasin D, I monitored phagocytic uptake of fluorescently-labelled beads. As anticipated, cytochalasin D pre-treatment almost fully diminished phagocytic uptake (Figure 73C).

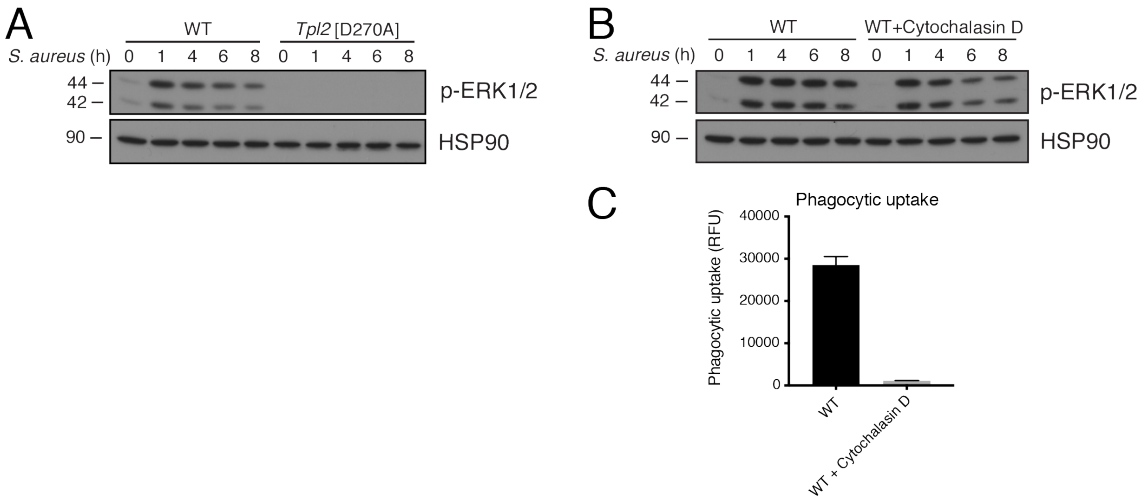

Figure 73 TPL-2 activates ERK1/2 from the cell surface following *S. aureus* infection

(**A-B**) BMDMs of the indicated genotypes were infected with *S. aureus* (MOI 10) for the times indicated. (**A**) Cell extracts from WT and *Tpl2*$^{D270A/D270A}$ BMDMs were immunoblotted with antibodies recognising p-ERK1/2 (T202/Y204) and HSP90. (**B**) Prior to bacterial infection, WT BMDMs were pre-treated with 10 µg/ml cytochalasin D (0.5 h), an inhibitor of actin polymerisation, which blocks phagocytic uptake of YFP-*S. aureus*. Cell extracts were immunoblotted with antibodies recognising p-ERK1/2 (T202/Y204) and HSP90. (**C**) Phagocytic uptake of fluorescently-labelled silica beads by WT BMDMs. Intracellular fluorescence was monitored 0.5 h following uptake of AF488-coupled beads by BMDMs. As positive control, BMDMs were pre-treated with 10 µg/ml cytochalasin D for 0.5 h. Error bars represent SEM. Cytochalasin D pre-treatment was carried out alongside treatments in panel (B). p, phospho.

RNA sequencing was used to determine the effect of *Tpl2*^{D270A} mutation on *S. aureus* induction of gene expression in BMDMs. Blocking TPL-2 catalytic activity had pronounced effects on the global transcriptome of *S. aureus*-infected BMDMs (Figure 74). *Tpl2*^{D270A} mutation significantly up- (2,326) and downregulated (1,924) genes upon bacterial infection in a time-dependent fashion. Some genes were significantly regulated by *Tpl2*^{D270A} mutation at 4 h post-infection (Figure 74A), while others were only regulated at 8 h post-infection (Figure 74B).

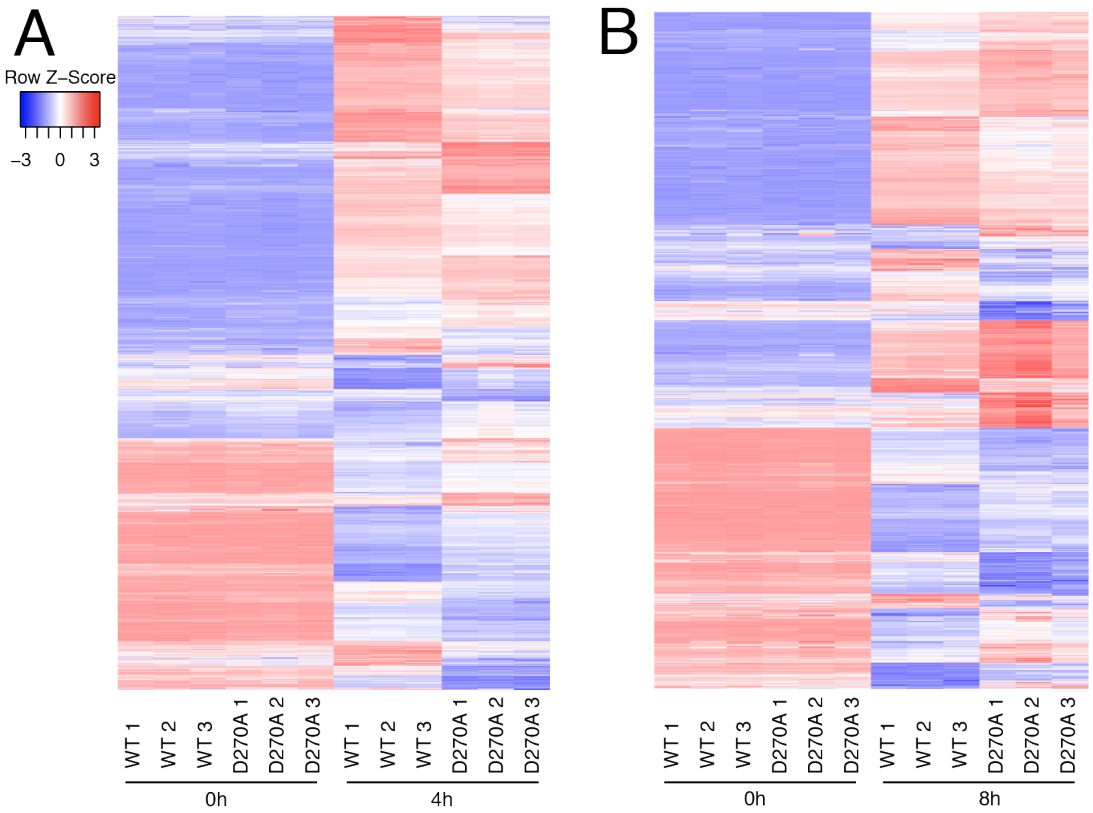

Figure 74 TPL-2 catalytic activity has pronounced effects on the global transcriptome of *S. aureus*-infected BMDMs

TPL-2-dependent transcriptome in response to *S. aureus* infection. Three biological replicates were included per genotype (n = 3). BMDMs of the indicated genotypes were infected with *S. aureus* (MOI 10) for 4 h or 8 h. Significantly upregulated genes are highlighted in red, significantly downregulated genes are highlighted in blue. (**A**) Heatmap showing expression of differentially regulated genes (adjusted *P* values < 0.05) between WT and *Tpl2*$^{D270A/D270A}$ BMDMs at 4 h post-infection. (**B**) Heatmap showing differentially regulated genes (adjusted *P* values < 0.05) between WT and *Tpl2*$^{D270A/D270A}$ BMDMs at 8 h post-infection.

Five out of the ten most significantly upregulated biological pathways in *Tpl2*$^{D270A/D270A}$ BMDMs relative to WT BMDMs at 4 h post-infection were implicated in type I interferon signalling (Figure 75A). In addition, five out of the ten most significantly downregulated biological pathways were implicated in MAP kinase-dependent innate immune signalling downstream of TLR2/4 and IL-1 (Figure 75B).

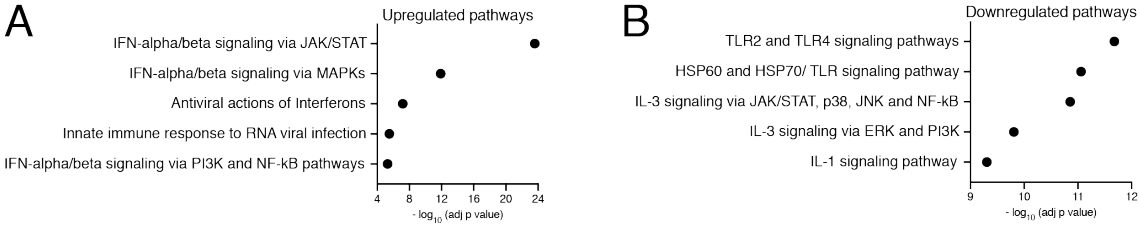

Figure 75 Selected pathways that are up- and downregulated by *Tpl2*^{D270A} mutation following *S. aureus* infection

Gene set enrichment analysis (GSEA) of significantly (**A**) upregulated and (**B**) downregulated biological pathways in *Tpl2*$^{D270A/D270A}$ relative to WT BMDMs 4 h following *S. aureus* infection. Pathways shown are selected from the ten most significantly up- or downregulated pathways, according to adjusted *P* value.

Consistent with these findings, expression of innate immune genes implicated in TLR2/4 and MAP kinase signalling was decreased in *Tpl2*$^{D270A/D270A}$ BMDMs relative to WT BMDMs at 4 h post-infection (Figure 76A). In addition, expression of key inflammatory mediators, including chemokines and cytokines, was significantly dysregulated in *Tpl2*$^{D270A/D270A}$ BMDMs relative to WT BMDMs following *S. aureus* infection (Figure 76B). More specifically, *Tpl2*^{D270A} mutation significantly decreased *Il23a*, *Ccl2*, *Il1b*, *Ccl7* and *Cxcl2* expression, while significantly increasing *Nos2*, *Il12a* and *Il12b* expression following *S. aureus* infection (Figure 76B).

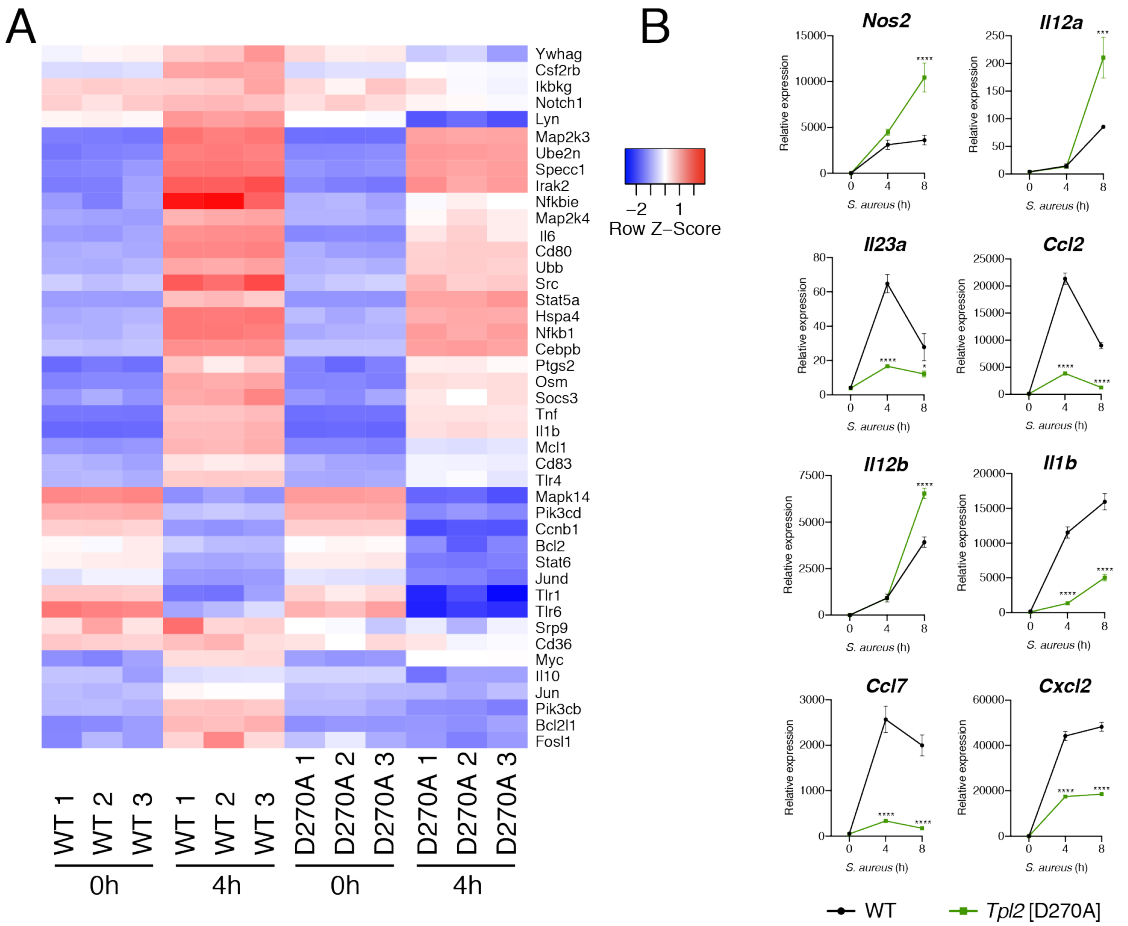

Figure 76 *Tpl2*^{D270A} mutation dysregulates expression of innate immune genes

(**A**) Heatmap showing relative expression of 43 selected innate immune genes between WT and *Tpl2*$^{D270A/D270A}$ BMDMs at 0 h and 4 h post-infection. Selected genes were involved in TLR2/4 signalling and JAK/STAT, p38α, JNK and NF-κB signalling pathways. Significantly upregulated genes are highlighted in red, significantly downregulated genes are highlighted in blue. All selected genes are differentially regulated, with adjusted *P* values < 0.05. (**B**) Relative expression values of selected genes that were significantly altered by *Tpl2*^{D270A} mutation following *S. aureus* infection of WT and *Tpl2*$^{D270A/D270A}$ BMDMs (n = 3). Data were analysed by a two-way ANOVA. Error bars represent SEM. * $P < 0.05$, *** $P < 0.001$, **** $P < 0.0001$.

TPL-2 is known to suppress type I interferon production during bacterial infection (McNab *et al*, 2013). Moreover, in the previous chapter, I provided experimental evidence that *Tpl2*^{D270A} mutation significantly increased expression of several *Ifna* genes following uptake of LPS-coated beads, whereas expression of *Ifna* genes was not regulated by TPL-2 following stimulation with soluble LPS (Figure 55).

Following *S. aureus* infection, *Tpl2*^{D270A} mutation significantly upregulated several biological pathways involved in type I interferon signalling (Figure 75A). In

accordance with these findings, *Tpl2*^{D270A} mutation significantly elevated expression of type I interferon genes, including *Ifnb1*, *Ifna1*, *Ifna2*, *Ifna4*, *Ifna5* and *Ifna6*, following *S. aureus* infection (Figure 77A). In line with this, expression of 63 ISGs was significantly upregulated in *Tpl2*$^{D270A/D270A}$ BMDMs relative to WT BMDMs 4 h after *S. aureus* infection (Figure 77B).

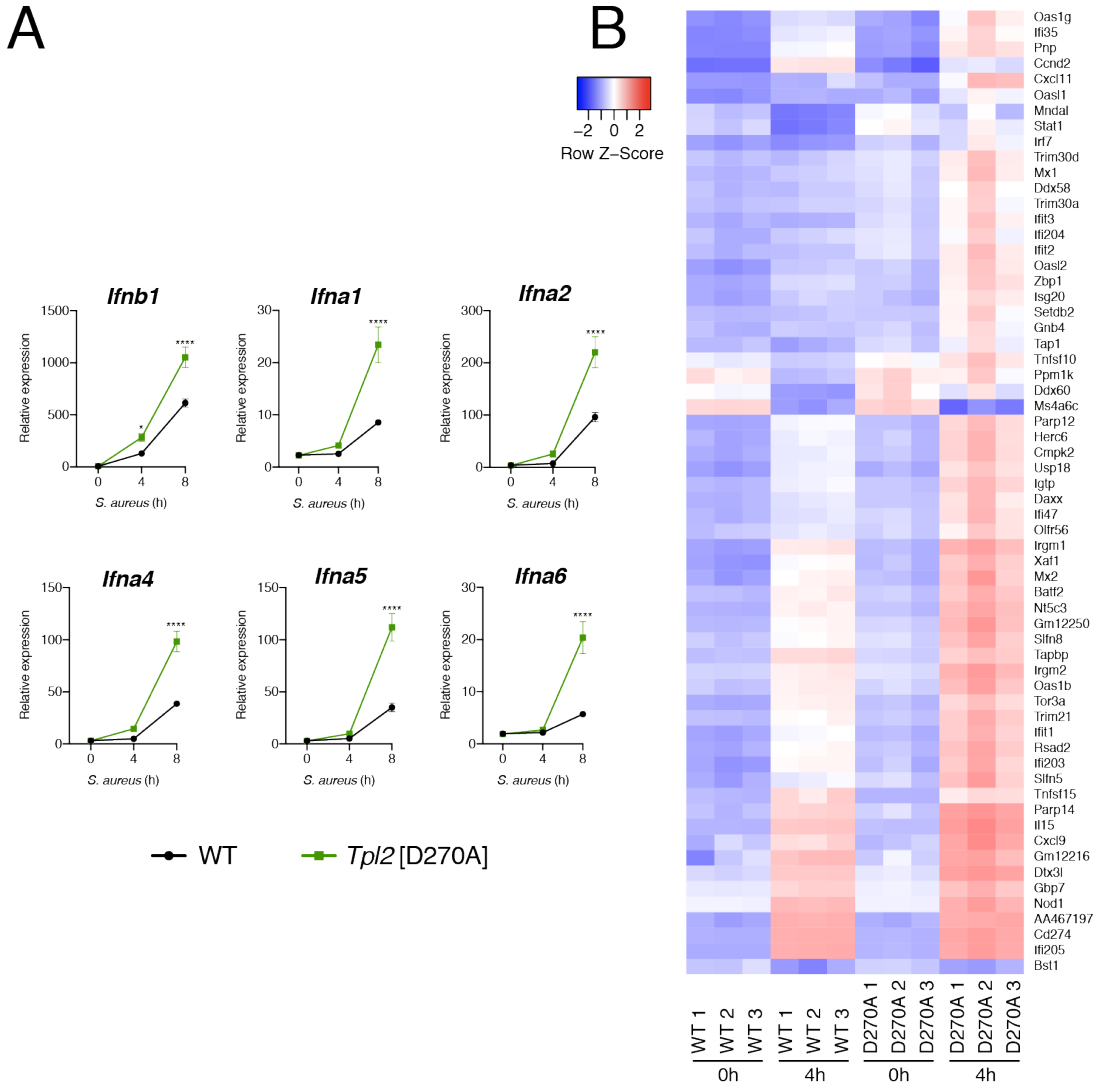

Figure 77 *Tpl2*^{D270A} mutation upregulates type I interferon and interferon-stimulated genes during *S. aureus* infection

(**A**) Relative expression values of type I interferon genes that were significantly upregulated by *Tpl2*^{D270A} mutation following *S. aureus* infection of WT and *Tpl2*$^{D270A/D270A}$ BMDMs (n = 3). Data were analysed by a two-way ANOVA. Error bars represent SEM. * P < 0.05, **** *P* < 0.0001. (**B**) Heatmap showing expression of 63 selected interferon-stimulated genes (ISGs) between WT and *Tpl2*$^{D270A/D270A}$ BMDMs at 0 h and 4 h post-infection. Significantly upregulated genes are highlighted in red,

significantly downregulated genes are highlighted in blue. All selected genes are differentially regulated, with adjusted *P* values < 0.05.

Together these results indicated that TPL-2 catalytic activity regulates, from the cell surface, early MAP kinase signalling that triggers gene expression of pro- and anti-inflammatory innate immune genes. Moreover, my findings confirmed that TPL-2 negatively regulates expression of type I interferons, including *Ifna* genes, following *S. aureus* infection. These observations using *S. aureus*, a more physiological stimulus, confirmed my previously obtained results with LPS-coated beads.

5.2.3.4 S. aureus stimulates TPL-2 activation of AKT signalling from the phagosome

My experiments with LPS-coated beads indicated that TPL-2 induces AKT activation following phagocytosis and showed that AKT signalling is critical for driving phagosome maturation in macrophages, consistent with the known role of PI3K-AKT signalling in regulating Rab GTPases and phagosomal acidification (Thi & Reiner, 2012). I therefore investigated whether TPL-2 also regulated AKT signalling following *S. aureus* infection. In response to *S. aureus* infection of WT BMDMs, AKT was strongly phosphorylated at S473 (Figure 78). Interestingly, AKT phosphorylation at S473 was substantially decreased in WT BMDMs pre-treated with cytochalasin D (Figure 78). This suggested that AKT phosphorylation in response to *S. aureus* infection was predominantly mediated from the endosomal compartment and not from the plasma membrane.

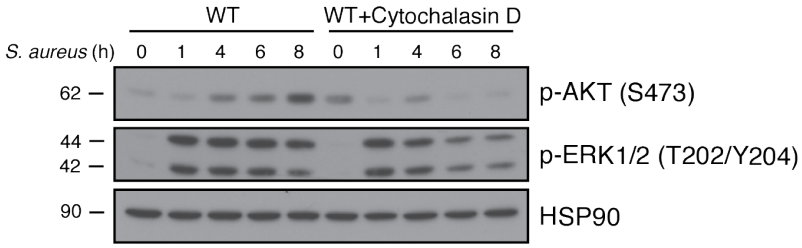

Figure 78 Endosomal activation of AKT following *S. aureus* infection

WT BMDMs were infected with *S. aureus* (MOI 10) for the times indicated. Prior to bacterial infection, WT BMDMs were pre-treated with 10 µg/ml cytochalasin D (0.5 h), an inhibitor of actin polymerisation, which blocks phagocytic uptake of YFP-*S. aureus*. Cell extracts were immunoblotted with antibodies recognising p-ERK1/2 (T202/Y204), p-AKT (S473) and HSP90. p, phospho.

Next, I investigated whether TPL-2 catalytic activity regulated AKT signalling following phagocytic uptake of *S. aureus*. Interestingly, AKT phosphorylation at S473 was strongly reduced in *Tpl2*$^{D270A/D270A}$ BMDMs compared to WT controls following *S. aureus* infection (Figure 79A). In addition, phosphorylation of p70S6K at T389 and S6 at S240/S244 was decreased by *Tpl2*^{D270A} mutation (Figure 79A). Moreover, phosphorylation of the AKT downstream target 4EBP1 at T37/T46 was reduced in *Tpl2*$^{D270A/D270A}$ BMDMs following phagocytosis of *S. aureus* (Figure 79A). While ERK1/2 activation was blocked by *Tpl2*^{D270A} mutation, phosphorylation of JNK1/2 at T183/Y185 remained unchanged (Figure 79A). Neither AKT nor MAP kinase signalling was impaired in BMDMs from *Abin2*$^{D310N/D310N}$ mice following phagocytic uptake of *S. aureus* (Figure 79A). Besides infecting BMDMs with *S. aureus*, I stimulated macrophages with Pam_3CSK_4, a soluble agonist of TLR2 (Tsolmongyn *et al*, 2013). Interestingly, phosphorylation of AKT at S473 and S6 at S240/S244 remained unaffected in *Tpl2*$^{D270A/D270A}$ BMDMs upon Pam_3CSK_4 stimulation (Figure 79B). These findings were in line with my previous observation that TPL-2 promoted AKT signalling from endosomal compartments and not from the cell surface.

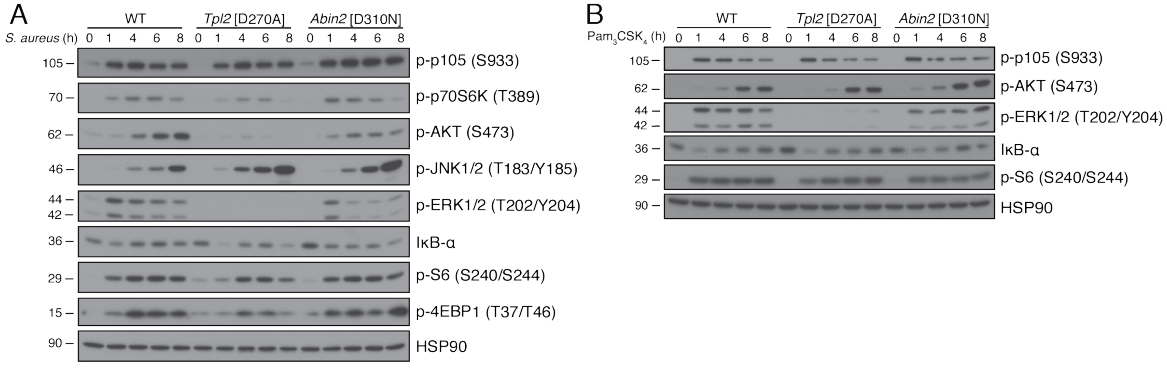

Figure 79 TPL-2 activates AKT signalling from endosomes following *S. aureus* infection

(**A**) BMDMs from WT, *Tpl2*$^{D270A/D270A}$ and *Abin2*$^{D310N/D310N}$ mice were infected with *S. aureus* (MOI 10) for the times indicated and cell extracts were immunoblotted with the antibodies indicated. (**B**) BMDMs from WT, *Tpl2*$^{D270A/D270A}$ and *Abin2*$^{D310N/D310N}$ mice were stimulated with 100 ng/ml Pam_3CSK_4 for the times indicated and cell extracts were immunoblotted with the antibodies indicated. p, phospho.

5.2.4 TPL-2 and ABIN-2 regulate macrophage killing of *Salmonella typhimurium*

Having shown that the TPL-2 complex was involved in promoting killing of several extracellular microbes, I set out to further study whether TPL-2 catalytic activity or ABIN-2 ubiquitin binding promoted killing of an intracellular bacterium. Here, I infected BMDMs with *S. typhimurium*, a Gram-negative intracellular pathogen. An infection efficiency of approximately 30% was achieved 1 h post-infection, with the percentage of infected cells remaining similar at 10 h post-infection (Figure 80A and B). In addition, GeoMean intensities of GFP^{high} BMDMs were calculated. Although GeoMean intensities increased from 1 h to 10 h post-infection, GeoMean intensities of GFP were comparable across all genotypes (Figure 80C). Infection rates confirmed that an MOI of 5 and a 10 h infection was appropriate to further study the functions of TPL-2 and ABIN-2 in the context of *S. typhimurium* infection.

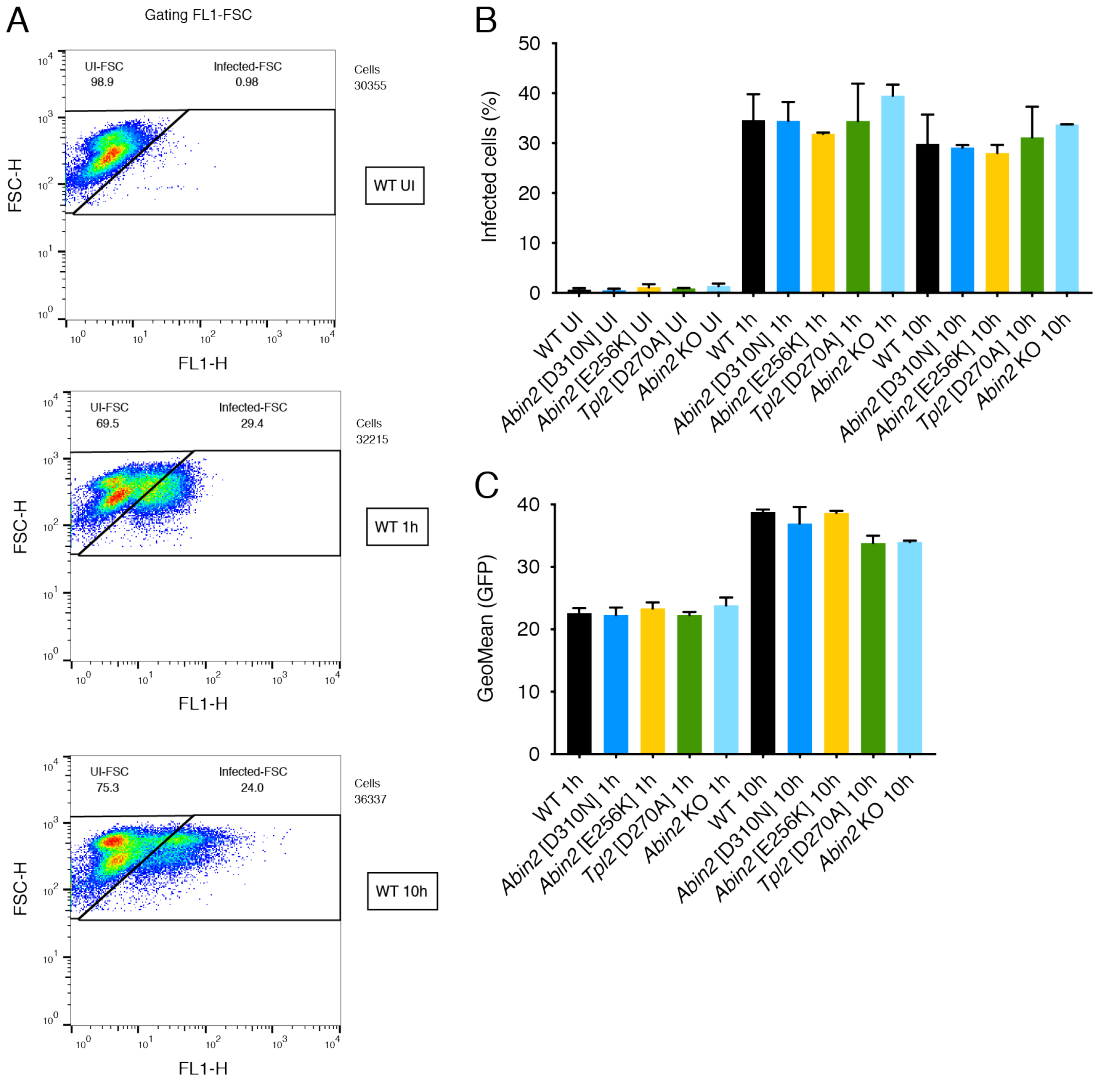

Figure 80 Infection of BMDMs with *S. typhimurium*

BMDMs from WT, *Tpl2*$^{D270A/D270A}$, *Abin2*$^{D310N/D310N}$, *Abin2*$^{E256K/E256K}$ and *Abin2*$^{-/-}$ mice were infected with GFP-*S. typhimurium* (MOI 5) for the times indicated. Cells were harvested and analysed by flow cytometry. (**A**) BMDMs were gated according to fluorescence at 530 nm (FL1), the optimal emission wavelength of GFP. GFP^{high} BMDMs were selected to calculate infection rates. (**B**) Infection efficiencies were calculated from panel (A) for all three biological replicates per genotype (n = 3). (**C**) GeoMean intensities of GFP^{high} BMDMs from panel (A) were calculated for all three biological replicates per genotype using FlowJo (Version 10.3.0) software (n = 3). UI, uninfected.

Phagocytic uptake of *S. typhimurium* into BMDMs was unchanged by *Tpl2*^{D270A} and *Abin2*^{D310N} mutation (Figure 81A). In accordance with my previous findings, the optimal time point for CFU analysis was 10 h post-infection since BMDMs from WT mice cleared approximately 50% of internalised *S. typhimurium* at this time point (Figure 81B). *Abin2*^{D310N} mutation significantly impaired bacterial killing of *S.*

typhimurium in BMDMs 10 h post-infection (Figure 81C). Strikingly, *Tpl2*^{D270A} mutation significantly accelerated bacterial killing of *S. typhimurium*, suggesting that loss of TPL-2 kinase activity was protective during *S. typhimurium* infection. Importantly, bafilomycin A1 pre-treatment of WT cells also resulted in decreased *S. typhimurium* CFU relative to WT controls, thus mimicking the effect of *Tpl2*^{D270A} mutation on *S. typhimurium* CFU in BMDMs (Figure 81C).

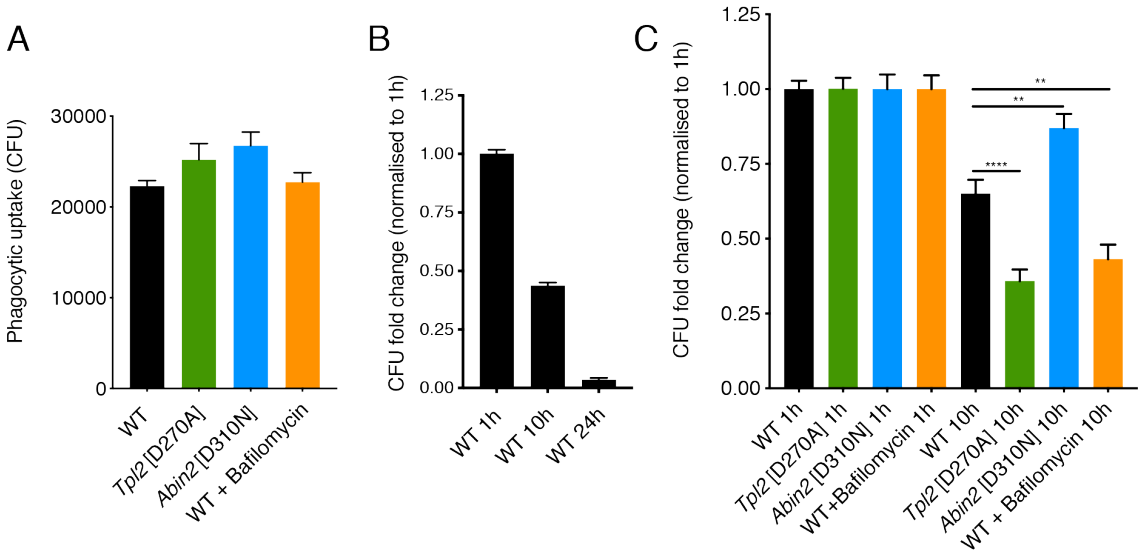

Figure 81 *Abin2*^{D310N} mutation impairs macrophage killing of *S. typhimurium*

BMDMs of the indicated genotypes were infected with GFP-*S. typhimurium* (MOI 5) for 0.5 h. As a control, WT cells were pre-treated with 1 µM bafilomycin A1 for 0.5 h to block V-ATPase-mediated acidification of phagosomes. Two biological replicates were analysed per genotype, each biological replicate was seeded in triplicates and plated in duplicates, thus providing 12 measurements per condition. (**A**) Phagocytic uptake (CFU) of GFP-labelled *S. typhimurium* into BMDMs of the indicated genotypes 1 h post-infection (n = 12). (**B-C**) *S. typhimurium* CFU were assessed at 10 h or 24 h after infection and normalised to CFU at 1 h (n = 12). Data were analysed by a one-way ANOVA. Error bars represent SEM. ** $P < 0.01$, **** $P < 0.0001$.

5.2.4.1 Impaired acidification resulting from loss of TPL-2 catalytic activity restricts S. typhimurium replication

As an intracellular bacterium, *S. typhimurium* has evolved complex mechanisms to exploit and evade host immune responses (Hurley *et al*, 2014). *S. typhimurium* encodes two type III secretion systems (T3SS) that deliver virulence effector proteins directly from the bacterial vacuole into host cells (Wang *et al*, 2020): Salmonella pathogenicity island 1 (SPI-1) and SPI-2 (Wang *et al*, 2020). Acidification of the *S.*

typhimurium phagosome stimulates assembly of the SPI-2 T3SS (Yu *et al*, 2010). Together with Dr Teresa Thurston (Imperial College London), we thus hypothesised that reduced *S. typhimurium* CFU in *Tpl2*$^{D270A/D270A}$ BMDMs may result from impaired acidification and lack of SPI-2 effector proteins, which are critical for *S. typhimurium* replication.

To test this, I infected BMDMs with *S. typhimurium ΔssaV*, a Salmonella mutant strain, which lacks the *ssaV* gene. The *ssaV* gene product is a component of the SPI-2 T3SS and critical for the secretion of effector proteins (Mesquita *et al*, 2012; Günster *et al*, 2017; Yu *et al*, 2010). Phagocytic uptake of *S. typhimurium ΔssaV* into BMDMs remained unchanged by *Tpl2*^{D270A} mutation (Figure 82A). As previously observed, *Tpl2*^{D270A} mutation, relative to WT cells, significantly increased bacterial killing of *S. typhimurium* (Figure 82B). However, *Tpl2*^{D270A} mutation did not accelerate bacterial killing upon infection with *S. typhimurium ΔssaV* (Figure 82B). This observation was consistent with reduced *S. typhimurium* CFU in *Tpl2*$^{D270A/D270A}$ BMDMs compared to WT cells resulting from impaired acidification due to loss of TPL-2 catalytic activity.

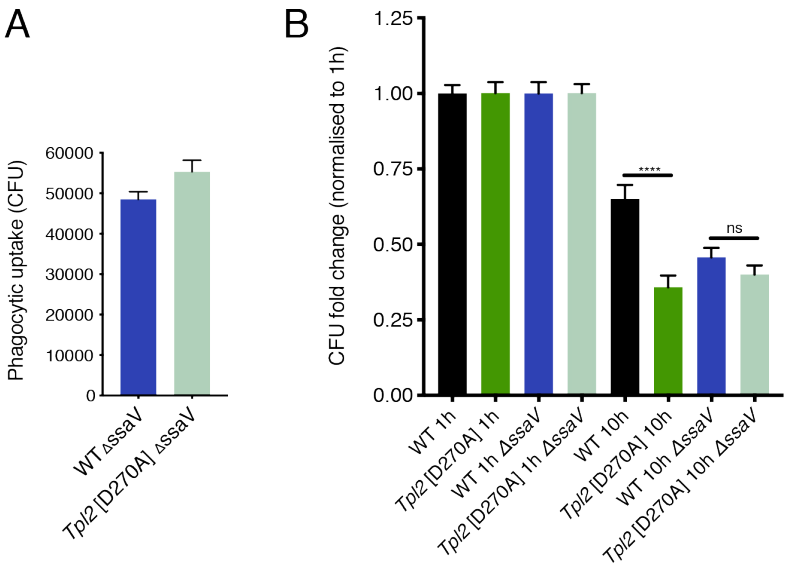

Figure 82 Impaired acidification mediated by *Tpl2*^{D270A} mutation restricts *S. typhimurium* growth

BMDMs of the indicated genotypes were infected with *S. typhimurium* or *S. typhimurium ΔssaV* (MOI 5) for 0.5 h. Two biological replicates were analysed per genotype, each biological replicate was seeded in triplicates and plated in duplicates, thus providing 12 measurements per condition. (**A**) Phagocytic uptake (CFU) of *S. typhimurium ΔssaV* into BMDMs of the indicated genotypes 1 h post-infection (n =

12). (**B**) *S. typhimurium* and *S. typhimurium ΔssaV* CFU were assessed at 10 h after infection and normalised to CFU at 1 h (n = 12). Data were analysed by a one-way ANOVA. Error bars represent SEM. **** $P < 0.0001$, not significant (ns).

5.2.4.2 S. typhimurium infection induces pyroptosis of macrophages independently of TPL-2 and ABIN-2

Pyroptosis is important for killing of *S. typhimurium* by macrophages (Thurston *et al*, 2016). I investigated whether *Abin2*^{D310N} or *Tpl2*^{D270A} mutation regulated pyroptosis following *S. typhimurium* infection, which may explain why *Abin2*^{D310N} mutation did not fully block killing of *S. typhimurium* by BMDMs.

To test levels of pyroptotic cell death, I analysed cytosolic LDH levels upon *S. typhimurium* infection. *S. typhimurium* infection caused a pronounced increase in LDH release, however, neither *Tpl2*^{D270A} nor *Abin2*^{D310N} mutation altered LDH levels at 10 h or 24 h post-infection (Figure 83A). Furthermore, comparable levels of the gasdermin D p30 cleavage product were detected in WT, *Tpl2*$^{D270A/D270A}$ and *Abin2*$^{D310N/D310N}$ BMDMs following *S. typhimurium* infection. These results suggested that neither TPL-2 catalytic activity nor ABIN-2 ubiquitin binding regulated pyroptosis following *S. typhimurium* infection (Figure 83B).

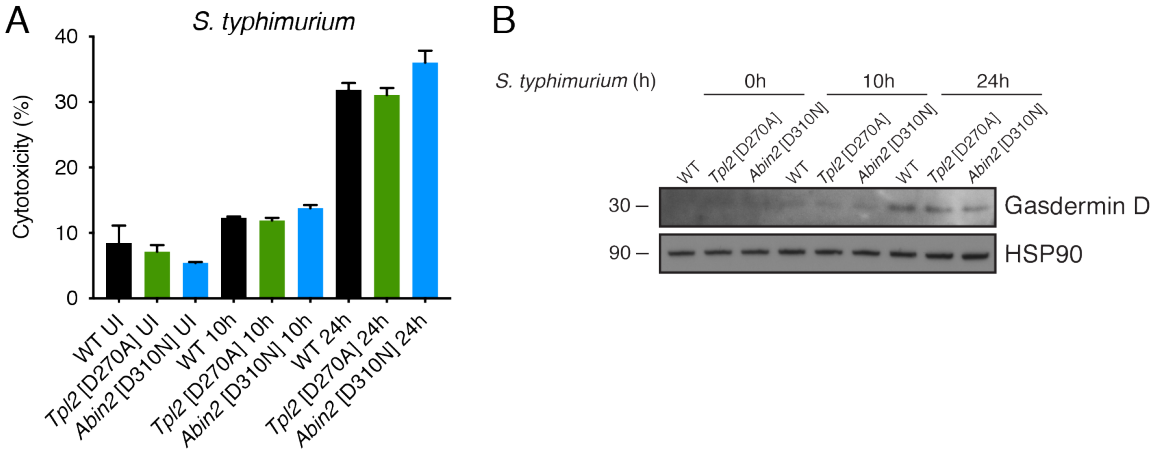

Figure 83 *Tpl2*^{D270A} and *Abin2*^{D310N} mutation do not impair pyroptosis upon *S. typhimurium* infection

BMDMs of the indicated genotypes were infected with GFP-*S. typhimurium* (MOI 5) for the times indicated. (**A**) Pyroptotic cell death following *S. typhimurium* infection was assayed by quantifying LDH release from the cytosol of BMDMs 10 h and 24 h post-infection. Supernatants were incubated with the cytotoxicity detection kit for 0.5 h and LDH levels were quantified by measuring absorbance at 490 nm (n = 4). (**B**)

Cell extracts from WT, *Tpl2*$^{D270A/D270A}$ and *Abin2*$^{D310N/D310N}$ BMDMs following *S. typhimurium* infection were immunoblotted for the gasdermin D p30 cleavage product. UI, uninfected.

5.3 Conclusion

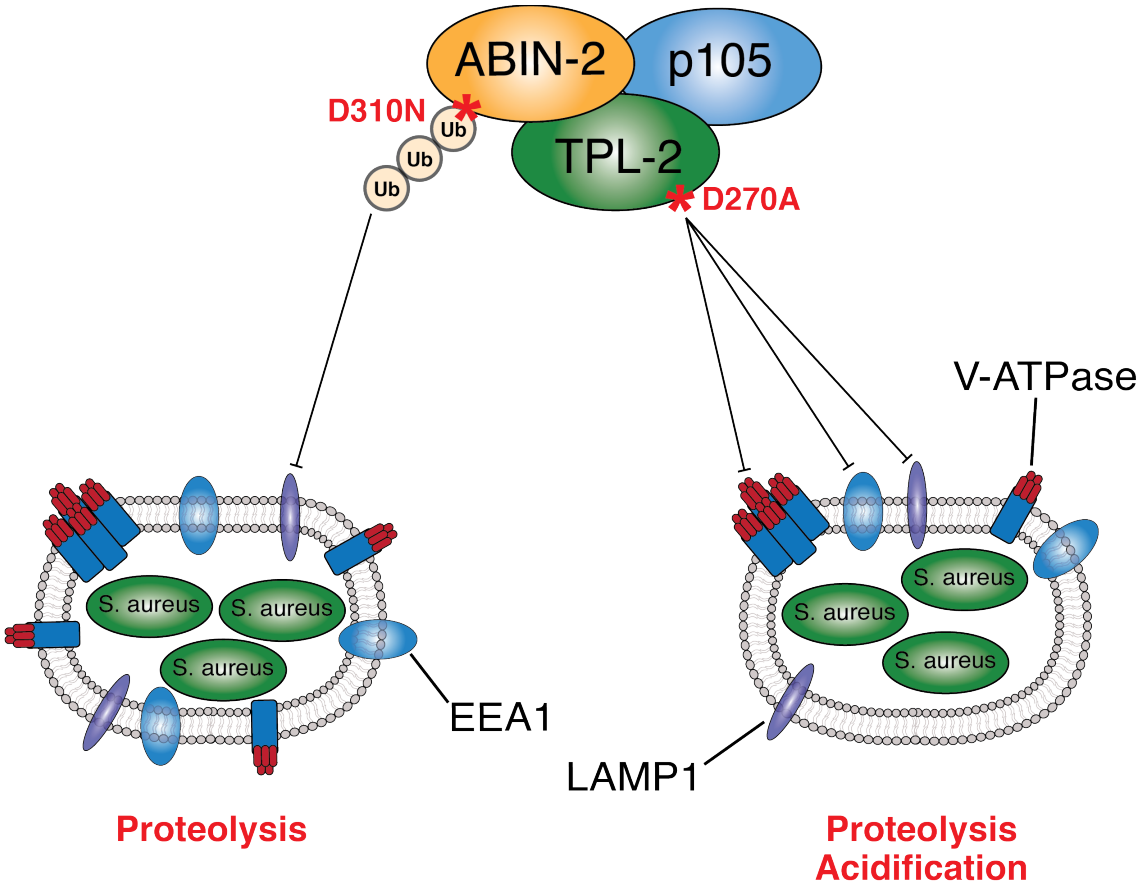

Figure 84 TPL-2 and ABIN-2 induce killing of *S. aureus* by promoting phagosome maturation

Both TPL-2 and ABIN-2 are important to mediate effective macrophage killing of *S. aureus* bacteria following internalisation. TPL-2 catalytic activity promotes co-localisation of EEA1 and LAMP1 with *S. aureus*-containing phagosomes. The kinase activity of TPL-2 is required for optimal cathepsin activity and acidification of phagosomes, which contain engulfed *S. aureus* bacteria. Ubiquitin binding to ABIN-2 is important for co-localisation of LAMP1 with *S. aureus*-containing phagosomes. Moreover, ubiquitin binding to ABIN-2 mediates optimal proteolytic activity within *S. aureus*-containing phagosomes.

5.3.1 ABIN-2 is a regulator of bacterial killing in macrophages

For the first time, my results in this chapter implicated ABIN-2 in the regulation of bacterial infection. I demonstrated that ubiquitin binding to ABIN-2 was required for efficient killing of bacteria following phagocytic uptake by macrophages. Importantly, ABIN-2 ubiquitin binding promoted killing of a diverse range of bacterial species, both Gram-negative and Gram-positive, as well as extracellular and intracellular. However, ABIN-2 was not required for efficient clearance of all bacterial species following infection of macrophages. While ABIN-2 ubiquitin binding promoted killing of *E. coli*, ABIN-2 was not required for clearance of internalised *C. rodentium*. As both species are Gram-negative extracellular enterobacteria, it suggests that other species-specific factors contribute to the differential requirement for ABIN-2 during infection with these bacteria.

Based on genomic studies, approximately one-third of the *C. rodentium* genome is unique when compared to *E. coli* (Petty *et al*, 2010). These *C. rodentium*-specific genes predominantly encode for proteins of secretion systems and virulence effector proteins (Petty *et al*, 2010). This may explain why *C. rodentium* is a pathogenic microbe causing colonic hyperplasia in mice, while *E. coli* K-12 is a non-pathogenic benign laboratory strain and gut commensal (Koli *et al*, 2011; Petty *et al*, 2010). Since *C. rodentium* encodes several secretion systems that allow for its escape from phagosomes, *C. rodentium* killing may become less dependent on fully functional phagosomes. Instead, clearance of *C. rodentium* in mice is dependent on NLRP3 inflammasome activation in the cytoplasm leading to inflammatory cell death and pyroptosis (Alipour *et al*, 2013; Song-Zhao *et al*, 2014). This may explain why defective phagosome maturation caused by *Abin2*^{D310N} mutation did not significantly impair killing of *C. rodentium* in murine macrophages. In future experiments, it will be important to show the effects of *Abin2*^{D310N} mutation on the maturation of phagosomes containing *E. coli* and *C. rodentium*. Since ABIN-2 is required for efficient killing of *E. coli*, it will be of particular interest to investigate whether loss of ubiquitin binding to ABIN-2 disrupts maturation of *E. coli* phagosomes. Specifically, it will be important to study whether cathepsin activity in *E. coli*-containing phagosomes is reduced by *Abin2*^{D310N} mutation.

My experiments indicated that ubiquitin binding to ABIN-2 was required for efficient killing of *Salmonella typhimurium*. *S. typhimurium* is a highly pathogenic Gram-negative bacterium that causes gastroenteritis and can have fatal outcomes in immunocompromised patients (Pham & McSorley, 2015). Ubiquitylation orchestrates many aspects of the host immune response to *S. typhimurium* infection, including the activation of inflammatory pathways (Fiskin *et al*, 2016). Ubiquitin also marks bacteria for removal by phagolysosomes and autophagosomes (Larock *et al*, 2015). ABIN-2 may function as a ubiquitin receptor to target ubiquitylated *S. typhimurium* bacteria to phagosomes. *S. typhimurium* is an intracellular pathogen that has evolved to escape from phagosomes and exploit the host machinery to drive its replication (Behnsen *et al*, 2015). Following *S. typhimurium* escape from the phagosomal lumen to the cytosol, *S. typhimurium* becomes heavily ubiquitylated, which results in the ubiquitin-dependent recruitment of autophagy receptors, including SQSTM1 and optineurin (OPTN) (Fiskin *et al*, 2016). While SQSTM1 strongly binds to K63-linked ubiquitin, OPTN contains, similar to ABIN-2, a UBAN domain that interacts with M1- and to a lesser extent K63-linked polyubiquitin chains (Wong & Holzbaur, 2014; Seibenhener *et al*, 2004; Li *et al*, 2018). Both SQSTM1 and OPTN recognise ubiquitylated *S. typhimurium* and mediate its delivery to autophagosomes, thus initiating *S. typhimurium* clearance by autophagy (Gomes & Dikic, 2014). In an analogous fashion to SQSTM1 and OPTN, ABIN-2 may function as an autophagy receptor that recognises ubiquitylated *S. typhimurium* in the cytosol following escape from the phagosome. In future experiments, it will be essential to decipher whether impaired *S. typhimurium* clearance in *Abin2*$^{D310N/D310N}$ BMDMs results from defects in phagosome maturation and/or autophagy. To investigate a potential function for ABIN-2 in mediating autophagosome formation during *S. typhimurium* infection, it will be of interest to investigate whether *Abin2*^{D310N} mutation disrupts LC3 co-localisation with bacteria following *S. typhimurium* infection. Moreover, monitoring cathepsin activity, phagosomal acidification and co-localisation of phagosomal markers, including EEA1 and LAMP1, with GFP-labelled *S. typhimurium* will provide insight as to whether *Abin2*^{D310N} mutation disrupts maturation of *S. typhimurium*-containing phagosomes.

5.3.2 ABIN-2 ubiquitin binding promotes phagosome maturation following *S. aureus* infection

My research revealed that loss of ubiquitin binding to ABIN-2 impaired killing of *S. aureus* by primary macrophages. Further studies demonstrated that *Abin2*^{D310N} mutation disrupted maturation of *S. aureus* phagosomes following phagocytic uptake of bacteria. The regulation of bacterial killing by ABIN-2 was restricted to its ability to interact with ubiquitin since *Abin2*^{E256K} mutation, which disrupts A20 binding, did not alter killing of *S. aureus*. Bafilomycin A1 pre-treatment only partially reduced, but not fully blocked, *S. aureus* killing. Given that bafilomycin A1 blocks phagosome maturation, my observations implied that an additional killing mechanism was involved in *S. aureus* clearance (Yamamoto *et al*, 1998). Macrophage killing of bacteria can be mediated by inflammasome activation and pyroptosis, which is induced by bacterial toxins or cytosolic bacteria that escape from phagosomes (Man *et al*, 2017). While pyroptosis-released bacteria are commonly killed by neutrophils, it has also been shown that pyroptosis can directly induce bacterial killing (Labbé & Saleh, 2008). I showed that ABIN-2 ubiquitin binding does not impair *S. aureus*-induced pyroptosis, which accounts for the partial block in bacterial killing by *Abin2*^{D310N} mutation. In addition, gasdermin D directly kills internalised bacteria (Liu *et al*, 2016; Evavold *et al*, 2018). *Abin2*^{D310N} mutation did not regulate *S. aureus*-induced gasdermin D cleavage, which provided a further explanation why loss of ABIN-2 ubiquitin binding did not fully block *S. aureus* killing.

ABIN-2 ubiquitin binding was required for optimal proteolysis within *S. aureus* phagosomes, as reflected by activity of the phagosomal protease cathepsin L. In contrast, ABIN-2 was not required for efficient acidification of *S. aureus* phagosomes. These observations mirrored my results obtained with silica and latex beads. While *Abin2*^{D310N} mutation did not regulate co-localisation of *S. aureus* phagosomes with EEA1, loss of ubiquitin binding to ABIN-2 impaired co-localisation of *S. aureus* phagosomes with LAMP1. These observations implied that ABIN-2 regulates phagosome maturation not at the early but at the late stage of maturation.

At present, the precise molecular mechanism by which ubiquitin binding to ABIN-2 regulates maturation of *S. aureus* phagosomes remains to be elucidated. However,

I provided initial evidence that loss of ABIN-2 ubiquitin binding reduced the percentage of ubiquitin$^+$ *S. aureus* phagosomes. It is important to note that I did not conclusively determine whether these ubiquitin modifications were directly attached to *S. aureus* bacteria, or whether the visualised ubiquitin puncta reflected ubiquitylated proteins on phagosomal membranes. It will be of interest to conduct further immunofluorescence studies to assess whether these ubiquitin puncta co-localise with phagosomal proteins, including LAMP1. The Trost laboratory and I have shown that K63-linked ubiquitin chains are highly abundant on latex bead phagosomes in macrophages (Guo *et al*, 2019). Therefore, the use of linkage-specific ubiquitin antibodies will shed light on chain topologies of ubiquitin puncta co-localising with *S. aureus* phagosomes in an ABIN-2-dependent manner.

Since ubiquitin regulates protein sorting to phagosomal membranes, my findings may suggest that ABIN-2 mediates trafficking of bactericidal ubiquitylated proteins to maturing phagosomes (Hicke & Dunn, 2003). Early studies demonstrated that translocation of ubiquitin to phagosomes is important to mediate the formation of MVBs. However, later studies indicated that ubiquitylation is important in directly promoting bacterial killing (Lee *et al*, 2005; Booth *et al*, 2002; Lawrence & Kornbluth, 2012). In support of this hypothesis, inhibition of deubiquitylases accelerates killing of phagosomal *L. monocytogenes* in primary macrophages (Burkholder *et al*, 2011). Strikingly, deubiquitylase inhibition significantly enhances the co-localisation of iNOS with *L. monocytogenes* phagosomes during infection (Burkholder *et al*, 2011). Moreover, it was previously proposed that ubiquitin localises to LAMP1$^+$ vesicles and that cathepsin-dependent proteolysis of ubiquitin yields products with anti-microbial potential that protect against *M. tuberculosis* infection (Alonso *et al*, 2007). Besides, recruitment of E3 ubiquitin ligases to phagosomes is critical to ensure efficient bacterial killing by macrophages (Lawrence & Kornbluth, 2012). During infection with *E. coli*, natural killer lytic-associated molecule (NKLAM), an E3 ubiquitin ligase generating K63-linked ubiquitin chains, promotes bacterial killing. Interestingly, NKLAM does not regulate phagocytic uptake or phagosomal acidification during *E. coli* infection (Lawrence & Kornbluth, 2012). These studies show that a protein of the ubiquitin system can promote bacterial killing without regulating phagocytic uptake or phagosomal acidification. Similarly to NKLAM, my findings indicated that ABIN-2 drives killing of bacteria without affecting acidification of phagosomes.

To further explore how ABIN-2 regulates maturation of *S. aureus* phagosomes, characterising the interactome of ABIN-2 following *S. aureus* infection will provide additional insight. More specifically, pulldowns of StrepII-ABIN-2 from *Abin2*$^{StrepII/StrepII}$ BMDMs following internalisation of *S. aureus* bacteria and subsequent MS analysis will likely identify regulators of phagosome maturation that are associated with ABIN-2 function. To determine whether *Abin2*^{Y231A} mutation promotes bacterial killing, *S. aureus* infection studies will reveal the potential importance of ESCRT-I binding to ABIN-2 in innate immune responses.

5.3.3 A novel role for TPL-2 in promoting bacterial killing by macrophages

In contrast to ABIN-2, TPL-2 has been implicated in driving immune responses to infection with several bacterial species, including *C. rodentium*, *L. monocytogenes*, and *M. tuberculosis* (Acuff *et al*, 2017b; McNab *et al*, 2013; Mielke *et al*, 2009). *Tpl2*$^{-/-}$ mice have been used to show that TPL-2 deficiency increases bacterial burden after infection due to defective innate immune responses. As previously discussed, *Tpl2*$^{-/-}$ mice are deficient in ABIN-2 as well as lacking TPL-2, and therefore findings from *Tpl2*$^{-/-}$ mice do not conclusively implicate TPL-2 catalytic activity in regulating bacterial killing. Although TPL-2 deficiency has been shown to increase bacterial burden in mice, TPL-2 has to date not been implicated in the regulation of phagosome maturation during infection.

Findings in this chapter demonstrated that TPL-2 catalytic activity was required for the efficient killing of *E. coli* and *C. rodentium*. Since *Tpl2*^{D270A} mutation impaired acidification of *C. rodentium* phagosomes, I showed for the first time that defective phagosome maturation resulting from inhibition of TPL-2 kinase activity underlies increased bacterial burden when TPL-2 function is lost. TPL-2-dependent defects in both phagosome maturation and expression of innate immune genes are likely to cooperatively contribute to increased *C. rodentium* infection when TPL-2 is absent.

My findings coincide with published *in vivo* infection models of *C. rodentium* and suggest that impaired phagosome maturation contributes, at least in part, to elevated

C. rodentium infection burden in *Tpl2*$^{-/-}$ mice (Acuff *et al*, 2017a, 2017b). Indeed, the Watford laboratory showed that TPL-2 promotes oxidative burst and bacterial killing by neutrophils during *C. rodentium* infection (Acuff *et al*, 2017b). Regulation of phagosome maturation in neutrophils differs from macrophages, whereby neutrophils are highly dependent on ROS generation (Nordenfelt & Tapper, 2011). Therefore, it is likely that phagosome maturation is regulated differently by TPL-2 in macrophages and neutrophils. Hence, future experiments addressing the function of TPL-2 in regulating phagosome maturation during bacterial infection in neutrophils will be of particular interest. While ubiquitin binding to ABIN-2 did not regulate killing of *C. rodentium*, TPL-2 catalytic activity was required for optimal killing of *C. rodentium*. At low pH, *C. rodentium* expresses secretion systems that mediate its escape from phagosomes (Araujo‐Garrido *et al*, 2020). Since *Tpl2*^{D270A} mutation impaired acidification of *C. rodentium* phagosomes, assembly of *C. rodentium* secretion systems may be inhibited in *Tpl2*$^{D270A/D270A}$ macrophages. Therefore, *C. rodentium* may be localised in non-microbicidal *Tpl2*$^{D270A/D270A}$ phagosomes for a prolonged period, thus enabling increased *C. rodentium* replication in the phagosomal lumen.

5.3.4 TPL-2 catalytic activity promotes phagosome maturation during *S. aureus* infection

The experimental evidence provided in this chapter demonstrated for the first time that TPL-2 catalytic activity is required for bacterial killing of *S. aureus* by macrophages. *Tpl2*^{D270A} mutation reduced cathepsin activity and blocked acidification of *S. aureus* phagosomes. Furthermore, decreased fractions of *S. aureus* phagosomes co-localised with EEA1 and LAMP1 when TPL-2 catalytic activity was blocked. Together, my results revealed that increased bacterial burden in *Tpl2*$^{D270A/D270A}$ macrophages following *S. aureus* infection resulted from impaired phagosome maturation. These findings were consistent with my previous observations using latex beads, which indicated that TPL-2 promotes both phagosomal proteolysis and acidification. Similar to inhibitory effects caused by *Abin2*^{D310N} mutation, *Tpl2*^{D270A} mutation only partially inhibited *S. aureus* killing. *Tpl2*^{D270A} mutation reduced bacterial killing to a similar extent as bafilomycin A1

treatment. Blocking phagosome maturation with bafilomycin A1 only reduces the rate of bacterial killing as other, phagosome-independent, killing mechanisms contribute to *S. aureus* clearance. The phagosome-independent killing of *S. aureus* via inflammasome activation and pyroptosis was, as with ABIN-2, not regulated by TPL-2. Moreover, gasdermin D directly kills internalised bacteria, in addition to inducing the release of pro-inflammatory IL-1β (Liu *et al*, 2016; Evavold *et al*, 2018). *Tpl2*^{D270A} mutation did not regulate *S. aureus*-induced gasdermin D cleavage, which provided further insights into why loss of TPL-2 catalytic activity did not fully block *S. aureus* killing.

In chapter four, I provided evidence that TPL-2-dependent phosphorylation of DMXL1 on S1903 induced phagosome acidification following uptake of beads. Although the detailed mechanism remains to be fully elucidated, it is likely that DMXL1 phosphorylation induces V-ATPase activity by promoting V_0 and V_1 complex assembly (Beyenbach & Wieczorek, 2006). Further studies are required to reveal the molecular mechanism by which TPL-2 catalytic activity promotes acidification of *S. aureus* phagosomes, however, my observations using beads suggest that TPL-2-dependent phosphorylation of DMXL1 may also regulate phagosome acidification via modulating V-ATPase assembly during *S. aureus* infection. Therefore, it will be important to determine whether DMXL1 phosphorylation at S1903 is induced by *S. aureus* infection and whether DMXL1 phosphorylation at S1903 is also regulated by TPL-2 catalytic activity following *S. aureus* infection.

I showed that TPL-2 catalytic activity was required for AKT activation following *S. aureus* infection of macrophages. Notably, I discovered that AKT activation was almost completely impaired if *S. aureus* internalisation is blocked by cytochalasin D (Agerer *et al*, 2005). This observation suggested that TPL-2-dependent AKT activation was mediated from phagosomes and not from the cell surface. Previous studies have shown that AKT signalling is activated following *S. aureus* infection and positively regulates phagocytosis (Lv *et al*, 2019; Oviedo-Boyso *et al*, 2011). In the previous chapter, I confirmed the importance of PI3K-AKT-mTOR signalling in driving phagosome proteolysis as well as acidification and described how this signalling axis regulates several aspects of phagosome maturation (Thi & Reiner, 2012). Activation of PI3K-AKT-mTOR signalling from phagosomal membranes may be an alternative

pathway, besides DMXL1 phosphorylation, by which TPL-2 promotes maturation of *S. aureus* phagosomes to induce bacterial killing.

5.3.5 TPL-2 catalytic activity suppresses type I interferon expression during *S. aureus* infection

In addition to its stimulatory effects on phagosome maturation, TPL-2 rapidly activated ERK1/2 MAP kinases from the plasma membrane and induced the expression of MAP kinase signature genes following *S. aureus* infection of BMDMs. Cytochalasin D pre-treatment did not block MAPK activation by *S. aureus*, which implied that TPL-2 signals from two different cellular locations following *S. aureus* infection.

Following *S. aureus* infection, *Tpl2*^{D270A} mutation decreased mRNA expression levels of numerous innate immune genes, including cytokines and chemokines. These observations coincided with previous findings implicating TPL-2 catalytic activity in the ERK1/2-dependent expression of innate immune genes following activation of PRRs (Gantke et al., 2011; Martel et al., 2013; Dr Michael Pattison, unpublished findings). TLR2 deficiency causes dramatic susceptibility to *S. aureus* infection *in vivo*, indicating that TLR2-induced signalling pathways mediate the innate immune response to *S. aureus* (Takeuchi *et al*, 2000). My results presented in this chapter are in line with previous studies showing that TPL-2 activates TLR2-induced innate immune signalling pathways in primary macrophages (Banerjee *et al*, 2006). Moreover, TPL-2 regulated MAPK pathways following Pam_3CSK_4 stimulation, which explains why immune signalling during *S. aureus* infection was dependent on TPL-2 (Yang *et al*, 2012).

Many TLRs, including TLR2, have the ability to signal from the endosomal compartment to trigger type I interferon expression (O'Neill & Bowie, 2007; Stack *et al*, 2014; Dietrich *et al*, 2010). Importantly, TLR2-dependent signalling from endosomes following *S. aureus* infection promotes type I interferon expression and bacterial survival (Musilova *et al*, 2019). Here, I provided evidence that upon *S. aureus* infection, TPL-2 catalytic activity strongly suppressed mRNA expression of

type I IFN genes, including *Ifnb1*, *Ifna1*, *Ifna2*, *Ifna5* and *Ifna6*, as well as multiple ISGs. As discussed, TPL-2 suppresses *Ifnb1* expression following TLR4 activation with soluble LPS. TPL-2-mediated inhibition of *Ifna* genes only occurred following internalisation of *S. aureu*s or LPS-coated beads, as previously outlined. These observations suggested that TPL-2 inhibits *Ifna* gene expression from endosomal compartments. This hypothesis coincides with previous studies demonstrating that TPL-2 suppresses *M. tuberculosis*-induced expression of *Ifna2*, *Ifna5* and *Ifna6* (McNab *et al*, 2013).

To consolidate that TLR-mediated pathways from the endosomal compartment induce type I IFN signalling, macrophages will be pre-treated with cytochalasin D to inhibit *S. aureus* internalisation. I hypothesise that cytochalasin D pre-treatment will abrogate expression of *Ifna* genes following *S. aureus* infection. This observation would confirm that TPL-2 suppresses *S. aureus*-induced type I IFN production from intracellular vesicles. Two protein kinases, TANK-binding kinase 1 (TBK1) and IKKε, drive type I IFN production during bacterial infection by phosphorylating the IRF3 transcription factor (Ikeda *et al*, 2007; Perry *et al*, 2004; Hemmi *et al*, 2004). To gain further insight into how TPL-2 regulates type I IFN production, it will be of interest to assess whether *Tpl2*^{D270A} mutation regulates TBK1 and IKKε phosphorylation during *S. aureus* infection. Moreover, monitoring TBK1 and IKKε phosphorylation following cytochalasin D pre-treatment upon *S. aureus* infection will reveal whether these kinases are phosphorylated downstream of TPL-2 from endosomal compartments. Lastly, pharmacological inhibition of TBK1 and IKKε following *S. aureus* internalisation, using the specific cell-permeable BX795 inhibitor, will confirm the potential requirement for TBK1 and IKKε activity to induce expression type I IFN genes during *S. aureus* infection (Clark *et al*, 2009).

Ifnar$^{-/-}$ mice, which cannot respond to type I IFNs, are substantially protected against *S. aureus* in the pneumonia lung infection model compared with WT control mice. Type I IFNs inhibit the transcription of *Il1b* and processing of IL-1β by inflammasomes, thereby reducing recruitment of neutrophils to sites of infection to increase susceptibility to *S. aureus* infection (Scumpia *et al*, 2017). TPL-2 activation of ERK1/2 also rapidly induces *Il1b* mRNA expression in macrophages following TLR

stimulation (McNab *et al*, 2013; Sriskantharajah *et al*, 2014). Consistent with this, I showed that *Il1b* mRNA levels were significantly decreased by *Tpl2*^{D270A} mutation following *S. aureus* infection. TPL-2 inhibition of type I IFN production and induction of IL-1β are therefore expected to promote more effective innate immune responses to *S. aureus* (Martin *et al*, 2009). It will thus be important to further investigate the immune responses, including tissue inflammation and bacterial burden, of *Tpl2*$^{D270A/D270A}$ mice to *S. aureus* infection *in vivo*. Similarly, TPL-2 inhibition of type I IFN gene expression is important for effective innate immune responses in mice to *L. monocytogenes* and *M. tuberculosis* (McNab *et al*, 2013; Mielke *et al*, 2009). This implies that TPL-2-dependent suppression of type I IFN gene expression is a common mechanism by which TPL-2 regulates anti-bacterial immune responses to a plethora of bacterial species.

5.3.6 Loss of TPL-2 catalytic activity protects against *S. typhimurium* infection

Since I demonstrated that TPL-2 expression protects against *E. coli*, *C. rodentium* and *S. aureus* infection, the initial observation that TPL-2 expression increases susceptibility to *S. typhimurium* infection was surprising. However, in contrast to other bacterial species studied here, *S. typhimurium* is a facultative intracellular bacterium that has acquired a comprehensive repertoire of immune evasion mechanisms to counteract and exploit innate and adaptive immune responses (Riquelme *et al*, 2011; Behnsen *et al*, 2015).

Although the low pH in the phagosomal lumen is generally a microbicidal milieu for internalised bacteria, phagosomal acidification is a prerequisite for *S. typhimurium* replication. Acidification of the *S. typhimurium* phagosome stimulates assembly of the SPI-2 T3SS (Yu *et al*, 2010; Rappl *et al*, 2003). The SPI-2 T3SS is important for the life cycle of *S. typhimurium* as this multiprotein complex delivers bacterial virulence effector proteins directly from the bacterial into the host cell cytosol (Wang *et al*, 2020). While *Tpl2*^{D270A} mutation accelerated bacterial killing of WT *S. typhimurium*, I showed that *Tpl2*^{D270A} mutation did not accelerate killing of an *S. typhimurium* mutant strain that lacked expression of SsaV. SsaV is located in the

inner bacterial membrane and is critical for the function of the SPI-2 T3SS (Yu *et al*, 2010). The T3SS translocates effectors, including SseF and SseJ, through the inner and outer bacterial membrane towards the T3SS needle, which penetrates the phagosomal membrane and delivers virulence effectors into the host cell cytosol (Mesquita *et al*, 2012; Günster *et al*, 2017; Yu *et al*, 2010). The *S. typhimurium* mutant strain lacking expression of SsaV is resistant to pH changes within the phagosomal lumen as acidification-induced SPI-2 T3SS assembly is blocked. Since SsaV deficiency rescued impaired *S. typhimurium* replication, it suggests that TPL-2-mediated phagosomal acidification is required for the assembly of the SPI-2 T3SS by *S. typhimurium* during infection. It also raises the possibility that pharmacological inhibition of TPL-2 may increase susceptibility to *S. typhimurium* infection. It will be of interest to investigate whether *Tpl2*$^{D270A/D270A}$ mice are protected against bacterial growth during *S. typhimurium* infection *in vivo*. To determine whether TPL-2 catalytic activity regulates secretion of *S. typhimurium* effector proteins from phagosomes, WT and *Tpl2*$^{D270A/D270A}$ macrophages will be infected with an *S. typhimurium* mutant strain expressing HA-tagged SseL, an effector protein that is translocated into host cells in a SPI-2-dependent manner. Immunoblotting will reveal whether *Tpl2*^{D270A} mutation impairs translocation of SseL effector proteins via the SPI-2 T3SS into the host cell cytosol.

Reference List

Van Acker GJD, Perides G, Weiss ER, Das S, Tsichlis PN & Steer ML (2007) Tumor progression locus-2 is a critical regulator of pancreatic and lung inflammation during acute pancreatitis. *J. Biol. Chem.* **282:** 22140–22149

Acuff N V., Latha K, Nagy T & Watford WT (2017a) Tpl2 Promotes Innate Cell Recruitment and Effector T Cell Differentiation To Limit Citrobacter rodentium Burden and Dissemination. *Infect. Immun.* **85:** 1–13

Acuff N V., Li X, Elmore J, Rada B & Watford WT (2017b) Tpl2 promotes neutrophil trafficking, oxidative burst, and bacterial killing. *J. Leukoc. Biol.* **101:** 1325–1333

Adachi O, Kawai T, Takeda K, Matsumoto M, Tsutsui H, Sakagami M, Nakanishi K & Akira S (1998) Targeted disruption of the MyD88 gene results in loss of IL-1- and IL- 18-mediated function. *Immunity* **9:** 143–150

Agerer F, Lux S, Michel A, Rohde M, Ohlsen K & Hauck CR (2005) Cellular invasion by Staphylococcus aureus reveals a functional link between focal adhesion kinase and cortactin in integrin-mediated internalisation. *J. Cell Sci.* **118:** 2189–2200

Agou F, Courtois G, Chiaravalli J, Baleux F, Coïc YM, Traincard F, Israël A & Véron M (2004) Inhibition of NF-κB activation by peptides targeting NF-κB essential modulator (NEMO) oligomerization. *J. Biol. Chem.* **279:** 54248–54257

Akira S, Uematsu S & Takeuchi O (2006) Pathogen recognition and innate immunity. *Cell* **124:** 783–801

Aktan F (2004) iNOS-mediated nitric oxide production and its regulation. *Life Sci.* **75:** 639–653

Akutsu M, Dikic I & Bremm A (2016) Ubiquitin chain diversity at a glance. *J. Cell Sci.* **129:** 875–880

Alexopoulou L, Holt A, Medzhitov R & Flavell R (2001) Recognition of double-stranded RNA and activation of NF-kappaB by Toll. *Nature* **413:** 732–738

Alipour M, Lou Y, Zimmerman D, Bording-Jorgensen MW, Sergi C, Liu JJ & Wine E (2013) A balanced IL-1β activity is required for host response to Citrobacter rodentium infection. *PLoS One* **8:**

Alonso S, Pethe K, Russell DG & Purdy GE (2007) Lysosomal killing of Mycobacterium mediated by ubiquitin-derived peptides is enhanced by autophagy. *Proc. Natl. Acad. Sci. U. S. A.* **104:** 6031–6036

Ananieva O, Darragh J, Johansen C, Carr JM, McIlrath J, Park JM, Wingate A, Monk CE, Toth R, Santos SG, Iversen L & Arthur JSC (2008) The kinases MSK1 and MSK2 act as negative regulators of Toll-like receptor signaling. *Nat. Immunol.* **9:** 1028–1036

Andersen-Nissen E, Smith KD, Strobe KL, Rassoulian Barrett SL, Cookson BT, Logan SM & Aderem A (2005) Evasion of Toll-like receptor 5 by flagellated bacteria. *Proc. Natl. Acad. Sci. U. S. A.* **102:** 9247–9252

Anderson CL, Shen L, Eicher DM, Wewers MD & Gill JK (1990) Phagocytosis mediated by three distinct Fcγ receptor classes on human leukocytes. *J. Exp. Med.* **171:** 1333–1345

Anderson KE, Chessa TAM, Davidson K, Henderson RB, Walker S, Tolmachova T, Grys K, Rausch O, Seabra MC, Tybulewicz VLJ, Stephens LR & Hawkins PT (2010) PtdIns3P and Rac direct the assembly of the NADPH oxidase on a novel, pre-phagosomal compartment during FcR-mediated phagocytosis in primary mouse neutrophils. *Blood* **116:** 4978–4989

Aoki M, Hamada F, Sugimoto T, Sumida S, Akiyama T & Toyoshima K (1993) The human cot proto-oncogene encodes two protein serine/threonine kinases with

different transforming activities by alternative initiation of translation. *J. Biol. Chem.* **268:** 22723–22732

Araki N, Johnson MT & Swanson JA (1996) A role for phosphoinositide 3-kinase in the completion of macropinocytosis and phagocytosis by macrophages. *J. Cell Biol.* **135:** 1249–1260

Araujo-Garrido JL, Bernal-Bayard J & Ramos-Morales F (2020) Type III secretion effectors with arginine n-glycosyltransferase activity. *Microorganisms* **8:**

Arnett E, Lehrer RI, Pratikhya P, Lu W & Seveau S (2011) Defensins enable macrophages to inhibit the intracellular proliferation of Listeria monocytogenes. *Cell. Microbiol.* **13:** 635–651

Arthur JSC & Ley SC (2013) Mitogen-activated protein kinases in innate immunity. *Nat. Rev. Immunol.* **13:** 679–692

Astarie-Dequeker C, N'Diaye EN, Le Cabec V, Rittig MG, Prandi J & Maridonneau-Parini I (1999) The mannose receptor mediates uptake of pathogenic and nonpathogenic mycobacteria and bypasses bactericidal responses in human macrophages. *Infect. Immun.* **67:** 469–477

Babior BM (2004) NADPH oxidase. *Curr. Opin. Immunol.* **16:** 42–47

Babu GR, Jin W, Norman L, Waterfield M, Chang M, Wu X, Zhang M & Sun SC (2006) Phosphorylation of NF-κB1/p105 by oncoprotein kinase Tpl2: Implications for a novel mechanism of Tpl2 regulation. *Biochim. Biophys. Acta - Mol. Cell Res.* **1763:** 174–181

Bain CC, Bravo-Blas A, Scott CL, Gomez Perdiguero E, Geissmann F, Henri S, Malissen B, Osborne LC, Artis D & Mowat AMI (2014) Constant replenishment from circulating monocytes maintains the macrophage pool in the intestine of adult mice. *Nat. Immunol.* **15:** 929–937

Bain J, McLauchlan H, Elliott M & Cohen P (2003) The specificities of protein kinase inhibitors: An update. *Biochem. J.* **371:** 199–204

Bain J, Plater L, Elliott M, Shpiro N, Hastie CJ, Mclauchlan H, Klevernic I, Arthur JSC, Alessi DR & Cohen P (2007) The selectivity of protein kinase inhibitors: A further update. *Biochem. J.* **408:** 297–315

Bandow K, Kusuyama J, Shamoto M, Kakimoto K, Ohnishi T & Matsuguchi T (2012) LPS-induced chemokine expression in both MyD88-dependent and -independent manners is regulated by Cot/Tpl2-ERK axis in macrophages. *FEBS Lett.* **586:** 1540–1546

Banerjee A, Gugasyan R, McMahon M & Gerondakis S (2006) Diverse Toll-like receptors utilize Tpl2 to activate extracellular signal-regulated kinase (ERK) in hemopoietic cells. *Proc. Natl. Acad. Sci. U. S. A.* **103:** 3274–3279

Banks CAS, Boanca G, Lee ZT, Eubanks CG, Hattem GL, Peak A, Weems LE, Conkright JJ, Florens L & Washburn MP (2016) TNIP2 is a hub protein in the NF- κ B network with both protein and RNA mediated interactions. *Mol. Cell. Proteomics* **15:** 3435–3449

Bardwell L (2006) Mechanisms of MAPK signalling specificity. *Biochem Soc Trans.* **34:** 837–841

Barnett SF, Defeo-Jones D, Fu S, Hancock PJ, Haskell KM, Jones RE, Kahana JA, Kral AM, Leander K, Lee LL, Malinowski J, McAvoy EM, Nahas DD, Robinson RG & Huber HE (2005) Identification and characterization of pleckstrin-homology-domain-dependent and isoenzyme-specific Akt inhibitors. *Biochem. J.* **385:** 399–408

Barton GM, Kagan JC & Medzhitov R (2006) Intracellular localization of Toll-like receptor 9 prevents recognition of self DNA but facilitates access to viral DNA. *Nat. Immunol.* **7:** 49–56

Behnsen J, Perez-Lopez A, Nuccio SP & Raffatellu M (2015) Exploiting host immunity: The Salmonella paradigm. *Trends Immunol.* **36:** 112–120

Beinke S, Deka J, Lang V, Belich MP, Walker PA, Howell S, Smerdon SJ, Gamblin SJ & Ley SC (2003) NF-κB1 p105 Negatively Regulates TPL-2 MEK Kinase Activity. *Mol. Cell. Biol.* **23:** 4739–4752

Beinke S, Robinson MJ, Hugunin M & Ley SC (2004) Lipopolysaccharide activation of the TPL-2/MEK/extracellular signal-regulated kinase mitogen-activated protein kinase cascade is regulated by IκB kinase-induced proteolysis of NF-κB1 p105. *Mol. Cell. Biol.* **24:** 9658–9667

Belich MP, Salmerón A, Johnston LH & Ley SC (1999) TPL-2 kinase regulates the proteolysis of the NF-kappaB-inhibitory protein NF-kappaB1 p105. *Nature* **397:** 363–368

Ben-Addi A, Mambole-Dema A, Brender C, Martin SR, Janzen J, Kjaer S, Smerdon SJ & Ley SC (2014) IκB kinase-induced interaction of TPL-2 kinase with 14-3-3 is essential for Toll-like receptor activation of ERK-1 and -2 MAP kinases. *Proc. Natl. Acad. Sci. U. S. A.* **111:** 2394–2403

Beutler B (2004) Innate immunity: An overview. *Mol. Immunol.* **40:** 845–859

Beyenbach KW & Wieczorek H (2006) The V-type H+ ATPase: Molecular structure and function, physiological roles and regulation. *J. Exp. Biol.* **209:** 577–589

Bhattacharyya RP, Reményi A, Yeh BJ & Lim WA (2006) Domains, Motifs, and Scaffolds: The Role of Modular Interactions in the Evolution and Wiring of Cell Signaling Circuits. *Annu. Rev. Biochem.* **75:** 655–680

Bidani A, Reisner BS, Haque AK, Wen J, Helmer RE, Tuazon DM & Heming TA (2000) Bactericidal Activity of Alveolar Macrophages is Suppressed by V-ATPase Inhibition. *Lung* **178:** 91–104

Binker MG, Cosen-Binker LI, Terebiznik MR, Mallo G V., Mccaw SE, Eskelinen EL, Willenborg M, Brumell JH, Saftig P, Grinstein S & Gray-Owen SD (2007) Arrested maturation of Neisseria -containing phagosomes in the absence of the lysosome-associated membrane proteins, LAMP-1 and LAMP-2. *Cell. Microbiol.* **9:** 2153–2166

Biondi RM & Nebreda AR (2003) Signalling specificity of Ser/Thr protein kinases through docking-site-mediated interactions. *Biochem. J.* **372:** 1–13

Blander JM & Medzhitov R (2004) Regulation of Phagosome Maturation by Signals from Toll-Like Receptors. *Science (80-.).* **304:** 1014–1018

Blasi E , Radzioch D , Merletti L VL (1989) Generation of macrophage cell line from fresh bone marrow cells with a myc/raf recombinant retrovirus. *Cancer Biochem Biophys* **10:** 303–317

Bone M, Nardo D De, Kalvakolanu D V & Latz E (2018) Chapter 4 - Immortalization of Murine Bone Marrow-Derived Macrophages. *Springer Sci.* **1784:** 35–49

Booth JW, Kim MK, Jankowski A, Schreiber AD & Grinstein S (2002) Contrasting requirements for ubiquitylation during Fc receptor-mediated endocytosis and phagocytosis. *EMBO J.* **21:** 251–258

Botos I, David M. S & Davies DR (2011) The Structural Biology of Toll-Like Receptors Istvan. *Structure* **19:** 447–459

Boulais J, Trost M, Landry CR, Dieckmann R, Levy ED, Soldati T, Michnick SW, Thibault P & Desjardins M (2010) Molecular characterization of the evolution of phagosomes. *Mol. Syst. Biol.* **6:** 1–14

Bouwmeester T, Bauch A, Ruffner H, Angrand PO, Bergamini G, Croughton K, Cruciat C, Eberhard D, Gagneur J, Ghidelli S, Hopf C, Huhse B, Mangano R, Michon AM, Schirle M, Schlegl J, Schwab M, Stein MA, Bauer A, Casari G, et al (2004) A physical and functional map of the human TNF-α/NF-κB signal transduction pathway. *Nat. Cell Biol.* **6:** 97–105

Bradford M (1976) A rapid and sensitive method for the quantitation of microgram quantities of protein utilizing the principle of protein-dye binding. *Anal. Biochem.* **72:** 248–254

Burkholder KM, Perry JW, Wobus CE, Donato NJ, Showalter HD, Kapuria V & O'Riordan MXD (2011) A small molecule deubiquitinase inhibitor increases localization of inducible nitric oxide synthase to the macrophage phagosome and enhances bacterial killing. *Infect. Immun.* **79:** 4850–4857

Burns K, Martinon F, Esslinger C, Pahl H, Schneider P, Bodmer JL, Di Marco F, French L & Tschopp J (1998) MyD88, an adapter protein involved in interleukin-1 signaling. *J. Biol. Chem.* **273:** 12203–12209

Butler MP, Hanly JA & Moynagh PN (2007) Kinase-active interleukin-1 receptor-associated kinases promote polyubiquitination and degradation of the Pellino family: Direct evidence for Pellino proteins being ubiquitin-protein isopeptide ligases. *J. Biol. Chem.* **282:** 29729–29737

Campbell L, Saville CR, Murray PJ, Cruickshank SM & Hardman MJ (2013) Local arginase 1 activity is required for cutaneous wound healing. *J. Invest. Dermatol.* **133:** 2461–2470

Campos MAS, Almeida IC, Takeuchi O, Akira S, Valente EP, Procópio DO, Travassos LR, Smith JA, Golenbock DT & Gazzinelli RT (2001) Activation of Toll-Like Receptor-2 by Glycosylphosphatidylinositol Anchors from a Protozoan Parasite. *J. Immunol.* **167:** 416–423

Cantalupo G, Alifano P, Roberti V, Bruni CB & Bucci C (2001) Rab-interacting lysosomal protein (RILP): The Rab7 effector required for transport to lysosomes. *EMBO J.* **20:** 683–693

Cantrell D (1996) T cell antigen receptor signal transduction pathways. *Annu. Rev. Immunol.* **14:** 259–274

Cardoso CMP, Jordao L & Vieira O V. (2010) Rab10 regulates phagosome maturation and its overexpression rescues Mycobacterium-containing phagosomes maturation. *Traffic* **11:** 221–235

Caron E & Hall A (1998) Identification of two distinct mechanisms of phagocytosis controlled by different Rho GTPases. *Science (80-.).* **282:** 1717–1721

Catrysse L, Vereecke L, Beyaert R & Loo G Van (2014) A20 in inflammation and autoimmunity. *Trends Immunol.* **35:** 22–31

Ceci JD, Patriotis CP, Tsatsanis C, Makris AM, Kovatch R, Swing DA, Jenkins NA, Tsichlis PN & Copeland NG (1997) Tpl-2 is an oncogenic kinase that is activated by carboxy-terminal truncation. *Genes Dev.* **11:** 688–700

Chakravortty D & Hensel M (2003) Inducible nitric oxide synthase and control of intracellular bacterial pathogens. *Microbes Infect.* **5:** 621–627

Chamberlain MD, Berry TR, Pastor MC & Anderson DH (2004) The p85α subunit of phosphatidylinositol 3′-kinase binds to and stimulates the GTPase activity of Rab proteins. *J. Biol. Chem.* **279:** 48607–48614

Chan SL, Mukasa T, Santelli E, Low LY & Pascual J (2010) The crystal structure of a TIR domain from Arabidopsis thaliana reveals a conserved helical region unique to plants. *Protein Sci.* **19:** 155–161

Chang C (2014) Autoimmunity: From black water fever to regulatory function. *J. Autoimmun.* **48–49:** 1–9

Chaplin DD (2010) Overview of the Immune Response. *J Allergy Clin Immunol* **125:** 2–39

Chau V, Tobias JW, Bachmair A, Marriott D, Ecker DJ, Gonda DK & Varshavsky A (1989) A multiubiquitin chain is confined to specific lysine in a targeted short-lived protein. *Science (80-.).* **243:** 1576–1583

Chen BC, Chen YH & Lin WW (1999) Involvement of p38 mitogen-activated protein kinase in lipopolysaccharide-induced iNOS and COX-2 expression in J774 macrophages. *Immunology* **97:** 124–129

Chen D, Jian Y, Liu X, Zhang Y, Liang J, Qi X, Du H, Zou W, Chen L, Chai Y, Ou G, Miao L, Wang Y & Yang C (2013) Clathrin and AP2 Are Required for Phagocytic

Receptor-Mediated Apoptotic Cell Clearance in Caenorhabditis elegans. *PLoS Genet.* **9:** 1–18

Chen J & Chen ZJ (2013) Regulation of NF-κB by ubiquitination. *Curr. Opin. Immunol.* **25:** 4–12

Chen L, Deng H, Cui H, Fang J, Zuo Z, Deng J, Li Y, Wang X & Zhao L (2018) Inflammatory responses and inflammation-associated diseases in organs. *Oncotarget* **9:** 7204–7218

Cheng H, Addona T, Keshishian H, Dahlstrand E, Lu C, Dorsch M, Li Z, Wang A, Ocain TD, Li P, Parsons TF, Jaffee B & Xu Y (2007) Regulation of IRAK-4 kinase activity via autophosphorylation within its activation loop. *Biochem. Biophys. Res. Commun.* **352:** 609–616

Cheung PCF, Campbell DG, Nebreda AR & Cohen P (2003) Feedback control of the protein kinase TAK1 by SAPK2a/p38α. *EMBO J.* **22:** 5793–5805

Chien CY, Liu WK, Chou CK & Su JY (2003) The A20-binding protein ABIN-2 exerts unexpected function in mediating transcriptional coactivation. *FEBS Lett.* **543:** 55–60

Cho J, Melnick M, Solidakis GP & Tsichlis PN (2005) Tpl2 (tumor progression locus 2) phosphorylation at Thr 290 is induced by lipopolysaccharide via an Iκ-B kinase-β-dependent pathway and is required for Tpl2 activation by external signals. *J. Biol. Chem.* **280:** 20442–20448

Cho J & Tsichlis PN (2005) Phosphorylation at Thr-290 regulates Tpl2 binding to NF-κB1/p105 and Tpl2 activation and degradation by lipopolysaccharide. *Proc. Natl. Acad. Sci. U. S. A.* **102:** 2350–2355

Chresta CM, Davies BR, Hickson I, Harding T, Cosulich S, Critchlow SE, Vincent JP, Ellston R, Jones D, Sini P, James D, Howard Z, Dudley P, Hughes G, Smith L, Maguire S, Hummersone M, Malagu K, Menear K, Jenkins R, et al (2010) AZD8055 is a potent, selective, and orally bioavailable ATP-competitive mammalian target of rapamycin kinase inhibitor with in vitro and in vivo antitumor activity. *Cancer Res.* **70:** 288–298

Christoforidis S, McBride HM, Burgoyne RD & Zerial M (1999) The Rab5 effector EEA1 is a core component of endosome docking. *Nature* **397:** 621–625

Chung H-Y, Morita E, von Schwedler U, Müller B, Kräusslich H-G & Sundquist WI (2008) NEDD4L Overexpression Rescues the Release and Infectivity of Human Immunodeficiency Virus Type 1 Constructs Lacking PTAP and YPXL Late Domains. *J. Virol.* **82:** 4884–4897

Ciechanover A, Hod Y & Hershko A (1978) A heat-stable polypeptide component of an ATP-dependent proteolytic system from reticulocytes. 1978. *Biochem. Biophys. Res. Commun.* **81:** 1100–1105

Ciuffreda L, Del Bufalo D, Desideri M, Di Sanza C, Stoppacciaro A, Ricciardi MR, Chiaretti S, Tavolaro S, Benassi B, Bellacosa A, Foá R, Tafuri A, Cognetti F, Anichini A, Zupi G & Milella M (2009) Growth-inhibitory and antiangiogenic activity of the MEK inhibitor PD0325901 in malignant melanoma with or without BRAF mutations. *Neoplasia* **11:** 720–731

Clague MJ, Urbé S & Komander D (2019) Breaking the chains: deubiquitylating enzyme specificity begets function. *Nat. Rev. Mol. Cell Biol.* **20:** 338–352

Clark AM, Reynolds SH, Anderson M & Wiest JS (2004) Mutational activation of the MAP3K8 protooncogene in lung cancer. *Genes. Chromosomes Cancer* **41:** 99–108

Clark K, Nanda S & Cohen P (2013) Molecular control of the NEMO family of ubiquitin-binding proteins. *Nat. Rev. Mol. Cell Biol.* **14:** 673–685

Clark K, Plater L, Peggie M & Cohen P (2009) Use of the pharmacological inhibitor BX795 to study the regulation and physiological roles of TBK1 and IκB Kinase ∈:A distinct upstream kinase mediates ser-172 phosphorylation and activation. *J. Biol. Chem.* **284:** 14136–14146

Cohen P (2000) The regulation of protein function by multisite phosphorylation - A 25 year update. *Trends Biochem. Sci.* **25:** 596–601

Cohen P (2002) The origins of protein phosphorylation. *Nat. Cell Biol.* **4:** 127–130

Cohen P (2009) Targeting protein kinases for the development of anti-inflammatory drugs. *Curr. Opin. Cell Biol.* **21:** 317–324

Cohen P (2014) The TLR and IL-1 signalling network at a glance. *J. Cell Sci.* **127:** 2383–2390

Cohen P & Alessi DR (2013) Kinase Drug Discovery – What ' s Next in the Field? *ACS Chem. Biol.* **8:** 96–104

Cohen S, Lahav-Baratz S & Ciechanover A (2006) Two distinct ubiquitin-dependent mechanisms are involved in NF-κB p105 proteolysis. *Biochem. Biophys. Res. Commun.* **345:** 7–13

Colaço A & Jäättelä M (2017) Ragulator-a multifaceted regulator of lysosomal signaling and trafficking. *J. Cell Biol.* **216:** 3895–3898

Collins JW, Keeney KM, Crepin VF, Rathinam VAK, Fitzgerald KA, Finlay BB & Frankel G (2014) Citrobacter rodentium: Infection, inflammation and the microbiota. *Nat. Rev. Microbiol.* **12:** 612–623

Collins RF, Schreiber AD, Grinstein S & Trimble WS (2002) Syntaxins 13 and 7 Function at Distinct Steps During Phagocytosis. *J. Immunol.* **169:** 3250–3256

Corrotte M, Chasserot-Golaz S, Huang P, Du G, Ktistakis NT, Frohman MA, Vitale N, Bader MF & Grant NJ (2006) Dynamics and function of phospholipase D and phosphatidic acid during phagocytosis. *Traffic* **7:** 365–377

Cox D, Berg JS, Cammer M, Chinegwundoh JO, Dale BM, Cheney RE & Greenberg S (2002) Myosin X is a downstream effector of PI(3)K during phagocytosis. *Nat. Cell Biol.* **4:** 469–477

Cox D, Lee DJ, Dale BM, Calafat J & Greenberg S (2000) A Rab11-containing rapidly recycling compartment in macrophages that promotes phagocytosis. *Proc. Natl. Acad. Sci. U. S. A.* **97:** 680–685

Damiani MT, Pavarotti M, Leiva N, Lindsay AJ, McCaffrey MW & Colombo MI (2004) Rab coupling protein associates with phagosomes and regulates recycling from phagosomal compartment. *Traffic* **5:** 785–797

Darnell JE, Kerr IM & Stark GR (1994) Jak-STAT pathways and transcriptional activation in response to IFNs and other extracellular signaling proteins. *Science (80-.).* **264:** 1415–1421

Dasi S, Choi J, Lambertz I, Kelliher MA, Eliopoulos AG, Du K & Tsichlis PN (2005) Tp12/Cot signals activate ERK, JNK, and NF-κB in a cell-type and stimulus-specific manner. *J. Biol. Chem.* **280:** 23748–23757

Davies LC, Jenkins SJ, Allen JE & Taylor PR (2013) Tissue-resident macrophages. *Nat. Immunol.* **14:** 986–995

Dean P, Heunis T, Härtlova A & Trost M (2019) Regulation of phagosome functions by post-translational modifications: a new paradigm. *Curr. Opin. Chem. Biol.* **48:** 73–80

DeCoursey TE (2010) Voltage Gated Proton Channels Find Their Dream Job Managing the Respiratory Burst in Phagocytes. *Physiol.* **25:** 27–40

Dedio J, KÖNIG P, WOHLFART P, SCHROEDER C, KUMMER W & MÜLLER-ESTERL W (2001) NOSIP, a novel modulator of endothelial nitric oxide synthase activity. *FASEB J.* **15:** 79–89

DeFilippis VR, Robinson B, Keck TM, Hansen SG, Nelson JA & Früh KJ (2006) Interferon Regulatory Factor 3 Is Necessary for Induction of Antiviral Genes during Human Cytomegalovirus Infection. *J. Virol.* **80:** 1032–1037

Deng L, Wang C, Spencer E, Yang L, Braun A, You J, Slaughter C, Pickart C & Chen ZJ (2000) Activation of the Iκb kinase complex by TRAF6 requires a dimeric ubiquitin-conjugating enzyme complex and a unique polyubiquitin chain. *Cell* **103:** 351–361

Deng W, Vallance BA, Li Y, Puente JL & Finlay BB (2003) Citrobacter rodentium translocated intimin receptor (Tir) is an essential virulence factor needed for actin condensation, intestinal colonization and colonic hyperplasia in mice. *Mol. Microbiol.* **48:** 95–115

Diamond G, Beckloff N, Weinberg A & Kisich KO (2009) The Roles of Antimicrobial Peptides in Innate Host Defense. *Curr. Pharm. Des.* **15:** 2377–92

Dietrich N, Lienenklaus S, Weiss S & Gekara NO (2010) Murine Toll-Like Receptor 2 Activation Induces Type I Interferon Responses from Endolysosomal Compartments. *PLoS One* **5:** 1–10

Dikic I, Wakatsuki S & Walters KJ (2009) Ubiquitin-binding domains from structures to functions. *Nat. Rev. Mol. Cell Biol.* **10:** 659–671

Dill BD, Gierlinski M, Härtlova A, Arandilla AG, Guo M, Clarke RG & Trost M (2015) Quantitative Proteome Analysis of Temporally Resolved Phagosomes Following Uptake Via Key Phagocytic Receptors. *Mol. Cell. Proteomics* **14:** 1334–1349

Dinarello CA, Gatti S & Bartfai T (1999) Fever: Links with an ancient receptor. *Curr. Biol.* **9:** 147–150

Dobin A, Davis CA, Schlesinger F, Drenkow J, Zaleski C, Jha S, Batut P, Chaisson M & Gingeras TR (2013) STAR: Ultrafast universal RNA-seq aligner. *Bioinformatics* **29:** 15–21

Dong G, Chanudet E, Zeng N, Appert A, Chen YW, Au WY, Hamoudi RA, Watkins AJ, Ye H, Liu H, Gao Z, Chuang SS, Srivastava G & Du MQ (2011) A20, ABIN-1/2, and CARD11 mutations and their prognostic value in gastrointestinal diffuse large B-cell lymphoma. *Clin. Cancer Res.* **17:** 1440–1451

Doyette A, Russel MRG, Hopkins CR & Woodman PG (2005) Depletion of TSG101 forms a mammalian 'class E' compartment: A multicisternal early endosome with multiple sorting defects. *J. Cell Sci.* **118:** 3003–3017

Driskell OJ, Mironov A, Allan VJ & Woodman PG (2007) Dynein is required for receptor sorting and the morphogenesis of early endosomes. *Nat. Cell Biol.* **9:** 113–120

Duclos S, Diez R, Garin J, Papadopoulou B, Descoteaux A, Stenmark H & Desjardins M (2000) Rab5 regulates the kiss and run fusion between phagosomes and endosomes and the acquisition of phagosome leishmanicidal properties in RAW 264.7 macrophages. *J. Cell Sci.* **113:** 3531–3541

Duffy JP, Harrington EM, Salituro FG, Cochran JE, Green J, Gao H, Bemis GW, Evindar G, Galullo VP, Ford PJ, Germann UA, Wilson KP, Bellon SF, Chen G, Taslimi P, Jones P, Huang C, Pazhanisamy S, Wang YM, Murcko MA, et al (2011) The discovery of VX-745: A novel and selective p38α kinase inhibitor. *ACS Med. Chem. Lett.* **2:** 758–763

Dumitru CD, Ceci JD, Tsatsanis C, Kontoyiannis D, Stamatakis K, Lin JH, Patriotis C, Jenkins NA, Copeland NG, Kollias G & Tsichlis PN (2000) TNFalpha induction by LPS is regulated posttranscriptionally via a Tpl2/ERK-dependent pathway. *Cell* **103:** 1071–1083

Duque GA & Descoteaux A (2014) Macrophage cytokines: Involvement in immunity and infectious diseases. *Front. Immunol.* **5:** 1–12

Van Dyken SJ & Locksley RM (2013) Interleukin-4- and Interleukin-13-Mediated Alternatively Activated Macrophages: Roles in Homeostasis and Disease. *Annu. Rev. Immunol.* **31:** 317–343

Ea CK, Deng L, Xia ZP, Pineda G & Chen ZJ (2006) Activation of IKK by TNFα Requires Site-Specific Ubiquitination of RIP1 and Polyubiquitin Binding by NEMO. *Mol. Cell* **22:** 245–257

Eaton S & Martin-Belmonte F (2014) Cargo sorting in the endocytic pathway: A key regulator of cell polarity and tissue dynamics. *Cold Spring Harb. Perspect. Biol.* **14:**

Echols N, Harrison P, Balasubramanian S, Luscombe NM, Paul B, Zhaolei Z & Gerstein M (2002) Comprehensive analysis of amino acid and nucleotide composition in

eukaryotic genomes, comparing genes and pseudogenes. *Nucleic Acids Res.* **30:** 2515–2523

Edimo WE, Janssens V, Waelkens E & Erneux C (2012) Reversible Ser/Thr SHIP phosphorylation: A new paradigm in phosphoinositide signalling?: Targeting of SHIP1/2 phosphatases may be controlled by phosphorylation on Ser and Thr residues. *BioEssays* **34:** 634–642

Eliopoulos AG, Dumitru CD, Wang CC, Cho J & Tsichlis PN (2002) Induction of COX-2 by LPS in macrophages is regulated by Tpl2-dependent CREB activation signals. *EMBO J.* **21:** 4831–4840

Eliopoulos AG, Wang CC, Dumitru CD & Tsichlis PN (2003) Tpl2 transduces CD40 and TNF signals that activate ERK and regulates IgE induction by CD40. *EMBO J.* **22:** 3855–3864

Emmerich CH, Bakshi S, Kelsall IR, Ortiz-Guerrero J, Shpiro N & Cohen P (2016) Lys63/Met1-hybrid ubiquitin chains are commonly formed during the activation of innate immune signalling. *Biochem. Biophys. Res. Commun.* **474:** 452–461

Emmerich CH, Ordureau A, Strickson S, Arthur JSC, Pedrioli PGA, Komander D & Cohen P (2013) Activation of the canonical IKK complex by K63/M1-linked hybrid ubiquitin chains. *Proc. Natl. Acad. Sci. United States Am.* **110:** 15247–15252

Erny KM, Peli J, Lambert JF, Muller V & Diggelmann H (1996) Involvement of the Tpl-2/cot oncogene in MMTV tumorigenesis. *Oncogene* **13:** 2015–2020

Etzioni A (2003) Immuno deficiency and autoinmunity. *Autoimmun Rev* **2:** 364–369

Evavold CL, Ruan J, Tan Y, Xia S, Wu H & Kagan JC (2018) The Pore-Forming Protein Gasdermin D Regulates Interleukin-1 Secretion from Living Macrophages. *Immunity* **48:** 35-44.e6

Fader CM & Colombo MI (2009) Autophagy and multivesicular bodies: two closely related partners. *Cell Death Differ.* **16:** 70–78

Fernández M, Manso R, Bernáldez F, López P, Martín-Duce A & Alemany S (2011) Involvement of Cot activity in the proliferation of ALCL lymphoma cells. *Biochem. Biophys. Res. Commun.* **411:** 655–660

Ferrell JE (1996) Tripping the switch fantastic: How a protein kinase cascade can convert graded inputs into switch-like outputs. *Trends Biochem. Sci.* **21:** 460–466

Fischer EH & Krebs EG (1955) Conversion of phosphorylase b to phosphorylase a in muscle extracts. *J. Biol. Chem.* **216:** 121–132

Fiskin E, Bionda T, Dikic I & Behrends C (2016) Global Analysis of Host and Bacterial Ubiquitinome in Response to Salmonella Typhimurium Infection. *Mol. Cell* **62:** 967–981

Flannagan RS, Cosío G & Grinstein S (2009) Antimicrobial mechanisms of phagocytes and bacterial evasion strategies. *Nat. Rev. Microbiol.* **7:** 355–366

Flannagan RS, Jaumouillé V & Grinstein S (2012) The Cell Biology of Phagocytosis. *Annu. Rev. Pathol. Mech. Dis.* **7:** 61–98

Foote JR, Patel AA, Yona S & Segal AW (2019) Variations in the phagosomal environment of human neutrophils and mononuclear phagocyte subsets. *Front. Immunol.* **10:** 1–11

Förstermann U & Sessa WC (2012) Nitric oxide synthases: Regulation and function. *Eur. Heart J.* **33:** 829–837

Fratti RA, Backer JM, Gruenberg J, Corvera S & Deretic V (2001) Role of phosphatidylinositol 3-kinase and Rab5 effectors in phagosomal biogenesis and mycobacterial phagosome maturation arrest. *J. Cell Biol.* **154:** 631–644

Freeman SA & Grinstein S (2014) Phagocytosis: receptors, signal integration, and the cytoskeleton. *mmunological Rev.* **262:** 193–215

Gandara ML, Lopez P, Hernando R, Castano JG & Alemany S (2003) The COOH-Terminal Domain of Wild-Type Cot Regulates Its Stability and Kinase Specific Activity. *Mol. Cell. Biol.* **23:** 7377–7390

Gandino L & Varesio L (1990) Immortalization of macrophages from mouse bone marrow and fetal liver. *Exp. Cell Res.* **188:** 192–198

Gantke T, Boussouf S, Janzen J, Morrice NA, Howell S, Mühlberger E & Ley SC (2013) Ebola virus VP35 induces high-level production of recombinant TPL-2-ABIN-2-NF-κB1 p105 complex in co-transfected HEK-293 cells. *Biochem. J.* **452:** 359–365

Gantke T, Sriskantharajah S & Ley SC (2011a) Regulation and function of TPL-2, an IB kinase-regulated MAP kinase kinase kinase. *Cell Res.* **21:** 131–145

Gantke T, Sriskantharajah S & Ley SC (2011b) Regulation and function of TPL-2, an IκB kinase-regulated MAP kinase kinase kinase. *Cell Res.* **21:** 131–145

Gantke T, Sriskantharajah S, Sadowski M & Ley SC (2012) IκB kinase regulation of the TPL-2/ERK MAPK pathway. *Immunol. Rev.* **246:** 168–182

Ganz T (2004) Antimicrobial polypeptides. *J. Leukoc. Biol.* **75:** 34–38

Geissmann F, Manz MG, Jung S, Sieweke MH, Merad M & Ley K (2010) Development of monocytes, macrophages and dendritic cells. *Science (80-.).* **327:** 656–661

George D, Friedman M, Allen H, Argiriadi M, Barberis C, Bischoff A, Clabbers A, Cusack K, Dixon R, Fix-Stenzel S, Gordon T, Janssen B, Jia Y, Moskey M, Quinn C, Salmeron JA, Wishart N, Woller K & Yu Z (2008) Discovery of thieno[2,3-c]pyridines as potent COT inhibitors. *Bioorganic Med. Chem. Lett.* **18:** 4952–4955

George D & Salmeron A (2009) Cot/Tpl-2 protein kinase as a target for the treatment of inflammatory disease. *Curr. Top. Med. Chem.* **9:** 611–22

Gerlach B, Cordier SM, Schmukle AC, Emmerich CH, Rieser E, Haas TL, Webb AI, Rickard JA, Anderton H, Wong WWL, Nachbur U, Gangoda L, Warnken U, Purcell AW, Silke J & Walczak H (2011) Linear ubiquitination prevents inflammation and regulates immune signalling. *Nature* **471:** 591–596

Ghazizadeh S, Bolen JB & Fleit HB (1994) Physical and functional association of Src-related protein tyrosine kinases with FcγRII in monocytic THP-1 cells. *J. Biol. Chem.* **269:** 8878–8884

Ghazizadeh S, Bolen JB & Fleit HB (1995) Tyrosine phosphorylation and association of Syk with FcγRII in monocytic THP-1 cells. *Biochem. J.* **305:** 669–674

Gillooly DJ, Morrow IC, Lindsay M, Gould R, Bryant NJ, Gaullier J, Parton RG & Stenmark H (2000) Localization of phosphatidylinositol 3-phosphate in yeast and mammalian cells. *EMBO J.* **19:** 4577–4588

Gilmore TD (2006) Introduction to NF-κB: Players, pathways, perspectives. *Oncogene* **25:** 6680–6684

Gkirtzimanaki K, Gkouskou KK, Oleksiewicz U, Nikolaidis G, Vyrla D, Liontos M, Pelekanou V, Kanellis DC, Evangelou K, Stathopoulos EN, Field JK, Tsichlis PN, Gorgoulis V, Liloglou T & Eliopoulos AG (2013) TPL2 kinase is a suppressor of lung carcinogenesis. *Proc. Natl. Acad. Sci. U. S. A.* **110:** E1470-9

Goldknopf IL & Busch H (1977) Isopeptide linkage between nonhistone and histone 2A polypeptides of chromosomal conjugate protein A24. *Proc. Natl. Acad. Sci. U. S. A.* **74:** 864–868

Goldstein G, Scheid M, Hammerling U, Schlesinger DH, Niall HD & Boyse EA (1975) Isolation of a polypeptide that has lymphocyte differentiating properties and is probably represented universally in living cells. *Proc. Natl. Acad. Sci. U. S. A.* **72:** 11–15

Gomes LC & Dikic I (2014) Autophagy in antimicrobial immunity. *Mol. Cell* **54:** 224–233

Gong D, Shi W, Yi S ju, Chen H, Groffen J & Heisterkamp N (2012) TGFβ signaling plays a critical role in promoting alternative macrophage activation. *BMC Immunol.* **13:** 1–10

Gordon S (2016) Phagocytosis: An Immunobiologic Process. *Immunity* **44:** 463–475

Graves AR, Curran PK, Smith CL & Mindell JA (2008) The Cl-/H+ antiporter ClC-7 is the primary chloride permeation pathway in lysosomes. *Nature* **453:** 788–792

Griffin BFM, Griffin JJA, Leider JE & Silverstein SC (1975) Requirements for

Circumferential Attachment of Particle-Bound Ligands to Specific Receptors on the Macrophage Plasma Membrane. *J. Exp. Med.* **142:** 1263–1282

Gringhuis SI, den Dunnen J, Litjens M, van der Vlist M, Wevers B, Bruijns SCM & Geijtenbeek TBH (2009) Dectin-1 directs T helper cell differentiation by controlling noncanonical NF-κB activation through Raf-1 and Syk. *Nat. Immunol.* **10:** 203–213

Gruenheid S, Pinner E, Desjardins M & Gros P (1997) Natural resistance to infection with intracellular pathogens: The Nramp1 protein is recruited to the membrane of the phagosome. *J. Exp. Med.* **185:** 717–730

Gu H, Botelho RJ, Yu M, Grinstein S & Neel BG (2003) Critical role for scaffolding adapter Gab2 in FcγR-mediated phagocytosis. *J. Cell Biol.* **161:** 1151–1161

Gulle H, Samstag A, Eibl MM & Wolf HM (1998) Physical and functional association of FcαR with protein tyrosine kinase Lyn. *Blood* **91:** 383–391

Guma M, Hammaker D, Topolewski K, Corr M, Boyle DL, Karin M & Firestein GS (2012) Pro- and anti-inflammatory functions of the p38 pathway in rheumatoid arthritis: Advantages of targeting upstream kinases MKK3 or MKK6. *Arthritis Rheum.* **64:** 2887–2895

Günster RA, Matthews SA, Holden DW & Thurston TLM (2017) SseK1 and SseK3 Type III Secretion System Effectors Inhibit NF-κB Signaling and Necroptotic Cell Death in Salmonella-Infected Macrophages. *Infect. Immun.* **85:** 1–18

Guo M, Härtlova A, Gierliński M, Prescott A, Castellvi J, Losa JH, Petersen SK, Wenzel UA, Dill BD, Emmerich CH, Ramon Y Cajal S, Russell DG & Trost M (2019) Triggering MSR1 promotes JNK-mediated inflammation in IL-4-activated macrophages. *EMBO J.* **38:** 1–15

Gutierrez MG (2013) The Process of Phagosome Maturation. *Small GTPases* **4:** 148–158

Gutmann S, Hinniger A, Fendrich G, Drückes P, Antz S, Mattes H, Möbitz H, Ofner S, Schmiedeberg N, Stojanovic A, Rieffel S, Strauss A, Troxler T, Glatthar R & Sparrer H (2015) The crystal structure of cancer Osaka thyroid kinase reveals an unexpected kinase domain fold. *J. Biol. Chem.* **290:** 15210–15218

Haas TL, Emmerich CH, Gerlach B, Schmukle AC, Cordier SM, Rieser E, Feltham R, Vince J, Warnken U, Wenger T, Koschny R, Komander D, Silke J & Walczak H (2009) Recruitment of the Linear Ubiquitin Chain Assembly Complex Stabilizes the TNF-R1 Signaling Complex and Is Required for TNF-Mediated Gene Induction. *Mol. Cell* **36:** 831–844

Häcker H & Karin M (2006) Regulation and function of IKK and IKK-related kinases. *Sci. Sig* **357:** 1–19

Haebig K, Gloeckner CJ, Miralles MG, Gillardon F, Schulte C, Riess O, Ueffing M, Biskup S & Bonin M (2010) ARHGEF7 (BETA-PIX) acts as guanine nucleotide exchange factor for leucine-rich repeat kinase 2. *PLoS One* **5:** 1–12

Hall JP, Kurdi Y, Hsu S, Cuozzo J, Liu J, Telliez JB, Seidl KJ, Winkler A, Hu Y, Green N, Askew GR, Tam S, Clark JD & Lin LL (2007) Pharmacologic inhibition of Tpl2 blocks inflammatory responses in primary human monocytes, synoviocytes, and blood. *J. Biol. Chem.* **282:** 33295–33304

Hamada F, Aoki M, Akiyama T & Toyoshima K (1993) Association of immunoglobulin G Fc receptor II with Src-like protein-tyrosine kinase Fgr in neutrophils. *Proc. Natl. Acad. Sci. U. S. A.* **90:** 6305–6309

Han MS, Jung DY, Morel C, Lakhani SA, Kim JK, Flavell RA & Davis (2013) JNK Expression by Macrophages Promotes Obesity-induced Insulin Resistance and Inflammation. *Science (80-.).* **11:** 218–222

Hanks SK, Quinn AM & Hunter T (1988) The protein kinase family: Conserved features and deduced phylogeny of the catalytic domains. *Science (80-.).* **241:** 42–52

Hanson PI, Roth R, Lin Y & Heuser JE (2008) Plasma membrane deformation by circular arrays of ESCRT-III protein filaments. *J. Cell Biol.* **180:** 389–402

Harrison RE, Bucci C, Vieira O V, Trina A, Grinstein S & Schroer TA (2003) Phagosomes Fuse with Late Endosomes and / or Lysosomes by Extension of Membrane Protrusions along Microtubules : Role of Rab7 and RILP. *Mol. Cell. Biol.* **23:** 6494–6506

Hassoun A, Linden PK & Friedman B (2017) Incidence, prevalence, and management of MRSA bacteremia across patient populations — a review of recent developments in MRSA management and treatment. *Crit. Care* **21:** 1–10

Hebron E, Hope C, Kim J, Jensen JL, Flanagan C, Bhatia N, Maroulakou I, Mitsiades C, Miyamoto S, Callander N, Hematti P & Asimakopoulos F (2013) MAP3K8 kinase regulates myeloma growth by cell-autonomous and non-autonomous mechanisms involving myeloma-associated monocytes/macrophages. *Br. J. Haematol.* **160:** 779–784

Heissmeyer V, Krappmann D, Hatada EN & Scheidereit C (2001) Shared Pathways of IκB Kinase-Induced SCFβTrCP-Mediated Ubiquitination and Degradation for the NF-κB Precursor p105 and IκBα. *Mol. Cell. Biol.* **21:** 1024–1035

Hemmi H, Takeuchi O, Sato S, Yamamoto M, Kaisho T, Sanjo H, Kawai T, Hoshino K, Takeda K & Akira S (2004) The roles of two IκB kinase-related kinases in lipopolysaccharide and double stranded RNA signaling and viral infection. *J. Exp. Med.* **199:** 1641–1650

Henne WM, Buchkovich NJ & Emr SD (2011) The ESCRT Pathway. *Dev. Cell* **21:** 77–91

Heride C, Urbé S & Clague MJ (2014) Ubiquitin code assembly and disassembly. *Curr. Biol.* **24:** R215–R220

Hershko A, Ciechanover A & Rose IA (1979) Resolution of the ATP dependent proteolytic system from reticulocytes: A component that interacts with ATP. *Proc. Natl. Acad. Sci. U. S. A.* **76:** 3107–3110

Heyninck K, Kreike MM & Beyaert R (2003) Structure-function analysis of the A20-binding inhibitor of NF-κB activation, ABIN-1. *FEBS Lett.* **536:** 135–140

Heyninck K, De Valck D, Vanden Berghe W, Van Criekinge W, Contreras R, Fiers W, Haegeman G & Beyaert R (1999) The zinc finger protein A20 inhibits TNF-induced NF-kB-dependent gene expression by interfering with an RIP- or TRAF2-mediated transactivation signal and directly binds to a novel NF-kB-inhibiting protein ABIN. *J. Cell Biol.* **145:** 1471–1482

Hicke L & Dunn R (2003) Regulation of Membrane Protein Transport by Ubiquitin and Ubiquitin-Binding Proteins. In *Annual Review of Cell and Developmental Biology*

Higgins LM, Frankel G, Douce G, Dougan G & MacDonald TT (1999) Citrobacter rodentium infection in mice elicits a mucosal Th1 cytokine response and lesions similar to those in murine inflammatory bowel disease. *Infect. Immun.* **67:** 3031–3039

Higgs HN & Pollard TD (2000) Activation by Cdc42 and PIP2 of Wiskott-Aldrich Syndrome protein (WASp) stimulates actin nucleation by Arp2/3 complex. *J. Cell Biol.* **150:** 1311–1320

Hildebrand JM, Yi Z, Buchta CM, Poovassery J, Stunz LL & Bishop GA (2011) Roles of tumor necrosis factor receptor associated factor 3 (TRAF3) and TRAF5 in immune cell functions. *Immunol. Rev.* **244:** 55–74

Hoebe K, Janssen EM, Kim SO, Alexopoulou L, Flavell RA, Han J & Beutler B (2003) Upregulation of costimulatory molecules induced by lipopolysaccharide and double-stranded RNA occurs by Trif-dependent and Trif-independent pathways. *Nat. Immunol.* **4:** 1223–1229

Hoffmann A, Natoli G & Ghosh G (2006) Transcriptional regulation via the NF-κB signaling module. *Oncogene* **25:** 6706–6716

Holland PM & Cooper JA (1999) Protein modification: Docking sites for kinases. *Curr. Biol.* **9:** 329–331

Holowka D, Sil D, Torigoe C & Baird B (2007) Insights into immunoglobulin E receptor signaling from structurally defined ligands. *Immunol. Rev.* **217:** 269–279

Holz MK, Ballif BA, Gygi SP & Blenis J (2005) mTOR and S6K1 mediate assembly of the translation preinitiation complex through dynamic protein interchange and ordered phosphorylation events. *Cell* **123:** 569–580

Hoppe AD & Swanson JA (2004) Cdc42, Rac1, and Rac2 Display Distinct Patterns of Activation during Phagocytosis. *Mol. Biol. Cell* **15:** 3509–3519

Hordijk PL (2006) Regulation of NADPH oxidases: The role of Rac proteins. *Circ. Res.* **98:** 453–462

Horgan CP, Hanscom SR & Mccaffrey MW (2013) Biochemical and Biophysical Research Communications GRAB is a binding partner for the Rab11a and Rab11b GTPases. *Biochem. Biophys. Res. Commun.* **441:** 214–219

Horng T, Barton GM & Medzhitov R (2001) TIRAP: an adapter molecule in the Toll signaling pathway. *Nat. Immunol.* **2:** 835–841

Hu H & Sun SC (2016) Ubiquitin signaling in immune responses. *Cell Res.* **26:** 457–483

Hu Y, Green N, Gavrin LK, Janz K, Kaila N, Li HQ, Thomason JR, Cuozzo JW, Hall JP, Hsu S, Nickerson-Nutter C, Telliez JB, Lin LL & Tam S (2006) Inhibition of Tpl2 kinase and TNFα production with quinoline-3-carbonitriles for the treatment of rheumatoid arthritis. *Bioorganic Med. Chem. Lett.* **16:** 6067–6072

Hu ZQ, Rao CL, Tang ML, Zhang Y, Lu XX, Chen JG, Mao C, Deng L, Li Q & Mao XH (2019) Rab32 GTpase, as a direct target of miR-30b/c, controls the intracellular survival of burkholderia pseudomallei by regulating phagosome maturation. *PLoS Pathog.* **15:** 1–27

Huang J & Manning BD (2008) The TSC1–TSC2 complex: a molecular switchboard controlling cell growth. *Biochem. J.* **412:** 179–190

Huang L, Verstrepen L, Heyninck K, Wullaert A, Revets H, De Baetselier P & Beyaert R (2008) ABINs inhibit EGF receptor-mediated NF-kappaB activation and growth of EGF receptor-overexpressing tumour cells. *Oncogene* **27:** 6131–6140

Hubeau M, Ngadjeua F, Puel A, Israel L, Feinberg J, Chrabieh M, Belani K, Bodemer C, Fabre I, Plebani A, Boisson-Dupuis S, Picard C, Fischer A, Israel A, Abel L, Veron M, Casanova JL, Agou F & Bustamante J (2011) New mechanism of X-linked anhidrotic ectodermal dysplasia with immunodeficiency: Impairment of ubiquitin binding despite normal folding of NEMO protein. *Blood* **118:** 926–935

Van Huffel S, Delaei F, Heyninck K, De Valck D & Beyaert R (2001) Identification of a Novel A20-binding Inhibitor of Nuclear Factor-kB Activation Termed ABIN-2. *J. Biol. Chem.* **276:** 30216–30223

Hughes DP, Marron MB & Brindle NPJ (2003) The antiinflammatory endothelial tyrosine kinase Tie2 interacts with a novel nuclear factor-κB inhibitor ABIN-2. *Circ. Res.* **92:** 630–636

Hukelmann JL, Anderson KE, Sinclair L V., Grzes KM, Murillo AB, Hawkins PT, Stephens LR, Lamond AI & Cantrell DA (2016) The cytotoxic T cell proteome and its shaping by the kinase mTOR. *Nat. Immunol.* **17:** 104–112

Hurley D, McCusker MP, Fanning S & Martins M (2014) Salmonella-host interactions - modulation of the host innate immune system. *Front. Immunol.* **5:** 1–11

Husebye H, Halaas Ø, Stenmark H, Tunheim G, Sandanger Ø, Bogen B, Brech A, Latz E & Espevik T (2006) Endocytic pathways regulate Toll-like receptor 4 signaling and link innate and adaptive immunity. *EMBO J.* **25:** 683–692

Husnjak K & Dikic I (2012) Ubiquitin-Binding Proteins: Decoders of Ubiquitin-Mediated Cellular Functions. *Annu. Rev. Biochem.* **81:** 291–322

Hutchins AP, Liu S, Diez D & Miranda-Saavedra D (2013) The repertoires of ubiquitinating and deubiquitinating enzymes in eukaryotic genomes. *Mol. Biol. Evol.* **30:** 1172–1187

Huynh KK, Eskelinen EL, Scott CC, Malevanets A, Saftig P & Grinstein S (2007) LAMP

proteins are required for fusion of lysosomes with phagosomes. *EMBO J.* **26:** 313–324

Hyung HL, Elia N, Ghirlando R, Lippincott-Schwartz J & Hurley JH (2008) Midbody targeting of the ESCRT machinery by a noncanonical coiled coil in CEP55. *Science (80-.).* **322:** 576–580

Iannacone M, Moseman EA, Tonti E, Bosurgi L, Junt T, Henrickson SE, Whelan SP, Guidotti LG & Von Andrian UH (2010) Subcapsular sinus macrophages prevent CNS invasion on peripheral infection with a neurotropic virus. *Nature* **465:** 1079–1083

Ihle JN, Witthuhn BA, Quelle FW, Yamamoto K, Thierfelder WE, Kreider B & Silvennoinen O (1994) Signaling by the cytokine receptor superfamily: JAKs and STATs. *Trends Biochem. Sci.* **19:** 222–227

Ikeda F & Dikic I (2008) Atypical ubiquitin chains: New molecular signals. 'Protein Modifications: Beyond the Usual Suspects' Review Series. *EMBO Rep.* **9:** 536–542

Ikeda F, Hecker CM, Rozenknop A, Nordmeier RD, Rogov V, Hofmann K, Akira S, Dötsch V & Dikic I (2007) Involvement of the ubiquitin-like domain of TBK1/IKK-i kinases in regulation of IFN-inducible genes. *EMBO J.* **26:** 3451–3462

Ingebritsen TS & Cohen P (1983) The Protein Phosphatases Involved in Cellular Regulation: 2. Glycogen Metabolism. *Eur. J. Biochem.* **132:** 255–261

Ip WKE, Sokolovska A, Charriere GM, Boyer L, Dejardin S, Cappillino MP, Yantosca LM, Takahashi K, Moore KJ, Lacy-Hulbert A & Stuart LM (2010) Phagocytosis and Phagosome Acidification Are Required for Pathogen Processing and MyD88-Dependent Responses to Staphylococcus aureus. *J. Immunol.* **184:** 7071–7081

Iwasaki A & Medzhitov R (2015) Control of adaptive immunity by the innate immune system. *Nat. Immunol.* **16:** 343–353

Iyer SS, Barton JA, Bourgoin S & Kusner DJ (2004) Phospholipases D1 and D2 Coordinately Regulate Macrophage Phagocytosis. *J. Immunol.* **173:** 2615–2623

Jabado N, Jankowski A, Dougaparsad S, Picard V, Grinstein S & Gros P (2000) Natural resistance to intracellular infections: Natural resistance-associated macrophage protein 1 (NRAMP1) functions as a pH-dependent manganese transporter at the phagosomal membrane. *J. Exp. Med.* **192:** 1237–1247

Jacque E, Schweighoffer E, Visekruna A, Papoutsopoulou S, Janzen J, Zillwood R, Tarlinton DM, Tybulewicz VLJ & Ley SC (2014) IKK-induced NF-κB1 p105 proteolysis is critical for B cell antibody responses to T cell-dependent antigen. *J. Exp. Med.* **211:** 2085–2101

Jakubzick C V., Randolph GJ & Henson PM (2017) Monocyte differentiation and antigen-presenting functions. *Nat. Rev. Immunol.* **17:** 349–362

Jancic C, Savina A, Wasmeier C, Tolmachova T, El-Benna J, Dang PMC, Pascolo S, Gougerot-Pocidalo MA, Raposo G, Seabra MC & Amigorena S (2007) Rab27a regulates phagosomal pH and NADPH oxidase recruitment to dendritic cell phagosomes. *Nat. Cell Biol.* **9:** 367–378

Janeway CA, Travers P, Walport M & Al E (2001) Principles of innate and adaptive immunity. *Immunobiol. Immune Syst. Heal. Dis. 5th Ed.*

Jeffrey PD, Russo AA, Polyak K, Gibbs E, Hurwitz J, Massagué J & Pavletich NP (1995) Mechanism of CDK activation revealed by the structure of a cyclinA-CDK2 complex. *Nature* **376:** 313–320

Jenssen H & Hancock REW (2009) Antimicrobial properties of lactoferrin. *Biochimie* **91:** 19–29

Jeong JH, Bhatia A, Toth Z, Oh S, Inn KS, Liao CP, Roy-Burman P, Melamed J, Coetzee GA & Jung JU (2011) TPL2/COT/MAP3K8 (TPL2) activation promotes androgen depletion-independent (ADI) prostate cancer growth. *PLoS One* **6:** 1–10

Jia J, Tarabykina S, Hansen C, Berchtold M & Cygler M (2001) Structure of apoptosis-linked protein ALG-2: Insights into Ca2+-induced changes in penta-EF-hand

proteins. *Structure* **9:** 267–275
Jiang X, Bomgarden R, Brown J, Drew DL, Robitaille AM, Viner R & Huhmer AR (2017) Sensitive and Accurate Quantitation of Phosphopeptides Using TMT Isobaric Labeling Technique. *J. Proteome Res.* **16:** 4244–4252
Jiang Y, Gram H, Zhao M, New L, Gu J, Feng L, Di Padova F, Ulevitch RJ & Han J (1997) Characterization of the structure and function of the fourth member of p38 group mitogen-activated protein kinases, p38δ. *J. Biol. Chem.* **272:** 30122–30128
Jin J, Li X, Gygi SP & Harper JW (2007) Dual E1 activation systems for ubiquitin differentially regulate E2 enzyme charging. *Nature* **447:** 1135–1138
Joffre OP, Segura E, Savina A & Amigorena S (2012) Cross-presentation by dendritic cells. *Nat. Rev. Immunol.* **12:** 557–569
Johansson M, Rocha N, Zwart W, Jordens I, Janssen L, Kuijl C, Olkkonen VM & Neefjes J (2007) Activation of endosomal dynein motors by stepwise assembly of Rab7-RILP-p150Glued, ORP1L, and the receptor βIII spectrin. *J. Cell Biol.* **176:** 459–471
Johnson SA, Pleiman CM, Pao L, Schneringer J, Hippen K & Cambier JC (1995) Phosphorylated immunoreceptor signaling motifs (ITAMs) exhibit unique abilities to bind and activate Lyn and Syk tyrosine kinases. *J. Immunol.* **155:** 4596–603
Jones DH, Nusbacher J & Anderson CL (1985) Fc receptor-mediated binding and endocytosis by human mononuclear phagocytes: Monomeric IgG is not endocytosed by U937 cells and monocytes. *J. Cell Biol.* **100:** 558–564
Junt T, Moseman EA, Iannacone M, Massberg S, Lang PA, Boes M, Fink K, Henrickson SE, Shayakhmetov DM, Di Paolo NC, Van Rooijen N, Mempel TR, Whelan SP & Von Andrian UH (2007) Subcapsular sinus macrophages in lymph nodes clear lymph-borne viruses and present them to antiviral B cells. *Nature* **450:** 110–114
Kagan JC & Medzhitov R (2006) Phosphoinositide-Mediated Adaptor Recruitment Controls Toll-like Receptor Signaling. *Cell* **125:** 943–955
Kagan JC, Su T, Horng T, Chow A, Akira S & Medzhitov R (2008a) TRAM couples endocytosis of Toll-like receptor 4 to the induction of interferon-β. *Nat. Immunol.* **9:** 361–368
Kagan JC, Su T, Horng T, Chow A, Akira S & Medzhitov R (2008b) TRAM couples endocytosis of Toll-like receptor 4 to the induction of interferon-β. *Nat. Immunol.* **9:** 361–368
Kaiser F, Cook D, Papoutsopoulou S, Rajsbaum R, Wu X, Yang H, Grant S, Ricciardi-castagnoli P, Tsichlis PN, Ley SC & Garra AO (2009) TPL-2 negatively regulates interferon-beta production in macrophages and myeloid dendritic cells. *J. Exp. Med.* **206:** 1863–1871
Kanayama A, Seth RB, Sun L, Ea CK, Hong M, Shaito A, Chiu YH, Deng L & Chen ZJ (2004) TAB2 and TAB3 activate the NF-κB pathway through binding to polyubiquitin chains. *Mol. Cell* **15:** 535–548
Kang YJ, Chen J, Otsuka M, Mols J, Ren S, Wang Y & Han J (2008) Macrophage Deletion of p38α Partially Impairs Lipopolysaccharide-Induced Cellular Activation. *J. Immunol.* **180:** 5075–5082
Katzmann DJ, Stefan CJ, Babst M & Emr SD (2003) Vps27 recruits ESCRT machinery to endosomes during MVB sorting. *J. Cell Biol.* **162:** 413–423
Kaufmann SHE & Dorhoi A (2016) Molecular Determinants in Phagocyte-Bacteria Interactions. *Immunity* **44:** 476–491
Kawai T & Adachi O (1999) Unresponsiveness of MyD88-Deficient Mice to Endotoxin. *Immunity* **11:** 115–122
Kawai T & Akira S (2006) TLR signaling. *Cell Death Differ.* **13:** 816–825
Kawai T & Akira S (2010) The role of pattern-recognition receptors in innate immunity: Update on toll-like receptors. *Nat. Immunol.* **11:** 373–384
Kawai T & Akira S (2011) Toll-like Receptors and Their Crosstalk with Other Innate Receptors in Infection and Immunity. *Immunity* **34:** 637–650

Kawai T, Takeuchi O, Fujita T, Inoue J, Mühlradt PF, Sato S, Hoshino K & Akira S (2001) Lipopolysaccharide Stimulates the MyD88-Independent Pathway and Results in Activation of IFN-Regulatory Factor 3 and the Expression of a Subset of Lipopolysaccharide-Inducible Genes. *J. Immunol.* **167:** 5887–5894

Kawasaki T & Kawai T (2014) Toll-like receptor signaling pathways. *Front. Immunol.* **5:** 1–8

Kim C, Sano Y, Todorova K, Carlson BA, Arpa L, Celada A, Lawrence T, Otsu K, Brissette JL, Arthur JSC & Park JM (2008) The kinase p38α serves cell type-specific inflammatory functions in skin injury and coordinates pro- and anti-inflammatory gene expression. *Nat. Immunol.* **9:** 1019–1027

Kinchen JM & Ravichandran KS (2008) Phagosome maturation: Going through the acid test. *Nat. Rev. Mol. Cell Biol.* **9:** 781–795

Kinchen JM & Ravichandran KS (2010) Identification of two evolutionarily conserved genes regulating processing of engulfed apoptotic cells. *Nature* **464:** 778–782

Kirisako T, Kamei K, Murata S, Kato M, Fukumoto H, Kanie M, Sano S, Tokunaga F, Tanaka K & Iwai K (2006) A ubiquitin ligase complex assembles linear polyubiquitin chains. *EMBO J.* **25:** 4877–4887

Kitano M, Nakaya M, Nakamura T, Nagata S & Matsuda M (2008) Imaging of Rab5 activity identifies essential regulators for phagosome maturation. *Nature* **453:** 241–245

Klose M, Salloum JE, Gonschior H & Linder S (2019) SNX3 drives maturation of Borrelia phagosomes by forming a hub for PI(3)P, Rab5a, and galectin-9. *J. Cell Biol.* **218:** 3039–3059

Kobayashi T, Stang E, Fang KS, De Moerloose P, Parton RG & Gruenberg J (1998) A lipid associated with the antiphospholipid syndrome regulates endosome structure and function. *Nature* **392:** 193–197

Kohio HP & Adamson AL (2013) Glycolytic control of vacuolar-type ATPase activity: A mechanism to regulate influenza viral infection. *Virology* **444:** 301–309

Kolaczkowska E & Kubes P (2013) Neutrophil recruitment and function in health and inflammation. *Nat. Rev. Immunol.* **13:** 159–175

Koli P, Sudan S, Fitzgerald D, Adhya S & Kar S (2011) Conversion of Commensal Escherichia Coli K-12 to an invasive form via expression of a mutant Histone-like protein. *MBio* **2:** 1–13

Koliaraki V, Roulis M & Kollias G (2012) Tpl2 regulates intestinal myofibroblast HGF release to suppress colitis-associated tumorigenesis. *J. Clin. Invest.* **122:** 4231–4242

Komander D & Rape M (2012) The Ubiquitin Code. *Annu. Rev. Biochem.* **81:** 203–229

Komander D, Reyes-Turcu F, Licchesi JDF, Odenwaelder P, Wilkinson KD & Barford D (2009) Molecular discrimination of structurally equivalent Lys 63-linked and linear polyubiquitin chains. *EMBO Rep.* **10:** 466–473

Kondo M (2010) Lymphoid and myeloid lineage commitment in multipotent hematopoietic progenitors. *Immunol. Rev.* **238:** 37–46

Kong L & Ge BX (2008) MyD88-independent activation of a novel actin-Cdc42/Rac pathway is required for Toll-like receptor-stimulated phagocytosis. *Cell Res.* **18:** 745–755

Kontoyiannis D, Boulougouris G, Manoloukos M, Armaka M, Apostolaki M, Pizarro T, Kotlyarov A, Forster I, Flavell R, Gaestel M, Tsichlis P, Cominelli F & Kollias G (2002) Genetic dissection of the cellular pathways and signaling mechanisms in modeled tumor necrosis factor-induced Crohn's-like inflammatory bowel disease. *J. Exp. Med.* **196:** 1563–1574

Kontoyiannis D, Pasparakis M, Pizarro TT, Cominelli F & Kollias G (1999) Impaired On/Off Regulation of TNF Biosynthesis in Mice Lacking TNF AU-Rich Elements. *Immunity* **10:** 387–398

Kostelansky MS, Schluter C, Tam YYC, Lee S, Ghirlando R, Beach B, Conibear E & Hurley JH (2007) Molecular Architecture and Functional Model of the Complete Yeast ESCRT-I Heterotetramer. *Cell* **129:** 485–498

Kulathu Y, Akutsu M, Bremm A, Hofmann K & Komander D (2009) Two-sided ubiquitin binding explains specificity of the TAB2 NZF domain. *Nat. Struct. Mol. Biol.* **16:** 1328–1330

Kumar A, Takada Y, Boriek AM & Aggarwal BB (2004) Nuclear factor-κB: Its role in health and disease. *J. Mol. Med.* **82:** 434–448

Kuriakose T, Tripp RA & Watford WT (2015) Tumor Progression Locus 2 Promotes Induction of IFNλ, Interferon Stimulated Genes and Antigen-Specific CD8+ T Cell Responses and Protects against Influenza Virus. *PLoS Pathog.* **11:** 1–22

Kyrmizi I, Ioannou M, Hatziapostolou M, Tsichlis PN, Boumpas DT & Tassiulas I (2013) Tpl2 kinase regulates FcγR signaling and immune thrombocytopenia in mice. *J. Leukoc. Biol.* **94:** 751–757

Labbé K & Saleh M (2008) Cell death in the host response to infection. *Cell Death Differ.* **15:** 1339–1349

Lai AY & Kondo M (2008) T and B lymphocyte differentiation from hematopoietic stem cell. *Semin Immunol.* **20:** 207–212

Laird MHW, Rhee SH, Perkins DJ, Medvedev AE, Piao W, Fenton MJ & Vogel SN (2009) TLR4/MyD88/PI3K interactions regulate TLR4 signaling. *J. Leukoc. Biol.* **85:** 966–977

Lamothe B, Besse A, Campos AD, Webster WK, Wu H & Darnay BG (2007) Site-specific Lys-63-linked tumor necrosis factor receptor-associated factor 6 auto-ubiquitination is a critical determinant of IκB kinase activation. *J. Biol. Chem.* **282:** 4102–4112

Lang V, Janzen J, Fischer GZ, Soneji Y, Beinke S, Salmerón A, Hay RT, Ben-Neriah Y & Ley SC (2003) BTrCP-Mediated Proteolysis of NF-kB1 p105 Requires Phosphorylation of p105 Serines 927 and 932. *Mol. Cell. Biol.* **23:** 402–413

Lang V, Symons A, Watton SJ, Janzen J, Soneji Y, Howell S, Ley SC & Beinke S (2004) ABIN-2 Forms a Ternary Complex with TPL-2 and NF- κ B1 p105 and Is Essential for TPL-2 Protein Stability. *Mol. Cell. Biol.* **24:** 5235–5248

Larock DL, Chaudhary A & Miller SI (2015) Salmonellae interactions with host processes. *Nat. Rev. Microbiol.* **13:** 191–205

Latz E, Visintin A, Lien E, Fitzgerald KA, Espevik T & Golenbock DT (2003) The LPS receptor generates inflammatory signals from the cell surface. *J. Endotoxin Res.* **9:** 375–380

Lauer J, Segeletz S, Cezanne A, Guaitoli G, Raimondi F, Gentzel M, Alva V, Habeck M, Kalaidzidis Y, Ueffing M, Lupas AN, Gloeckner CJ & Zerial M (2019) Auto-regulation of Rab5 GEF activity in rabex5 by allosteric structural changes, catalytic core dynamics and ubiquitin binding. *Elife* **8:** 1–22

Lawrence DW & Kornbluth J (2012) E3 Ubiquitin ligase NKLAM is a macrophage phagosome protein and plays a role in bacterial killing. *Cell Immunol.* **279:** 46–52

Lebman BYDA, Coffman RL, Med JE & Rockefeller T (1988) Interleukin 4 causes isotype switching to IgE in T cell-stimulated clonal B cell cultures. *J. Exp. Med.* **168:** 853–862

Lee HW, Joo KM, Lim JE, Cho HJ, Cho HJ, Park MC, Seo HJ, Seo S Il, Lee J Il, Kim S, Jeong BC & Nam DH (2013) Tpl2 kinase impacts Tumor growth and metastasis of clear cell renal cell carcinoma. *Mol. Cancer Res.* **11:** 1375–1386

Lee KY (2019) M1 and M2 polarization of macrophages: a mini-review. *Med. Biol. Sci. Eng.* **2:** 1–5

Lee WL, Kim MK, Schreiber AD & Grinstein S (2005) Role of ubiquitin and proteasomes in phagosome maturation. *Mol. Biol. Cell* **16:** 2077–2090

Lefebvre C, Legouis R & Culetto E (2018a) ESCRT and autophagies: Endosomal functions and beyond. *Semin. Cell Dev. Biol.* **74:** 21–28

Lefebvre C, Legouis R & Culetto E (2018b) ESCRT and autophagies: Endosomal functions and beyond. *Semin. Cell Dev. Biol.* **74:** 21–28

Lemaitre B, Nicolas E, Michaut L, Reichhart JM & Hoffmann JA (1996) The dorsoventral regulatory gene cassette spatzle/Toll/Cactus controls the potent antifungal response in Drosophila adults. *Cell* **86:** 973–983

Lennartz MR (2008) Phospholipases and Phagocytosis. In *Molecular Mechanisms of Phagocytosis*

Lennon-Duménil AM, Bakker AH, Maehr R, Fiebiger E, Overkleeft HS, Rosemblatt M, Ploegh HL & Lagaudrière-Gesbert C (2002) Analysis of protease activity in live antigen-presenting cells shows regulation of the phagosomal proteolytic contents during dendritic cell activation. *J. Exp. Med.* **196:** 529–539

Ley K (2017) M1 Means Kill; M2 Means Heal. *J. Immunol.* **199:** 2191–2193

Li B & Dewey CN (2011) RSEM: accurate transcript quantification from RNA-Seq data with or without a reference genome. *BMC Bioinformatics* **12:** 1–16

Li F, Xu D, Wang Y, Zhou Z, Liu J, Hu S, Gong Y, Yuan J & Pan L (2018) Structural insights into the ubiquitin recognition by OPTN (optineurin) and its regulation by TBK1-mediated phosphorylation. *Autophagy* **14:** 66–79

Li J, Chai QY & Liu CH (2016) The ubiquitin system: A critical regulator of innate immunity and pathogen-host interactions. *Cell. Mol. Immunol.* **13:** 560–576

Li W, Bengtson MH, Ulbrich A, Matsuda A, Reddy VA, Orth A, Chanda SK, Batalov S & Joazeiro CAP (2008) Genome-Wide and Functional Annotation of Human E3 Ubiquitin Ligases Identifies MULAN, a Mitochondrial E3 that Regulates the Organelle's Dynamics and Signaling. *PLoS One* **3:** 1–14

Libby P & Goldberg AL (1978) Leupeptin, a protease inhibitor, decreases protein degradation in normal and diseased muscles. *Science (80-.).* **199:** 534–536

Liberman R, Bond S, Shainheit MG, Stadecker MJ & Forgac M (2014) Regulated assembly of vacuolar ATPase is increased during cluster disruption-induced maturation of dendritic cells through a phosphatidylinositol 3-Kinase/mTOR-dependent pathway. *J. Biol. Chem.* **289:** 1355–1363

Lin KM, Hu W, Troutman TD, Jennings M, Brewer T, Li X, Nanda S, Cohen P, Thomas JA & Pasare C (2014) IRAK-1 bypasses priming and directly links TLRs torapid NLRP3 inflammasome activation. *Proc. Natl. Acad. Sci. U. S. A.* **111:** 775–780

Lin SC, Lo YC & Wu H (2010) Helical assembly in the MyD88-IRAK4-IRAK2 complex in TLR/IL-1R signalling. *Nature* **465:** 885–890

Lindsay AJ, Hendrick AG, Cantalupo G, Senic-Matuglia F, Goud B, Bucci C & McCaffrey MW (2002) Rab coupling protein (RCP), a novel Rab4 and Rab11 effector protein. *J. Biol. Chem.* **277:** 12190–12199

Lindsley CW, Zhao Z, Leister WH, Robinson RG, Barnett SF, Defeo-Jones D, Jones RE, Hartman GD, Huff JR, Huber HE & Duggan ME (2005) Allosteric Akt (PKB) inhibitors: Discovery and SAR of isozyme selective inhibitors. *Bioorganic Med. Chem. Lett.* **15:** 761–764

Liu J, Li M, Li L, Chen S & Wang X (2018) Ubiquitination of the PI3-kinase VPS-34 promotes VPS-34 stability and phagosome maturation. *J. Cell Biol.* **217:** 347–360

Liu W-K, Yen P-F, Chien C-Y, Fann M-J, Su J-Y & Chou C-K (2004) The inhibitor ABIN-2 disrupts the interaction of receptor-interacting protein with the kinase subunit IKKgamma to block activation of the transcription factor NF-kappaB and potentiate apoptosis. *Biochem. J.* **378:** 867–76

Liu WK, Chien CY, Chou CK & Su JY (2003) An LKB1-interacting protein negatively regulates TNFα-induced NF-κB activation. *J. Biomed. Sci.* **10:**

Liu X, Zhang Z, Ruan J, Pan Y, Magupalli VG, Wu H & Lieberman J (2016) Inflammasome-activated gasdermin D causes pyroptosis by forming membrane pores. *Nature* **535:** 153–158

Lo YC, Lin SC, Rospigliosi CC, Conze DB, Wu CJ, Ashwell JD, Eliezer D & Wu H (2009)

Structural Basis for Recognition of Diubiquitins by NEMO. *Mol. Cell* **33:** 602–615

López-Pelaéz M, Fumagalli S, Sanz C, Herrero C, Guerra S, Fernandez M & Alemany S (2012) Cot/tpl2-MKK1/2-Erk1/2 controls mTORC1-mediated mRNA translation in Toll-like receptor-activated macrophages. *Mol. Biol. Cell* **23:** 2982–2992

López-Peláez M, Soria-Castro I, Boscá L, Fernández M & Alemany S (2011) Cot/tpl2 activity is required for TLR-induced activation of the Akt p70 S6k pathway in macrophages: Implications for NO synthase 2 expression. *Eur. J. Immunol.* **41:** 1733–1741

Love MI, Huber W & Anders S (2014) Moderated estimation of fold change and dispersion for RNA-seq data with DESeq2. *Genome Biol.* **15:** 1–21

Lu YC, Yeh WC & Ohashi PS (2008) LPS/TLR4 signal transduction pathway. *Cytokine* **42:** 145–151

Luciano BS, Hsu S, Channavajhala PL, Lin LL & Cuozzo JW (2004) Phosphorylation of threonine 290 in the Activation Loop of Tp12/Cot is necessary but not sufficient for kinase activity. *J. Biol. Chem.* **279:** 52117–52123

Lukacs GL, Rotstein OD & Grinstein S (1990) Phagosomal acidification is mediated by a vacuolar-type H+-ATPase in murine macrophages. *J. Biol. Chem.* **265:** 21099–21107

Lukacs GL, Rotstein OD & Grinstein S (1991) Determinants of the Phagosornal pH in Macrophages. *J. Biol. Chem.* **266:** 24540–24548

Lund AH, Turner G, Trubetskoy A, Verhoeven E, Wientjens E, Hulsman D, Russell R, DePinho RA, Lenz J & van Lohuizen M (2002) Genome-wide retroviral insertional tagging of genes involved in cancer in Cdkn2a-deficient mice. *Nat. Genet.* **32:** 160–165

Lv Y, Fang L, Ding P & Liu R (2019) PI3K/Akt-Beclin1 signaling pathway positively regulates phagocytosis and negatively mediates NF-κB-dependent inflammation in Staphylococcus aureus-infected macrophages. *Biochem. Biophys. Res. Commun.* **510:** 284–289

MacLean B, Tomazela DM, Shulman N, Chambers M, Finney GL, Frewen B, Kern R, Tabb DL, Liebler DC & MacCoss MJ (2010) Skyline: An open source document editor for creating and analyzing targeted proteomics experiments. *Bioinformatics* **26:** 966–968

Makris A, Patriotis C, Bear SE & Tsichlis PN (1993) Genomic organization and expression of Tpl-2 in normal cells and Moloney murine leukemia virus-induced rat T-cell lymphomas: activation by provirus insertion. *J. Virol.* **67:** 4283–4289

Man SM, Karki R & Kanneganti TD (2017) Molecular mechanisms and functions of pyroptosis, inflammatory caspases and inflammasomes in infectious diseases. *Immunol. Rev.* **277:** 61–75

Manders EMM, Verbeek FJ & Aten JA (1993) Measurement of co-localization of objects in dual-colour confocal images. *J. Microsc.* **169:** 375–382

Manil-Segalén M, Lefebvre C, Culetto E, Manil-segalén M, Lefebvre C, Culetto E & Legouis R (2015) Need an ESCRT for autophagosomal maturation ? Need an ESCRT for autophagosomal maturation ? **0889:** 566–571

Mansfield PJ, Shayman JA & Boxer LA (2000) Regulation of polymorphonuclear leukocyte phagocytosis by myosin light chain kinase after activation of mitogen-activated protein kinase. *Blood* **95:** 2407–2412

Mantegazza AR, Savina A, Vermeulen M, Pérez L, Geffner J, Hermine O, Rosenzweig SD, Faure F & Amigorena S (2008) NADPH oxidase controls phagosomal pH and antigen cross-presentation in human dendritic cells. *Blood* **112:** 4712–4722

Mantovani A, Sica A, Sozzani S, Allavena P, Vecchi A & Locati M (2004) The chemokine system in diverse forms of macrophage activation and polarization. *Trends Immunol.* **25:** 677–686

Mantovani A, Sozzani S, Locati M, Allavena P & Sica A (2002) Macrophage polarization:

Tumor-associated macrophages as a paradigm for polarized M2 mononuclear phagocytes. *Trends Immunol.* **23:** 549–555

Mantovani B, Rabinovitch M & Nussenzweig V (1972) Different roles of the macrophage receptor sites for complement (C3) and for immunoglobulin (IgG). *J. Exp. Med.* **135:** 780–792

Mao Y, Nickitenko A, Duan X, Lloyd TE, Wu MN, Bellen H & Quiocho FA (2000) Crystal structure of the VHS and FYVE tandem domains of Hrs, a protein involved in membrane trafficking and signal transduction. *Cell* **100:** 447–456

Marienfeld RB, Palkowitsch L & Ghosh S (2006) Dimerization of the IκB Kinase-Binding Domain of NEMO Is Required for Tumor Necrosis Factor Alpha-Induced NF-κB Activity. *Mol. Cell. Biol.* **26:** 9209–9219

Marjuki H, Gornitzky A, Marathe BM, Ilyushina NA, Jerry R, Desai G, Webby RJ & Webster RG (2011) Influenza A Virus-Induced Early Activation of ERK and PI3K Mediates V-ATPase-Dependent Intracellular pH Change Required for Fusion. *Cell Microbiol.* **13:** 587–601

Marshansky V & Futai M (2008) The V-type H+-ATPase in vesicular trafficking: targeting, regulation and function. *Curr. Opin. Cell Biol.* **20:** 415–426

Martel G, Bérubé J & Rousseau S (2013) The Protein Kinase TPL2 Is Essential for ERK1/ERK2 Activation and Cytokine Gene Expression in Airway Epithelial Cells Exposed to Pathogen-Associated Molecular Patterns (PAMPs). *PLoS One* **8:** 1–9

Martin E, Nathan C & Xie QW (1994) Role of interferon regulatory factor 1 in induction of nitric oxide synthase. *J. Exp. Med.* **180:** 977–984

Martin FJ, Gomez MI, Wetzel DM, Memmi G, Seaghdha MO, Soong G, Schindler C & Prince A (2009) Staphylococcus aureus activates type I IFN signaling in mice and humans through the Xr repeated sequences of protein A. *J. Clin. Invest.* **119:** 1931–1939

Martinez FO & Gordon S (2014) The M1 and M2 paradigm of macrophage activation: Time for reassessment. *F1000Prime Rep.* **6:** 1–13

Martinez FO, Helming L & Gordon S (2009) Alternative Activation of Macrophages: An Immunologic Functional Perspective. *Annu. Rev. Immunol.* **27:** 451–483

Mastroeni P, Vazquez-Torres A, Fang FC, Xu Y, Khan S, Hormaeche CE & Dougan G (2000) Antimicrobial actions of the nadph phagocyte oxidase and inducible nitric oxide synthase in experimental salmonellosis. I. Effects on microbial killing by activated peritoneal macrophages in vitro. *J. Exp. Med.* **192:** 237–247

May RC, Caron E, Hall A & Machesky LM (2000) Involvement of the Arp2/3 complex in phagocytosis mediated by FcγR or CR3. *Nat. Cell Biol.* **2:** 246–248

McBride HM, Rybin V, Murphy C, Giner A, Teasdale R & Zerial M (1999) Oligomeric complexes link Rab5 effectors with NSF and drive membrane fusion via interactions between EEA1 and syntaxin 13. *Cell* **98:** 377–386

McGaha TL, Chen Y, Ravishankar B, Rooijen N Van & Karlsson MCI (2011) Marginal zone macrophages suppress innate and adaptive immunity to apoptotic cells in the spleen. *Blood* **117:** 5403–5412

McNab FW, Ewbank J, Rajsbaum R, Stavropoulos E, Martirosyan A, Redford PS, Wu X, Graham CM, Saraiva M, Tsichlis P, Chaussabel D, Ley SC & O'Garra A (2013) TPL-2-ERK1/2 Signaling Promotes Host Resistance against Intracellular Bacterial Infection by Negative Regulation of Type I IFN Production. *J. Immunol.* **191:** 1732–1743

McWhirter SM, Fitzgerald KA, Rosains J, Rowe DC, Golenbock DT & Maniatis T (2004) IFN-regulatory factor 3-dependent gene expression is defective in Tbk1-deficient mouse embryonic fibroblasts. *Proc. Natl. Acad. Sci. U. S. A.* **101:** 233–238

Mendoza H, Campbell DG, Burness K, Hastie J, Ronkina N, Shim JH, Arthur JSC, Davis RJ, Gaestel M, Johnson GL, Ghosh S & Cohen P (2008) Roles for TAB1 in regulating the IL-1-dependent phosphorylation of the TAB3 regulatory subunit and

activity of the TAK1 complex. *Biochem. J.* **409:** 711–722
Merkulova M, Păunescu TG, Azroyan A, Marshansky V, Breton S & Brown D (2015) Mapping the H + (V) -ATPase interactome : identification of proteins involved in trafficking , folding , assembly and phosphorylation. *Sci. Rep.* **5:** 1–15
Mesquita FS, Thomas M, Sachse M, Santos AJM, Figueira R & Holden DW (2012) The Salmonella deubiquitinase SseI inhibits selective autophagy of cytosolic aggregates. *PLoS Pathog.* **8:** 1–14
Metcalf D & Isaacs AM (2010) The role of ESCRT proteins in fusion events involving lysosomes, endosomes and autophagosomes. *Biochem. Soc. Trans.* **38:** 1469–1473
Mettlen M, Chen P-H, Srinivasan S, Danuser G & Schmid SL (2018) Regulation of Clathrin-Mediated Endocytosis. *Annu Rev Biochem* **87:** 871–896
Mielke LA, Elkins KL, Wei L, Starr R, Tsichlis PN, O'Shea JJ & Watford WT (2009) Tumor Progression Locus 2 (Map3k8) Is Critical for Host Defense against Listeria monocytogenes and IL-1β Production . *J. Immunol.* **183:** 7984–7993
Mikkers H, Allen J, Knipscheer P, Romeyn L, Hart A, Vink E & Berns A (2002) High-throughput retroviral tagging to identify components of specific signaling pathways in cancer. *Nat. Genet.* **32:** 153–159
Mishra A, Eathiraj S, Corvera S & Lambright DG (2010) Structural basis for Rab GTPase recognition and endosome tethering by the C2H2 zinc finger of Early Endosomal Autoantigen 1 (EEA1). *Proc. Natl. Acad. Sci. U. S. A.* **107:** 10866–10871
Miyauchi J, Sasadaira H, Watanabe K & Watanabe Y (1985) Ultrastructural immunocytochemical localization of lysozyme in human monocytes and macrophages. *Cell Tissue Res.* **242:** 269–277
Miyoshi J, Higashi T, Mukai H, Ohuchi T & Kakunaga T (1991) Structure and transforming potential of the human cot oncogene encoding a putative protein kinase. *Mol. Cell. Biol.* **11:** 4088–4096
Mogensen TH (2009) Pathogen recognition and inflammatory signaling in innate immune defenses. *Clin. Microbiol. Rev.* **22:** 240–273
Molloy A & Winterbourn C (1990) Release of iron from phagocytosed Escherichia coli and uptake by neutrophil lactoferrin. *Blood* **75:** 984–989
Moodie SA, Willumsen BM, Weber MJ & Wolfman A (1993) Complexes of Ras·GTP with Raf-1 and mitogen-activated protein kinase kinase. *Science (80-.).* **260:** 1658–1661
Moorthy AK, Savinova O V., Ho JQ, Wang VYF, Vu D & Ghosh G (2006) The 20S proteasome processes NF-κB1 p105 into p50 in a translation-independent manner. *EMBO J.* **25:** 1945–1956
Morrison DK (2012) MAP kinase pathways. *Cold Spring Harb. Perspect. Biol.* **4:** 1–5
Motshwene PG, Moncrieffe MC, Grossmann JG, Kao C, Ayaluru M, Sandercock AM, Robinson C V., Latz E & Gay NJ (2009) An Oligomeric Signaling Platform formed by the toll-like receptor signal transducers MyD88 and IRAK-4. *J. Biol. Chem.* **284:** 25404–25411
Moulder MPC, Witting K, Berlin I, Pruneda JN, Wu K-P, Chang J-G, Merkx R, Bialas J, Groettrup M, Vertegaal ACO, Schulman BA, Komander D, Neefjes J, Oualid F El & Huib O (2016) A cascading activity-based probe sequentially targets E1–E2–E3 ubiquitin enzymes. *Nat Chem Biol.* **12:** 523–530
Mukaka MM (2012) Statistics corner: A guide to appropriate use of correlation coefficient in medical research. *Malawi Med. J.* **24:** 69–71
Mukherjee S, Ghosh R & Maxfield F (1997) Endocytosis. *Physiol Rev* **77:** 759–803
Murray PJ & Wynn TA (2011) Protective and pathogenic functions of macrophage subsets. *Nat. Rev. Immunol.* **11:** 723–737
Musilova J, Mulcahy ME, Kuijk MM, McLoughlin RM & Bowie AG (2019) Toll-like receptor 2-dependent endosomal signaling by Staphylococcus aureus in monocytes induces type i interferon and promotes intracellular survival. *J. Biol. Chem.* **294:** 17031–

17042
Muzio M, Ni J, Feng P & Dixit VM (1997) IRAK (Pelle) family member IRAK-2 and MyD88 as proximal mediators of IL- 1 signaling. *Science (80-.).* **278:** 1612–1615
Muzioł T, Pineda-Molina E, Ravelli RB, Zamborlini A, Usami Y, Göttlinger H & Weissenhorn W (2006) Structural Basis for Budding by the ESCRT-III Factor CHMP3. *Dev. Cell* **10:** 821–830
Nagano F, Kawabe H, Nakanishi H, Shinohara M, Deguchi-Tawarada M, Takeuchi M, Sasaki T & Takai Y (2002) Rabconnectin-3, a novel protein that binds both GDP/GTP exchange protein and GTPase-activating protein for Rab3 small G protein family. *J. Biol. Chem.* **277:** 9629–9632
Nanda SK, Nagamori T, Windheim M, Amu S, Aviello G, Patterson-Kane J, Arthur JSC, Ley SC, Fallon P & Cohen P (2018) ABIN2 Function Is Required To Suppress DSS-Induced Colitis by a Tpl2-Independent Mechanism. *J. Immunol.* **201:** 3373–3382
Nanda SK, Venigalla RKC, Ordureau A, Patterson-Kane JC, Powell DW, Toth R, Arthur JSC & Cohen P (2011) Polyubiquitin binding to ABIN1 is required to prevent autoimmunity. *J. Exp. Med.* **208:** 1215–28
Netea MG, Kullberg BJ & Van der Meer JWM (2000) Circulating Cytokines as Mediators of Fever. *Clin. Infect. Dis.* **31:** S178–S184
Neumann Y, Bruns SA, Rohde M, Prajsnar TK, Foster SJ & Schmitz I (2016) Intracellular Staphylococcus aureus eludes selective autophagy by activating a host cell kinase. *Autophagy* **12:** 2069–2084
Newman S, Fan L, Pribnow A, Silkov A, Rice S V., Lee S, Shao Y, Shaner B, Mulder H, Nakitandwe J, Shurtleff S, Azzato EM, Wu G, Zhou X, Barnhill R, Easton J, Nichols KE, Ellison DW, Downing JR, Pappo A, et al (2019) Clinical genome sequencing uncovers potentially targetable truncations and fusions of MAP3K8 in spitzoid and other melanomas. *Nat. Med.* **25:** 597–602
Ng EL, Wang Y & Tang BL (2007) Rab22B's role in trans-Golgi network membrane dynamics. *Biochem. Biophys. Res. Commun.* **361:** 751–757
Nielsen E, Severin F, Backer JM, Hyman AA & Zerial M (1999) Rab5 regulates motility of early endosomes on microtubules. *Nat. Cell Biol.* **1:** 376–382
Nordenfelt P & Tapper H (2011) Phagosome dynamics during phagocytosis by neutrophils. *J. Leukoc. Biol.* **90:** 271–284
O'Keefe SJ, Mudgett JS, Cupo S, Parsons JN, Chartrain NA, Fitzgerald C, Chen SL, Lowitz K, Rasa C, Visco D, Luell S, Carballo-Jane E, Owens K & Zaller DM (2007) Chemical genetics define the roles of p38α and p38β in acute and chronic inflammation. *J. Biol. Chem.* **282:** 34663–34671
O'Neill LAJ & Bowie AG (2007) The family of five: TIR-domain-containing adaptors in Toll-like receptor signalling. *Nat. Rev. Immunol.* **7:** 353–364
Ochiai H, Sakai S, Hirabayashi T, Shimizu Y & Terasawa K (1995) Inhibitory effect of bafilomycin A1, a specific inhibitor of vacuolar-type proton pump, on the growth of influenza A and B viruses in MDCK cells. *Antiviral Res.* **27:** 425–430
Odin JA, Edberg JC, Painter CJ, Kimberly RP & Unkeless JC (1991) Regulation of phagocytosis and [Ca2+]i flux by distinct regions of an Fc receptor. *Science (80-.).* **254:** 1785–1788
Odorizzi G (2006) The multiple personalities of Alix. *J. Cell Sci.* **119:** 3025–3032
Oeckinghaus A & Ghosh S (2009) The NF-kappaB family of transcription factors and its regulation. *Cold Spring Harb. Perspect. Biol.* **1:** 1–14
Ohnishi H, Tochio H, Kato Z, Orii KE, Li A, Kimura T, Hiroaki H, Kondo N & Shirakawa M (2009) Structural basis for the multiple interactions of the MyD88 TIR domain in TLR4 signaling. *Proc. Natl. Acad. Sci. U. S. A.* **106:** 10260–10265
Ohtake F, Saeki Y, Ishido S, Kanno J & Tanaka K (2016) The K48-K63 Branched Ubiquitin Chain Regulates NF-κB Signaling. *Mol. Cell* **64:** 251–266
Okumura M, Ichioka F, Kobayashi R, Suzuki H, Yoshida H, Shibata H & Maki M (2009)

Penta-EF-hand protein ALG-2 functions as a Ca2+-dependent adaptor that bridges Alix and TSG101. *Biochem. Biophys. Res. Commun.* **386:** 237–241

Ordureau A, Smith H, Windheim M, Peggie M, Carrick E, Morrice N & Cohen P (2008) The IRAK-catalysed activation of the E3 ligase function of Pellino isoforms induces the Lys63 -linked polyubiquitination of IRAK1. *Biochem. J.* **409:** 43–52

Orian A (2000) SCFbeta-TrCP ubiquitin ligase-mediated processing of NF-kappaB p105 requires phosphorylation of its C-terminus by IkappaB kinase. *EMBO J.* **19:** 2580–2591

Oviedo-Boyso J, Cortés-Vieyra R, Huante-Mendoza A, Yu HB, Valdez-Alarcón JJ, Bravo-Patiño A, Cajero-Juárez M, Finlay BB & Baizabal-Aguirre VM (2011) The phosphoinositide-3-kinase-akt signaling pathway is important for Staphylococcus aureus internalization by endothelial cells. *Infect. Immun.* **79:** 4569–4577

Pagès G & Pouysségur J (2004) MAP Kinase Signaling Humana Press

Palecanda A, Paulauskis J, Al-Mutairi E, Imrich A, Qin G, Suzuki H, Kodama T, Tryggvason K, Koziel H & Kobzik L (1999) Role of the scavenger receptor MARCO in alveolar macrophage binding of unopsonized environmental particles. *J. Exp. Med.* **189:** 1497–1506

Papoutsopoulou S, Symons A, Tharmalingham T, Belich MP, Kaiser F, Kioussis D, O'Garra A, Tybulewicz V & Ley SC (2006) ABIN-2 is required for optimal activation of Erk MAP kinase in innate immune responses. *Nat. Immunol.* **7:** 606–615

Park BS & Lee JO (2013) Recognition of lipopolysaccharide pattern by TLR4 complexes. *Exp. Mol. Med.* **45:** e66-9

Parker DC (1993) T cell-dependent B cell activation. *Annu. Rev. Immunol.* **11:** 331–360

Parra KJ & Kane PM (1998) Reversible Association between the V1 and V0 Domains of Yeast Vacuolar H+-ATPase Is an Unconventional Glucose-Induced Effect. *Mol. Cell. Biol.* **18:** 7064–7074

Parsons DW, Jones S, Zhang X, Lin JCH, Leary RJ, Angenendt P, Mankoo P, Carter H, Siu IM, Gallia GL, Olivi A, McLendon R, Rasheed BA, Keir S, Nikolskaya T, Nikolsky Y, Busam DA, Tekleab H, Diaz LA, Hartigan J, et al (2008) An integrated genomic analysis of human glioblastoma multiforme. *Science (80-.).* **321:** 1807–1812

Patriotis C, Makris a, Bear SE & Tsichlis PN (1993) Tumor progression locus 2 (Tpl-2) encodes a protein kinase involved in the progression of rodent T-cell lymphomas and in T-cell activation. *Proc. Natl. Acad. Sci. U. S. A.* **90:** 2251–5

Pattison MJ, Mitchell O, Flynn HR, Chen C-S, Yang H-T, Ben-Addi H, Boeing S, Snijders AP & Ley SC (2016) TLR and TNF-R1 activation of the MKK3/MKK6-p38 axis in macrophages is mediated by TPL-2 kinase. *Biochem. J.* **473:** 2845–2861

Pauls E, Nanda SK, Smith H, Toth R, Arthur JSC & Cohen P (2013) Two Phases of Inflammatory Mediator Production Defined by the Study of IRAK2 and IRAK1 Knock-in Mice. *J. Immunol.* **191:** 2717–2730

Pautz A, Art J, Hahn S, Nowag S, Voss C & Kleinert H (2010) Regulation of the expression of inducible nitric oxide synthase. *Nitric Oxide - Biol. Chem.* **23:** 75–93

Pauwels AM, Trost M, Beyaert R & Hoffmann E (2017) Patterns, Receptors, and Signals: Regulation of Phagosome Maturation. *Trends Immunol.* **38:** 407–422

Pawson T & Scott JD (1997) Signaling through scaffold, anchoring, and adaptor proteins. *Science (80-.).* **278:** 2075–2080

Peiser L, Gough PJ, Kodama T & Gordon S (2000) Macrophage Class A Scavenger Receptor-Mediated Phagocytosis of Escherichia coli : Role of Cell Heterogeneity , Microbial Strain , and Culture Conditions In Vitro. **68:** 1953–1963

Perry AK, Chow EK, Goodnough JB, Yeh WC & Cheng G (2004) Differential requirement for TANK-binding kinase-1 in type I interferon responses to toll-like receptor activation and viral infection. *J. Exp. Med.* **199:** 1651–1658

Perugorria MJ, Murphy LB, Fullard N, Chakraborty JB, Vyrla D, Wilson CL, Oakley F, Mann J & Mann DA (2013) Tumor progression locus 2/Cot is required for activation

of extracellular regulated kinase in liver injury and toll-like receptor-induced TIMP-1 gene transcription in hepatic stellate cells in mice. *Hepatology* **57:** 1238–1249

Petty NK, Bulgin R, Crepin VF, Cerdeño-Tárraga AM, Schroeder GN, Quail MA, Lennard N, Corton C, Barron A, Clark L, Toribio AL, Parkhill J, Dougan G, Frankel G & Thomson NR (2010) The Citrobacter rodentium genome sequence reveals convergent evolution with human pathogenic Escherichia coli. *J. Bacteriol.* **192:** 525–538

Pham OH & McSorley SJ (2015) Protective host immune responses to Salmonella infection. *Future Microbiol.* **10:** 101–110

Pinna LA & Ruzzene M (1996) How do protein kinases recognize their substrates? *Biochim. Biophys. Acta - Mol. Cell Res.* **1314:** 191–225

Plüddemann A, Mukhopadhyay S & Gordon S (2011) Innate immunity to intracellular pathogens: Macrophage receptors and responses to microbial entry. *Immunol. Rev.* **240:** 11–24

Poltorak A, He X, Smirnova I, Liu MY, Van Huffel C, Du X, Birdwell D, Alejos E, Silva M, Galanos C, Freudenberg M, Ricciardi-Castagnoli P, Layton B & Beutler B (1998a) Defective LPS signaling in C3H/HeJ and C57BL/10ScCr mice: Mutations in Tlr4 gene. *Science (80-.).* **282:** 2085–2088

Poltorak A, Smirnova I, He X, Liu MY, Van Huffel C, Birdwell D, Alejos E, Silva M, Du X, Thompson P, Chan EKL, Ledesma J, Roe B, Clifton S, Vogel SN & Beutler B (1998b) Genetic and physical mapping of the Lps locus: Identification of the toll-4 receptor as a candidate gene in the critical region. *Blood Cells, Mol. Dis.* **24:** 340–355

Poteryaev D, Datta S, Ackema K, Zerial M & Spang A (2010) Identification of the switch in early-to-late endosome transition. *Cell* **141:** 497–508

Pugin J, Heumann D, Tomasz A, Kravchenko V V., Akamatsu Y, Nishijima M, Glauser MP, Tobias PS & Ulevitch RJ (1994) CD14 Is a pattern recognition receptor. *Immunity* **1:** 509–516

Pugin J, Schurer-Maly CC, Leturcq D, Moriarty A, Ulevitch RJ & Tobias PS (1993) Lipopolysaccharide activation of human endothelial and epithelial cells is mediated by lipopolysaccharide-binding protein and soluble CD14. *Proc. Natl. Acad. Sci. U. S. A.* **90:** 2744–2748

Pullen N & Thomas G (1997) The modular phosphorylation and activation of p70(s6k). *FEBS Lett.* **410:** 78–82

Rahighi S, Ikeda F, Kawasaki M, Akutsu M, Suzuki N, Kato R, Kensche T, Uejima T, Bloor S, Komander D, Randow F, Wakatsuki S & Dikic I (2009) Specific Recognition of Linear Ubiquitin Chains by NEMO Is Important for NF-κB Activation. *Cell* **136:** 1098–1109

Raiborg C, Wesche J, Malerød L & Stenmark H (2006) Flat clathrin coats on endosomes mediate degradative protein sorting by scaffolding Hrs in dynamic microdomains. *J. Cell Sci.* **119:** 2414–2424

Rappl C, Deiwick J & Hensel M (2003) Acidic pH is required for the functional assembly of the type III secretion system encoded by Salmonella pathogenicity island 2. *FEMS Microbiol. Lett.* **226:** 363–372

Rath M, Müller I, Kropf P, Closs EI & Munder M (2014) Metabolism via arginase or nitric oxide synthase: Two competing arginine pathways in macrophages. *Front. Immunol.* **5:** 1–10

Rincón M & Davis RJ (2009) Regulation of the immune response by stress-activated protein kinases. *Immunol. Rev.* **228:** 212–224

Rink J, Ghigo E, Kalaidzidis Y & Zerial M (2005) Rab conversion as a mechanism of progression from early to late endosomes. *Cell* **122:** 735–749

Riquelme S, Wozniak A, Kalergis A & Bueno S (2011) Evasion of Host Immunity by Virulent Salmonella: Implications for Vaccine Design. *Curr. Med. Chem.* **18:** 5666–

5675
Risso A (2000) Leukocyte antimicrobial peptides: multifunctional effector molecules of innate immunity. *J. Leukoc. Biol.* **68:** 785–92
Robinson MJ, Beinke S, Kouroumalis A, Tsichlis PN & Ley SC (2007) Phosphorylation of TPL-2 on Serine 400 Is Essential for Lipopolysaccharide Activation of Extracellular Signal-Regulated Kinase in Macrophages. *Mol. Cell. Biol.* **27:** 7355–7364
Roche PA & Furuta K (2015) The ins and outs of MHC class II-mediated antigen processing and presentation. *Nat. Rev. Immunol.* **15:** 203–216
Roger T, Froidevaux C, Le Roy D, Reymond MK, Chanson AL, Mauri D, Burns K, Riederer BM, Akira S & Calandra T (2009) Protection from lethal Gram-negative bacterial sepsis by targeting Toll-like receptor 4. *Proc. Natl. Acad. Sci. U. S. A.* **106:** 2348–2352
Roget K, Ben-Addi A, Mambole-Dema A, Gantke T, Yang H-T, Janzen J, Morrice N, Abbott D & Ley SC (2012) IkB Kinase 2 Regulates TPL-2 Activation of Extracellular Signal-Regulated Kinases 1 and 2 by Direct Phosphorylation of TPL-2 Serine 400. *Mol. Cell. Biol.* **32:** 4684–4690
Roh JS & Sohn DH (2018) Damage-Associated Molecular Patterns in Inflammatory Diseases. *Immune Netw.* **18:** 1–14
Rosales C & Uribe-Querol E (2017) Phagocytosis: A Fundamental Process in Immunity. *Biomed Res. Int.*
Ross GD, Reed W, Dalzell JG, Becker SE & Hogg N (1992) Macrophage cytoskeleton association with CR3 and CR4 regulates receptor mobility and phagocytosis of iC3b-opsonized erythrocytes. *J. Leukoc. Biol.* **51:** 109–117
Roszer T (2015) Understanding the Mysterious M2 Macrophage through Activation Markers and Effector Mechanisms. *Mediators Inflamm.* **2015:** 1–16
Roulis M, Nikolaou C, Kotsaki E, Kaffe E, Karagianni N, Koliaraki V, Salpea K, Ragoussis J, Aidinis V, Martini E, Becker C, Herschman HR, Vetrano S, Danese S & Kollias G (2014) Intestinal myofibroblast-specific Tpl2-Cox-2-PGE2 pathway links innate sensing to epithelial homeostasis. *Proc. Natl. Acad. Sci. U. S. A.* **111:** E4658–E4667
Roux PP & Blenis J (2004) ERK and p38 MAPK-Activated Protein Kinases: a Family of Protein Kinases with Diverse Biological Functions. *Microbiol. Mol. Biol. Rev.* **68:** 320–344
Roux PP & Topisirovic I (2018) Signaling Pathways Involved in the Regulation of mRNA Translation. *Mol. Cell. Biol.* **38:** 1–26
Rowe DC, McGettrick AF, Latz E, Monks BG, Gay NJ, Yamamoto M, Akira S, O'Neill LA, Fitzgerald KA & Golenbock DT (2006) The myristoylation of TRIF-related adaptor molecule is essential for Toll-like receptor 4 signal transduction. *Proc. Natl. Acad. Sci. U. S. A.* **103:** 6299–6304
Rupper AC, Rodriguez-Paris JM, Grove BD & Cardelli JA (2001) p110-Related PI 3-kinases regulate phagosome-phagosome fusion and phagosomal pH through a PKB/Akt dependent pathway in Dictyostelium. *J. Cell Sci.* **114:** 1283–1295
Russell DA, Pottier RH & Valenzeno DP (1995) In vivo spectroscopic properties of the fluorescent pH indicator biscarboxyethyl carboxyfluorescein. *J. Photochem. Photobiol. B Biol.* **29:** 17–22
Russell DG, Vanderven BC, Glennie S, Mwandumba H & Heyderman RS (2009) The macrophage marches on its phagosome: Dynamic assays of phagosome function. *Nat. Rev. Immunol.* **9:** 594–600
Rybicka JM, Balce DR, Chaudhuri S, Allan ERO & Yates RM (2012) Phagosomal proteolysis in dendritic cells is modulated by NADPH oxidase in a pH-independent manner. *EMBO J.* **31:** 932–944
Rybicka JM, Balce DR, Khan MF, Krohn RM & Yates RM (2010) NADPH oxidase activity

controls phagosomal proteolysis in macrophages through modulation of the lumenal redox environment of phagosomes. *Proc. Natl. Acad. Sci. U. S. A.* **107:** 10496–10501

Ryder P V., Vistein R, Gokhale A, Seaman MN, Puthenveedu MA & Faundez V (2013) The WASH complex, an endosomal Arp2/3 activator, interacts with the Hermansky-Pudlak syndrome complex BLOC-1 and its cargo phosphatidylinositol-4- kinase type IIα. *Mol. Biol. Cell* **24:** 2269–2284

Salmerón A, Janzen J, Soneji Y, Bump N, Kamens J, Allen H & Ley SC (2001) Direct Phosphorylation of NF-κB1 p105 by the IκB Kinase Complex on Serine 927 Is Essential for Signal-induced p105 Proteolysis. *J. Biol. Chem.* **276:** 22215–22222

Sanchez-Muñoz F, Dominguez-Lopez A & Yamamoto-Furusho JK (2008) Role of cytokines in inflammatory bowel disease. *World J. Gastroenterol.* **14:** 4280–4288

Sanger A, Hirst J, Davies AK & Robinson MS (2019) Adaptor protein complexes and disease at a glance. *J. Cell Sci.* **132:** 1–8

Sano H, Peck GR, Kettenbach AN, Gerber SA & Lienhard GE (2011) Insulin-stimulated GLUT4 protein translocation in adipocytes requires the rab10 guanine nucleotide exchange factor dennd4C. *J. Biol. Chem.* **286:** 16541–16545

Sarbassov DD, Guertin DA, Ali SM & Sabatini DM (2005) Phosphorylation and regulation of Akt/PKB by the rictor-mTOR complex. *Science (80-.).* **307:** 1098–1101

Sato S, Sanjo H, Takeda K, Ninomiya-Tsuji J, Yamamoto M, Kawai T, Matsumoto K, Takeuchi O & Akira S (2005) Essential function for the kinase TAK1 in innate and adaptive immune responses. *Nat. Immunol.* **6:** 1087–1095

Savina A, Jancic C, Hugues S, Guermonprez P, Vargas P, Moura IC, Lennon-Duménil AM, Seabra MC, Raposo G & Amigorena S (2006) NOX2 Controls Phagosomal pH to Regulate Antigen Processing during Crosspresentation by Dendritic Cells. *Cell* **126:** 205–218

Savinova O V., Hoffmann A & Ghosh G (2009) The Nfkb1 and Nfkb2 Proteins p105 and p100 Function as the Core of High-Molecular-Weight Heterogeneous Complexes. *Mol. Cell* **34:** 591–602

Schaeffer HJ & Weber MJ (1999) Mitogen-Activated Protein Kinases: Specific Messages from Ubiquitous Messengers. *Mol. Cell. Biol.* **19:** 2435–2444

Schliwa M (1982) Action of cytochalasin D on cytoskeletal networks. *J. Cell Biol.* **92:** 79–91

Schmidt O & Teis D (2012) The ESCRT machinery. *Curr. Biol.* **22:** R116–R120

Schroder K, Hertzog P, Ravasi T & Hume DA (2004) IFN Gamma an Overview. *J. Leukoc. Biol.* **75:** 163–189

Schuijs MJ, Willart MA, Vergote K, Gras D, Deswarte K, Ege MJ, Madeira FB, Beyaert R, Van Loo G, Bracher F, Von Mutius E, Chanez P, Lambrecht BN & Hammad H (2015) Farm dust and endotoxin protect against allergy through A20 induction in lung epithelial cells. *Science (80-.).* **349:** 1106–1110

Schulman BA, Lindstrom DL & Harlow E (1998) Substrate recruitment to cyclin-dependent kinase 2 by a multipurpose docking site on cyclin A. *Proc. Natl. Acad. Sci. U. S. A.* **95:** 10453–10458

Schwartz DC & Hochstrasser M (2003) A superfamily of protein tags: Ubiquitin, SUMO and related modifiers. *Trends Biochem. Sci.* **28:** 321–328

Scumpia PO, Botten GA, Norman JS, Kelly-Scumpia KM, Spreafico R, Ruccia AR, Purbey PK, Thomas BJ, Modlin RL & Smale ST (2017) Opposing roles of Toll-like receptor and cytosolic DNA-STING signaling pathways for Staphylococcus aureus cutaneous host defense. *PLoS Pathog.* **13:** 1–30

Searle S, Bright NA, Roach TIA, Atkinson PGP, Barton CH, Meloen RH & Blackwell JM (1998) Localisation of Nramp1 in macrophages: Modulation with activation and infection. *J. Cell Sci.* **111:** 2855–2866

Seibenhener ML, Babu JR, Geetha T, Wong HC, Krishna NR & Wooten MW (2004)

Sequestosome 1/p62 Is a Polyubiquitin Chain Binding Protein Involved in Ubiquitin Proteasome Degradation. *Mol. Cell. Biol.* **24:** 8055–8068

Seilie ES & Wardenburg JB (2017) Staphylococcus aureus pore-forming toxins: the interface of pathogen and host complexity. *Semin Cell Dev Biol.* **72:** 101–116

Senger K, Pham VC, Varfolomeev E, Hackney JA, Corzo CA, Collier J, Lau VWC, Huang Z, Hamidzhadeh K, Caplazi P, Peng I, Setiadi AF, Francis R, Paler-Martinez A, Kwon YC, Ramirez-Carrozzi V, Sun Y, Grigg PW, Roose-Girma M, Jeet S, et al (2017) The kinase TPL2 activates ERK and p38 signaling to promote neutrophilic inflammation. *Sci. Signal.* **10:**

Serbina N V., Salazar-Mather TP, Biron CA, Kuziel WA & Pamer EG (2003) TNF/iNOS-producing dendritic cells mediate innate immune defense against bacterial infection. *Immunity* **19:** 59–70

Sethi N, Yan Y, Quek D, Schupbach T & Kang Y (2010) Rabconnectin-3 is a functional regulator of mammalian notch signaling. *J. Biol. Chem.* **285:** 34757–34764

Seto S, Tsujimura K & Koide Y (2011) Rab GTPases Regulating Phagosome Maturation Are Differentially Recruited to Mycobacterial Phagosomes. *Traffic* **12:** 407–420

Sette P, Jadwin JA, Dussupt V, Bello NF & Bouamr F (2010) The ESCRT-Associated Protein Alix Recruits the Ubiquitin Ligase Nedd4-1 To Facilitate HIV-1 Release through the LYPXnL L Domain Motif. *J. Virol.* **84:** 8181–8192

Shapouri-Moghaddam A, Mohammadian S, Vazini H, Taghadosi M, Esmaeili SA, Mardani F, Seifi B, Mohammadi A, Afshari JT & Sahebkar A (2018) Macrophage plasticity, polarization, and function in health and disease. *J. Cell. Physiol.* **233:** 6425–6440

Shen H, Tesar BM, Walker WE & Goldstein DR (2008) Dual Signaling of MyD88 and TRIF are Critical for Maximal TLR4- Induced Dendritic Cell Maturation. *J Immunol.* **181:** 1849–1858

Shields SB & Piper RC (2011) How ubiquitin functions with ESCRTs. *Traffic* **12:** 1306–1317

Da Silva Correia J, Soldau K, Christen U, Tobias PS & Ulevitch RJ (2001) Lipopolysaccharide is in close proximity to each of the proteins in its membrane receptor complex. Transfer from CD14 to TLR4 and MD-2. *J. Biol. Chem.* **276:** 21129–21135

Da Silva Correia J & Ulevitch RJ (2002) MD-2 and TLR4 N-linked glycosylations are important for a functional lipopolysaccharide receptor. *J. Biol. Chem.* **277:** 1845–1854

Simonsen A, Lippe R, Christoforidis S, Gaullier J-M, Brech A, Callaghan J, Toh B-H, Murphy C, Zerial M & Stenmark H (1998) EEA1 links PI(3)K function to Rab5 regulation of endosome fusion. *Nature* **394:** 494–498

Smith-Garvin JE, Koretzky GA & Jordan MS (2009) T Cell Activation. *Annu Rev Immunol.* **27:** 591–619

Smith H, Liu XY, Dai L, Goh ETH, Chan AT, Xi J, Seh CC, Qureshi IA, Lescar J, Ruedl C, Gourlay R, Morton S, Hough J, McIver EG, Cohen P & Cheung PCF (2011) The role of TBK1 and IKKε in the expression and activation of Pellino 1. *Biochem. J.* **434:** 537–548

Soliman M, Seo JY, Kim DS, Kim JY, Park JG, Alfajaro MM, Baek Y Bin, Cho EH, Kwon J, Choi JS, Kang M Il, Park SI & Cho KO (2018) Activation of PI3K, Akt, and ERK during early rotavirus infection leads to V-ATPase-dependent endosomal acidification required for uncoating. *PLoS Pathog.* **14:** 1–32

Song-Zhao GX, Srinivasan N, Pott J, Baban D, Frankel G & Maloy KJ (2014) Nlrp3 activation in the intestinal epithelium protects against a mucosal pathogen. *Mucosal Immunol.* **7:** 763–774

Soond SM, Everson B, Riches DWH & Murphy G (2005) ERK-mediated phosphorylation of Thr735 in TNFα-converting enzyme and its potential role in TACE protein

trafficking. *J. Cell Sci.* **118:** 2371–2380
Spence J, Sadis S, Haas AL & Finley D (1995) A ubiquitin mutant with specific defects in DNA repair and multiubiquitination. *Mol. Cell. Biol.* **15:** 1265–1273
Spencer E, Jiang J & Chen ZJ (1999) Signal-induced ubiquitination of IκBα by the F-box protein Slimb/β- TrCP. *Genes Dev.* **13:** 284–294
Sriskantharajah S, Belich MP, Papoutsopoulou S, Janzen J, Tybulewicz V, Seddon B & Ley SC (2009) Proteolysis of NF-κB1 p105 is essential for T cell antigen receptor-induced proliferation. *Nat. Immunol.* **10:** 38–47
Sriskantharajah S, Gückel E, Tsakiri N, Kierdorf K, Brender C, Ben-Addi A, Veldhoen M, Tsichlis PN, Stockinger B, O'Garra A, Prinz M, Kollias G & Ley SC (2014) Regulation of Experimental Autoimmune Encephalomyelitis by TPL-2 Kinase. *J. Immunol.* **192:** 3518–29
Stack J, Doyle SL, Connolly DJ, Reinert LS, O'Keeffe KM, McLoughlin RM, Paludan SR & Bowie AG (2014) TRAM Is Required for TLR2 Endosomal Signaling to Type I IFN Induction. *J. Immunol.* **193:** 6090–6102
Stafford MJ, Morrice NA, Peggie MW & Cohen P (2006) Interleukin-1 stimulated activation of the COT catalytic subunit through the phosphorylation of Thr290 and Ser62. *FEBS Lett.* **580:** 4010–4014
Steinberg BE, Huynh KK, Brodovitch A, Jabs S, Stauber T, Jentsch TJ & Grinstein S (2010) A cation counterflux supports lysosomal acidification. *J. Cell Biol.* **189:** 1171–1186
Stenmark H (2009) Rab GTPases as coordinators of vesicle traffic. *Nat. Rev. Mol. Cell Biol.* **10:** 513–525
Straub RH & Schradin C (2016) Chronic inflammatory systemic diseases – an evolutionary trade-off between acutely beneficial but chronically harmful programs. *Evol. Med. Public Heal.* **2016:** 37–51
Stuart LM, Deng J, Silver JM, Takahashi K, Tseng AA, Hennessy EJ, Ezekowitz RAB & Moore KJ (2005) Response to Staphylococcus aureus requires CD36-mediated phagocytosis triggered by the COOH-terminal cytoplasmic domain. *J. Cell Biol.* **170:** 477–485
Stuchell MD, Garrus JE, Müller B, Stray KM, Ghaffarian S, McKinnon R, Kräusslich HG, Morham SG & Sundquist WI (2004) The human endosomal sorting complex required for transport (ESCRT-I) and its role in HIV-1 budding. *J. Biol. Chem.* **279:** 36059–36071
Sturgill-Koszycki S, Schlesinger PH, Chakraborty P, Haddix PL, Collins HL, Fok AK, Allen RD, Gluck SL, Heuser J & Russell DG (1994) Lack of acidification in Mycobacterium phagosomes produced by exclusion of the vesicular proton-ATPase. *Science (80-.).* **263:** 678–681
Sulahian TH, Imrich A, DeLoid G, Winkler AR & Kobzik L (2008) Signaling pathways required for macrophage scavenger receptor-mediated phagocytosis: Analysis by scanning cytometry. *Respir. Res.* **9:** 1–15
Swatek KN & Komander D (2016) Ubiquitin modifications. *Cell Res.* **26:** 399–422
Symons A, Beinke S & Ley SC (2006) MAP kinase kinase kinases and innate immunity. *Trends Immunol.* **27:** 40–48
Tae WK, Staschke K, Bulek K, Yao J, Peters K, Oh KH, Vandenburg Y, Xiao H, Qian W, Hamilton T, Min B, Sen G, Gilmour R & Li X (2007) A critical role for IRAK4 kinase activity in Toll-like receptor-mediated innate immunity. *J. Exp. Med.* **204:** 1025–1036
Takeuchi O & Akira S (2010) Pattern Recognition Receptors and Inflammation. *Cell* **140:** 805–820
Takeuchi O, Hoshino K & Akira S (2000) Cutting Edge: TLR2-Deficient and MyD88-Deficient Mice Are Highly Susceptible to Staphylococcus aureus Infection . *J. Immunol.* **165:** 5392–5396

Tan Y, Zanoni I, Cullen TW, Goodman AL & Kagan JC (2015) Mechanisms of Toll-like receptor 4 endocytosis reveal a common immune-evasion strategy used by pathogenic and commensal bacteria. *Physiol. Behav.* **43:** 909–922

Taniuchi I (2018) CD4 Helper and CD8 Cytotoxic T Cell Differentiation. *Annu. Rev. Immunol.* **36:** 579–601

Tanner JJ, Frey BB, Pemberton T & Henzl MT (2016) EF5 Is the High-Affinity Mg2+ Site in ALG-2. *Biochemistry* **55:** 5128–5141

Tarabykina S, Møller AL, Durussel I, Cox J & Berchtold MW (2000) Two forms of the apoptosis-linked protein ALG-2 with different Ca2+ affinities and target recognition. *J. Biol. Chem.* **275:** 10514–10518

Teijaro JR (2016) Type I interferons in viral control and immune regulation. *Curr. Opin. Virol.* **16:** 31–40

Tenno T, Fujiwara K, Tochio H, Iwai K, Morita EH, Hayashi H, Murata S, Hiroaki H, Sato M, Tanaka K & Shirakawa M (2004) Structural basis for distinct roles of Lys63- and Lys48-linked polyubiquitin chains. *Genes to Cells* **9:** 865–875

Thi EP & Reiner NE (2012) Phosphatidylinositol 3-kinases and their roles in phagosome maturation. *J. Leukoc. Biol.* **92:** 553–566

Thoma B, Grell M, Pfizenmaier K & Scheurich P (1990) Identification of a 60-kD tumor necrosis factor (TNF) receptor as the major signal transducing component in TNF responses. *J. Exp. Med.* **172:** 1019–1023

Thurston TLM, Matthews SA, Jennings E, Alix E, Shao F, Shenoy AR, Birrell MA & Holden DW (2016) Growth inhibition of cytosolic Salmonella by caspase-1 and caspase-11 precedes host cell death. *Nat. Commun.* **7:** 1–15

Tobias PS, Soldau K & Ulevitch RJ (1986) Isolation of a lipopolysaccharide-binding acute phase reactant from rabbit serum. *J. Exp. Med.* **164:** 777–793

Tomczak MF, Gadjeva M, Wang YY, Brown K, Maroulakou I, Tsichlis PN, Erdman SE, Fox JG & Horwitz BH (2006) Defective Activation of ERK in Macrophages Lacking the p50/p105 Subunit of NF-κB Is Responsible for Elevated Expression of IL-12 p40 Observed after Challenge with Helicobacter hepaticus . *J. Immunol.* **176:** 1244–1251

Tournier C, Dong C, Turner TK, Jones SN, Flavell RA & Davis RJ (2001) MKK7 is an essential component of the JNK signal transduction pathway activated by proinflammatory cytokines. *Genes Dev.* **15:** 1419–1426

Towbin H, Staehelin T & Gordon J (1979) Electrophoretic transfer of proteins from polyacrylamide gels to nitrocellulose sheets: procedure and some applications. *Proc. Natl. Acad. Sci. U. S. A.* **76:** 4350–4354

Traer CJ, Rutherford AC, Palmer KJ, Wassmer T, Oakley J, Attar N, Carlton JG, Kremerskothen J, Stephens DJ & Cullen PJ (2007) SNX4 coordinates endosomal sorting of TfnR with dynein-mediated transport into the endocytic recycling compartment. *Nat. Cell Biol.* **9:** 1370–1380

Traub LM & Lukacs GL (2007) Decoding ubiquitin sorting signals for clathrin-dependent endocytosis by CLASPs. *J. Cell Sci.* **120:** 543–553

Tridandapani S, Lyden TW, Smith JL, Carter JE, Coggeshall KM & Anderson CL (2000) The adapter protein LAT enhances Fcγ receptor-mediated signal transduction in myeloid cells. *J. Biol. Chem.* **275:** 20480–20487

Trost M, English L, Lemieux S, Courcelles M, Desjardins M & Thibault P (2009) The Phagosomal Proteome in Interferon-γ-Activated Macrophages. *Immunity* **30:** 143–154

Tsai RK & Discher DE (2008) Inhibition of 'self' engulfment through deactivation of myosin-II at the phagocytic synapse between human cells. *J. Cell Biol.* **180:** 989–1003

Tsolmongyn B, Koide N, Jambalganiin U, Odkhuu E, Naiki Y, Komatsu T, Yoshida T & Yokochi T (2013) A Toll-like receptor 2 ligand, Pam3CSK4, augments interferon-γ-

induced nitric oxide production via a physical association between MyD88 and interferon-γ receptor in vascular endothelial cells. *Immunology* **140:** 352–361

Turk B, Dolenc I, Turk V & Bieth JG (1993) Kinetics of the pH-induced Inactivation of Human Cathepsin L. *Biochemistry* **32:** 375–380

Turk B, Turk D & Turk V (2000) Lysosomal cysteine proteases: More than scavengers. *Biochim. Biophys. Acta - Protein Struct. Mol. Enzymol.* **1477:** 98–111

Tuttle AM, Hoffman TL & Schilling TF (2014) Rabconnectin-3a Regulates Vesicle Endocytosis and Canonical Wnt Signaling in Zebrafish Neural Crest Migration. *PLoS Biol.* **12:** 1–14

Tuveson DA & Jacks T (1999) Modeling human lung cancer in mice: similarities and shortcomings. *Oncogene* **18:** 5318–24

Tzeng E, Billiar TR, Robbins PD, Loftus M & Stuehr DJ (1995) Expression of human inducible nitric oxide synthase in a tetrahydrobiopterin (H4B)-deficient cell line: H4B promotes assembly of enzyme subunits into an active dimer. *Proc. Natl. Acad. Sci. U. S. A.* **92:** 11771–11775

Ubersax JA & Ferrell JE (2007) Mechanisms of specificity in protein phosphorylation. *Nat. Rev. Mol. Cell Biol.* **8:** 530–541

Unbekandt M & Olson MF (2014) The actin-myosin regulatory MRCK kinases: Regulation, biological functions and associations with human cancer. *J. Mol. Med.* **92:** 217–225

Uribe-Quero E & Rosales C (2017) Control of phagocytosis by microbial pathogens. *Front. Immunol.* **8:** 1–23

Vachon E, Martin R, Kwok V, Cherepanov V, Chow CW, Doerschuk CM, Plumb J, Grinstein S & Downey GP (2007) CD44-mediated phagocytosis induces inside-out activation of complement receptor-3 in murine macrophages. *Blood* **110:** 4492–4502

Varadan R, Assfalg M, Haririnia A, Raasi S, Pickart C & Fushman D (2004) Solution Conformation of Lys63-linked Di-ubiquitin Chain Provides Clues to Functional Diversity of Polyubiquitin Signaling. *J. Biol. Chem.* **279:** 7055–7063

Varol C, Mildner A & Jung S (2015) Macrophages: Development and tissue specialization. *Annu. Rev. Immunol.* **33:** 643–675

Ventura S, Cano F, Kannan Y, Breyer F, Pattison MJ, Wilson MS & Ley SC (2018) A20-binding inhibitor of NF-κB (ABIN) 2 negatively regulates allergic airway inflammation. *J. Exp. Med.* **215:** 2737–2747

Vergne I, Fratti R, Hill P, Chua J, Belisle J & Deretic V (2004) Mycobacterium tuberculosis Phagosome Maturation Arrest: Mycobacterial Phosphatidylinositol Analog Phosphatidylinositol Mannoside Stimulates Early Endosomal Fusion. *Mol. Biol. Cell* **15:** 751–760

Verstrepen L, Carpentier I, Verhelst K & Beyaert R (2009) ABINs: A20 binding inhibitors of NF-kB and apoptosis signaling. *Biochem. Pharmacol.* **78:** 105–114

Vieira O V., Botelho RJ, Rameh L, Brachmann SM, Matsuo T, Davidson HW, Schreiber A, Backer JM, Cantley LC & Grinstein S (2001) Distinct roles of class I and class III phosphatidylinositol 3-kinases in phagosome formation and maturation. *J. Cell Biol.* **155:** 19–25

Vieira O V., Bucci C, Harrison RE, Trimble WS, Lanzetti L, Gruenberg J, Schreiber AD, Stahl PD & Grinstein S (2003a) Modulation of Rab5 and Rab7 Recruitment to Phagosomes by Phosphatidylinositol 3-Kinase. *Mol. Cell. Biol.* **23:** 2501–2514

Vieira O V, Bucci C, Harrison RE, Trimble WS, Lanzetti L, Gruenberg J, Schreiber AD, Stahl PD & Grinstein S (2003b) Modulation of Rab5 and Rab7 Recruitment to Phagosomes by Phosphatidylinositol 3-Kinase. **23:** 2501–2514

Vieira SM, Lemos HP, Grespan R, Napimoga MH, Dal-Secco D, Freitas A, Cunha TM, Verri WA, Souza DA, Jamur MC, Fernandes KS, Oliver C, Silva JS, Teixeira MM & Cunha FQ (2009) A crucial role for TNF-α in mediating neutrophil influx induced by

endogenously generated or exogenous chemokines, KC/CXCL1 and LIX/CXCL5. *Br. J. Pharmacol.* **158:** 779–789

Wagner S, Carpentier I, Rogov V, Kreike M, Ikeda F, Löhr F, Wu CJ, Ashwell JD, Dötsch V, Dikic I & Beyaert R (2008) Ubiquitin binding mediates the NF-κB inhibitory potential of ABIN proteins. *Oncogene* **27:** 3739–3745

Wagner SA, Satpathy S, Beli P & Choudhary C (2016) SPATA2 links CYLD to the TNF-α receptor signaling complex and modulates the receptor signaling outcomes. *EMBO J.* **35:** 1868–1884

Walsh MC, Kim GK, Maurizio PL, Molnar EE & Choi Y (2008) TRAF6 autoubiquitination-independent activation of the NFκB and MAPK pathways in response to IL-1 and RANKL. *PLoS One* **3:** 1–11

Wang C, Deng L, Hong M, Akkaraju GR, Inoue JI & Chen ZJ (2001) TAK1 is a ubiquitin-dependent kinase of MKK and IKK. *Nature* **412:** 346–351

Wang J, Ren J, Wu B, Feng S, Cai G, Tuluc F, Peränen J & Guo W (2015) Activation of Rab8 guanine nucleotide exchange factor Rabin8 by ERK1/2 in response to EGF signaling. *Proc. Natl. Acad. Sci. U. S. A.* **112:** 148–153

Wang M, Qazi IH, Wang L, Zhou G & Han H (2020) Salmonella virulence and immune escape. *Microorganisms* **8:** 1–25

Wang S, Deng S, Cao Y, Zhang R, Wang Z, Jiang X, Wang J, Zhang X, Zhang J, Liu G & Lian Z (2018) Overexpression of Toll-Like Receptor 4 Contributes to Phagocytosis of Salmonella Enterica Serovar Typhimurium via Phosphoinositide 3-Kinase Signaling in Sheep. *Cell. Physiol. Biochem.* **49:** 662–677

Wang T & Hong W (2002) Interorganellar Regulation of Lysosome Positioning by the Golgi Apparatus through Rab34 Interaction with Rab-interacting Lysosomal Protein. *Mol. Biol. Cell* **13:** 4317–4332

Warren LL, Moo-Kyung K, Schreiber AD & Grinstein S (2005) Role of Ubiquitin and Proteasomes in Phagosome Maturation. *Mol Biol Cell* **16:** 2077–2090

Wasmeier C, Romao M, Plowright L, Bennett DC, Raposo G & Seabra MC (2006) Rab38 and Rab32 control post-Golgi trafficking of melanogenic enzymes. *J. Cell Biol.* **175:** 271–281

Waterfield M, Jin W, Reiley W, Zhang M & Sun S-C (2004) IκB Kinase Is an Essential Component of the Tpl2 Signaling Pathway. *Mol. Cell. Biol.* **24:** 6040–6048

Waterfield MR, Zhang M, Norman LP & Sun SC (2003) NF-κB1/p105 regulates lipopolysaccharide-stimulated MAP kinase signaling by governing the stability and function of the Tpl2 kinase. *Mol. Cell* **11:** 685–694

Watford WT, Hissong BD, Durant LR, Yamane H, Muul LM, Kanno Y, Tato CM, Ramos HL, Berger AE, Mielke L, Pesu M, Solomon B, Frucht DM, Paul WE, Sher A, Jankovic D, Tsichlis PN & O'Shea JJ (2008) Tpl2 kinase regulates T cell interferon-γ production and host resistance to toxoplasma gondii. *J. Exp. Med.* **205:** 2803–2812

Watford WT, Wang C-C, Tsatsanis C, Mielke LA, Eliopoulos AG, Daskalakis C, Charles N, Odom S, Rivera J, O'Shea J & Tsichlis PN (2010) Ablation of Tumor Progression Locus 2 Promotes a Type 2 Th Cell Response in Ovalbumin-Immunized Mice. *J. Immunol.* **184:** 105–113

Webb L V., Ventura S & Ley SC (2019) ABIN-2, of the TPL-2 Signaling Complex, Modulates Mammalian Inflammation. *Trends Immunol.* **40:** 1–10

Wellbrock C, Karasarides M & Marais R (2004) The RAF proteins take centre stage. *Nat. Rev. Mol. Cell Biol.* **5:** 875–885

Wesche H, Gao X, Li X, Kirschning CJ, Stark GR & Cao Z (1999) IRAK-M Is a Novel Member of the Pelle / Interleukin-1 Receptor-associated Kinase (IRAK) Family. *J. Biol. Chem.* **274:** 19403–19410

White M V. (1990) The role of histamine in allergic diseases. *J. Allergy Clin. Immunol.* **86:** 599–605

Whitley P, Reaves BJ, Hashimoto M, Riley AM, Potter BVL & Holman GD (2003) Identification of mammalian Vps24p as an effector of phosphatidylinositol 3,5-bisphosphate-dependent endosome compartmentalization. *J. Biol. Chem.* **278:** 38786–38795

Wijk SJL & Timmers HTM (2010) The family of ubiquitin-conjugating enzymes (E2s): deciding between life and death of proteins. *FASEB J.* **24:** 981–993

Williams RL & Urbé S (2007) The emerging shape of the ESCRT machinery. *Nat. Rev. Mol. Cell Biol.* **8:** 355–368

Wilson LJ, Linley A, Hammond DE, Hood FE, Coulson JM, MacEwan DJ, Ross SJ, Slupsky JR, Smith PD, Eyers PA & Prior IA (2018) New Perspectives, opportunities, and challenges in exploring the human protein kinome. *Cancer Res.* **78:** 15–29

Winston JT, Strack P, Beer-Romero P, Chu CY, Elledge SJ & Harper JW (1999) The SCFbeta-TRCP-ubiquitin ligase complex associates specifically with phosphorylated destruction motifs in IkappaBalpha and beta-catenin and stimulates IkappaBalpha ubiquitination in vitro. *Genes Dev* **13:** 270–283

Winterbourn CC (2008) Reconciling the chemistry and biology of reactive oxygen species. *Nat. Chem. Biol.* **4:** 278–286

Wong YC & Holzbaur ELF (2014) Optineurin is an autophagy receptor for damaged mitochondria in parkin-mediated mitophagy that is disrupted by an ALS-linked mutation. *Proc. Natl. Acad. Sci. U. S. A.* **111:** E4439–E4448

Wright SD, Tobias PS, Ulevitch RJ & Ramos RA (1989) Lipopolysaccharide (LPS) binding protein opsonizes LPS-bearing particles for recognition by a novel receptor on macrophages. *J. Exp. Med.* **170:** 1231–1241

Wu J, Green N, Hotchandani R, Hu Y, Condon J, Huang A, Kaila N, Li HQ, Guler S, Li W, Tam SY, Wang Q, Pelker J, Marusic S, Hsu S, Perry Hall J, Telliez JB, Cui J & Lin LL (2009) Selective inhibitors of tumor progression loci-2 (Tpl2) kinase with potent inhibition of TNF-α production in human whole blood. *Bioorganic Med. Chem. Lett.* **19:** 3485–3488

Wullaert A, Verstrepen L, Van Huffel S, Adib-Conquy M, Cornelis S, Kreike M, Haegman M, El Bakkouri K, Sanders M, Verhelst K, Carpentier I, Cavaillon JM, Heyninck K & Beyaert R (2007) LIND/ABIN-3 is a novel lipopolysaccharide-inducible inhibitor of NF-κB activation. *J. Biol. Chem.* **282:** 81–90

Wurmser AE, Sato TK & Emr SD (2000) New component of the vacuolar class C-Vps complex couples nucleotide exchange on the Ypt7 GTPase to SNARE-dependent docking and fusion. *J. Cell Biol.* **151:** 551–562

Wynn T, Chawla A & Pollard JW (2013) Origins and Hallmarks of Macrophages: Development, Homeostasis, and Disease. *Nature* **496:** 445–455

Xia ZP, Sun L, Chen X, Pineda G, Jiang X, Adhikari A, Zeng W & Chen ZJ (2009) Direct activation of protein kinases by unanchored polyubiquitin chains. *Nature* **461:** 114–119

Xu D, Matsumoto ML, McKenzie BS & Zarrin AA (2018) TPL2 kinase action and control of inflammation. *Pharmacol. Res.* **129:** 188–193

Yamamoto A, Tagawa Y, Yoshimori T, Moriyama Y, Masaki R & Tashiro Y (1998) Bafilomycin A1 Prevents Maturation of Autophagic Vacuoles by Inhibiting Fusion between Autophagosomesand Lysosomesin Rat HepatomaCell Line ,. *Cell Struct. Funct.* **23:** 33–42

Yamamoto M, Sato S, Hemmi H, Hoshino K, Kaisho T, Sanjo H, Takeuchi O, Sugiyama M, Okabe M, Takeda K & Akira S (2003a) Role of adaptor TRIF in the MyD88-independent toll-like receptor signaling pathway. *Science (80-.).*

Yamamoto M, Sato S, Hemmi H, Uematsu S, Hoshino K, Kaisho T, Takeuchi O, Takeda K & Akira S (2003b) TRAM is specifically involved in the Toll-like receptor 4-mediated MyD88-independent signaling pathway. *Nat. Immunol.* **4:** 1144–1150

Yamaoka S, Courtois G, Bessia C, Whiteside ST, Weil R, Agou F, Kirk HE, Kay RJ &

Israël A (1998) Complementation cloning of NEMO, a component of the IκB kinase complex essential for NF-κB activation. *Cell* **93:** 1231–1240

Yang D, Tournier C, Wysk M, Lu HT, Xu J, Davis RJ & Flavell RA (1997) Targeted disruption of the MKK4 gene causes embryonic death, inhibition of c-Jun NH2-terminal kinase activation, and defects in AP-1 transcriptional activity. *Proc. Natl. Acad. Sci. U. S. A.* **94:** 3004–3009

Yang H-T, Papoutsopoulou S, Belich M, Brender C, Janzen J, Gantke T, Handley M & Ley SC (2012) Coordinate Regulation of TPL-2 and NF-kB Signaling in Macrophages by NF-kB1 p105. *Mol. Cell. Biol.* **32:** 3438–3451

Yang L, Zheng L, Chng WJ & Ding JL (2019) Comprehensive Analysis of ERK1/2 Substrates for Potential Combination Immunotherapies. *Trends Pharmacol. Sci.* **40:** 897–910

Yaron A, Hatzubai A, Davis M, Lavon I, Amit S, Manning AM, Andersen JS, Mann M, Mercurio F & Ben-Neriah Y (1998) Identification of the receptor component of the IkBa-ubiquitin ligase. *Nature* **396:** 590–594

Yates RM, Hermetter A & Russell DG (2005) The kinetics of phagosome maturation as a function of phagosome/lysosome fusion and acquisition of hydrolytic activity. *Traffic* **6:** 413–420

Yates RM & Russell DG (2005) Phagosome maturation proceeds independently of stimulation of toll-like receptors 2 and 4. *Immunity* **23:** 409–417

Yates RM & Russell DG (2008) Real-time spectrofluorometric assays for the lumenal environment of the maturing phagosome. *Methods Mol Biol.* **445:** 311–325

Ye H, Arron JR, Lamothe B, Cirilli M, Kobayashi T, Shevde NK, Segal D, Dzivenu OK, Vologodskaia M, Yim M, Du K, Singh S, Pike JW, Darnay BG, Choi Y & Wu H (2002) Distinct molecular mechanism for initiating TRAF6 signalling. *Nature* **418:** 443–447

Ye J, Xie X, Tarassishin L & Horwitz MS (2000) Regulation of the NF-κB activation pathway by isolated domains of FIP3/IKKγ, a component of the IκB-α kinase complex. *J. Biol. Chem.* **275:** 9882–9889

Yoneyama M, Suhara W, Fukuhara Y, Fukuda M, Nishida E & Fujita T (1998) Direct triggering of the type I interferon system by virus infection: Activation of a transcription factor complex containing IRF-3 and CBP/p300. *EMBO J.* **17:** 1087–1095

Yoshimori T, Yamamoto A, Moriyama Y, Futai M & Tashir Y (1991) Bafilomycin A1, a Specific Inhibitor of Vacuolar-type H+-ATPase, Inhibits Acidification and Protein Degradation in Lysosomes of Cultured Cells. *J. Biol. Chem.* **266:** 17707–17712

Yu M, Lowell CA, Neel BG & Gu H (2006) Scaffolding Adapter Grb2-Associated Binder 2 Requires Syk to Transmit Signals from FcεRI. *J. Immunol.* **176:** 2421–2429

Yu XJ, McGourty K, Liu M, Unsworth KE & Holden DW (2010) pH sensing by intracellular salmonella induces effector translocation. *Science (80-.).* **328:** 1040–1043

Zandi E, Rothwarf DM, Delhase M, Hayakawa M & Karin M (1997) The IκB kinase complex (IKK) contains two kinase subunits, IKKα and IKKβ, necessary for Iκb phosphorylation and NF-κB activation. *Cell* **91:** 243–252

Zanoni I, Ostuni R, Marek LR, Barresi S, Barbalat R, Barton GM, Granucci F & Kagan JC (2011) CD14 controls the LPS-induced endocytosis of toll-like receptor 4. *Cell* **147:** 868–880

Zaru R, Edgar AJ, Hanauer A & Watts C (2015) Structural and Functional Basis for p38-MK2-Activated Rsk Signaling in Toll-Like Receptor-Stimulated Dendritic Cells. *Mol. Cell. Biol.* **35:** 132–140

Zarubin T & Han J (2005) Activation and signaling of the p38 MAP kinase pathway. *Cell Res.* **15:** 11–18

Zeigerer A, Gilleron J, Bogorad RL, Marsico G, Nonaka H, Seifert S, Epstein-Barash H, Kuchimanchi S, Peng CG, Ruda VM, Conte-Zerial P Del, Hengstler JG, Kalaidzidis Y, Koteliansky V & Zerial M (2012) Rab5 is necessary for the biogenesis of the

endolysosomal system in vivo. *Nature* **485:** 465–470

Zhang CY, Bai N, Zhang ZH, Liang N, Dong L, Xiang R & Liu CH (2012) TLR2 signaling subpathways regulate TLR9 signaling for the effective induction of IL-12 upon stimulation by heat-killed Brucella abortus. *Cell. Mol. Immunol.* **9:** 324–333

Zhang J-M & An J (2007) Cytokines, Inflammation and Pain. *Int Anesth. Clin.* **45:** 27–37

Zhang J, Clark K, Lawrence T, Peggie MW & Cohen P (2014) An unexpected twist to the activation of IKKβ: TAK1 primes IKKβ for activation by autophosphorylation. *Biochem. J.* **461:** 531–537

Zhang SY, Jouanguy E, Ugolini S, Smahi A, Elain G, Romero P, Segal D, Sancho-Shimizu V, Lorenzo L, Puel A, Picard C, Chapgier A, Plancoulaine S, Titeux M, Cognet C, Von Bernuth H, Ku CL, Casrouge A, Zhang XX, Barreiro L, et al (2007) TLR3 deficiency in patients with herpes simplex encephalitis. *Science (80-.).* **317:** 1522–1527

Zhang W, Sloan-Lancaster J, Kitchen J, Trible RP & Samelson LE (1998) LAT: The ZAP-70 tyrosine kinase substrate that links T cell receptor to cellular activation. *Cell* **92:** 83–92

Zhang Y, Lu W & Hong M (2010) The membrane-bound structure and topology of a human α-defensin indicate a dimer pore mechanism for membrane disruption. *Biochemistry* **49:** 9770–9782

Zhu G, Wu CJ, Zhao Y & Ashwell JD (2007) Optineurin Negatively Regulates TNFα-Induced NF-κB Activation by Competing with NEMO for Ubiquitinated RIP. *Curr. Biol.* **17:** 1438–1443

Zhu H, Liang Z & Li G (2009) Rabex-5 Is a Rab22 Effector and Mediates a Rab22-Rab5 Signaling Cascade in Endocytosis. *Mol. Biol. Cell* **20:** 4524–4530

Zolov SN, Bridges D, Zhang Y, Lee WW, Riehle E, Verma R, Lenk GM, Converso-Baran K, Weide T, Albin RL, Saltiel AR, Meisler MH, Russell MW & Weisman LS (2012) In vivo, Pikfyve generates PI(3,5)P2, which serves as both a signaling lipid and the major precursor for PI5P. *Proc. Natl. Acad. Sci. U. S. A.* **109:** 17472–17477

Zou H, Li Q, Lin SC, Wu Z, Han J & Ye Z (2007) Differential requirement of MKK4 and MKK7 in JNK activation by distinct scaffold proteins. *FEBS Lett.* **581:** 196–202

Zougman A, Selby PJ & Banks RE (2014) Suspension trapping (STrap) sample preparation method for bottom-up proteomics analysis. *Proteomics* **14:** 1006–1010